UNIVERSITY OF SOUTHAMPTON
FACULTY OF PHYSICAL SCIENCES AND ENGINEERING
SCHOOL OF ELECTRONICS AND COMPUTER SCIENCE

Mobile Social Networking Aided Content Dissemination in Heterogeneous Networks

by

Jie Hu
B. Eng., MSc.
Southampton Wireless Group

Thesis for the degree of Doctor of Philosophy

October 2015

SUPERVISOR:

Professor Lajos Hanzo
FREng, FIEEE, FIEE, DSc, EIC IEEE Press
Chair of Southampton Wireless Group

and

Professor Lie-Liang Yang
SMIEEE, FIET, PhD
Southampton Wireless Group

Faculty of Physical Sciences and Engineering
University of Southampton
Southampton SO17 1BJ
United Kingdom

Dedicated to my family

UNIVERSITY OF SOUTHAMPTON

ABSTRACT

FACULTY OF PHYSICAL SCIENCES AND ENGINEERING
SOUTHAMPTON WIRELESS GROUP

Doctor of Philosophy

MOBILE SOCIAL NETWORKING AIDED CONTENT DISSEMINATION IN HETEROGENEOUS NETWORKS

by Jie Hu

Thanks to the rapid development of the wireless Internet, numerous mobile applications provide platforms for Mobile Users (MUs) to share any Information of Common Interest (IoCI) with their friends. For example, mobile applications of Facebook and Twitter enable MUs to share information via posts and status updates. Similarly, the mobile application of *Wase* (http://www.waze.com/) enables the drivers to share the real-time traffic information collected by themselves. However, at the time of writing, the dissemination process of the IoCI is predominantly supported by the Centralised Infrastructure (CI) based communication. In order to receive the IoCI, the mobile devices of MUs have to be connected either to a Base Station (BS) or to a Wi-Fi hotspot. However, the CI-based information dissemination faces the following three limitations: i) intermittent connectivity in rural areas; ii) overloaded CI-based network; iii) inefficient data service in densely populated areas. Due to the rapid development of the powerful mobile computing technique, mobile devices are typically equipped with large storage capacity, say dozens or possibly hundreds of Giga Bytes. Furthermore, they support multiple communication standards, such as Infrared, Bluetooth and Wi-Fi modules, in support of direct peer-to-peer communications. As a result, this treatise contributed towards mitigating the above-mentioned design problems in the conventional CI-based information dissemination by seeking assistance both from the opportunistic contacts and opportunistic multicast amongst MUs, who share common interest in the same information. This results in an integrated cellular and opportunistic network. Since mobile devices are carried by MUs, exploring the social behaviours exhibited by individuals and the social relationships amongst MUs may assist us in enhancing the communication experience.

We firstly study an integrated cellular and large-scale opportunistic network, where the MUs are sparsely distributed within a large area. Due to the large size of the area and the sparse distribution of the MUs, the connectivity between a BS and a MU as well as that between a pair of MUs exhibit an intermittent nature. As a result, the information delivery has to be realised by the opportunistic contact between a transmitter and receiver pair, when the receiver enter the range of the transmitter. However, successful information delivery requires that the duration of this opportunistic contact has to be longer than the downloading period of the information. This integrated network is relied upon for disseminating delay-tolerant IoCI amongst the MUs. We model the information dissemination in this integrated network by a Continuous-Time-Pure-Birth-Markov-Chain (CT-PBMC) and further derive its relevant delay metrics and information delivery ratio. With the assistance of large-scale opportunistic networks, the information delivery ratio before the IoCI expires may be doubled, when compared to the conventional CI-based information dissemination. Furthermore, upon modelling the contact history of the MUs as a social network, social centrality based schemes are proposed for the sake of off-loading tele-traffic from the potentially congested CI to the large-scale opportunistic network. As demonstrated by our simulation results, in the scenario considered, as many as 58% MUs can be served by the large-scale opportunistic network before the IoCI expires.

In the above-mentioned large-scale networks, the MUs tend to be dispersed. By contrast, in the densely populated scenario, where numerous MUs can be found within a small area, classic BS-aided multicast is often invoked as a traditional measure of disseminating the IoCI by relying on the broadcast nature of the wireless channels. However, BS-aided multicasting becomes inefficient, when the number of MUs is high.

If we efficiently exploit the redundant copies of the IoCI held by the already served MUs and activate these IoCI holders as potential relays for the next stage of cooperative multicast, the resultant diversity gain beneficially accelerates the information dissemination process. This approach may be regarded as opportunistic cooperative multicast, since no deterministic relay selection scheme is required. Its promising advantages experienced during disseminating the delay-sensitive IoCI across the densely populated area considered motivate us to study an integrated cellular and small-scale opportunistic network. By jointly considering both the effects of the channel model in the physical layer, as well as the resource scheduling in the Medium-Access-Control (MAC) layer and the information dissemination protocol in the network layer, we model the information dissemination process by a Discrete-Time-Pure-Birth-Markov-Chain (DT-PBMC). Apart from the above-mentioned factors related to wireless transmission, we also consider various MUs' social characteristics, such as their altruistic behaviours and their geographic social relationships. Relying upon the above-mentioned DT-PBMC, we are capable of studying the delay versus energy dissipation trade-off during the information dissemination process. As demonstrated by our simulation results, the integrated cellular and small-scale opportunistic network considered is capable of substantially reducing the total information dissemination delay and the total energy dissipation of the classic BS-aided multicast. However, these benefits are achieved at the cost of the additional energy dissipated by the individual MUs. In order to further reduce both the information dissemination delay and the energy dissipation, Social Network Analysis (SNA) tools are relied upon for proposing a range of efficient resource scheduling approaches in the MAC layer. As demonstrated by our simulation results, the so-called shortest-shortest-distance scheduling regime outperforms its counterparts in terms of both its delay and energy metrics.

Since the distance-related path-loss predetermines the successful information delivery in the scenario of the integrated cellular and small-scale opportunistic network, it is crucial for us to study the statistical properties of the random distance between a transmitter and receiver pair. As a result, we derive the closed-form distributions of both the random distance between a pair of MUs and that between a BS and MU pair for different scenarios. Apart from assisting us in analysing the information dissemination process, these results may be further relied upon for evaluating the path-loss, the throughput, the spectral efficiency and the outage probability in mobile networks.

Although mobile communication techniques evolved from the well known analog '1G' mobile networks to the emerging heterogeneous '5G' mobile networks, the operational systems still rely on the CI-dominated 'Comm 1.0' era. Explicitly, direct interaction amongst the MUs without any aid of the CI is rare. Since powerful mobile devices and pervasive social networking services are popular amongst the MUs, more direct interaction amongst the MUs would be advocated for the sake of achieving a more reliable, more prompt, and more energy-efficient communication experience. This treatise may contribute in a modest way towards the new 'Comm 2.0' era and may inspire further efforts from both the industrial and academic communities so as to embrace both the opportunities and the challenges of this new era from both the technical and economic perspectives.

Declaration of Authorship

I, **Jie Hu**, declare that the thesis entitled **MOBILE SOCIAL NETWORKING AIDED CONTENT DISSEMINATION IN HETEROGENEOUS NETWORKS** and the work presented in it are my own and has been generated by me as the result of my own original research. I confirm that:

- This work was done wholly or mainly while in candidature for a research degree at this University;
- Where any part of this thesis has previously been submitted for a degree or any other qualification at this University or any other institution, this has been clearly stated;
- Where I have consulted the published work of others, this is always clearly attributed;
- Where I have quoted from the work of others, the source is always given. With the exception of such quotations, this thesis is entirely my own work;
- I have acknowledged all main sources of help;
- Where the thesis is based on work done by myself jointly with others, I have made clear exactly what was done by others and what I have contributed myself;
- Parts of this work have been published.

Signed: ..... Date: .....

Acknowledgements

I would like to express my heartfelt gratitude to Professor Lajos Hanzo and Professor Lie-Liang Yang for their patience, insightful advice and continuous support and encouragement of my research. Their instructive and inspiring advice have always stimulated and guided me during my four years study.

Many thanks to my colleagues and the staff of the Southampton Wireless Group for the valuable discussions and comments throughout my research. Special thanks to my colleagues, Dr. Rong Zhang, Dr. Mohammed El-Hajjar, Dr. Bo Zhang, Dr. Jiayi Zhang and Dr. Wenbo Zhang as well as Dr. Halil Yetgin for their technical support and collaborative work. Many thanks to my friends, Dr. Jia Shi, Dr. Wei Liang, Dr. Hua Sun, Dr. Shaoshi Yang, for their altruistic support during my life in Southampton.

I would like to express my warmest gratitude to my father, Yujin, my mother, Liying, for their lifelong support, for their eternal love and for their understanding and faith on me.

List of Publications

Journals:

1. **Jie Hu**, Lie-Liang Yang and Lajos Hanzo, "Maximum Average Service Rate and Optimal Queue Scheduling of Delay-Constrained Hybrid Cognitive Ratio in Nakagami Fading Channels", *IEEE Transactions on Vehicular Technology*, vol. 62, no. 5, pp. 2220-2229, June 2013.

2. **Jie Hu**, Lie-Liang Yang and Lajos Hanzo, "Mobile Social Networking Aided Content Dissemination in Heterogeneous Networks," *China Communications*, vol. 10, no. 6, pp. 1-12, June 2013.

3. **Jie Hu**, Lie-Liang Yang and Lajos Hanzo, "Distributed Cooperative Social Multicast Aided Content Dissemination in Random Mobile Networks," *IEEE Transactions on Vehicular Technology*, vol. 64, no. 7, pp. 3075-2229, July 2014.

4. Bo Zhang, **Jie Hu**, Ying Huang, Mohammed El-Hajjar and Lajos Hanzo, "Outage Analysis of Superposition-Modulation-Aided Network-Coded Cooperation in the Presence of Network Coding Noise," *IEEE Transactions on Vehicular Technology*, vol. 64, no. 2, pp. 493-501, February 2015.

5. **Jie Hu**, Lie-Liang Yang, H. Vincent Poor and Lajos Hanzo, "Bridging the Social and Wireless Networking Divide: Information Dissemination in Integrated Cellular and Opportunistic Networks," *IEEE Access, early access*, September 2015.

6. **Jie Hu**, Lie-Liang Yang and Lajos Hanzo, "Delay Analysis of Social Group Multicast Aided Content Dissemination in Cellular Systems," *submitted to IEEE Transactions on Communication, under major revision*, September 2015.

7. **Jie Hu**, Lie-Liang Yang and Lajos Hanzo, "Energy-Efficient Cross-Layer Design of Wireless Mesh Networking for Content Sharing in Online Social Networks," *to be submitted*, September 2015.

8. **Jie Hu**, Lie-Liang Yang and Lajos Hanzo, "Stochastic Geometry and Performance Analysis of MUs obeying Uniform Mobility Model in Cellular Systems," *to be submitted*, October 2015.

Conferences:

1. **Jie Hu**, Lie-Liang Yang and Lajos Hanzo, "Optimal Queue Scheduling for Hybrid Cognitive Radio Maintaining Maximum Average Service Rate under Delay Constraints," *2012 IEEE Global Communications Conference (GlOBECOM)*, pp. 1398-1403, Anaheim, USA, December 2012.

2. **Jie Hu**, Lie-Liang Yang and Lajos Hanzo, "Throughput and Delay Analysis of Wireless Multicast in Distributed Mobile Social Networks Based on Geographic Social Relationships, " *2014 IEEE Wireless Communications and Networking Conference (WCNC)*, pp. 1874-1879, Istanbul, Turkey, April 2014.

3. **Jie Hu**, Lie-Liang Yang and Lajos Hanzo, "Cooperative Multicast Aided Picocellular Hybrid Information Dissemination in Mobil Social Networks: Delay/Energy Evaluation and Relay Selection," *2014 IEEE Wireless Communications and Networking Conference (WCNC)*, pp. 3207-3212 , Istanbul, Turkey, April 2014.

Contents

Glossary

ACK	ACKnowledgement
ana	analytical
BCCH	BroadCast Control Channel
BS	Base Station
BSs	Base Stations
BSSHM	BS-aided-Single-Hop Multicast
CCDF	Complementary Cumulative Distribution Function
CDF	Cumulative Distribution Function
CDFs	Cumulative Distribution Functions
CDMA	Code-Division-Multiple-Access
CI	Centralised Infrastructure
CMM	Community-based Mobility Model
COs	Content Owners
CSMA	Carrier-Sense-Multiple-Access
CSs	Content Seekers
CT-PBMC	Continuous-Time-Pure-Birth-Markov-Chain
DT-PBMC	Discrete-Time-Pure-Birth-Markov-Chain
DTNs	Delay-Tolerant Networks
FA	Factor of Altruism
HCMM	Home-cell Community-based Mobility Model
i.i.d.	independently and identically distributed
IC	Information Controller
ICI	Inter-Cell Interference
IM	Information Multicaster
IMs	information multicasters
IoCI	Information of Common Interest
IoCI	Information of Common interest
IOs	Information Owners
LTE-A	Long-Term-Evolution-Advanced

MAC Medium-Access-Control
MANET Mobile *Ad hoc* NETwork
MANETs Mobile *Ad hoc* NETworks
MSC Mobile Switching Centre
MSN Mobile Social Networking
MSNs Mobile Social Networks
MU Mobile User
MUs Mobile Users

NW Newmann-Watts

OFDMA Orthogonal-Frequency-Division-Multiple-Access
OLPC One Laptop Per Child
opp opportunistic

P2P Peer-to-Peer
PBMC Pure-Birth based Markov Chain
PDF Probability Density Function
PDFs Probability Density Functions
PHY PHYsical
PL Path-Loss
PMF Probability Mass Function
POs Packet Owners
PPP Poisson-Point-Process
PSD Power Spectrum Density
PUCCH Physical Uplink Control CHannel

QoS Quality of Service
QPSK Quadrature Phase-Shift Keying

RD Random Direction
reg regular
RMSE Root-Mean-Square-Error
RU Roadside Unit
RW Random Walk
RWP Random Way-Point

sim simulation
SNA Social Network Analysis
SNR Signal-to-Noise-Ratio
SPM Social Pressure Metric
SPRP Successful Packet Reception Probability

TCN Telephone Call Network
TDF Tail Distribution Function
TDMA Time-Division-Multiple-Access
tot total
TS Time Slot

TSs	Time Slots
uMUs	unserved Mobile Users
WS	Watts-Strogatz

List of Symbols

Special Symbols

Note that the generic subscript l in the symbols throughout the entire treatise represents 'b' for characterising the corresponding feature of the transmission between a BS and a MU, while l represents 's' for characterising the corresponding feature of the transmission between a pair of MUs.

Specific Symbols in Chapter 2

L: The file size.

B: The transmission rate.

T_L: The life Time of the Information of Common Interest (IoCI).

T_{IC} & $\overline{T}_{IC}$: The inter-contact duration between a mobile transmitter and receiver pair and its average value.

T_C & $\overline{T}_C$: The contact duration between a mobile transmitter and receiver pair and its average value.

$\overline{F}_{T_C,l}(\cdot)$: The Complementary Cumulative Distribution Function (CCDF) of the contact duration between a mobile transmitter and receiver pair.

$V_{\min}$&$V_{\max}$: The minimum and maximum speed of a Mobile User (MU) obeying a Random Direction (RD) mobility model.

$V_{\max}$: The maximum speed of a MU obeying a RD mobility model.

S: The area of the square-shaped mobility region.

r & R: The transmission range of a MU (a mobile node) and that of a BS (a static node).

V^*: The relative speed between a mobile transmitter and receiver pair.

λ_l: The average contact rate between a transmitter and receiver pair.

$\widetilde{\lambda}_l$: The effective average contact rate between a transmitter and receiver pair when jointly considering both the inter-contact duration, contact duration and the minimum information transmission time required.

N: The total number of MUs in the area studied.

$\widetilde{\lambda}_n$: The transition rate from state n to state $(n+1)$.

T_n: The transition delay from state n to state $(n+1)$.

Λ: The transition rate matrix of the Continuous-Time-Pure-Birth-Markov-Chain (CT-PBMC).

T_D: The dissemination delay that is spent for disseminating the IoCI to all the MUs in a large-scale opportunistic network.

T_I: The individual delay of a specific MU successfully receiving the IoCI.

$p_n(t)$: The probability of the CT-PBMC studied staying at state n after a time period t.

$SPM_{i,j}\&\omega_{i,j}$: The Social Pressure Metric (SPM) and its reciprocal between MU_i and MU_j.

Generic Symbols in Chapters 3-6

N: The total number of MUs in a MSN group studied.

$|h_l(t)|^2$: The square of the fading amplitude during the t-th Time Slot (TS).

$\Omega_l(y_l)$: The Path-Loss (PL) when the distance between a transmitter and receiver pair is y_l.

c: The speed of light.

$f_{l,c}$: The carrier frequency.

d_0: The reference distance defining the edge of the near-field of the transmit antenna.

$P_{l,0}$: The received power at the reference point which is d_0 m away from the transmit antenna.

$P_{l,r}$: The average received power at a receiver end.

κ: The PL exponent.

N_0: The power spectrum density of the white noise.

W_l: The transmission bandwidth.

γ: The pre-defined Signal-to-Noise-Ratio (SNR) threshold for successful packet reception.

$\mathbf{P}_i(t)$: The position of the i-th MSN user during the t-th time interval.

Y_l: The random distance between a transmitter and receiver pair.

R: The radius of the circular area studied.

$\mu_l(y_l)$: The Successful Packet Reception Probability (SPRP) of a wireless link during a specific TS , given that the distance between a transmitter and receiver pair is y_l.

$\overline{\mu}_l$: The average SPRP of a wireless link between a transmitter and receiver pair.

$f_{Y_l}(y_l)$: The accurate PDF of the random distance Y_l between a transmitter and receiver pair.

$\widetilde{f}_{Y_l}(y_l)$: The approximate PDF of the random distance Y_l between a transmitter and receiver pair.

$p_{n,n+m}(t)$: The transition probability from state n to state $(n+m)$ in the Discrete-Time-Pure-Birth-Markov-Chain (DT-PBMC) during the t-th TS or transmission frame.

$\overline{p}_{n,n+m}$: The average transition probability from state n to state $(n+m)$ in the DT-PBMC.

Specific Symbols in Chapter 3

q: The Factor of Altruism (FA).

Δt: The duration of a virtual mini-TS.

n_k: The number of Packet Owners (POs) willing to forward the packet of common interest when the Pure-Birth based Markov Chain (PBMC) transits from state k to state $(k+1)$.

T_k: The transition delay from state k to $(k+1)$.

T_D: The dissemination delay that is spent for disseminating the packet of common interest across the MSN group.

m & θ: The shape and scale parameters of a Gamma distribution.

$\Pr_k$: The probability of a specific MSN user successfully receiving the packet of common interest in state k.

$T_{\mathcal{A}}$: The individual user-delay of a specific MSN user $\mathcal{A}$ successfully receiving the packet of common interest.

$T_{W,k}$: The transmit time of an individual MSN user during the transition from state k to state $(k+1)$.

T_W: The transmit time of an individual MSN user involved in forwarding the packet of common interest during the packet dissemination process.

P_l^{tx}: The transmit power of a transmitter.

P_l^{rx}: The signal processing power for recovering a received packet at a receiver end.

E_k: The energy dissipation of the transition from state k to state $(k+1)$.

E_D: The total energy dissipated during disseminating the packet of common interest across the target MSN group.

E_I: The energy dissipated by an individual MSN user during the packet dissemination process.

$\mathcal{R}_{MSN}$: The expected number of replicas of the packet off-loaded from the BS to the MSN group.

r_{MSN}: The tele-traffic off-loading ratio.

Specific Symbols in Chapter 4

U: The number of initial Content Owners (COs).

$\varphi_s(y_s)$: The social strength between a pair of MUs when they are y_s m away from each other.

$\overline{\varphi}_s$: The average social strength between a pair of MUs.

r: The neighbourhood range.

α: The social exponent.

$\nu_s(y_s)$: The social unicast throughput of a social wireless link connecting a transmitter and receiver pair when they are y_s m away.

$\overline{\nu}$: The average social unicast throughput of a social wireless link connecting a transmitter and receiver pair.

$\mathbb{P}(t)$: The random transition matrix of the DT-PBMC during the t-th transmission frame.

$\mathbf{Q}(t)$ & $\overline{\mathbf{Q}}$: The random transition matrix between the transient states of the DT-PBMC during the t-th transmission frame and its expected matrix.

$\mathbf{Q_0}(t)$: The random vector of absorbing probabilities in the DT-PBMC during the t-th transmission frame

K: The content dissemination delay when the content of common interest is disseminated from the initial COs across the MSN studied.

Specific Symbols in Chapter 5

The random matrices, namely $\mathbf{P}(t)$, $\mathbf{Q}(t)$ and $\mathbf{Q_0}(t)$, and their corresponding expected matrices, namely $\overline{\mathbf{P}}$, $\overline{\mathbf{Q}}$ and $\overline{\mathbf{Q_0}}$, hold the same definitions as those defined in Chapter 4.

n_0: The number of TSs provided for cooperative-multicast-aided spontaneous dissemination.

$\Omega_{l,0}$: The free-space PL at the reference point which is d_0 m away from the transmit antenna.

$P_{l,t}$: The transmit power of a transmitter.

$\lambda_s(y_s, \mathcal{L})$: The throughput of a wireless link connecting a pair of MUs, when they are y_s m away from each other and $\mathcal{L}$ TSs are allocated to the transmitter.

$\overline{\lambda}_s(\mathcal{L})$: The average throughput of a wireless link connecting a pair of MUs, when $\mathcal{L}$ TSs are allocated to the transmitter.

A: The size of a specific target group of MUs.

$\Pr_n$: The probability that the transient boundary is at state n of the DT-PBMC.

$\mathbf{Q}_n(t)$: The sub-matrix of $\mathbf{Q}(t)$ containing its entries in the first n rows and n columns.

$\widetilde{\mathbf{Q}}_n(t)$: The revised $N \times N$ matrix, whose top-left sub-matrix is $\mathbf{Q}_n(t)$ and all the other elements are filled by zeros.

$\widehat{\mathbf{Q}}_n$: The expected matrix of the random matrix $\widetilde{\mathbf{Q}}_n(t)$.

K_G: The group delay, namely the dely when the entire group $\mathcal{A}$ of MUs has successfully received the IoCI.

K_I: The individual delay, namely the delay of a specific MU receiving the IoCI.

K_D: The dissemination delay, which represents the delay when all the N MUs in the cell have successfully received the IoCI.

K_b: The BS-aided multicast delay K_b, which is the delay of the BS-adied first stage of information dissemination.

K^{bm}: The BS-adied-single-hop-multicast delay, namely the delay when only the BS is the sole transmitter for multicasting the IoCI.

Specific Symbols in Chapter 6

r: The radius of the circular area studied.

a: The side length of the square area studied.

d: The distance from the location of the BS to the centre of the area studied.

Specific Symbols in Chapter 7

$\mathcal{F}_i$: The content file, which is ranked at the i-th position of the popular content list.

F: The number of content files in the popular content list.

$\mathcal{C}(q)$: The total cost function with respect to the FA q, which is in the non-cooperative gaming modelling.

$T_I(q)$: The delay of an individual MU successfully receiving the content of common interest during the content dissemination process with respect to the FA q.

$E_I(q)$: The energy dissipated by an individual MU during the content dissemination process with respect to the FA q.

Special Operations

$\|\cdot\|$: The cardinality operation on a set.

$(\cdot)^T$: The transpose of a matrix.

$\lceil\cdot\rceil$: Rounding a numerical value to its nearest higher integer.

$\lfloor\cdot\rfloor$: Rounding a numerical value to its nearest lower integer.

$\binom{\cdot}{\cdot}$: Binomial coefficient operation.

$\sum$: The summation of all elements.

$\prod$: The product of all elements.

$\forall$: For all elements within a certain range.

$\int$: The integration operation.

$\lim$: The limitation operation.

$\mathcal{E}[\cdot]$: The expectation operation.

$Var[\cdot]$: The variance operation.

$\exp(\cdot)$: The exponential operation.

$\log(\cdot)$: The logarithm operation.

$\ln(\cdot)$: The natural logarithm operation.

$\max[\cdot]$: The maximum value of a vector/matrix.

$\min[\cdot]$: The minimum value of a vector/matrix.

$mod(x, y)$: The remainder after the division of x by y.

$f_X(x)$: The Probability Density Function (PDF) of a random variable X.

$F_X(x)$: The Cumulative Distribution Function (CDF) of a random variable X.

$\overline{F}_X(x)$: The Complementary Cumulative Distribution Function (CCDF) of a random variable X.

$\Pr(\cdot)$: The probability of an arbitrary event occurring.

$O(\cdot)$: The notation describing the order of a given function.

Chapter 1

Introduction: An Overview of the Social Network Analysis and Its Application in Wireless Communication

1.1 Background

At the time of writing, we are witnessing a dramatic increase of the number of mobile devices and connections. The white paper published by Cisco in 2014 [1] predicted that by the end of 2014, the number of mobile-connected devices would exceed the number of people on earth and this number would break through the 10 billion limit by 2018. Accommodating the huge amount of tele-traffic generated by billions of mobile devices is a 'mission impossible' for the conventional Centralised Infrastructure (CI) based communication system. However, most of the mobile devices are equipped with multiple communication modes, which makes device-to-device communication [2] and the Internet of things [3] become attractive solutions. Furthermore, since mobile devices are held by people, communication between mobile devices is featured by the social behaviours of people, which stimulates the cross-disciplinary research area of *mobile social networks* [4] based on the combination of social science and wireless communication and networking. The growing research interest can be observed in Figure 1.1.

1.2 Social Network Analysis

Let us first provide a brief survey over the research area of Social Network Analysis (SNA). To most people, the phrase 'social network' refers to online social networking services such as *Facebook* (http://www.facebook.com) and *Twitter* (http://www.twitter.com). However, the research of social networks dates back farther than the emergence of the Internet. The true foundation of this field is attributed to Moreno, who studied social interactions within groups of people and published his research entitled *Who Shall Survive* [21] in 1934. Unfortunately, traditional data collection methods such as interviews and questionnaires [22] as well as observations [23] are extremely inefficient. Hence, research on SNA progressed slowly in the early decades of the 20-th century, until the invention of computer technology and online social networking services. Since then, the research community became more prosperous than ever before. In the rest of Section 1.2, we will characterise the structure of social networks and introduce the new research trends in terms of nodes' and edges' importance evaluation (centralities), communities and small-world phenomenons, as

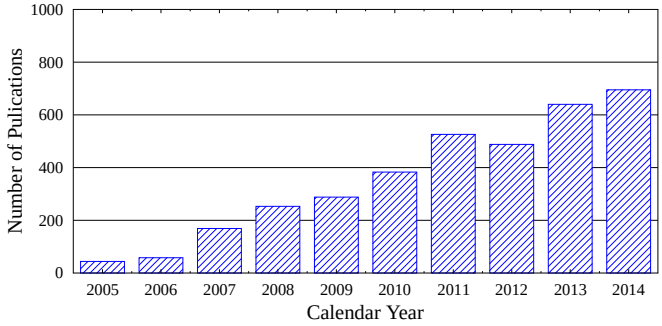

(a) IEEE Digital Library

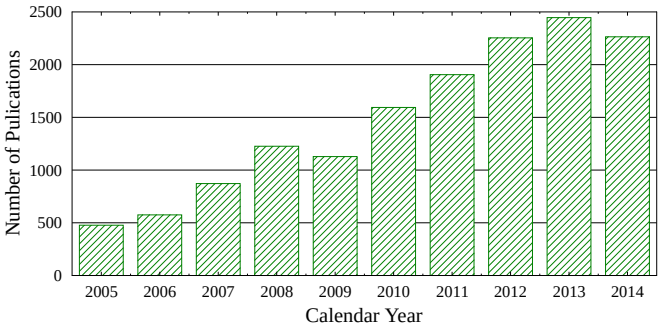

(b) ACM Digital Library

Figure 1.1: The number of publications including the searching term 'mobile social network' in both the IEEE digital library and the ACM digital library from the calendar year 2005 to 2014.

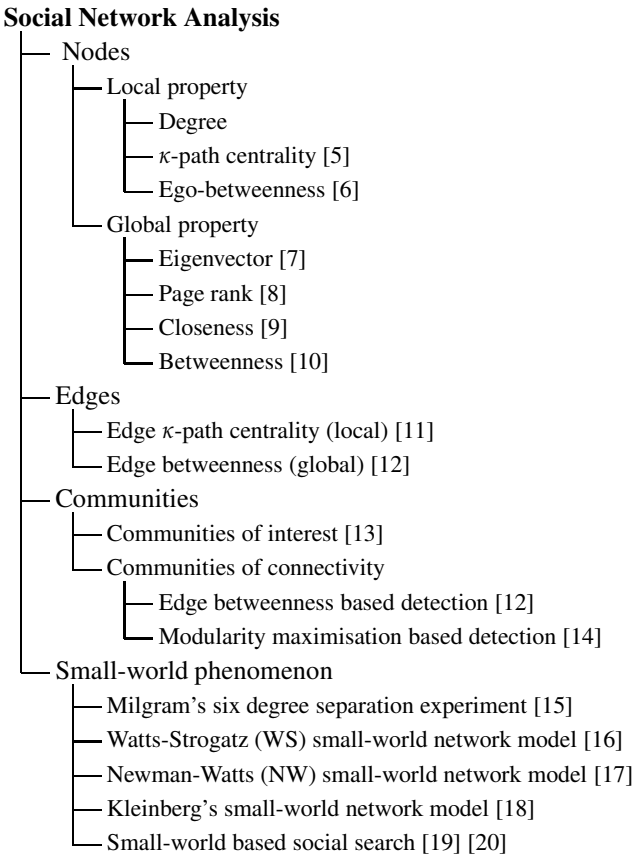

Figure 1.2: The research in social network analysis

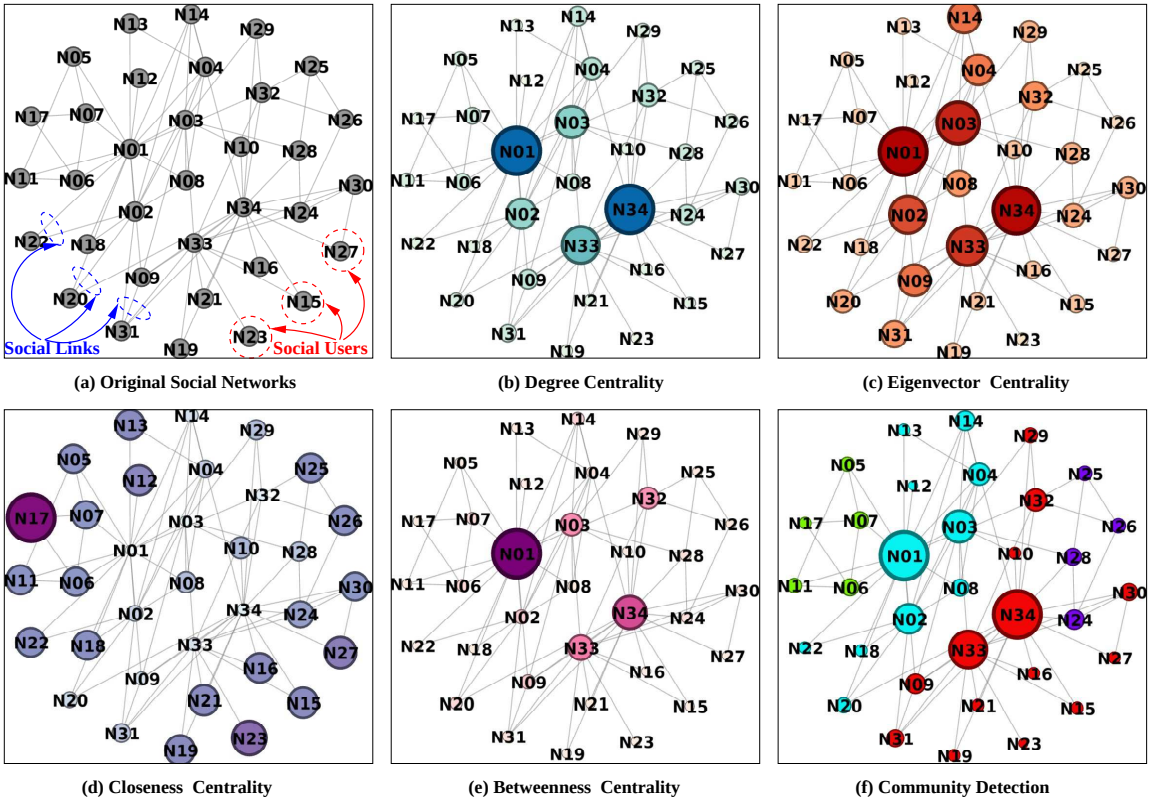

Figure 1.3: Unweighted and undirected friendship network between members of a karate club. This social network shows the pattern of friendships between the members of a karate club at an American university. The data were collected and published in [24]. The calculation process of degree, eigenvector, closeness, and betweenness centralities for the node 'N06' is exemplified in Table 1.1.

summarised in Figure 1.2.

1.2.1 Structure of Social Networks

A social network is comprised of social users (represented by nodes) and social links (represented by edges). A pair of social users is said to be connected by a social link, if they share a friendship, as portrayed in Figure 1.3(a). Mathematically, the structure of a generic social network having N nodes can be characterised by an adjacency matrix $A = [a_{ij}]_{N\times N}$, where $a_{ij} = 1$ if there is a social link spanning from node i to node j and $a_{ij} = 0$, otherwise. The social network of Figure 1.3(a) characterises the friendships amongst the members of a karate club at an American university [24]. An edge represents that a pair of individuals consistently were observed to interact also outside the normal activities of the club (karate classes and club meetings). The social network of Figure 1.3(a) is an unweighted and undirected graph, which indicates that all the social links have the same strength and they are symmetrical. The social network of Figure 1.3(a) can be characterised by the adjacency matrix A_{kara}, as shown in Eq.(1.1). Furthermore, a social link can be assigned a weight for the sake of characterising the strength of the friendship between a pair of social users. Sometimes, a pair of social users share 'unsymmetrical' friendships, which can be characterised by directional social links in social networks.

$$A_{kara} = \begin{pmatrix}
0&1&1&1&1&1&1&1&1&0&1&1&1&1&0&0&0&1&0&1&0&1&0&0&0&0&0&0&0&0&0&0&1&0&0\\
1&0&1&1&0&0&0&1&0&0&0&0&0&1&0&0&0&1&0&1&0&1&0&0&0&0&0&0&0&0&0&1&0&0&0\\
1&1&0&1&0&0&0&1&1&1&0&0&0&1&0&0&0&0&0&0&0&0&0&0&0&0&0&0&1&1&0&0&0&1&0\\
1&1&1&0&0&0&0&1&0&0&0&0&1&1&0&0&0&0&0&0&0&0&0&0&0&0&0&0&0&0&0&0&0&0&0\\
1&0&0&0&0&0&1&0&0&0&1&0&0&0&0&0&0&0&0&0&0&0&0&0&0&0&0&0&0&0&0&0&0&0&0\\
1&0&0&0&0&0&1&0&0&0&1&0&0&0&0&0&1&0&0&0&0&0&0&0&0&0&0&0&0&0&0&0&0&0&0\\
1&0&0&0&1&1&0&0&0&0&0&0&0&0&0&1&0&0&0&0&0&0&0&0&0&0&0&0&0&0&0&0&0&0&0\\
1&1&1&1&0&0&0&0&0&0&0&0&0&0&0&0&0&0&0&0&0&0&0&0&0&0&0&0&0&0&0&0&0&0&0\\
1&0&1&0&0&0&0&0&0&0&0&0&0&0&0&0&0&0&0&0&0&0&0&0&0&0&0&0&0&0&0&1&0&1&1\\
0&0&1&0&0&0&0&0&0&0&0&0&0&0&0&0&0&0&0&0&0&0&0&0&0&0&0&0&0&0&0&0&0&0&1\\
1&0&0&0&1&1&0&0&0&0&0&0&0&0&0&0&0&0&0&0&0&0&0&0&0&0&0&0&0&0&0&0&0&0&0\\
1&0&0&0&0&0&0&0&0&0&0&0&0&0&0&0&0&0&0&0&0&0&0&0&0&0&0&0&0&0&0&0&0&0&0\\
1&0&0&1&0&0&0&0&0&0&0&0&0&0&0&0&0&0&0&0&0&0&0&0&0&0&0&0&0&0&0&0&0&0&0\\
1&1&1&1&0&0&0&0&0&0&0&0&0&0&0&0&0&0&0&0&0&0&0&0&0&0&0&0&0&0&0&0&0&0&1\\
0&0&0&0&0&0&0&0&0&0&0&0&0&0&0&0&0&0&0&0&0&0&0&0&0&0&0&0&0&0&0&0&1&1&\\
0&0&0&0&0&0&0&0&0&0&0&0&0&0&0&0&0&0&0&0&0&0&0&0&0&0&0&0&0&0&0&0&1&1&\\
0&0&0&0&0&1&1&0&0&0&0&0&0&0&0&0&0&0&0&0&0&0&0&0&0&0&0&0&0&0&0&0&0&0&\\
1&1&0&0&0&0&0&0&0&0&0&0&0&0&0&0&0&0&0&0&0&0&0&0&0&0&0&0&0&0&0&0&0&0&\\
0&0&0&0&0&0&0&0&0&0&0&0&0&0&0&0&0&0&0&0&0&0&0&0&0&0&0&0&0&0&0&0&1&1&\\
1&1&0&0&0&0&0&0&0&0&0&0&0&0&0&0&0&0&0&0&0&0&0&0&0&0&0&0&0&0&0&0&0&1&\\
0&0&0&0&0&0&0&0&0&0&0&0&0&0&0&0&0&0&0&0&0&0&0&0&0&0&0&0&0&0&0&0&1&1&\\
1&1&0&0&0&0&0&0&0&0&0&0&0&0&0&0&0&0&0&0&0&0&0&0&0&0&0&0&0&0&0&0&0&0&\\
0&0&0&0&0&0&0&0&0&0&0&0&0&0&0&0&0&0&0&0&0&0&0&0&0&0&0&0&0&0&0&0&1&0&\\
0&0&0&0&0&0&0&0&0&0&0&0&0&0&0&0&0&0&0&0&0&0&0&0&0&0&1&0&1&0&1&0&0&1&1\\
0&0&0&0&0&0&0&0&0&0&0&0&0&0&0&0&0&0&0&0&0&0&0&0&0&0&1&0&1&0&0&0&1&0&0\\
0&0&0&0&0&0&0&0&0&0&0&0&0&0&0&0&0&0&0&0&0&0&0&0&0&1&1&0&0&0&0&0&1&0&0\\
0&0&0&0&0&0&0&0&0&0&0&0&0&0&0&0&0&0&0&0&0&0&0&0&0&0&0&0&0&0&0&1&0&0&1\\
0&0&1&0&0&0&0&0&0&0&0&0&0&0&0&0&0&0&0&0&0&0&0&1&1&0&0&0&0&0&0&0&0&1&\\
0&0&1&0&0&0&0&0&0&0&0&0&0&0&0&0&0&0&0&0&0&0&0&0&0&0&0&0&0&0&0&1&0&1&\\
0&0&0&0&0&0&0&0&0&0&0&0&0&0&0&0&0&0&0&0&0&0&0&1&0&0&1&0&0&0&0&0&1&1&\\
0&1&0&0&0&0&0&0&1&0&0&0&0&0&0&0&0&0&0&0&0&0&0&0&0&0&0&0&0&0&0&0&1&1&\\
1&0&0&0&0&0&0&0&0&0&0&0&0&0&0&0&0&0&0&0&0&0&0&0&1&1&0&0&1&0&0&0&1&1&\\
0&0&1&0&0&0&0&0&1&0&0&0&0&0&1&1&0&0&1&0&1&0&1&1&0&0&0&0&0&1&1&1&0&1&\\
0&0&0&0&0&0&0&0&0&1&1&0&0&0&1&1&1&0&0&1&1&1&0&0&1&0&0&1&1&1&1&1&1&1&0
\end{pmatrix} \tag{1.1}$$

1.2.2 Evaluating Nodes in Social Networks

In order to fully exploit the characteristics of a social network, the identification of the principal social users inside the social network is quite important. Such an identification requires an *importance measure* (also referred to as *centrality*) to weigh social users and social links.

The most straightforward approach is to directly count the number of neighbours that a social user is directly connected to in the social network studied, which is referred to as the *degree centrality*. Figure 1.3(b) portrays the degrees for all the nodes in the social network of the karate club [24]. A darker node that is also characterised by a larger size has a higher value of degree centrality. We observe from Figure 1.3(b) that 'N01' and 'N34' have the highest degrees, sequentially followed by 'N33' and 'N03'. The degree centrality is also applied often for characterising the 'impact factor' of an academic journal by quantifying how often a specific journal is cited by others. Survey journals of the research community usually have a higher impact factor than pure research journals. However, the degree centrality only characterises the local topological properties of a node in a social network, since only the neighbourhood of a node is taken into account. Unfortunately, this measurement is not capable of characterising the global role of a node in the entire social network.

A natural extension of the degree centrality is the *eigenvector centrality*. In the definition of the degree centrality, every neighbour is equally treated without any bias. By contrast, a more important neighbour may provide higher weight for the calculation of the eigenvector centrality [7]. As a result, a node having fewer high-weight neighbours may still outrank another node having more low-weight neighbours, i.e. if

the neighbours of the former node are more important than those of the latter. Figure 1.3(c) portrays the eigenvector centralities for all the nodes in the social network of the karate club [24]. We observe from Figure 1.3(c) that 'N03' outranks 'N33', although 'N03' has fewer neighbours than 'N33'. This is because the neighbours of 'N03' are more important than those of 'N33'. The eigenvector centrality is also routinely applied in the citation network of journals for characterising the 'eigenfactor' of an academic journal. As an example, research journals in the communication community often outrank survey journals in terms of their eigenfactor. Furthermore, as a variant of the eigenvector centrality, *PageRank centrality* has been proposed for ranking the webpages provided by the Google search engine [8].

Another global measure is referred to as *closeness centrality* [9]. This measure evaluates how 'close' a node is to all the other nodes in a network. Figure 1.3(d) portrays the closeness centralities for all the nodes in the social network of the karate club. We observe from Figure 1.3(d) that 'N17' is the closest node to all the other nodes in the social network, although the number of its neighbours is quite low, as shown in Figure 1.3(b).

Betweenness centrality [10] is another global measure, which relies on the idea that in social networks information flows along the *shortest path* in terms of the number of hops between a pair of end-users. As a result, a node would have a high betweenness centrality, if a large number of end-to-end shortest paths cross it. As shown in Figure 1.3(e), 'N01' has the highest betweenness centrality in the social network of the karate club. The authors of [25] further relaxed the assumption that information only flows along the shortest paths and proposed a new betweenness centrality based on random walks. However, the original computation of betweenness centrality requires the global knowledge of the social network studied. If the social network is quite large, having millions of nodes in it, even the most efficient algorithm for computing the betweenness centrality has the complexity of $O(MN)$ [26], where M and N represents the numbers of edges and nodes, respectively. As a further advance, the authors of [5] proposed κ-*path centrality*, where the computation only relies on the information flows along the paths that are shorter than κ hops. They found that κ-path centrality metric matches the original betweenness centrality closely, while significantly reducing the complexity of its computation to $O(\kappa^3 N^{2-2\alpha} \log N)$. The *egocentric network* concept of [27] represents the network surrounding the individual studied within a radius of 1 hops. Moreover, the *ego-betweenness* [6] is a special case of κ-path centrality for $\kappa = 2$.

The aforementioned betweenness centrality of nodes can be readily extended in order to characterise the betweenness centrality for edges, which plays a vital role in community detection [12]. Similar to [5], a κ-*path edge betweenness* was proposed in [11] and the corresponding computational complexity was reduced to $O(\kappa M)$, where M is the number of edges in the social network studied.

Table 1.1 exemplifies the calculation process of the degree, of the eigenvector, the closeness and the betweenness centralities for the node 'N06' in the social network of the karate club, as shown in Figure 1.3.

1.2.3 Community Detection

According to different node classification principles, we have the following two types of community:

- A *community of interest*, which is "a set of people assembled around a topic of common interest. Its members take part in the community to exchange information, to obtain answers to personal questions or problems, to improve their understanding of a subject, to share common passions or to play" [13].
- A *community of connectivity*, which is a group of nodes in social networks densely connected to each other and weakly coupled with nodes residing outside the community itself.

These two types of community may convert into each other. People sharing common interests are often tightly connected to each other in social networks. Vice versa, people that are strongly connected to each

Table 1.1: Various centralities of node 'N06' in the social network of Figure 1.3

Centrality	**Calculation Process**	**Value**	**Complexity**[a]
Degree	Node N06 has 4 neighbours in total, which are N01, N07, N11 and N17. The number of neighbours is derived by summing the entries in the 6-th row of the adjacent matrix A_{kara} of Eq.(1.1).	$Deg(\text{N06}) = 4$	$O(\min(M,N))$
Eigenvector	Given the adjacency matrix A_{kara} of Eq.(1.1), according to the formula $A_{kara}x = \lambda x$, find the eigenvalue $\lambda_{\max} = 6.67$ having the largest absolute value and derive its corresponding eigenvector x. The eigenvector centrality of N06 is the 6-th entry of x.	$Eig(\text{N06}) = 0.226$	$O(C \cdot N^2)$ [28], C is the No. of the iterations in the invoked algorithm.
Closeness	Given the adjacency matrix A_{kara} of Eq.(1.1), we find the shortest path between N06 and an arbitrary node j. Calculate the number of hops of this shortest path, defined as $d_{6,j}$. For example, the shortest path between N06 and N12 is $N06 \rightarrow N01 \rightarrow N12$ having $d_{6,12} = 2$ hops. Repeat this computing process for all the nodes. Then the closeness of N06 is derived as $\sum_{j=1,j\neq 6}^{34} 1/d_{6,j}$.	$Clo(\text{N06}) = 2.6$	$O(M + N \log N)$ [9]
Betweenness	Given the adjacency matrix A_{kara} of Eq.(1.1), we find all the shortest paths between an arbitrary pair of nodes, i and j. The total number of these paths is g_{ij}. Amongst these paths, $g_{ij}(k)$ paths cross node k. For example, there are $g_{7,11} = 3$ shortest paths between N07 and N11. Amongst these, only $g_{7,11}(6) = 1$ shortest path cross N06. Repeat this computing process for all possible pairs. Then the betweenness of N06 is derived as $\sum_{i=1}^{34}\sum_{j=1}^{34} g_{ij}(6)/g_{ij}/2$, for $i \neq 6$ and $j \neq 6$.	$Bet(\text{N06}) = 15.8$	$O(MN)$ [26]

[a] M and N represents the numbers of edges and nodes, respectively.

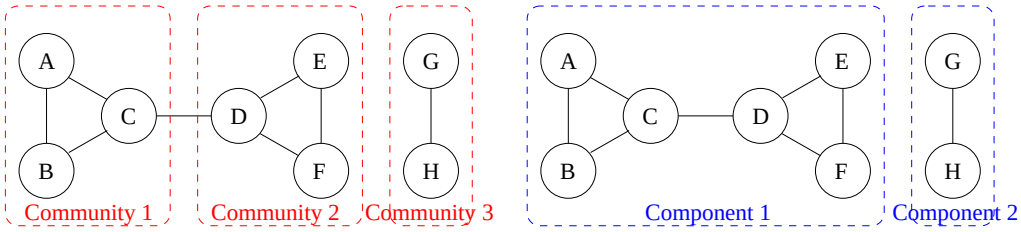

(a) Dividing a social network into communities (b) Dividing a social network into components

Figure 1.4: An example for highlighting the difference between the concepts of community and component

other may tend to cultivate common interests due to frequent communication with each other. The community of interest is the focus of our research in the following chapters. However, in this section, we would like to briefly introduce the detection of communities of connectivity.

As mentioned above, edge betweenness was invoked in the community detection algorithm developed in [12]. After calculating the betweenness for all edges, the specific edge having the highest betweenness is removed. Then, the betweenness of the edges affected by the former removal edges is recalculated. This procedure is repeated until the underlying community structure of the network is completely discovered.

Modularity was designed to quantify the grade of division across a network into modules [29]. The authors of [14] develop a community detection algorithm based on modularity maximisation, which iteratively optimises the formulation of local communities until the achievable global modularity can no longer be improved by tentatively imposing perturbations on the current community state. This algorithm is exploited for discovering the community structure of the social network, such as the karate club, as shown in Figure 1.3(f). We observe from Figure 1.3(f) that the social network is divided into four communities and different communities are filled by different colours and patterns. The largest community has 14 members, while the smallest community has only 4 members.

Apart from communities, we have another similar concept concerning the connectivity of social networks constituted by a diverse range of *connected components*. In SNA, a connected component is a sub-network in which any two nodes are connected to each other by multi-hop links. A node in a component is *not connected* to any other nodes residing outside this component. This property constitutes the main difference between the concepts of components and communities, since nodes residing in different communities may still find a multi-hop link connecting each other. It is quite straightforward to find all connected components in a social network in linear time, when either a breadth-first search or a depth-first search algorithm is invoked.

As portrayed in Figure 1.4(a), a social network having six nodes may for example be divided into three communities. Community 1 is comprised of Nodes A, B and C, Community 2 consists of Nodes D, E and F, and Community 3 includes Nodes G and H. We observe from Figure 1.4(a) that although Nodes A and E belong to different communities, they are still connected by a multi-hop link $A \rightarrow C \rightarrow D \rightarrow E$. By contrast, in Figure 1.4(b), the same social network is divided into two components. Component 1 is comprised of Nodes A to F and Component 2 only includes Nodes G and H. We observe from Figure 1.4(b) that since Node A and Node G belong to different components, no multi-hop link connects this pair of nodes in the social network.

Note that the concept of connected components is exploited in Chapter 2 later for designing a tele-traffic off-loading scheme.

1.2.4 Small-World Phenomenon

The small-world phenomenon of social networks was firstly revealed by Milgram's famous experiment [15]:

In order to deliver a letter from a source person to a target person, the source would initially be given basic information about the target, including his address and occupation. Then the source would be instructed to send the letter to someone on a first-name basis in an effort to transmit the letter to the target as efficaciously as possible. Anyone subsequently receiving the letter would be given the same instructions, and the chain of communication would continue until the target was reached.

Over many trials, Milgram found that the average number of hops in successful chains lie between five and six, which is referred to as the 'six degrees of separation' principle. Generally speaking, a small-world network is a type of mathematical graph in which most nodes are not neighbours of one another, but most nodes can be reached from every other by a small number of hops or steps.

There are two mathematical models that may be used for constructing a small-world network from a regular network[1], namely the Watts-Strogatz (WS) [16] model and the Newmann-Watts (NW) model [17]. In the WS model, a small-world network is constructed by 'rewiring' a few links in an existing regular network [16]. By contrast, in the NW model [17], a small-world network is constructed via adding a few new links without changing any existing links of the original regular network. Moreover, the link rewiring probability (or the link adding probability) in the WS (or the NW) model can be expressed by $p \propto 1/(d_{i,j})^{\alpha}$ [18], where $d_{i,j}$ represents the minimum number of hops spanning from node i to node j in the original regular network and α is a basic structural parameter that quantifies how clustered the network is. This model is known as Kleinberg's small-world network model. In a nutshell, small-world networks typically have a high clustering coefficient, but a low average path length quantified in terms of the number of hops.

Let us consider an example of the small-world phenomenon exhibited by a social network whose social users are distributed across a two-dimensional social surface, as portrayed in Figure 4.6. A specific position in this two-dimensional surface represents a specific social profile. The distance between a pair of positions in this social surface represents the social difference between a pair of social profiles. As a result, the closer a pair of social users are to each other in this surface, the more common features they share with each other

[1] In the SNA, a regular network is defined as a network, where each node has the same number of neighbours

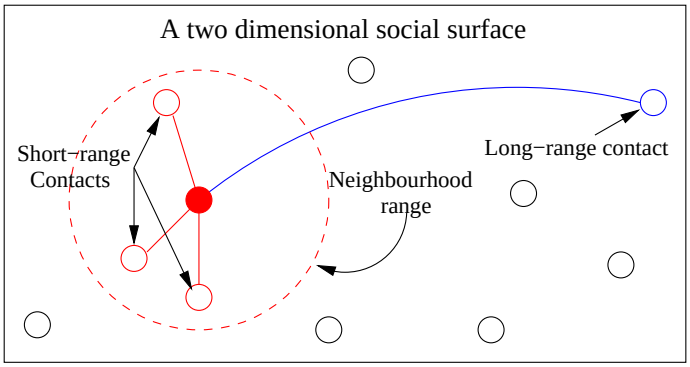

Figure 1.5: An example for the small-world phenomenon exhibited by a social network whose social users are distributed in a two-dimensional social surface. The small circles represent social users and the solid lines represent the social links.

and hence the more likely they become each other's contact. Furthermore, a neighbourhood range is defined for a social user. The social user maintains regular contacts with the others residing in this neighbourhood range, but may only have occasional contacts outside this neighbourhood range. Consequently, the contacts of a social user are categorised into short-range contacts and long-range ones. Short-range contacts represent other social users residing inside the neighbourhood range of the communication initiator. Having a shorter neighbourhood range indicates a more dense clustering of local social users, which may enhance the privacy and security of local social users, but may hamper the prompt information dissemination across the entire social network. A social user normally has quite a few long-range contacts too. Long-range contacts represent the social users outside the neighbourhood range, but who are still reachable in a single hop from the communication initiator. These long-range contacts are capable of significantly reducing the average number of hops spanning from the communication initiator to all the other social users in the entire social network. Hence, having a higher number of long-range contacts may significantly reduce the information transmission delay, as demonstrated in [19] and [20]. However, having more long-range contacts may expose the social user to more untrusted peers and hence it is associated with a higher risk of leaking the private information of the social user to other malicious attackers. As a result, for the small-world phenomenon based social network design, we have to strike a balance between the efficiency of the information transmission and the security of private information. In Chapter 4 of this treatise, a similar small-world network model is relied upon for characterising the geographic social relationships amongst social users.

The major contributions in SNA research are summarised in Table 1.2.

1.3 When Social Networks Meet Telecommunication Networks

At the time of writing, there are remarkable advances in the cross-disciplinary research area of SNA aided telecommunication networking and signal processing, which seamlessly bridge telecommunications networks and social networks [30]. These advances are portrayed in Figure 1.6. The central box of Figure 1.6 summarises the commonly-adopted SNA tools, which have been detailed in Section 1.2. The outer shell of boxes in Figure 1.6 provides a glimpse of some of the applications of the SNA in the research of the telecommunication. We will briefly introduce these applications in the rest of Section 1.3.

1.3.1 Communication Networking Modelling

Firstly, SNA can be exploited for modelling and optimising generic communication networks. The authors of [31] modelled the Telephone Call Network (TCN) by a scale-free social network [32], where nodes represented telephone numbers and two nodes were connected if calls were made between the corresponding

Table 1.2: Major contributions in the SNA research

Year	Author	Contribution
1934	Moreno *et al.* [21]	pioneered the SNA research.
1969	Milgram *et al.* [15]	identified the small-world phenomenon in social networks by a letter delivery experiment.
1977	Zachary [24]	constructed a social network by observing people's behaviours in a karate club.
	Freeman [10]	proposed betweenness centrality for evaluating the importance of nodes.
1982	Freeman [27]	defined the centred graphs and studied the structure of egocentric networks.
1988	Freeman [23]	investigated the capabilities of humans in processing social information relying on data collected by observation.
1998	Watts *et al.* [16]	constructed a small-world network by rewiring a few links in a regular network.
1999	Newman *et al.* [17]	constructed a small-world network by adding some new links without changing any existing links of the original regular network.
2000	Kleinberg [18]	modelled the link rewiring probability as an inversely-proportional value of the social separation in terms of the number of hops in the original regular network.
2001	Newman [26]	proposed an algorithm for computing betweenness, whose complexity is $O(MN)$.
2002	Marsden [6]	proposed ego-betweenness centrality for egocentric networks.
	Girvan *et al.* [12]	proposed a community detection algorithm based on the edge betweenness centrality.
2003	Henri *et al.* [13]	provided the definition of the community of interest.
2005	Newman [25]	proposed a new betweenness centrality by assuming that the information flows in the social network according to the random walk law.
2006	Newman [29]	designed modularity to quantify the grade of division across a network into modules.
2007	Bonacich [7]	proposed the eigenvector centrality concept for evaluating the importance of the nodes.
2008	Chen *et al.* [9]	summarised the closeness centrality in the social network.
	Blondel *et al.* [14]	proposed an algorithm in order to detect the community structure of the social network with the aid of the modularity concept.
2011	Tripathi *et al.* [5]	proposed the κ-path centrality relying on the information flows along the paths that are shorter than κ hops.
2012	Meo *et al.* [11]	proposed the κ-path centrality for characterising the importance of an edge in a social network.
2014	Inaltekin *et al.* [20]	mathematically demonstrated Milgram's 'six degrees of separation' theory in the context of the social search.

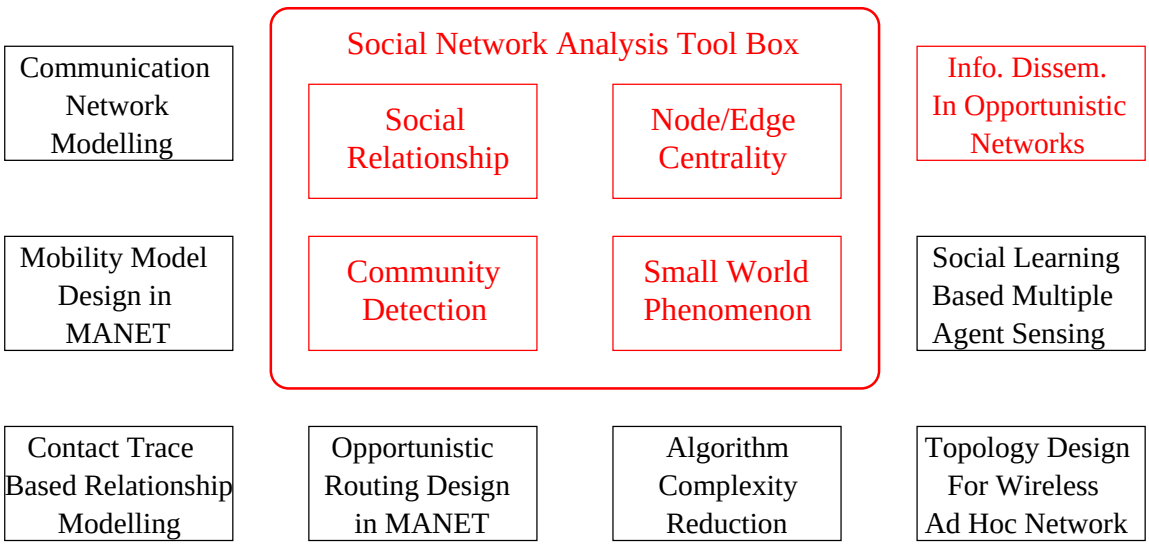

Figure 1.6: The cross-disiplinary research in social network analysis aided telecommunications

telephone numbers. Based on this social network model, a preferential call blocking scheme was proposed in order to mitigate the adverse effect of a sudden surge in the number of telephone calls, which potentially resulted in an overloaded telephone network. The authors of [33] studied the performance of generic communication networks and linked the degree as well as betweenness centralities to the node activation probability. Following in-depth experiments relying on various mathematical network models as well as on the Internet constructed at the autonomous system level [34], their resource allocation scheme based on the node activation probability was shown to outperform both the uniform and the degree-based schemes.

1.3.2 Mobility Model Design

Secondly, SNA can be exploited for designing mobility models, which are capable of reflecting the social relationships amongst the Mobile Users (MUs). Based on the mobile phone data collected by the Reality Mining project [35], the self-reported social relationship between a pair of individuals exhibits a distinctive behavioural signature as quantified in terms of their physical proximity and calling patterns. The landmark research disseminated in [35] confirms that the social relationships amongst the MUs affect their mobility patterns. Relying on this fact, the authors of [36] proposed a Community-based Mobility Model (CMM). In CMM, a MU is more likely to move towards a specific place, where most of his/her friends are staying. The CMM captures the behaviours of MUs moving in groups and between groups. As an evolution of CMM, the Home-cell Community-based Mobility Model (HCMM) is proposed in [37]. Apart from the friendship cohesion inherited from CMM, HCMM also accounts for the associated spatial attraction, where a MU may be inclined to move towards a specific place defined as 'home'.

1.3.3 Contact Trace Based Relationship Modelling

Thirdly, SNA can be exploited for modelling the social relationships between a pair of MUs according to their contact trace. In a Mobile *Ad hoc* NETwork (MANET), when a pair of MUs enter each other's transmission range, their contact can be readily established. During an observation period, if a MU encounters another MU, we establish a social relationship between them. However, the qualities of the social relationships vary amongst the different MU pairs. In [38], the qualities of the social relationships are characterised by the associated encounter frequency, the total or average contact period and the average separation period. However, all of the above-mentioned metrics are biased, when evaluating the qualities of the social relationships. Imagine that we have a pair of MUs making 10 short contacts with each other during the observation period, where the total contact duration is 5 minutes. By contrast, another pair of MUs may only make contact with each other once during the observation period, but the contact duration is 30 minutes. If the contact frequency is our prime criterion, the social relationship of the first pair of MUs is weighed higher than that of the latter pair. By contrast, according to the total contact period based criterion, the latter pair is assigned a higher weight than the first pair. As a further innovation, the Social Pressure Metric (SPM) was proposed in [39] for overcoming the inherent bias of the above-mentioned metrics and for the sake of accurately and fairly characterising the qualities of the social relationships. The SPM will be relied upon for modelling the strength of the social relationship between an arbitrary pair of MUs in Chapter 2, where more details will be revealed concerning this metric.

1.3.4 Opportunistic Routing Design

Fourthly, SNA can be exploited for efficient routing design in MANETs. Due to the intermittent nature of MANETs, data forwarding is realised by opportunistic contacts amongst MUs. When modelling the social relationships between any pair of MUs with the aid of the contact trace, their contact opportunities can be characterised by the associated social graph. Hence various centralities can be invoked for evaluating the

personal importance of the MUs in a MANET. If the current message holder makes a contact with another intermediate relay, it may compare its own centrality to that of the relay. If the message holder's centrality is lower than that of the relay, the message is passed to the relay and deleted from the current message holder. Otherwise, no message exchange occurs between the message holder and the relay. As a result, the message is always kept in MUs associated with a higher centrality, because this sort of MUs may provide a higher chance of forwarding the message to the final destination. In [40], the degree of connectivity is exploited for formulating a data-forwarding strategy, since the intermediate MUs associated with higher degree values are more likely to have the final destination within a single-hop reach. The so-called BUBBLE forwarding algorithm [41] is capable of accounting for the global betweenness centralities of the MUs, since the intermediate MUs associated with higher betweenness values are more effective in terms of their inter-community message delivery, especially in the situation, when the final destination is not within the same community as the source. Furthermore, the SimBet [42] routing policy was proposed for exploiting the local ego-betweenness [6]. The reason as to why the ego-betweenness is relied upon in the SimBet routing policy is two-folds. Firstly, the importance of MUs can be evaluated in terms of their ego-betweenness without the global knowledge of the entire MANET, which guarantees the flexibility of this routing protocol. Secondly, the ego-betweenness aided ranking approach matches the conventional betweenness aided one quite closely, which guarantees the efficiency of this routing protocol.

1.3.5 Algorithmic Complexity Reduction

Furthermore, SNA can be exploited for reducing the algorithmic complexity. A coalitional game approach is proposed in [43] in order to cooperatively deliver packets in hybrid wireless mobile networks. After modelling the MUs' contact history by a social network, the authors found that a pair of MUs separated by multiple hops – rather than a single hop – have a reduced influence on each other in the corresponding social network. As a result, the designers did not have to invest extra complexity into finding the optimal solution based on the entire global network. Therefore, the MUs are divided into communities according to the specific structure of the social network, where members within the same community have a strong influence on each other. Following the community detection phase, finding the gaming-aided solution of the game model is carried out independently for all the communities. Let us imagine that we have N MUs in this coalitional game and that these MUs can be equally divided into M communities. The complexity imposed by finding the optimal solution based on the global network is $O(N^2)$, as demonstrated in [43]. By contrast, the complexity of finding the optimal solution within a specific community is $O(N^2/M^2)$ and hence that of finding the optimal solutions for all of the communities is on the order of $M \cdot O(N^2/M^2) = O(N^2/M)$. As demonstrated by this simple example, compared to finding the global gaming-aided solution, the complexity of finding the solution of the game model is significantly reduced with the aid of the community detection technique.

1.3.6 Topology Design for Wireless *Ad Hoc* Networks

Moreover, the small-world phenomenon can be exploited for constructing wireless *ad hoc* networks. The core of this issue is how to establish a 'long-range contact' amongst the communication nodes so as to significantly reduce the average number of hops but still to retain the benefits of clustering in wireless *ad hoc* networks. In [44], the communication nodes are assumed to be equipped with two transceivers, one dedicated to maintaining short-range communications with their neighbours and the other is for realising long-range communications with distant peers. The probability of creating a direct wireless link between a pair of distant communication nodes is jointly determined by considering both the residual battery energy of nodes as well as by the multi-hop transmission distance and the geographical distance between the nodes, whilst also taking the constraints of the radio transmission range into account. As a result, an energy efficient

wireless network topology may be created by relying on the small-world principle. Directional beamforming (BF) is invoked in [45] for creating a long-range direct link between a pair of 'central' nodes in wireless *ad hoc* networks in order to preserve the validity of the small-world phenomenon. Here, betweenness centrality is relied upon for characterising how central a communication node is in the wireless *ad hoc* network considered. Although establishing a directional beam towards a certain node may result in losing some of its connections in other directions, the average number of hops between all pairs of nodes can be significantly reduced and consequently it enhances the reliability of the wireless *ad hoc* network. In [46], a twin-layer heterogeneous *ad hoc* network is established so as to embrace the small-world phenomenon. The lower layer network is comprised of ordinary nodes, which are further divided into several local communities. The intra-community communication is carried out by the direct communications amongst the community members. Each community has a super relay and only the most 'central' node of this community is connected to this super relay. All of the super relays belonging to different communities can also be connected subject to their transmission range and geographic positions. These super relays constitute an upper layer network. The inter-community communication is fulfilled with the aid of this upper layer network. This twin-layer network architecture embraces two distinctive features of the small-world phenomenon, namely its high-density clustering and low average path length.

1.3.7 Social Learning based Multi-Agents Sensing

Additionally, an agent, which could be either a 'physical sensor[2]' or a 'social sensor[3]', may make a sensing decision by jointly exploiting both its own local observation as well as the decisions made by the surrounding agents. This is regarded as social learning based multi-agent sensing [47]. In this application, by exchanging information with their peers, agents form a community in order to collaboratively achieve a common goal with a better 'utility' than that achieved by them individually. In [47], a social learning protocol was discussed in detail and a strategy of making a global sensing decision was proposed for the sake of minimising both the detection delay and the false alarm penalties. Furthermore, based on this original social learning protocol, the authors of [48] resolved the associated privacy concern as well as the biased sensing-induced misinformation propagation.

1.3.8 Information Dissemination in Opportunistic Networks

Finally, SNA can be exploited for realising information dissemination in opportunistic networks. In this application, MUs form a community of interest, as introduced in Section 1.2.3. Based on the multifunctional mobile devices owned by numerous subscribers, the Information of Common Interest (IoCI) can be spontaneously disseminated across the community without the aid of any CI. For instance, the crowd participating in the inauguration of the new Pope's identity may form a community of interest in order to share close-up video-clips of the Pope on the podium. Similarly, supporters in a football stadium may also form a community of interest so as to share video-clips of a spectacular goal from different angles or the score updates from another stadium. The tools of SNA are capable of assisting us in designing an efficient strategy for information dissemination. In the following chapters of this treatise, we mainly focus our attention on revealing the details of information dissemination in integrated cellular and opportunistic networks.

The major contributions in SNA aided telecommunication research are summarised in Table 1.3.

[2]Examples of physical sensors include sound sensors, chemical sensors and temperature sensors. A physical sensor aims to detect a state change of a natural phenomenon.

[3]Examples of social sensors include Twitter posts, Facebook status updates, and ratings in online reputation systems such as Yelp and Tripadvisor. A social sensor aims to infer social relationships and human activities

Table 1.3: Major contributions in the SNA aided telecommunication research

Year	Authors	SNA Tool	Contribution
2005	Eagle *et al.* [35]	Social Relationship	found a close match between the self-reported social relationships of the MUs and the mobility behaviours of the MUs.
2007	Musolesi *et al.* [36]	Social Relationship	designed a mobility model based on social network theory.
2008	Costa *et al.* [40]	Degree Centrality	designed a routing protocol based on degree centrality.
2009	Tam *et al.* [31]	Social Network	modelled a telephone network by a social network prototype.
	Li *et al.* [38]	Social Relationship	modelled the qualities of the social relationships by the encounter frequency, average/total contact duration/separation period.
	Daly *et al.* [42]	Ego-Betweenness	designed a routing protocol based on ego-betweenness centrality.
2010	Boldrini *et al.* [37]	Social Relationship	designed a mobility model based on both social network theory and spatial attraction.
2011	Hui *et al.* [41]	Betweenness and Community Detec.	designed a routing protocol based on betweenness centrality as well as community detection.
2012	Bulut *et al.* [39]	Social Relationship	proposed SPM so as to accurately model the quality of the contact trace based social relationships.
	Banerjee *et al.* [45]	Small-World Phenomenon	invoked a directional BF technique so as to preserve the small-world phenomenon in wireless *ad hoc* networks.
2013	Wu *et al.* [33]	Degree Centrality Betweenness	proposed a resource allocation scheme based on node activation probability, which is defined by their degree and betweenness.
	Niyato *et al.* [43]	Community Detection	reduced the complexity of finding a game-solution by exploiting the community detection technique.
	Zhang *et al.* [44]	Small-World Phenomenon	created an energy efficient wireless *ad hoc* network topology by exploiting the small-world phenomenon.
	Gu *et al.* [46]	Small-World Phenomenon	proposed a twin-layer heterogeneous network architecture so as to embrace the small-world phenomenon.
	Krishnamurthy *et al.* [47]	Social Network	proposed a social learning protocol for multi-agent aided sensing by exploiting information exchange in social networks.
2014	Krishnamurthy *et al.* [48]	Social Network	resolved privacy and misinformation propagation issues in social learning.

1.4 Motivations and Contributions

1.4.1 Design Dilemmas of Information Dissemination in Centralised Infrastructure Based System

As discussed, an increasing number of MUs share common interests in the same information. For instances, drivers have to receive the traffic information in rural areas; urban residents are interested in the weather forecast before they go to work; Attendees are keen on reading the program before their conference gets started; Football fans in the stadium are curious about the score update from their championship contender's match... However, CI based techniques exhibit the following limitations in disseminating the IoCI:

- *Intermittent connectivity in rural areas.* Suffering from coverage limitations of the CI in rural areas, the wireless links between the MUs and Base Stations (BSs) are prone to intermittent connections due to the high mobilities of the MUs. The same limitations are encountered, when most of the CI is destroyed by a natural disaster [49], such as an earthquake, a tsunami etc. The traditional measures of improving and recovering the wireless connection include building more BSs in the rural area, and increasing the transmit power of the existing BSs so as to cover a larger geographic area as well as deploying more relay stations. However, due to the sparse user distribution in rural areas, the aforementioned measures are believed to be of low-return investment for the network operators. The network operators are keen on finding a robust and flexible approach of improving the connectivity in rural areas, which is worth investing into.

- *Overloaded centralised infrastructure.* As we witness an explosive growth of the tele-traffic demand,

most of the existing BSs are overloaded, which results in significant degradation of the Quality of Service (QoS) for the MUs. The traditional measures of increasing the network capacity include the employment of small-cells [50] in order to off-load the potentially excessive data traffic from the macro-cells. Moreover, the increasing tele-traffic imposes serious Inter-Cell Interference (ICI) [51]. In order to further increase the attainable network capacity and to mitigate the adverse effects of ICI, Wi-Fi hotspots are deployed by the network operators for off-loading tele-traffic from cellular networks [52], because the 802.11 Wi-Fi systems [53] operates in a spectrum band different from that of classic cellular communication. However, these traditional measures are based on the centralised management of the entire CI, which imposes a high cost on the network operators in terms of both deployment and maintenance expenses. How to exploit the common interest of MUs and how to utilise the redundant copies of the IoCI saved in the storage of the MUs' devices poses a substantial challenge for the network operators in order to relieve their congested CI from the heavy tele-traffic load.

- *Inefficient data service in densely populated area.* In the densely populated scenarios, such as a football stadium, an open air festival and a conference venue, there are likely to be hundreds of MUs crowding in a very small area having a radius of 50 meters. Since people temporarily get together for a specific event and rarely visit this place again after the event, it is unwise to invest into costly CI for these scenarios. The traditional measure of efficiently delivering the IoCI is to allow the CI to multicast the IoCI by exploiting the broadcast nature of wireless channels rather than to consume excessive resources for establishing dedicated channels [54]. However, when the number of requesters is huge, the CI will impose both a long delay and a low throughput during the multicasting of the IoCI to all the requesters [55]. How to further improve the efficiency of the information dissemination process across densely populated areas via the cooperation of the MUs without extra investment into the CI is still an open dilemma for the network operators.

1.4.2 Improving the Information Dissemination

Fortunately, the smart multifunctional mobile devices that are equipped both with large storage capacity and multiple communication modes are popular amongst the MUs. These devices are capable of receiving the IoCI from both the CI and other devices, carrying it in their own storage and finally forwarding it to their peers. Hence, they can be 'employed' by CI in order to more efficiently deliver the information to the targets. As a result, it is possible for us to solve the aforementioned design dilemma of CI based information dissemination by exploiting the opportunistic communication amongst the MUs based on either opportunistic contacts [4] [56] within large-scale opportunistic networks or with the aid of opportunistic multicast scheduling [5] [57] within small-scale opportunistic networks. Here, the adjective 'large-scale' indicates a large area covered by an opportunistic network, which has a size of several kilometres and it is far larger than the transmission range of the MUs. Moreover, having a 'large-scale' opportunistic network also indicates imposing a longer latency on delivering the IoCI, which may even be on the order of hours. By contrast, the terminology of 'small-scale' indicates a small area quantified in terms of metres, which is comparable to the transmission range of MUs. Moreover, having a 'small-scale' opportunistic network also indicates a lower latency in delivering the IoCI, which is on the order of a transmission frame duration, say milliseconds.

[4] The information delivery is completed by the contact of the source and the target, when the target comes within the source's transmission range. No pre-decided deterministic routing is required.

[5] All the MUs holding the IoCI are potential relays for the next stage of multicast. No pre-decided deterministic relay selection is required.

1.4.3 Novel Contributions and Thesis Organisation

Motivated by the above-mentioned background, in this thesis, we aim for bridging the social and wireless networking divide and study the information dissemination in integrated cellular and opportunistic networks. The basic idea is that MUs form a community of interest in order to cooperatively disseminate the IoCI across the entire network.

First of all, we will study integrated cellular and large-scale opportunistic networks in the interest of improving the dissemination of the delay-tolerant IoCI in Chapter 2. The novel contributions of this chapter are summarised as follows.

- In Chapter 2, in order to resolve the first two dilemmas introduced in Section 1.4.1, we will identify two application scenarios of the information dissemination in integrated cellular and large-scale opportunistic networks, namely that of improving the connectivity of cellular networks and that of off-loading tele-traffic from the congested CI. Then we will classify the various factors that may influence the information dissemination process into two main categories. The class of factors that are independent of the MUs' mobilities include the *transmission range* of the BS/MUs, the *transmission rate* of both the cellular and opportunistic links as well as the *file size* and *life time* of the IoCI. By contrast, the factors related to the MUs' mobility patterns include both the *inter-contact duration* and the *contact duration*. Their statistical properties will be investigated. By considering the joint impact of the above-mentioned factors, we will provide a Continuous-Time-Pure-Birth-Markov-Chain (CT-PBMC) based analytical framework for characterising a range of performance metrics pertaining to the information dissemination process in an integrated network. Furthermore, according to their contact histories, we will weigh the social relationships amongst the MUs relying on the SPM [39]. After analysing the resultant social contact graph using the tools of SNA, several tele-traffic off-loading schemes will be conceived in order to increase the number of MUs served by the opportunistic network. These original contributions were disseminated in [58].

Then, we will focus our attention on the issues of information dissemination in integrated cellular and small-scale opportunistic networks in Chapters 3 to 5. The novel contributions of Chapters 3 to 5 are summarised as follows:

- In Chapter 3, we will study mobile social networking aided content dissemination in the context of cellular systems relying on altruistic human behaviour. We will consider the dissemination process of a single packet of the content of common interest. The dissemination process of this packet is completed with the aid of the joint effort of both the BS-aided multicast and of the cooperative multicast of the Packet Owners (POs)[6] . Once a number of hitherto unserved Mobile Users (uMUs) have successfully received the packet of common interest, the POs may refresh their decisions as to whether they will forward the packet in the forthcoming stage. The probability of the POs forwarding the packet will be defined as a Factor of Altruism (FA). If no POs are willing to multicast the packet in a specific stage, the BS has to take over the task of multicasting the packet, until some uMUs successfully receive the packet. We will consider the effects of channel attenuation imposed by both the path-loss and the non-dispersive multipath fading as a more realistic physical layer model. Since the success of packet reception at the receiver end depends on the received signal strength, we will no longer have to consider having a fixed transmission range in this scenario. A realistic energy model will be invoked for evaluating the energy dissipation during the packet dissemination process. The energy dissipation of an individual MU is comprised of the transmit energy assigned to forwarding a packet plus the signal processing energy required for recovering a contaminated packet. Then, we will approximate the above-mentioned information dissemination process by an approximate CT-PBMC model subject

[6]Packet owners referred to the MUs who have successfully received the packet of the commonly interested content.

to the assumption that the basic transmission unit in our system is a virtual mini-slot, whose duration is far shorter than a single time slot. Based on this approximate CT-PBMC model, various delay and energy metrics will be derived in closed-form. We will study the energy-dissipation versus delay tradeoff in the scenario, when the MUs move within a circular area by obeying a uniform mobility model and in the realistic scenario, when the MUs move around within a densely populated subway station. These contributions were first disseminated in our works [59] and [60].

- In Chapter 4, we will study distributed multi-stage cooperative social multicast aided content dissemination in random mobile networks. The content dissemination process is initiated by some of the content owners and it is terminated, when all the MUs within the studied area have successfully received copies of the content of common interest without any CI-based transmission. The effects of social constraints on the multicast performance will also be taken into consideration, where a content owner is unwilling to multicast the content to all the uMUs, but he/she would altruistically multicast it to the content owner's hitherto unserved social contacts. The pertinent geographic social relationships will be exploited for characterising the social strength between an arbitrary pair of MUs. We will rely on a similar physical layer model to that in Chapter 3, but additionally we will further design a practical Time-Division-Multiple-Access (TDMA) scheme for the Medium-Access-Control (MAC) layer. With the aid of this TDMA scheme, we will be able to carry out the necessary control signalling exchange required for resource scheduling. Furthermore, we will also be able to avoid adverse interferences and packet collisions, when multiple content owners simultaneously multicast the content of common interest during the content dissemination process. However, we will only consider an idealised resource scheduling approach in this chapter, where each content owner is guaranteed to have a single dedicated time slot for multicasting the content. Assuming that the MUs move within a circular area by obeying the uniform mobility model, we will derive the average social unicast throughput in closed-form. Based on the social unicast throughput, we will further model the content dissemination process by a Discrete-Time-Pure-Birth-Markov-Chain (DT-PBMC) by relaxing the idealised assumptions made in Chapter 3 in order to accurately characterise the content dissemination process. Four theorems will be proposed based on the DT-PBMC in order to assist the derivation of the dissemination delay. Furthermore, we will also demonstrate the advantages of our multi-stage cooperative social multicast protocol over its counterparts, including the non-cooperative direct social multicast protocol, the single-stage cooperative social multicast protocol and the non-cooperative gossip based social unicast protocol. These contributions were the basis of our publications [61] and [62].

- In Chapter 5, we will study a hybrid information dissemination scheme in the context of the integrated cellular and small-scale opportunistic networks considered. This hybrid information dissemination scheme is comprised of two main stages, namely the BS-aided multicast stage and the cooperative multicast-aided spontaneous dissemination stage. At the very beginning of the hybrid information dissemination process, the BS first multicasts the IoCI until at least a single uMUs successfully receives it. Then the IoCI is spontaneously disseminated amongst the MUs themselves with the aid of multi-stage cooperative multicast. Once an uMU has successfully received the IoCI, it may join the Information Multicaster (IM) set in order to seek a time slot for its own multicast. This spontaneous dissemination is continued, until all of the MUs successfully receive the IoCI. Similarly to Chapter 4, we will still adopt a TDMA scheme in the MAC layer, but consider a more practical scenario, where only a limited number of time slots is reserved for the spontaneous dissemination stage. In order to efficiently exploit the limited number of time slots, a round-robin resource scheduling scheme will be implemented by randomly sorting the IMs. Assuming that the MUs move within a circular area by obeying the uniform mobility model, we will derive the l-th moment of the throughput for both the cellular link between the BS and a MU as well as for the opportunistic link between a pair of MUs. Then we will further calculate the average throughput of the opportunistic link, when multiple time slots are assigned to it. By modelling the hybrid information dissemination scheme using a DT-PBMC, we will provide a

generic analytical framework for evaluating various delay metrics, namely the group delay, the individual delay and the dissemination delay as well as the conventional BS-aided single-hop multicast delay[7]. In order to further enhance the information dissemination process, we will propose a range of resource scheduling approaches. Inspired by the centrality concept of SNA, we sort the IMs according to their different importance for the uMUs and then apply the round-robin algorithm to the sorted IM set. These centrality-based resource scheduling approaches include the shortest-longest-distance scheduling, the shortest-shortest-distance scheduling, the shortest-sum-distance scheduling and the highest-sum-rate scheduling regimes. We will demonstrate the advantage of our hybrid information dissemination scheme over the conventional BS-aided-single-hop-multicast and demonstrate that the shortest-shortest-distance scheduling regime outperforms its rivals. These contributions formulate the novelty claims of [58] and [63].

The statistical properties of the random distance between a BS and a MU as well as that between a pair of MUs are crucial for accurately analysing the various delay and energy metrics during the information dissemination process. Given this motivation, we will address it in the next chapter:

- In Chapter 6, we will analyse the stochastic geometrical properties of cellular networks. We will characterise either the Cumulative Distribution Functions (CDFs) or the Probability Density Functions (PDFs) in closed-form for a random distance between a BS and a MU in two scenarios. In the first scenario, a MU moves within the entire cellular area by obeying the uniform mobility model, whose shape is either a circle or a regular polygon. The BS is located at the centre of the cell. In the second scenario, a MU moves within a specific bounded area, whose shape is either a circle or a square, while the BS is located at an arbitrary position, either inside or outside this specific bounded area. We will then evaluate both the CDF and the PDF of the random distance between a pair of MUs, when the MUs move within either a circular area or a square area. The Monte-Carlo simulation results will demonstrate the accuracy of our analytical derivations. The results of Chapter 6 will be relied upon for deriving the closed-form throughput performance of both the cellular links and of the opportunistic links of Chapters 3 to 5. These contributions are included in our upcoming work [64].

Finally, we will conclude in Chapter 7 by summarising our key conclusions and by comparing the difference between the main features of the integrated cellular and large-scale opportunistic network as well as those of its small-scale counterpart. We expound by presenting the evolution of our analytical framework for characterising the information dissemination process in integrated cellular and small-scale opportunistic networks, as well as by providing further insights concerning the information dissemination process in diverse scenarios.

The schematic of Figure 1.7 outlines the organisation of the thesis for the readers' convenience.

[7]Please refer to Chapter 5 for the definition of these delay metrics.

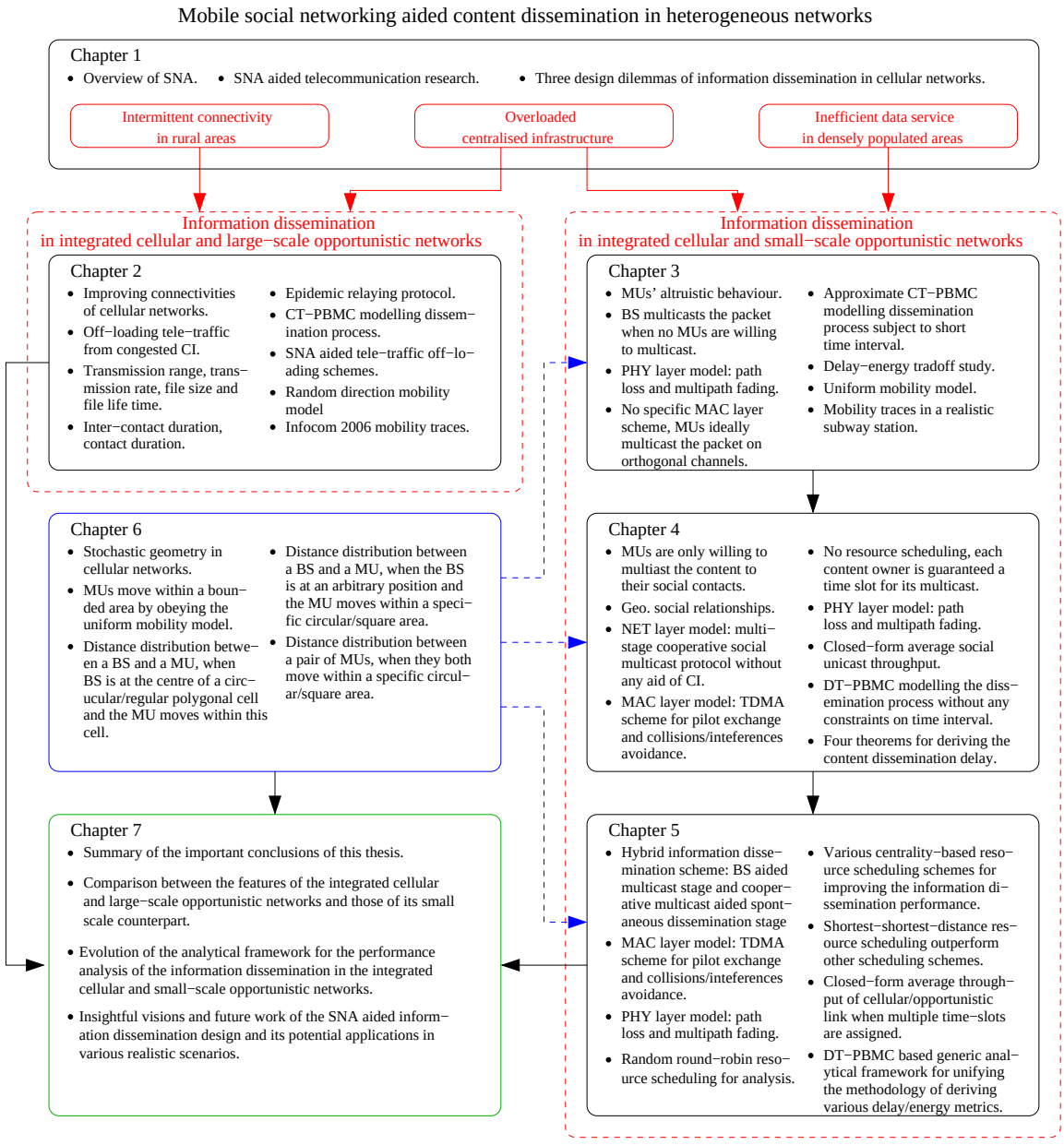

Figure 1.7: Schematic of the structure of the thesis.

Chapter 2

Information Dissemination in Integrated Cellular and Large-scale Opportunistic Networks

2.1 Introduction

2.1.1 Background

Humans are social beings and hence they often share common interest in specific pieces of information. For example, people driving to the city centre are eager to acquire the real-time traffic and road information for the sake of finding time-efficient routes towards their destinations. In every morning, people on their way to work or school are curious about the weather forecast and keen to know about the updates on public transport. Moreover, the social events occurring right across the globe constitute an important part of people's daily life [65]. These social events, such as meetings, conferences, exhibitions, sports events, entertainment etc. are typically organised and planned by using program guides. The organisers and planners have conventionally distributed the program guides to the attendees in form of paper-based documents. However, thanks to the rapid development of smart mobile devices and the mobile Internet, the distribution of these Information of Common Interest (IoCI) can also be completed by appropriate mobile applications in electronic format. The *Google Maps* (http://www.google.co.uk/maps/about/) mobile application is capable for example of flexibility designing an optimal route, relying on the real-time traffic and road information. The *BBC Weather* mobile application (http://www.bbc.co.uk/weather/about/19086178) provides real-time weather information for its users, while the *Moovit* (http://moovitapp.com/) mobile application provides real-time public transport information. Finally, the *GenieConnect* (http://www.geniemobile.com) mobile application offers access to event information and facilitates the distribution of program guides.

However, this information dissemination driven by mobile applications is supported by a Centralised Infrastructure (CI). The mobile devices are connected to either cellular networks or to Wi-Fi access points so as to receive information. If there are not any interactions amongst the Mobile Users (MUs), they are unaware of their peers' existence. Hence, MUs have to request the IoCI with the aid of their CI-based communication. As a result, numerous dedicated channels have to be established for delivering the same copies of the IoCI, which is a waste of precious spectral resources and may impose congestions on the CI. Fortunately, some mobile applications have already provided interaction functions for MUs, which might offer another opportunity for the MUs to receive the IoCI directly from their peers. For example, the *Wase*

(http://www.waze.com/) mobile application provides a platform for sharing real-time traffic and road information collected by the drivers themselves and the *Grupio* (http://www.grupio.com) mobile application facilitates for conference attendees to communicate and to share the relevant event information with each other. During the information dissemination process, the copies of the IoCI are saved in the mobile devices. As the MUs may be readily aware of their peers' quest for the IoCI, exploiting the redundancy of the IoCI and supporting direct communications[1] amongst the MUs may provide us with an appealing information dissemination scheme as an alternative to the low-efficiency CI-based one. Due to the intermittent nature of Mobile *Ad hoc* NETworks (MANETs) [66], which is incurred by the high mobility of the MUs, it is almost impossible to maintain deterministic routing information between any transmitter and receiver pairs. As a result, the opportunistic contacts of the MUs have to be invoked for designing an information dissemination scheme across a sparsely populated large-scale area [67].

In order to disseminate the IoCI to all the MUs in a distributed manner, the store-carry-forward mode of [68] is exploited. Once a MU receives the IoCI, it first saves the IoCI in its own storage, then carries the IoCI as it moves and forwards it to other hitherto unserved Mobile Users (uMUs). However, in large-scale opportunistic networks, MUs are sparsely distributed across a large area, their transmission range is much smaller than the size of the area studied. Any information exchange can only be completed, when the MUs are within each other's transmission range. Moreover, since it rarely occurs that an uMU simultaneously enters the transmission range of multiple Information Owners (IOs) or vice versa, sophisticated Medium-Access-Control (MAC) protocols, such as interference/contention avoidance and resource scheduling [69], become dispensable. As a consequence, the information dissemination is dominated by the mobility pattern of MUs, and the corresponding delay metrics exhibit similar to the *inter-contact duration*[2] between a pair of MUs, which is the main feature of Delay-Tolerant Networks (DTNs) [70].

In order to enhance the efficiency of the information dissemination process, in this chapter, we propose to integrate opportunistic networks into conventional cellular networks. With the aid of opportunistic networks, a pair of dilemmas related to the dissemination of the IoCI within cellular networks, which have been discussed in Chapter 1, can be resolved.

2.1.2 Two Application Scenarios

As portrayed in Figure 2.1, integrated cellular and large-scale opportunistic networks can be applied in the following two scenarios.

2.1.2.1 Improving Connectivity of Cellular Networks

If the Base Stations (BSs) are sparsely distributed in a large area [71], the MUs may lose their connections to the BSs since they are likely to be out of the BSs' coverage. In this case, opportunistic communication between a pair of MUs can be invoked for the sake of disseminating important messages. As shown in Figure 2.1(a), when MU1 and MU4 move into the coverage of the BS, they successfully receive the IoCI from the BS. Thereafter, they carry the IoCI and roam within the area studied. Once they meet other uMUs, the IoCI is delivered via the opportunistic links between them. As a result, opportunistic communication increases the chance of the IoCI's successful reception for those MUs that are not within the coverage of the BS. This integrated network can be exploited for supporting emergency communication as well when most of the BSs are destroyed by a natural disaster [49]. Furthermore, if we consider the BS to be a Roadside Unit (RU), the scenario of Figure 2.1(a) can be naturally extended to a hybrid vehicular network [72], where RU-to-vehicle and vehicle-to-vehicle communications cooperate in order to disseminate the important traffic information,

[1] Direct communication amongst the MUs is possible since current smart mobile devices are equipped with various communication functions, such as the distributed Wi-Fi networking, the Bluetooth and infrared aided peer-to-peer transmission.

[2] The statistical properties of the inter-contact duration will be introduced in Section 2.2.4

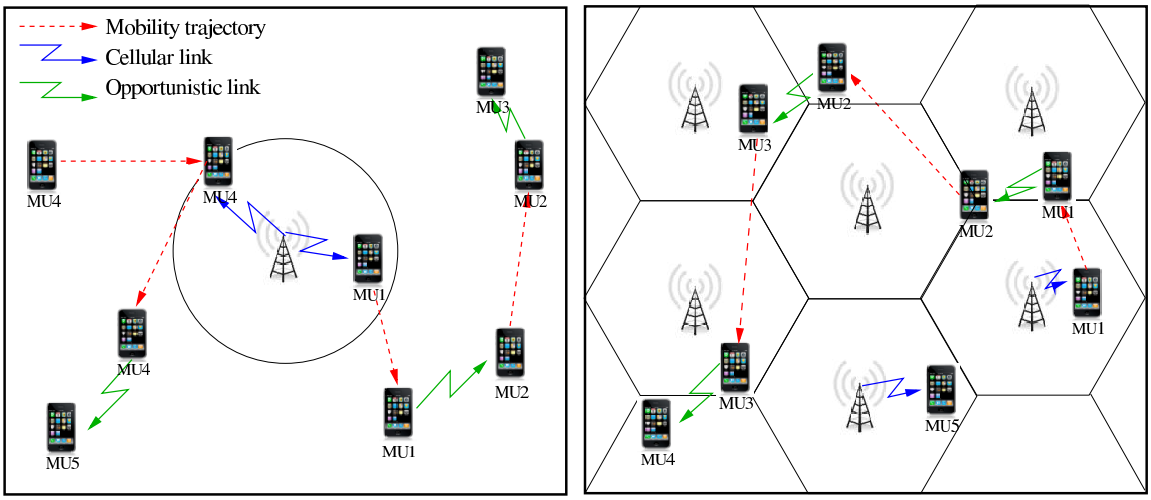

(a) Improving the connectivity of cellular networks

(b) Off–loading tele–traffic from cellular networks

Figure 2.1: Two application scenarios for the integrated cellular and large-scale opportunistic networks

for example. In Section 2.4, we will introduce a mathematical tool for analysing the delay metrics of this scenario.

2.1.2.2 Off-Loading Tele-Traffic from Cellular Networks

Due to the intrinsic unicast nature of cellular communications, multiple dedicated cellular links have to be established for the sake of disseminating the IoCI to all the requesters, which absorbs a large fraction of the BSs' resources. Apart from improving the connectivity of cellular networks, large-scale opportunistic networks are also capable of off-loading some tele-traffic from cellular networks so as to save BSs' precious resources [73]. As shown in Figure 2.1(b), the BSs firstly inject some copies of the IoCI into the opportunistic networks. Thereafter, the IoCI is disseminated via opportunistic contacts of MUs as well as via direct injections from the BSs. Since all the MUs are covered by the cellular networks, the information delivery of a cellular link is prompt and the delay is substantially shorter than the inter-contact duration of MUs. Our goal of this application is to disseminate the IoCI to as many MUs as possible via the large-scale opportunistic network before the IoCI expires. In Section 2.5, we will highlight the specific characteristics of this scenario.

2.1.3 Novel Contribution

Against this background, our novel contributions in this chapter are summarised as follows:

- We provide a detailed introduction to the information dissemination process of integrated cellular and large-scale opportunistic networks, and discuss its typical applications both in the scenario of improving the connectivity of the classic cellular networks and in the scenario of off-loading tele-traffic from the cellular networks to the opportunistic networks.
- We characterise the impact of both the mobility-related factors and that of a range of other factors on the information dissemination process. Specifically, we demonstrate that the contact duration between a pair of MUs obeying a random direction based mobility model is exponentially distributed. By contrast, the contact duration between a BS (static node) and a MU can be closely approximated by the Gamma distribution.

- We also survey three protocols conceived for aiding the information dissemination in integrated cellular and opportunistic networks, namely the conventional direct transmission protocol, the two-hop relaying protocol and the epidemic relaying protocol. The epidemic relaying protocol is invoked in our information dissemination model.
- By jointly considering both the contact duration as well as the well-known exponentially distributed inter-contact duration, we model the information dissemination process by a Continuous-Time-Pure-Birth-Markov-Chain (CT-PBMC), when a homogeneous mobility model is assumed for all the MUs. Furthermore, we additionally demonstrate that heterogeneous mobility can also be handled with the aid of an equivalent mathematical transformation.
- Furthermore, the tools of Social Network Analysis (SNA) are invoked for carefully selecting the initial IoCI receiver set in order to off-load as much tele-traffic as possible from cellular networks to opportunistic networks.

2.1.4 Chapter Organisation

The rest of this chapter is organised as follows:

- In Section 2.2, we characterise the impact of various factors on the information dissemination process.
- In Section 2.3, we provide a survey of the protocols that can be invoked for aiding the information dissemination in integrated cellular and large-scale opportunistic networks.
- In Section 2.4, we model the information dissemination in an integrated cellular and large-scale opportunistic network by a CT-PBMC, based on which various performance metrics are analysed.
- In Section 2.5, SNA aided tele-traffic off-loading schemes are proposed for resolving the congestion of cellular networks.
- In Section 2.6, our numerical results are provided for characterising the statistical properties of the inter-contact duration and contact duration between a pair of MUs, while demonstrating the ability of our integrated network to improve the connectivity of the conventional cellular network and its ability to off-load the tele-traffic from the congested cellular network.
- In Section 2.7, we conclude this chapter.

2.2 Factors Affecting the Information Dissemination

Let us first introduce the factors affecting the information dissemination performance of the integrated cellular and large-scale opportunistic networks, which are unrelated to the mobility of MUs.

2.2.1 Transmission Range

In practice, the transmission range r is determined by a specific short-range communication technique employed for information transmission. For instance, the transmission range is up to 60 meters for Bluetooth [74], whilst it could be upto 250 meters for Wi-Fi according to the family of 802.11 protocols [53]. Theoretically, the transmission range is jointly determined by transmit power, wireless channel's attenuation, as well as by the interference. For instance, *effective transmission range* [75] is defined as the maximum value of the range satisfying the condition that the received power remains higher than a pre-defined threshold with a high probability.

2.2.2 File Size and Transmission Rate

Since the wireless link can only be established when the source and the target are within each other's transmission range, as to whether the file can be successfully delivered or not depends on the file size L, on the transmission rate B and on their contact duration[3]. The file size varies from Kilobytes (for text messages) to Megabytes (for multimedia contents), while the transmission rate depends on bandwidth and transmit power, on the channel attenuation, on the interference, as well as on the specific choice of the modulation and coding schemes. Since adaptive power control [76] is widely adopted in practical communication, a minimum transmission rate B can usually be achieved at the receiver end. If this is the case, the transmission duration becomes L/B time units.

2.2.3 Life Time of the Information of Common Interest

IoCI considered in this chapter may belong to the category of time-sensitive information, such as weather forecast, traffic information etc. This type of information would only attract the interest of MUs for a short period, which is defined by the life time T_L [77]. Once the IoCI is firstly generated, it would be disseminated in the integrated cellular and large-scale opportunistic networks for a period of T_L. After this period, the uMUs might lose their interest in it and the IoCI might be discarded since it is no longer up-to-date. The value of T_L depends on the mobile application's specific requirements.

Apart from the factors which are unrelated to the mobility of the MUs, the mobility-related factors also crucially affect the information dissemination performance in the integrated networks.

2.2.4 Inter-Contact Duration

Let MU_i and MU_j move according to a specific mobility model. These two MUs are within each other's transmission range at time 0, and then they move out of range at time instant t_1. If these two MUs next come within the transmission range of each other again at time t_2, then the time duration $T_{IC} = (t_2 - t_1)$ is defined as the *inter-contact duration* of MU_i and MU_j.

Let us consider the following random direction mobility model [78] as an example.

Definition 2.1 (Random Direction (RD) mobility model)**.** *In this model, a MU uniformly assumes a specific speed from the region* $[V_{\min}, V_{\max}]$ *and uniformly chooses a particular direction from the region* $[0, 2\pi)$*. Then this MU moves along the chosen direction with the chosen speed for an exponentially distributed travelling time. After this movement, the MU again randomly chooses a speed, a direction and a travelling time for its next movement.*

According to [79], the expected inter-contact duration between a pair of MUs obeying the RD mobility model is given by

$$\overline{T}_{IC} = \frac{S}{2rV^*}, \tag{2.1}$$

where S is the area of the square-shaped mobility region, r is the transmission range and V^* is the average relative speed[4] between a pair of MUs, whose value is given by [80]

$$V^* = 1.27\overline{V} = \frac{1.27(V_{\min} + V_{\max})}{2}. \tag{2.2}$$

[3]This will be introduced in Section 2.2.5

[4]The relative speed between a moving node and a static node is $V^* = \overline{V}$, which can be substituted in Eq.(2.1) for the sake of calculating the average inter-contact duration between the BS and a MU.

Furthermore, the *contact rate* is defined as $\lambda_s = 1/\overline{T}_{IC}$, and the number of contacts during a specific period can be modelled by a Poisson process with a rate of λ_s [79]. In our following discourse, we also denote the rate of contact occurrences between the BS and a MU as λ_b.

As demonstrated in [79], the inter-contact duration of the RD model and that of the Random Way-Point (RWP) model [78] strictly obey the exponential distribution, while the inter-contact duration of the Random Walk (RW) model [78] also has an exponentially distributed tail. The inter-contact duration of the InfoCom 2006 mobility trace may be approximated by a certain inverse power-law distribution [81], but this approximation is believed to be over-pessimistic. Furthermore, the authors of [82] found that most of the realistic mobility traces, such as those of the InfoCom [81] and UCSD [83] datasets, can be closely approximated by a mixed power-law and exponential distribution. After a characteristic time, which may be on the order of half a day, the Complementary Cumulative Distribution Function (CCDF) of the inter-contact duration decays exponentially. As supported by the above-mentioned researches, it is reasonable for researchers to assume the exponentially distributed inter-contact duration in the delay analysis of large-scale opportunistic networks [84] [85].

Our numerical results are provided in Section 2.6.1 for the sake of demonstrating that the inter-contact duration between a pair of MUs is an exponentially distributed random variable, provided that this pair of MUs moves within a square area by obeying a RD mobility model.

2.2.5 Contact Duration

Let MU_i and MU_j move according to a specific mobility model. We assume that these two MUs come within the transmission range of each other at time instant 0. The contact duration T_C is defined as a period during which they initially remain in contact with each other before they move out of each other's transmission range.

Let us again consider the RD mobility model as an example. According to [86], the average contact duration between a pair of MUs is given by

$$\overline{T}_C = \frac{\pi r}{2V^*}, \tag{2.3}$$

where r is the transmission range and V^* is the average relative speed given by Eq.(2.2).

However, the CCDF of the contact duration has not been characterised in the open literature for the popular synthetic mobility models, such as the RD, RWP and RW mobility models. The authors of [87] found that the contact duration obeys the Pareto distribution for the encounter trace collected by Bluetooth devices. By contrast, the authors of [88] found that for vehicular mobility traces, the contact duration is closely approximated by a mixed power-law and exponential distribution. In contrast to the inter-contact duration reported in [82], the CCDF of the contact duration exponentially decays before reaching a specific characteristic time, which is on the order of 100 seconds. As a result, researchers may reasonably assume an exponential distribution for characterising the statistical properties of the contact duration.

Our numerical results are provided in Section 2.6.1 for the sake of demonstrating that the contact duration between a pair of MUs is an exponentially distributed random variable and that between a MU and a centrally-located BS follows a Gamma distribution, when the MUs move within a square area by obeying a RD mobility model.

The authors of [89] proposed a contact-duration-aware data replication scheme by assuming Pareto-distributed contact duration. However, the impact of contact duration on the information dissemination of large-scale opportunistic networks has been to a degree neglected in the existing literature. Researchers often assume that the bandwidth provided for the transmission between a pair of MUs is extremely high and the file size is relatively small [40]- [42]. Even if the file size is large, the file is assumed to be divided into small data chunks. In this case, the existing studies do not focus on transmitting the entire file but on transmitting

a single data chunk [90] [91]. According to these assumptions, if a pair of MUs is in contact, the file (or the data chunk) may be delivered promptly. Hence, it has been deemed unnecessary to account for the contact duration when characterising the information dissemination performance. However, these assumptions are somewhat impractical. To this end, we assume in this chapter that the success of file delivery depends on the following two events:

- The target MU enters the transmission range of the source MU with a rate of λ_s;
- The contact duration between the source and the target must be longer than the required transmission time that is defined as L/B, where L is the file size and B is the transmission rate.

Therefore, the probability of successfully delivering a file during a single contact is given by $\overline{F}_{T_C}(L/B) = \Pr(T_C > L/B)$, which is the CCDF of the contact duration T_C. For this reason, we propose a thinned Poisson process for the *effective contact* model between a pair of MUs with a rate of $\widetilde{\lambda}_s = \overline{F}_{T_C}(L/B)\lambda_s$. Since both the original contact processes and the contact durations between any pairs of MUs are independent of each other [79], the effective contact processes are independent as well.

2.3 Protocols for Information Dissemination

In the open literature, there are three commonly-adopted protocols for information dissemination, which are portrayed in Figures 2.2 and 2.3.

2.3.1 Direct Transmission

In this protocol, information is disseminated only by the BS without any assistance from the opportunistic communication between the MUs [92]. All the MUs receive the IoCI only when they move into the transmission range of the BS.

As shown in Figure 2.2(a), during the first observation period, only MU1 enters the transmission range of the BS and hence receives the IoCI. During the second observation period, although MU2 is in close proximity of MU1, it cannot fetch the IoCI from MU1, since MU1 is not capable of delivering any information to its peers according to the direct transmission protocol. Meanwhile, MU3 enters the BS's range and receives the IoCI from the BS. Since no uMUs are in the BS's range during the third observation period, none of the uMUs can successfully receive their desired IoCI. Following these three observation periods, only MU1 and MU3 succeed in receiving the IoCI.

2.3.2 Two-Hop Relaying

In this protocol, only the specific MUs that flawlessly receive the IoCI from the BS are relied upon for further disseminating the IoCI to the other uMUs [90].

As shown in Figure 2.2(b), during the first observation period, MU1 enters the coverage of the BS, hence it successfully receives the IoCI from the BS and then it is employed by the BS for further disseminating the IoCI to the other uMUs. During the second observation period, MU1 relays the IoCI to the MU2, since MU2 comes into its transmission range. However, MU2 is not capable of further delivering the IoCI, because it is not directly employed by the BS. Meanwhile, MU3 comes into the BS's range and is also employed by the BS for disseminating the IoCI. As a result, during the third observation period, MU3 delivers the IoCI to MU4, but MU5 cannot fetch the desired IoCI from MU2. Compared to the direct transmission protocol, following these three observation periods, we additionally have MU2 in the successful receiver set.

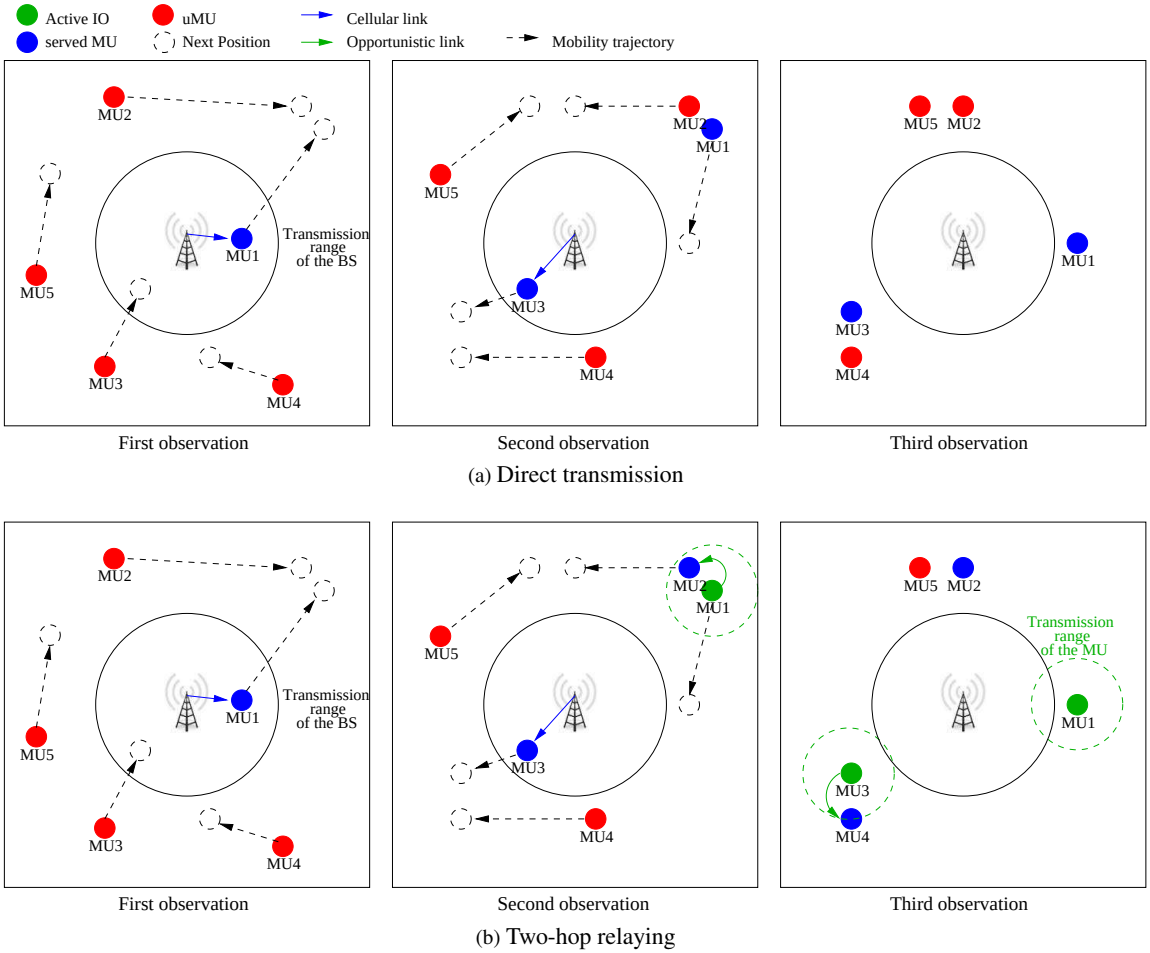

Figure 2.2: Examples of (a) the direct transmission protocol and (b) the two-hop relaying protocol during three consecutive observations. Same mobility traces of five MUs are invoked in both of these examples.

2.3.3 Epidemic Relaying

In this protocol, the MUs carrying the IoCI may deliver it to any uMUs that are within their transmission range [93]. The epidemic relaying protocol is often criticised for its low efficiency in terms of supporting end-to-end communication, because multiple copies of the information are generated, which consumes a large fraction of the resources. However, this low-efficiency problem does not exist in the scenario of information dissemination, because all the MUs in the community are innately interested in the information distributed.

As shown in Figure 2.3, after successfully receiving the IoCI from the BS during the first observation period, MU1 then relays the IoCI to MU2 in the subsequent period, when MU2 comes into its transmission range. Afterwards, when MU5 is in close proximity of MU2 during the third period, MU2 successfully delivers the IoCI to MU5 according to the epidemic relaying protocol. Similarly, since MU3 fetches the IoCI from the BS during the second observation period, it then successfully forwards the IoCI to MU4 during the third period. As a result, we observe from Figure 2.3 that all of the five MUs successfully receive their desired IoCI at the end of these three periods, which obviously outperforms both the direct transmission and the two-hop relaying protocols of Figure 2.2.

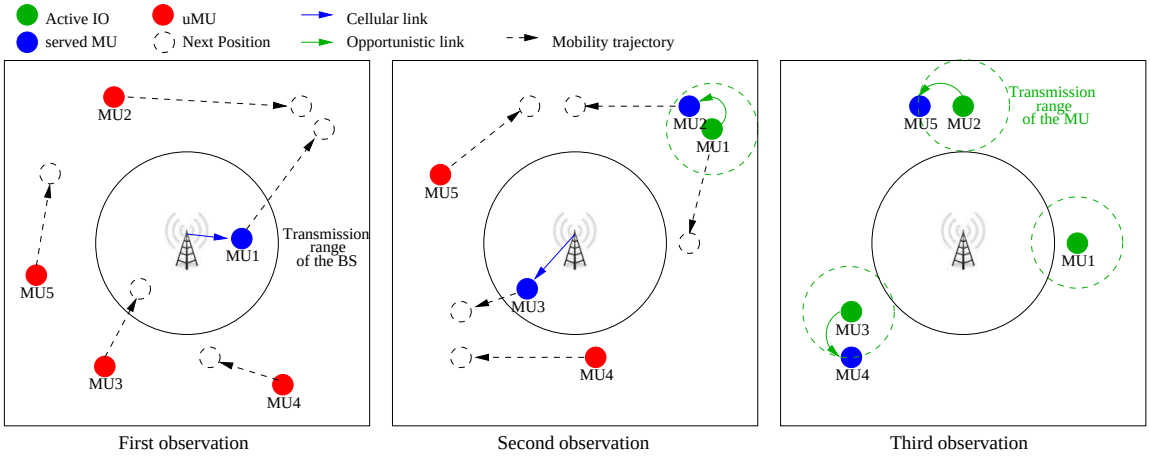

Figure 2.3: Examples of the epidemic relaying protocol during three consecutive observations. Same mobility traces of five MUs are invoked as in Figure 2.2.

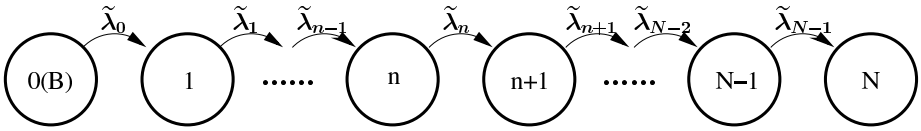

Figure 2.4: The information dissemination process is modelled by a continuous-time-pure-birth Markov chain.

2.4 Continuous-Time-Pure-Birth-Markov-Chain Aided Performance Analysis

Let us now introduce the mathematical tool for analysing the delay metrics of integrated cellular and large-scale opportunistic networks. We first consider its application in the scenario of improving the connectivity of the cellular networks, as shown in Figure 2.1(a). A slight adjustment of this methodology makes it fit also for the scenario of off-loading the tele-traffic from the cellular networks, as shown in Figure 2.1(b).

We assume that all the N MUs roam in a bounded area, and the IoCI is disseminated according to the *epidemic relaying* protocol. The contact between any pair of MUs obeys an independent homogeneous Poisson process with a rate of λ_s. Correspondingly, the contact duration between any pair of MUs also obeys an independent homogeneous distribution, whose CCDF is $\overline{F}_{T_C,s}(t_C)$. If the size of the IoCI is L, and the transmission rate provided for the opportunistic links is B_s, the successful IoCI delivery during a single contact is achieved with a probability of $\overline{F}_{T_C,s}(L/B_s)$. As a result, the effective contact between any pair of MUs can be modelled by a thinned Poisson process [94] with a rate of $\widetilde{\lambda}_s = \lambda_s \overline{F}_{T_C,s}(L/B_s)$.

We assume having only a single BS in the area studied, as shown in Figure 2.1(a), and the contact between any MUs and the BS also obeys an independent homogeneous Poisson process with a rate of λ_b. Correspondingly, the contact duration between any MU and the BS also obeys an independent homogeneous distribution, whose CCDF is $\overline{F}_{T_C,b}(t_C)$. Similarly, the effective contact between any MU and the BS can be modelled by another homogeneous thinned Poisson process having a rate of $\widetilde{\lambda}_b = \lambda_b \overline{F}_{T_C,b}(L/B_b)$.

As a result, we may model the information dissemination process by a CT-PBMC, as shown in Figure 2.4. State n of the CT-PBMC represents that currently there are n MUs having the IoCI in their own storage, which are referred to as IOs. Observe from Figure 2.4 that there are two special states. The first one is the *initial state* 0, which represents that only the BS owns the IoCI at the beginning of the information dissemination process. The other one is the final state N, namely the *absorbing state*, which represents that all the MUs successfully receive the IoCI. The rest of the states are defined as the *transient states*.

Furthermore, $\{\widetilde{\lambda}_n, n = 0, 1, \cdots, (N-1)\}$ represent the rates of the state transitions from state n to state $(n+1)$. Specifically, for state n, we have n IOs and $(N-n)$ uMUs. Consequently, the transition rate is given by

$$\widetilde{\lambda}_n = (N-n)\widetilde{\lambda}_b + n(N-n)\widetilde{\lambda}_s, \tag{2.4}$$

where $\widetilde{\lambda}_b$ and $\widetilde{\lambda}_s$ have already been defined in the above paragraphs. Note that if we let $\widetilde{\lambda}_s = 0$ in Eq.(2.4), the resultant transition rates only include the BS-related terms, which can be relied on for analysing the attainable performance of the direct transmission protocol, as introduced in Section 2.3.1. The $(N \times N)$-element transition rate matrix [95] is given by

$$\Lambda = \begin{pmatrix} -\widetilde{\lambda}_0 & \widetilde{\lambda}_0 & 0 & \cdots & 0 \\ 0 & -\widetilde{\lambda}_1 & \widetilde{\lambda}_1 & \cdots & 0 \\ \vdots & \ddots & \ddots & \ddots & \vdots \\ 0 & 0 & \ddots & -\widetilde{\lambda}_{N-2} & \widetilde{\lambda}_{N-2} \\ 0 & 0 & 0 & \cdots & -\widetilde{\lambda}_{N-1} \end{pmatrix}. \tag{2.5}$$

Given this transition rate matrix, we are able to derive some delay metrics with the aid of the CT-PBMC.

2.4.1 The Dissemination Delay

The dissemination delay T_D is defined as the time that is spent for disseminating the IoCI to all the N MUs in the area studied. According to the properties of the CT-PBMC, a specific transition delay T_n from state n to state $(n+1)$ obeys an exponential distribution with a rate of $\widetilde{\lambda}_n$. Therefore, the dissemination delay is obtained as $T_D = \sum_{n=0}^{N-1} T_n$, which obeys a hypo-exponential distribution [94]. Since the state transition delays $\{T_n, n = 0, 1, \cdots, (N-1)\}$ are independent of each other, the expectation of the dissemination delay is derived as

$$\mathcal{E}[T_D] = \sum_{n=0}^{N-1} \frac{1}{\widetilde{\lambda}_n} = \sum_{n=0}^{N-1} \frac{1}{(N-n)\widetilde{\lambda}_b + n(N-n)\lambda_s}. \tag{2.6}$$

The dissemination delay T_D is expressed as a phase-type distribution [95], whose CCDF is given by

$$\Pr(T_D > t_D) = \boldsymbol{\alpha}^T \times \exp(t_D \Lambda) \times \mathbf{1}, \tag{2.7}$$

where $\boldsymbol{\alpha}$ is a $(N \times 1)$-elements column vector, whose first element is one and all the other elements are zeros, $\mathbf{1}$ is a $(N \times 1)$-elements column vector, whose elements are all ones. Thanks to the existence of the term $(N-n)\widetilde{\lambda}_b$ in Eq.(2.4), the transition rate obeys $\widetilde{\lambda}_n \neq \widetilde{\lambda}_m$ for all $n \neq m$. Hence, we may directly formulate the CCDF of the hypo-exponential distributed dissemination delay T_D [94] as

$$\Pr(T_D > t_D) = \sum_{n=0}^{N-1} \left(\prod_{m=0, m\neq n}^{N-1} \frac{\widetilde{\lambda}_m}{\widetilde{\lambda}_m - \widetilde{\lambda}_n} \right) \exp(-\widetilde{\lambda}_n t_D), \tag{2.8}$$

which is based on an equivalent transformation of Eq.(2.7).

2.4.2 The Individual Delay

The individual delay T_I of a specific MU is defined as the time of this MU successfully receiving the IoCI. This is also the end-to-end delay between the BS and a specific MU when the epidemic relaying protocol is invoked for the information dissemination. The target MU may receive the IoCI during any of the states spanning from 1 to N in the sequence of the state transitions of the CT-PBMC. When considering the transition from state n to $(n+1)$ $(0 \leq n \leq N-1)$, the target MU may successfully receive the IoCI

with a probability of $1/(N-n)$, and it may fail to receive it with a probability of $(N-n-1)/(N-n)$. Specifically, the probability $P_{n+1}^{(I)}$of the target MU receiving the IoCI at state $(n+1)$, which naturally implies that it has not received the IoCI at any of the previous states, may be expressed as

$$\Pr_{n+1}^{(I)} = \frac{1}{N-n}\prod_{m=0}^{n-1}\frac{N-m-1}{N-m} = \frac{1}{N}, 0 \leq n \leq (N-1). \tag{2.9}$$

Given that the target MU receives the IoCI at state $(n+1)$, the CT-PBMC can be considered as being absorbed at this state. Similarly to Eq.(2.7), the conditional expectation and the CCDF of T_I is expressed as

$$\mathcal{E}[T_I|n+1] = \sum_{m=0}^{n}\frac{1}{\widetilde{\lambda}_m},\ 0 \leq n \leq (N-1), \tag{2.10}$$

$$\Pr(T_I > t_I|n+1) = \boldsymbol{\alpha}^T \times \exp(t_I\Lambda) \times \mathbf{1}_{n+1}, \tag{2.11}$$

where $\mathbf{1}_{n+1}$ is a $(N \times 1)$-element column vector, whose first $(n+1)$ elements are ones and all the other elements are zeros. After further manipulations relying on the Bayesian principle [94], the CCDF of T_I may be expressed as

$$\begin{aligned}\Pr(T_I > t_I) &= \sum_{n=0}^{N-1}\Pr(T_I > t_I|n+1)\Pr_{n+1}^{(I)} \\ &= \sum_{n=0}^{N-1}\frac{\boldsymbol{\alpha}^T \times \exp(t_I\Lambda) \times \mathbf{1}_{n+1}}{N} \\ &= \frac{\boldsymbol{\alpha}^T \times \exp(t_I\Lambda)}{N} \times \sum_{n=0}^{N-1}\mathbf{1}_{n+1} \\ &= \frac{\boldsymbol{\alpha}^T \times \exp(t_I\Lambda) \times \boldsymbol{\eta}}{N},\end{aligned} \tag{2.12}$$

where $\boldsymbol{\eta} = (N, N-1, \cdots, 1)^T$. Similarly, the expectation of T_I may be expressed as

$$\mathcal{E}[T_I] = \sum_{n=0}^{N-1}\mathcal{E}[T_I|n+1]\Pr_{n+1}^{(I)} = \sum_{n=0}^{N-1}\frac{1}{N}\sum_{m=0}^{n}\frac{1}{\widetilde{\lambda}_m} = \sum_{n=0}^{N-1}\frac{N-n}{N}\frac{1}{\widetilde{\lambda}_n}, \tag{2.13}$$

where $\widetilde{\lambda}_n$ in Eq.(2.13) is given by Eq.(2.4).

2.4.3 The Number of the Information Owners at an Arbitrary Time Instant

As introduced in Section 2.2.4, if the IoCI has a useful life time T_L, it is important for us to determine how many MUs can successfully receive the IoCI before it expires. The following theorem provides the closed-form expression for calculating the probability of the CT-PBMC remaining in an arbitrary state at an arbitrary time instant.

Theorem 2.1. *Let us denote the probability of the CT-PBMC remaining in state n at time instant t as $p_n(t)$ for $0 \leq n \leq N$. The closed-form expression of $p_n(t)$ is formulated as:*

$$p_n(t) = \begin{cases} \exp(-\widetilde{\lambda}_0 t), & n = 0, \\ \left(\prod_{m=0}^{n-1}\widetilde{\lambda}_m\right)\sum_{i=0}^{n}\frac{\exp(-\widetilde{\lambda}_i t)}{\prod_{j=0,j\neq i}^{n}(\widetilde{\lambda}_j - \widetilde{\lambda}_i)}, & 0 < n < N, \\ 1 - \sum_{n=0}^{N-1} p_n(t), & n = N. \end{cases} \tag{2.14}$$

Proof. Please refer to Appendix 2.A for the proof. □

Let $t = T_L$ in Theorem 2.1, we may derive the average number of MUs successfully receiving the IoCI before the IoCI expires, which is expressed as $\overline{n} = \sum_{n=0}^{N} n p_n(T_L)$.

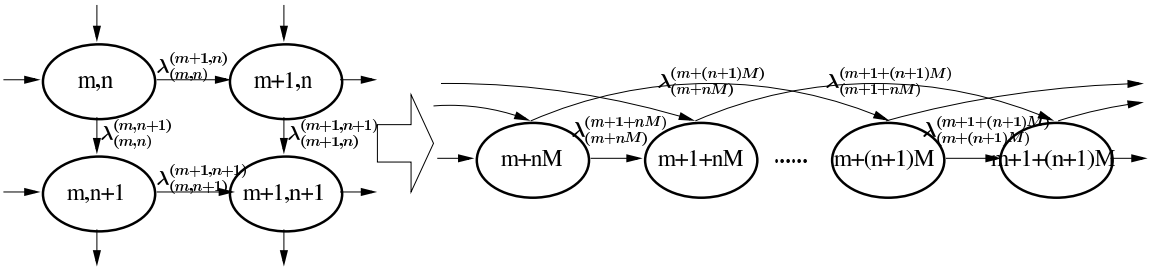

Figure 2.5: Two-dimensional CT-PBMC for capturing the heterogeneous MUs' mobility patterns and the equivalent transformation into its one-dimensional version. There are two categories of MUs, namely the super MUs and the ordinary MUs.

2.4.4 Heterogeneous Mobile Users

Assuming a homogeneous mobility pattern in the above analysis is somewhat idealised for adequately reflecting the real characteristics of the MUs. In the existing literature [96] [97], often the multi-dimensional Markov chain is invoked for capturing the heterogeneous MUs' mobility patterns. In this section, we will show that after some equivalent mathematical transformations, the analytical framework introduced in Section 2.4 can be further exploited for deriving various performance metrics, when the MUs' heterogeneous mobility patterns are taken into account.

The authors of [96] modelled the epidemic relaying protocol based end-to-end communication by a two-dimensional CT-PBMC, as shown in Figure 2.5. Let us first consider how to map their model onto the analytical framework of this section. In their model, two types of MUs are assumed, namely number M of super MUs and number N of ordinary MUs. Jointly considering the impact of both the inter-contact duration and contact duration, the effective contact rate between a pair of super MUs is $\widetilde{\lambda}_{\mathcal{SS}}$, and that between a pair of ordinary MUs is $\widetilde{\lambda}_{\mathcal{NN}}$, while that between a super MU and a ordinary one is $\widetilde{\lambda}_{\mathcal{SN}}$. Additionally, the effective contact rate between a super MU and the BS is $\widetilde{\lambda}_{\mathcal{BS}}$, while that between an ordinary MU and the BS is $\widetilde{\lambda}_{\mathcal{BN}}$.

As portrayed in Figure 2.5, state (m,n) represents that we currently have m super MUs and n ordinary MUs that have successfully received the IoCI. When the epidemic relaying protocol is implemented, the transition rates from this state to its neighbouring states may be expressed as

$$\begin{cases} \lambda_{(m,n)}^{(m+1,n)} = (M-m)(\widetilde{\lambda}_{\mathcal{BS}} + m\widetilde{\lambda}_{\mathcal{SS}} + n\widetilde{\lambda}_{\mathcal{NS}}), \\ \lambda_{(m,n)}^{(m,n+1)} = (N-n)(\widetilde{\lambda}_{\mathcal{BN}} + m\widetilde{\lambda}_{\mathcal{NS}} + n\widetilde{\lambda}_{\mathcal{NN}}). \end{cases} \tag{2.15}$$

However, before analysing any of the performance metrics of this two-dimensional CT-PBMC, we have to equivalently transform it into a one-dimensional version, as shown in Figure 2.5. State (m,n) for $0 \leq m \leq M$ and $0 \leq n \leq N$ in the two-dimensional CT-PBMC can be transformed into state $(m+nM)$ in its transformed one-dimensional version. Furthermore, the corresponding transition rates $\lambda_{(m,n)}^{(m+1,n)}$ and $\lambda_{(m,n)}^{(m,n+1)}$ are also equivalently transformed into $\lambda_{(m+nM)}^{(m+1+nM)}$ and $\lambda_{(m+nM)}^{(m+(n+1)M)}$, respectively. After this transformation, our analytical framework introduced in Section 2.4 can be invoked for analysing the various performance metrics. However, we have to employ a phase-type-distribution similar to that of Eq.(2.7), for the sake of characterising the performance of this two-dimensional CT-PBMC. This methodology can then be naturally extended to the multi-dimensional CT-PBMC.

Similarly, the authors of [97] rely on a pair of communities for their model. The MUs in the same community share the same mobility pattern, while the MUs belonging to the different communities have different mobility patterns. Hence, we classify the solutions provided in both [96] and [97] into the same category.

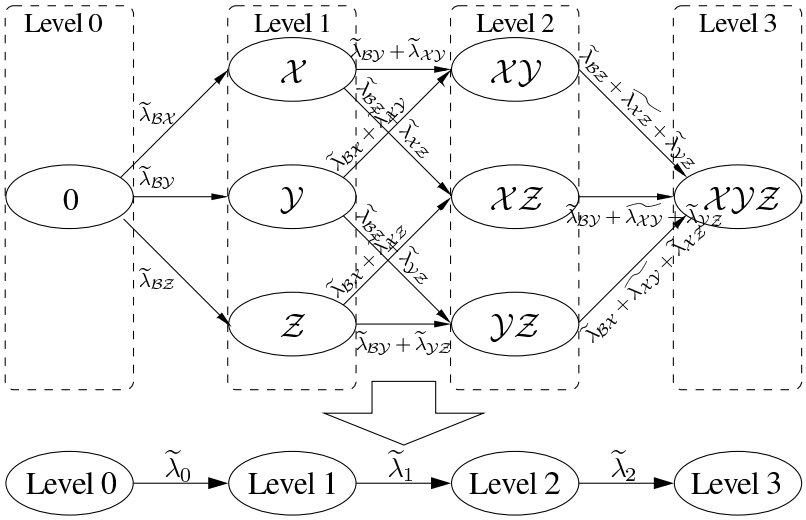

Figure 2.6: An example of the CT-PBMC for modelling completely heterogeneous mobility patterns of MUs and its transformation towards a typical one-dimensional version.

The authors of [91] assumed completely heterogeneous mobility patterns for MUs. We extend this model to our integrated cellular and large-scale opportunistic network. We denote the set of the MUs in the networks as $\boldsymbol{\mathcal{N}}$. When jointly considering the impact of both the inter-contact duration and the contact duration, any pairs of MUs have different effective contact rates, which are denoted as $\{\widetilde{\lambda}_{\mathcal{XY}}|\mathcal{X},\mathcal{Y}\in\boldsymbol{\mathcal{N}}\}$. Furthermore, the effective contact rates between the BS and any MU are different as well, which are denoted as $\{\widetilde{\lambda}_{\mathcal{BX}}|\mathcal{X}\in\boldsymbol{\mathcal{N}}\}$.

Figure 2.6 portrays an example of CT-PBMC for modelling the completely heterogeneous mobility patterns of MUs in an integrated network, which consists of three MUs, say $\boldsymbol{\mathcal{N}}=\{\mathcal{X},\mathcal{Y},\mathcal{Z}\}$. According to the number of MUs successfully receiving the IoCI, the CT-PBMC is divided into three levels. In Level 0, only the BS owns the IoCI. Level 1 is comprised of three states, say states $\mathcal{X}$, $\mathcal{Y}$ and $\mathcal{Z}$, representing the corresponding MUs that own the IoCI. Level 2 is comprised of three states as well, say states $\mathcal{XY}$, $\mathcal{XZ}$ and $\mathcal{YZ}$. Finally, level 3 only has a single state, which is state $\mathcal{XYZ}$, representing that all the MUs have received the IoCI. Let us consider a single state transition as an example, say from state $\mathcal{X}$ to state $\mathcal{XY}$, in order to explain how to derive the corresponding transition rate. MU $\mathcal{Y}$ can only successfully receive the IoCI if $\mathcal{Y}$ 'meets' either $\mathcal{X}$ or the BS. Hence, the corresponding state transition delay is equal to the minimum of two exponential variables associated with the rates of $\widetilde{\lambda}_{\mathcal{XY}}$ and $\widetilde{\lambda}_{\mathcal{BY}}$. Since the effective inter-contact durations[5] are exponentially distributed, this minimum is also an exponential random variable with a rate of $\widetilde{\lambda}_{\mathcal{BY}}+\widetilde{\lambda}_{\mathcal{XY}}$.

If we extend the CT-PBMC of Figure 2.6 to a more generic model having $|\boldsymbol{\mathcal{N}}|=N$ MUs, level n, which represents that n MUs have successfully received the IoCI, consists of $\binom{N}{n}$ different states. We further establish a simplified one-dimensional CT-PBMC, whose states represent the different levels of the original CT-PBMC, as shown at the bottom of Figure 2.6. As demonstrated in [91], if the specific values of the transition rates $\{\widetilde{\lambda}_{\mathcal{XY}}|\mathcal{X},\mathcal{Y}\in\boldsymbol{\mathcal{N}}\}$ obey a distribution with a mean of $\widehat{\lambda}_s$ and those of the transition rates $\{\widetilde{\lambda}_{\mathcal{BX}}|\mathcal{X}\in\boldsymbol{\mathcal{N}}\}$ obey another distribution with a mean of $\widehat{\lambda}_b$, then the transition rate between level n and level $(n+1)$ in the simplified one-dimensional CT-PBMC should be $\widetilde{\lambda}_n=(N-n)(\widehat{\lambda}_b+n\widehat{\lambda}_s)$. As a result, the model characterising completely heterogeneous mobility patterns of the MUs can also be found using the analytical framework of Section 2.4.

[5]The duration between two consecutive effective contacts is defined as the effective inter-contact duration.

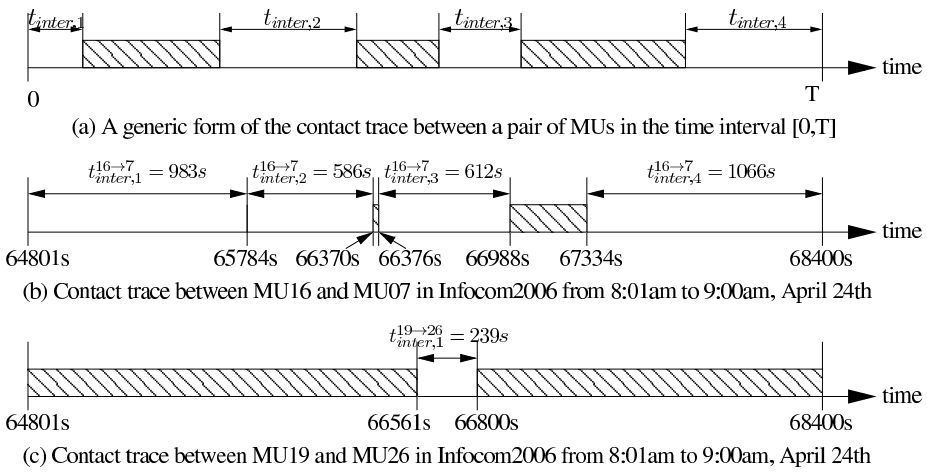

(a) A generic form of the contact trace between a pair of MUs in the time interval [0,T]

(b) Contact trace between MU16 and MU07 in Infocom2006 from 8:01am to 9:00am, April 24th

(c) Contact trace between MU19 and MU26 in Infocom2006 from 8:01am to 9:00am, April 24th

Figure 2.7: Examples of the contact trace between a pair of MUs in the time interval $[0, T]$. For the Infocom2006 contact trace, the observation period is $T = 3600$ second(s), from 8:01 am to 9:00 am, on April 24th. Shaded boxes represent the contact duration between MUs. Both the SPMs and the 'friendship' weights of the contact traces as presented in (b) and (c) are provided in Table 2.1.

2.5 Social Network Analysis Aided Tele-traffic Off-loading

As shown in Figure 2.1(b), in the application of off-loading the tele-traffic from the cellular system, all the MUs roam within the coverage of the cellular network. As a result, the contact rates between the BSs and the MUs are infinite, which indicates that the inter-contact duration is zero and that the MUs are always capable of connecting to the BSs. Moreover, the transmission delay from the BSs to the MUs only depends on the transmission rate of the wireless channels connecting them, which is far shorter than the inter-contact duration between the MUs. Hence, it is reasonable to assume that the information transmission between the BSs and the MUs can be promptly completed [91].

However, transmitting the IoCI to multiple requesters via multiple dedicated cellular links imposes a heavy traffic load on the BSs. Consequently, opportunistic communications amongst the MUs are adopted for off-loading the tele-traffic from the overloaded BSs. To this end, the BSs initially disseminate some copies of the IoCI to a group $\mathcal{D}$ of MUs via dedicated cellular links, whose size is $|\mathcal{D}| = D$. Then, the IoCI is disseminated to the rest of the MUs by their peers via opportunistic communications. During this information dissemination process, the BSs might further inject the IoCI into the large-scale opportunistic network at any time instant. However, in order to reduce the IoCI copies to be injected by the BS, the optimal strategy to be adopted by the BSs is demonstrated in [91] to be that of initially sending the IoCI to some MUs before embarking on the information dissemination across the opportunistic network and finally transmitting the IoCI to the uMUs right before the IoCI expires.

According to the aforementioned optimal strategy in [91], after the initial IoCI injection, we have $|\mathcal{D}| = D$ MUs that have successfully received the IoCI and the BSs are no longer invoked for disseminating the IoCI before it expires. Hence, the initial state of the CT-PBMC as shown in Figure 2.4 is state D, rather than state 0. Furthermore, the state transition rate is re-derived after deleting all the BS-related terms. After this slight adjustment, our analytical framework of Section 2.4 can also be exploited for analysing the performance metrics in the specific application of off-loading the tele-traffic from the cellular networks.

Another issue in this application scenario is how to select the initial receiver set $\mathcal{D}$ for receiving the IoCI from the BSs before the information dissemination commences so that more MUs can receive the IoCI via the opportunistic networks before it expires. In order to achieve this goal, the concept of 'centrality' borrowed from the tools of SNA [59] is exploited for evaluating the specific significance of an individual MU in the opportunistic networks.

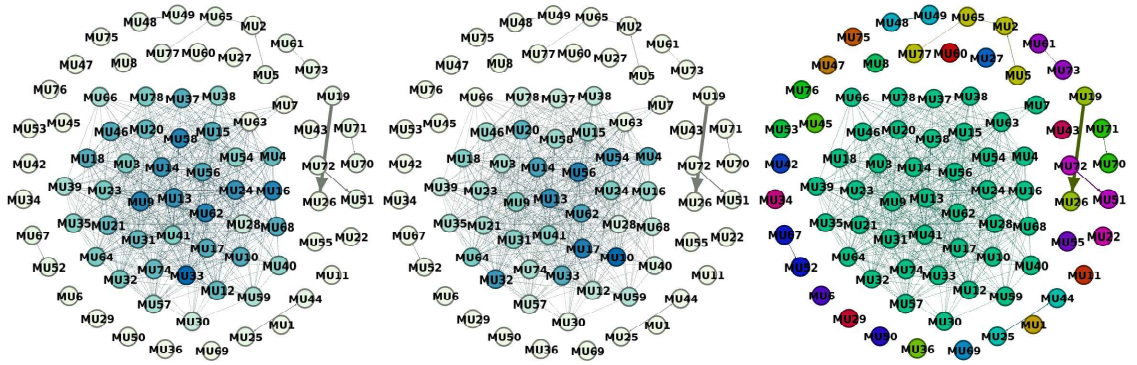

(a) Out-degree (b) Betweenness (c) Component

Figure 2.8: The social contact graph extracted from the InfoCom 2006 mobility trace [81] between 8:01am and 9:00am on 24th April, 2006. The weights of the 'friendships' between arbitrary pairs MUs are evaluated by the reciprocals of the corresponding SPMs. Only the 'friendships' having a weight higher than 0.0033 s^{-1} are retained in this social contact graph.

Table 2.1: Calculating the SPMs and the 'friendship' weights between two pairs of MUs in Infocom2006 from 8:01am to 9:00am, April 24th. The contact traces in this observation period are provided in Figure 2.7

Pair	Calculation	SPM	Weight	Verdict
MU16 ↓ MU07	Observe from Figure 2.7(b) that for this pair, there are 3 contact events during the observing period. Hence, we have 4 inter-contact durations, namely $t^{16\to7}_{inter,1} = 983$s, $t^{16\to7}_{inter,2} = 586$s, $t^{16\to7}_{inter,3} = 612$s and $t^{16\to7}_{inter,4} = 1066$s.Then the SPM is derived as $SPM = \left((t^{16\to7}_{inter,1})^2 + (t^{16\to7}_{inter,2})^2 + (t^{16\to7}_{inter,3})^2 + (t^{16\to7}_{inter,4})^2\right)/2/3600$. The weight is the reciprocal of this SPM.	391.7	0.0026	<0.0033 Discard
MU19 ↓ MU26	Observe from Figure 2.7(c) that for this pair, there are 2 contact events during the observing period. Hence, we have one inter-contact duration, namely $t^{19\to26}_{inter,1} = 239$s. Then the SPM is derived as $SPM = (t^{19\to26}_{inter,1})^2/2/3600$. The weight is the reciprocal of this SPM.	7.934	0.1260	>0.0033 Retain

Before evaluating the centrality[6] of an individual MU, we have to extract a social contact graph from the contact traces and quantify the grade of 'friendship' between a pair of MUs according to their contact-history, as shown in Figure 2.7. We account for the encounter-related properties with the aid of the so-called Social Pressure Metric (SPM) [39]. Explicitly, the SPM between MU_i and MU_j is defined as $SPM_{i,j} = (\sum_{x=1}^{n} t^2_{inter,x})/(2T)$, whose reciprocal $\omega_{i,j} = (2T)/(\sum_{x=1}^{n} t^2_{inter,x})$ represents the weight of the 'friendship' between MUs. The larger the value of $\omega_{i,j}$, the closer the friendship and hence the higher the forwarding probability between MU_i and MU_j.

Let us consider the realistic mobility trace of Infocom 2006 [81] as an example. We study the contact traces of the $N = 78$ MUs (exclude all the static nodes and external nodes) for one hour, between 8:01am and 9:00am on 24th April, 2006, namely on the opening day of the conference. The SPMs between all pairs of MUs are calculated for this time period, whose reciprocals are invoked for defining the weighst of their friendships. The length of the observing period is $T = 3600$ s. The weight threshold is set to be $1/5$ min^{-1} (0.0033 s^{-1}). All the friendships, whose weights are lower than this threshold, are discarded. In Table 2.1, we exemplify the calculation of the SPMs and the 'friendship' weights for the pair of MU16 and MU07 as well as for the pair of MU19 and MU26. As a result, we obtain a directed social contact graph for the 78 MUs, as shown in Figure 2.8. With the aid of the tools of SNA, the following strategies may be designed for

[6]Centrality describes how 'central' a node is in a network [59]. There are various types of centrality, such as degree, betweenness, closeness, as introduced in Chapter 1

selecting the initial receiver set.

- *Random selection:* Without considering any social network features, the initial receiver set $\mathcal{D}$ is randomly selected. Although we cannot guarantee a better delivery ratio before the IoCI expires, improved fairness amongst the MUs can be achieved, as claimed in [91].

- *Out-degree-based selection: Out-degree* of a MU is defined as the number of the social links that emerge from this MU and terminate at its neighbours in the directed social contact graph [59]. As shown in Figure 2.8(a), a node filled by a darker colour exhibits a higher out-degree value. Before the information dissemination commences, the MUs having the $|\mathcal{D}| = D$ highest out-degrees are selected as the initial receivers.

- *Betweenness-based selection:* The betweenness [59] for MU k is calculated as

$$C_B(k) = \sum_{j=1, j\neq k}^{N} \sum_{i=1, i\neq k}^{N} \frac{g_{i,j}(k)}{g_{i,j}},$$

  where $g_{i,j}$ is the total number of shortest paths, in terms of the number of hops, linking MU i and MU j in the social contact graph, and $g_{i,j}(k)$ is the number of those shortest paths that include MU k. The betweenness identifies 'bridge MUs' that act as links between different node clusters. As shown in Figure 2.8(b), a node filled by a darker colour has a higher value of betweenness. Before the information dissemination process, the MUs having the $|\mathcal{D}| = D$ highest betweenness values are selected as the initial receivers.

- *Component-based selection:* As shown in Figure 2.8(c), the social contact graph is naturally divided into different components. The MUs in the same component are connected to its peers via direct links or multi-hop links, while the MUs in different components are disconnected. In Figure 2.8(c), the nodes belonging to the same component are filled by the same colour. The social contact graph of Figure 2.8(c) is comprised of 28 components, amongst which the largest one has 40 MUs. In order to allow more MUs to receive the IoCI via the opportunistic networks, the initial receivers should cover as many different components as possible. We sort the components according to their size and select a MU belonging to this component having the highest betweenness as the component 'head'. All these component 'heads' have higher priorities to be included into the initial receiver set than other MUs, and by the same rationale, the 'head' of a larger component has a higher priority to be selected than the head of a smaller component. According to this principle, we may obtain the initial receiver set $\mathcal{D}$.

Apart from the aforementioned ones, there are other types of centralities conceived for different purposes. Google's well-known ranking algorithm, namely *page rank*, measures the likelihood of nodes having important friends in a social graph [98]. Ego-betweenness [6] is exploited for designing the opportunistic routing protocol in [42] without any global knowledge of the network. In contrast to traditional centralities that are based on unweighted networks, the *cumulative contact probability* concept of [99] is used for reflecting the properties of weighted networks. Interested readers may refer to the related references for further information.

2.6 Numerical Results

In this section, we first characterise the inter-contact duration and contact duration between a pair of MUs and those between a BS and MU pair. Then we demonstrate the capability of the integrated cellular and large-scale opportunistic network in terms of improving the connectivity of the conventional cellular network and in terms of off-loading the tele-traffic from the congested CI.

Table 2.2: Simulation parameters for the RD mobility model

Description	Simulation Parameters
Simulation Area	A 2000×2000 m^2 square area
BS Location	The centre of the square area
Average Duration	10 minutes
Speed region	2 m/s $\sim$ 4 m/s
Direction region	0 radian $\sim$ 2π radian

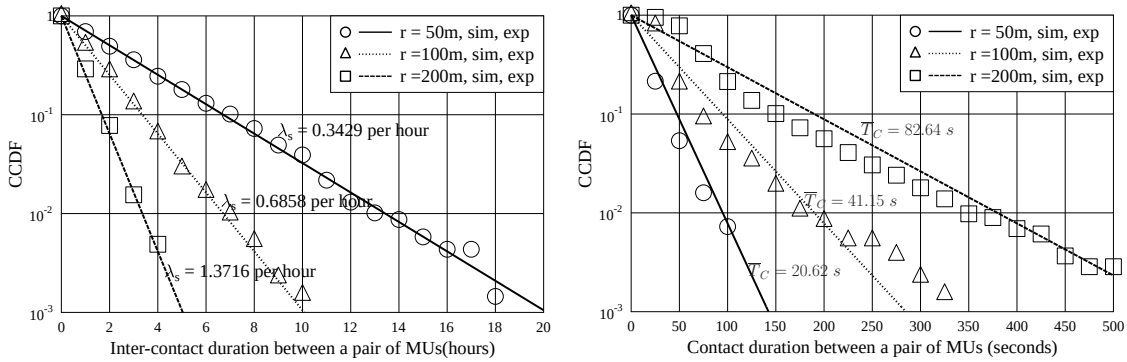

(a) Inter-contact duration

(b) Contact duration

Figure 2.9: The CCDFs of both the inter-contact duration and the contact duration between a pair of MUs (mobile nodes), which are paramerised by their transmission range. This pair of MUs move within a 2000×2000 (m^2) square area by obeying a RD mobility model. Their transmission range r takes a value from the set $\{50, 100, 200\}$ m. Other parameters related to the RD mobility model are listed in Table 2.2. The average contact rates are caclulated by taking the reciprocal of Eq.(2.1) and the average contact durations are calculated by Eq.(2.3).

2.6.1 Inter-Contact Duration and Contact Duration

Let us now consider some simulation results obtained from the following RD mobility model:

- The simulation area is a 2000×2000 (m^2) square area;
- The BS is located at the centre of the square area.
- The duration of a single movement obeys an exponential distribution with a mean of 10 minutes;
- The speed of a single movement is uniformly chosen from the region of $[2, 4]$ (m/s);
- The direction of a single movement is also uniformly chosen from the region of $[0, 2\pi)$;
- A MU would bounce back if he/she hits the boundary of the square area during a single movement.

The most important parameters of the RD mobility model are also summarised in Table 2.2 for the readers' convenience.

We first study the CCDF of both the inter-contact duration and of the contact duration between a pair of MUs, as depicted in Figure 2.9. We calculate the average contact rates between this pair of MUs by taking the reciprocal of Eq.(2.1). Observe from Figure 2.9(a) that increasing the transmission range r of the MUs may increase the opportunities for this pair of MUs to make contact with each other. For example, this pair of MUs makes on average 0.3429 contacts per hour, when the transmission range is 50 m. However, this number is increased to 1.3716 per hour, when the transmission range is increased to 200 m. As portrayed in Figure

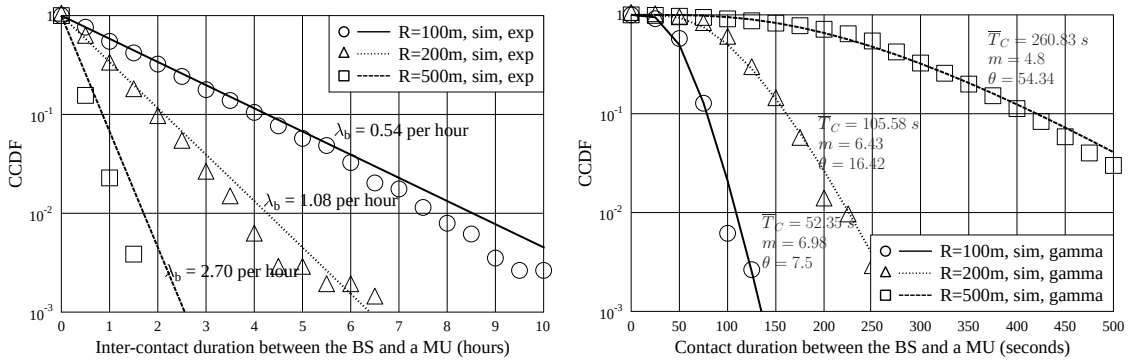

(a) Inter-contact duration (b) Contact duration

Figure 2.10: The CCDFs of both the inter-contact duration and the contact duration between a MU (mobile node) and a BS (static node), which are paramerised by the transmission range of the BS. The MU moves within a 2000×2000 (m^2) square area by obeying a RD mobility model, while the BS is fixed at the centre of the square area. The transmission range R of the BS takes a value from the set $\{100, 200, 500\}$ m. Other parameters related to the RD mobility model are listed in Table 2.2. The average contact rates are caclulated by taking the reciprocal of Eq.(2.1) and the average contact durations are calculated by Eq.(2.3).

2.9(a), the simulated CCDFs of the inter-contact durations are closely approximated by the exponential distributions associated with the means derived by Eq.(2.1).

Observe from Figure 2.9(b) that increasing the transmission range r of the MUs may prolong their contact duration. For example, the average contact duration between this pair of MUs is only 20.62 s when the transmission range is 50 m, but it is almost quadrupled as the transmission range is increased to 200 m. As portrayed in Figure 2.9(b), the simulated CCDFs of the contact durations are closely approximated by the exponential distributions associated with the means derived by Eq.(2.3).

Let us now study the CCDFs of both the inter-contact duration and the contact duration between a MU and a BS, as portrayed in Figure 2.10. We derive the average contact rates between the MU and the BS by taking the reciprocal of Eq.(2.1). Observe from Figure 2.10(a) that the probability of opportunities for the MU to contact the BS is increased, as the transmission range of the BS increases. For example, when the transmission range of the BS is $R = 100$ m, the MU contacts the BS 0.54 times per hour on average, but the contact becomes more frequent, say 2.7 times per hour, as we increase the transmission range of the BS from 100 m to 500 m. As shown in Figure 2.10(a), the simulated CCDFs of the inter-contact durations are closely approximated by the exponential distributions associated with the means derived by Eq.(2.1).

Observe from Figure 2.10(b) that increasing the transmission range of the BS is capable of prolonging the contact duration between the MU and the BS. For example, when the BS's transmission range is $R = 100$ m, the average duration of a single contact is 52.35 s, but it is increased to 260.83 s as the BS's transmission range is increased to $R = 500$ m. However, as presented in Figure 2.10(b), we surprisingly find that the contact duration between the MU and the BS can be closely approximated by a Gamma distributed random variable. For example, when the transmission range of the BS is $R = 200$ m, the simulated CCDF of the contact duration is accurately approximated by a Gamma distribution associated with a shape parameter $m = 6.43$ and a scale parameter of $\theta = 16.42$. In order to obtain the accurate value of the shape parameter m and that of the scale parameter θ, we have to derive the closed-form results for the mean and the variance of the contact duration. Although the mean is given by Eq.(2.3), we have not derived its accurate variance, which we expect to tackle in our future work. At this stage, we embark on numerically deriving the variance of the contact duration.

Table 2.3: Simulation parameters for improving the cellular networks' connectivity

	BS to MUs	MUs to MUs
Tx Range	$R = 100$ m	$r = 50$ m
Tx Rate	$B_b = 1$ Mbps	$B_s = 2$ Mbps
File Size	$L = 40$ Mb (5 MB)	
File Life Time	From 1 hour to 2 hour	
Number of MUs	From 10 to 100	

2.6.2 Improving the Connectivity of Cellular Networks

In this scenario, we adopt a homogeneous RD mobility model for all the MUs. The parameters of this RD model are the same as those used in Section 2.6.1, which have been summarised in Table 2.2. Furthermore, as shown in Table 2.3, we assume that the transmission range of the BS is 100 m, while that of the MUs is 50 m. The transmission rate of the cellular link is $B_b = 1$ Mbps and that of the opportunistic link is $B_s = 2$ Mbps. The epidemic relaying protocol, as introduced in Section 2.3.3, is used for facilitating the information dissemination process. The file size of the IoCI is set to 40 Mb (5 MB). Once the uMUs enter the transmission range of the IOs (including the BS and the served MUs), their cellular/opportunistic links are established for delivering the IoCI. In some occasions, an uMU may enter the transmission ranges of several IOs. This uMU is only allowed to select a single IO for downloading the IoCI. If the IoCI is not successfully downloaded but this uMU is still within the transmission range of other IOs, it may choose another IO for continually downloading the IoCI. If the IoCI is not successfully downloaded and this uMU is no longer within any IO's transmission range, the data received by the uMU so far are discarded. This principle is also implemented for studying the tele-traffic off-loading scenario in the next section.

The average successful delivery ratio before the IoCI expires is plotted in Figure 2.11. The analytical results (ana) in Figure 2.11 are obtained by the following steps:

- Both the contact process between the BS and the MU and that between a pair of MUs are modelled by Poisson processes. The contact rate λ_b between the BS and the MUs is approximated to be $\lambda_b = 0.54$ per hour according to Eq.(2.1), while the contact rate λ_s between a pair of MUs is approximately $\lambda_s = 0.3429$ per hour according to Eq.(2.1).
- The contact duration between the BS and the MU is modelled by a Gamma distribution having a shape parameter of $m = 6.98$ and a scale parameter of $\theta = 7.5$, as shown in Figure 2.10(b). The contact duration between a pair of MUs is modelled by an exponential distribution having a mean of $\overline{T}_C = 20.62$ seconds, which is derived from Eq.(2.3).
- With the aid of CT-PBMC, as introduced in Section 2.4, the state probabilities $\{p_n(T_L)\}$ are calculated by Eq.(2.14) when the life time $T_L = \{1.0, 1.5, 2.0\}$ hours are achieved. Furthermore, the average successful delivery ratio is obtained as $\overline{n}/N = \sum_{n=0}^{N} np_n(T_L)/N$, where N is the total number of MUs in the area studied.

As shown in Figure 2.11, we observe that having more MUs may significantly increases the average delivery ratio, since the probability of successfully delivering the IoCI is greatly enhanced, when more MUs participate in the information dissemination process. The delivery ratio increases from 45% to 100%, when the life time of the IoCI is one hour, as the number of MUs increases from 10 to 80. Naturally, if the MUs can tolerate a longer latency of receiving the IoCI, which indicates a longer life time, the delivery ratio is also improved.

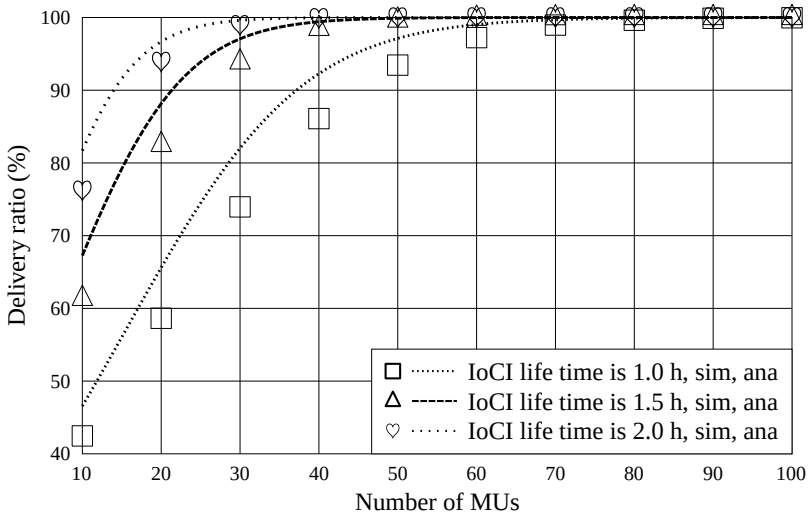

Figure 2.11: The average successful delivery ratio before the expiry of the IoCI. The RD mobility model defined in Section 2.6.1 is invoked for modelling the movement of the MUs. The mobility-related parameters are provided by Table 2.2, while the other parameters are given by Table 2.3.

Table 2.4: Centralities of the initial receiver set according to different selection schemes

	MU33	MU09	MU16	MU58	MU62	MU13	MU14	MU24	MU10	MU15
Out-degree	**23**	**21**	**21**	**21**	**21**	**20**	**20**	**20**	**18**	**18**
Betweenness	33.6	20.0	21.9	21.2	34.6	37.6	35.1	28.1	42.9	24.6
Com.ID(size)	2(40)	2(40)	2(40)	2(40)	2(40)	2(40)	2(40)	2(40)	2(40)	2(40)

(a) Out-degree based selection

	MU10	MU17	MU56	MU13	MU32	MU54	MU14	MU62	MU04	MU33
Out-degree	18	18	18	20	16	14	20	21	17	23
Betweenness	**42.9**	**39.8**	**39.0**	**37.7**	**36.4**	**36.4**	**35.1**	**34.6**	**33.9**	**33.6**
Com.ID(size)	2(40)	2(40)	2(40)	2(40)	2(40)	2(40)	2(40)	2(40)	2(40)	2(40)

(b) Betweenness based selection

	MU10	MU65	MU19	MU25	MU48	MU51	MU52	MU61	MU70	MU76
Out-degree	18	1	1	1	1	1	1	1	1	0
Betweenness	42.9	1	0	0	0	0	0	0	0	0
Com.ID(size)	**2(40)**	**1(4)**	**6(2)**	**8(2)**	**17(2)**	**19(2)**	**20(2)**	**24(2)**	**26(2)**	**28(1)**

(c) Component based selection

2.6.3 Tele-Traffic Off-Loading

On the opening day of an academic conference, the organisers are keen on finding an efficient way of disseminating the conference program to the attendees. Again, as an example, the contact traces of InfoCom 2006 [81] is employed. We study the period spanning from 8:01 am to 9:00 am on the opening day of the conference, April 24th, 2006, in order to study how much the opportunistic network would assist us in disseminating the IoCI. The file size of the IoCI is 40 Mb (5MB). Since the traces were collected via Bluetooth devices, we assume that the opportunistic link between a pair of MUs is realised by Bluetooth and the transmission rate is 1 Mbps. Bluetooth is a half-duplex peer-to-peer communication technique. Hence, while a source is transmitting data to a target, extra links cannot be established even if another uMUs enters the transmission range of the source. Furthermore, corresponding to [73], we assume that an uMU will acquire the IoCI from his/her geographic neighbours with a probability of $p_{pull} = 0.001$ during every contact.

Moreover, random selection, out-degree based selection and betweenness-based selection as well as component-based selection are invoked for appointing the initial receiver set directly acquiring the IoCI

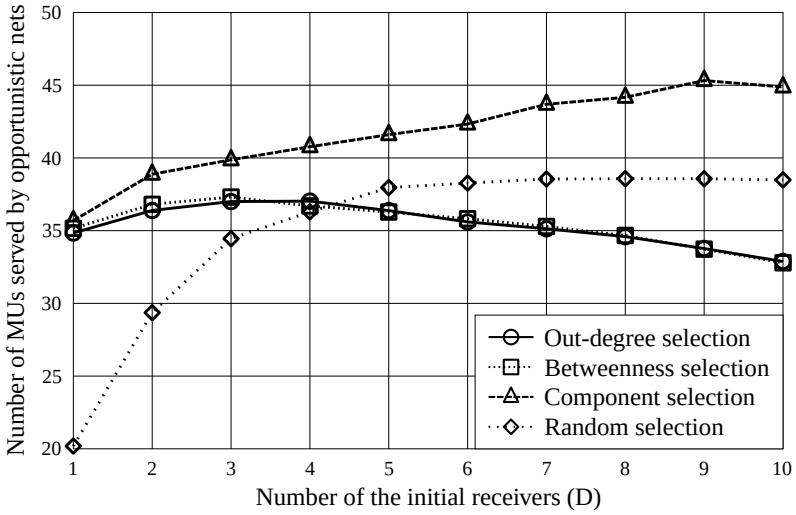

Figure 2.12: The average number of MUs receiving the IoCI via the opportunistic network. The period spanning from 8:01am to 9:00am on April 24th during InfoCom 2006 is studied. The file size of the IoCI is 40 Mb (5 MB). The transmission rate of the Bluetooth enabling opportunistic link is 1 Mbps. An uMU will fetch the IoCI from his/her geographic neighbours with a probability of $p_{pull} = 0.001$.

from the CI. Based on the social contact graph of the MUs, as shown in Figure 2.8, the initial receiver set is determined as follows, if the number of initial receivers is 10:

- For the random selection, by definition, the initial receiver set is randomly selected for every round of the simulation.
- For the out-degree-based selection, the initial receiver set is determined from Figure 2.8(a) as {MU33, MU9, MU16, MU58, MU62, MU13, MU14, MU24, MU10, MU15}. The out-degrees and other centralities of this receiver set are listed in Table 2.4(a).
- For the betweenness-based selection, the initial receiver set is determined from Figure 2.8(b) as {MU10, MU17, MU56, MU13, MU32, MU54, MU14, MU62, MU4, MU33}. The betweenness and other centralities of this receiver set are listed in Table 2.4(b).
- For the component based selection, the initial receiver set is determined from Figure 2.8(c) as {MU10, MU65, MU19, MU25, MU48, MU51, MU52, MU61, MU70, MU76}. The component IDs and the component sizes as well as other centralities of this receiver set are listed in Table 2.4(c).

The computation process of the above-mentioned metrics, including the out-degree, the betweenness and the component ID as well as the component size is omitted for reasons of space-economy, since it obeys the same methodology as shown in Table 1.1 of Chapter 1.

As shown in Figure 2.12, we study the impact of the number of the initial receivers on the number of MUs served by the opportunistic network. The number of MUs served by the opportunistic network also indicates the amount of tele-traffic off-loaded from the CI. Observe from Figure 2.12 that the number of MUs served by the opportunistic network firstly increases as we increase the number of initial receivers. But after reaching the peak, it then slowly reduces as we further increase the number of the initial receivers. For different initial receiver selection approaches, the peaks appear at different positions. Specifically, for both the out-degree and betweenness-based selection approaches, the peaks appear when the number of the initial receivers is 3; for component-based selection, the peak appears when the number of the initial receivers is 9; for random selection, the peak appears when the number of the initial receivers is 8.

Furthermore, as shown in Figure 2.12, the pair of centrality based selection methods, namely the out-degree and betweenness based ones, have nearly the same performance because all the initial receivers selected by these two methods belong to the largest component, as shown in Figure 2.8(c) and Tables 2.4(a)(b). Therefore, the MUs belonging to the other 27 components cannot receive the IoCI via the opportunistic network. Observe from Figure 2.12 that the component-based selection performs the best, because more isolated components are covered by the initial receivers. Moreover, when the number of initial receivers is low, the random selection perform worst, because the MUs belonging to an isolated component are likely to be selected, which seriously degrades the performance. However, when the number of initial receivers is high, the random selection outperforms the two centrality-based methods, because it is more likely to cover more MUs in the opportunistic network.

2.7 Chapter Conclusions

In this chapter, we studied the information dissemination in an integrated cellular and large-scale opportunistic network. Here the terminology 'large-scale' indicates the following two features of this integrated network:

- In this integrated network, the MUs are sparsely distributed in a large area, which results in intermittent connectivities between the MUs and the BSs as well as amongst the MUs themselves. Successful information delivery can be achieved by the opportunistic contacts between the MUs and the BSs as well as amongst the MUs themselves.
- In this integrated network, the successful information delivery suffers from a relatively 'large' delay, since the uMUs have to enter the transmission range of the IOs so as to fetch the information. The underlying long inter-contact duration results in a long information delivery delay for the sparsely distributed MUs. As a result, only delay-tolerant information is suitable for the dissemination in this integrated network.

In Section 2.1, we firstly exemplified the increasing demand of MUs for disseminating the IoCI in an integrated cellular and large-scale opportunistic network and introduced some of the commercial mobile applications that can be relied upon for realising the information dissemination amongst MUs. Then, we focused our attention on two application scenarios of our integrated networks, namely on improving the connectivities of cellular networks and on off-loading the tele-traffic from the congested CI.

In Section 2.2, we elaborated on the various factors that may affect the information dissemination performance. Amongst the factors that are independent of the node mobilities, we discussed the transmission range, the file size and transmission rate as well as the life time of the IoCI. Furthermore, in the category of mobility related-factors, we investigated both the effects of the inter-contact duration and of the contact duration. Moreover, for the RD mobility model, we provided closed-form equations for calculating both the average inter-contact duration and the average contact duration. By jointly considering the impact of these mobility-related factors, we defined the concept of effective contact process and modelled it by a thinned Poisson process.

In Section 2.3, we surveyed three protocols that can be invoked for disseminating the IoCI in an integrated cellular and opportunistic network, namely the direct transmission protocol, the two-hop relaying protocol and the epidemic relaying protocol. We highlighted the advantages of the epidemic relaying protocol in terms of its delivery ratio over the other two protocols via a simple example.

In Section 2.4, we modelled the information dissemination process in an integrated cellular and opportunistic network by a CT-PBMC. In this CT-PBMC model, we accounted for the impact of various factors on the information dissemination performance, as introduced in Section 2.2. Specifically, we assumed that

all the MUs move within an area by following a homogeneous mobility model. We focused our attention on deriving closed-form formulas for the following performance metrics:

- The dissemination delay, which was the time duration that elapsed since the IoCI was generated at the central server, until it was successfully received by all the subscribers.
- The individual delay, which was the time duration that elapsed since the IoCI was generated at the central server, until it was successfully received by a specific subscriber.
- The delivery ratio, which is the percentage of the MUs successfully receiving the IoCI before it expires.

We demonstrated furthermore that our analytical framework is also fit for calculating the corresponding performance metrics when heterogeneous mobility patterns of the MUs are considered.

In Section 2.5, we established a social contact graph for the MUs according to their contact history. Basically, a 'friendship' can be established between a pair of MUs, if they contact each other during the observation period. The reciprocal of the SPM is exploited for evaluating the strength of these virtual 'friendships'. Only if the weights of the 'friendships' exceed a pre-defined threshold, they could be retained in the social contact graph. Based on this social contact graph, various strategies were designed for selecting the initial receiver set, namely the random selection, the out-degree-based selection, the betweenness-based selection as well as the component-based selection.

In Section 2.6, numerical results were provided for characterising the statistical properties of both the inter-contact duration and of the contact duration between a pair of MUs and those between a MU and a BS. Furthermore, we also demonstrated the capability of the integrated network in terms of improving the connectivities of the cellular network and in terms of off-loading the tele-traffic from the congested CI. Our conclusions are as follows:

- Both the inter-contact duration and the contact duration between a pair of MUs could be approximated by exponentially distributed random variables, when both the MUs moved within a square area by obeying the RD mobility model, as presented in Figure 2.9.
- The inter-contact duration between a MU and a BS may be approximated by an exponentially distributed random variable, while the contact duration between them may be approximated by a Gamma distributed random variable, when the MU move within a square area by obeying the RD mobility model and the BS was located at the centre of this square area, as shown in Figure 2.10.
- In the scenario of improving the connectivities of cellular networks, our numerical results seen in Figure 2.11 suggested that increasing the social participation of the MUs is capable of significantly enhancing the average delivery ratio of the IoCI before it expires. Furthermore, if the MUs are capable of tolerating a longer latency of receiving the IoCI, which was reflected by a longer life time of the IoCI, the average delivery ratio may be remarkably improved.
- The quantitative comparison between our epidemic relaying aided information dissemination scheme and the BS-assisted direct transmission scheme is provided in Table 2.5. In contrast to the epidemic relaying protocol, we observe from Table 2.5 that varying the number of MUs may not affect the average delivery ratio, when the BS-assisted direct transmission scheme is implemented, because no opportunistic links are established for delivering the IoCI.
- In the scenario of the tele-traffic off-loading application, our numerical results seen in Figure 2.12 suggested that increasing the size of the initial receiver set may result in an increased number of MUs served by the opportunistic networks. However, further increasing this size may reduce the capability of the opportunistic network to off-load the tele-traffic.

Table 2.5: Quantitative comparison between our epidemic relaying aided information dissemination scheme and the BS-assisted direct transmission scheme in terms of the average delivery ratio. All the simulation parameters are provided by both Tables 2.2 and 2.3. Note that we only present the simulation results in this table. For more detailed results of our epidemic relaying aided information dissemination scheme, please refer to Figure 2.11.

	Number of MUs ($N = 10$)			Number of MUs ($N = 20$)		
IoCI life time	$T_L = 1.0$ h	$T_L = 1.5$ h	$T_L = 2.0$ h	$T_L = 1.0$ h	$T_L = 1.5$ h	$T_L = 2.0$ h
Average delivery ratio, direct transmission	31.8 %	43.7 %	53.5%	31.8 %	43.7 %	53.5 %
Average delivery ratio, epidemic relaying	42.5 %	61.4 %	76.2 %	58.6 %	82.5 %	93.9%

Table 2.6: Quantitative comparison amongst different selection approaches for the initial receiver set in terms of the average number of MUs served by the opportunistic network, which is summarised from Figure 2.12. Please refer to the caption of Figure 2.12 for the detailed parameters.

	Average number of MUs served by opportunistic networks			
Size of the initial receiver set	Random selection	Out-degree selection	Betweenness selection	Component selection
$D = 2$	29.4 MUs	36.4 MUs	36.8 MUs	38.9 MUs
$D = 4$	36.3 MUs	37.0 MUs	36.7 MUs	40.8 MUs
$D = 6$	38.3 MUs	35.6 MUs	35.8 MUs	42.3 MUs
$D = 8$	38.6 MUs	34.6 MUs	34.7 MUs	44.2 MUs
$D = 10$	38.5 MUs	32.9 MUs	32.8 MUs	44.9 MUs

- We also observed from Figure 2.12 that the component-based selection approach always performed best over its counterparts. The centrality-based selection approaches, including both the out-degree and the betweenness-based selections, had almost the same performance. When we had a small initial receiver set, the centrality-based approaches outperformed the random selection. However, the random selection was more capable of off-loading tele-traffic than both of the centrality-based selection approaches. The quantitative comparison amongst different selection approaches is provided in Table 2.6.

Since the information dissemination in a sparsely populated opportunistic network is dominated by the encounter properties of the MUs, it is reasonable for us to assume that the successful information delivery depends on the event that the target enters the source's transmission range and lingers within the range for a sufficiently long period. However, this simplified physical layer model is not appropriate, when the MUs are distributed in a small-scale area, where all the MUs might appear within each other's transmission range. When we consider both the shadow-fading and the multipath fading effects, the shape of a MU's transmission range is no longer a regular circle. Moreover, the geographic position of a target determines the channel's attenuation represented by the path-loss. If the target is closer to the source, it may receive a stronger signal and its probability of recovering the original information becomes higher. As a result, in the following chapters, we will focus our attention on resolving the information dissemination issues in a small-scale scenario by considering more specific realistic physical layer models. We will also consider the impact of both the MUs' altruistic behaviours and their social relationships on the attainable information dissemination performance.

Appendix

2.A Proof of Theorem 2.1

For the specific case of $1 \leq n \leq (N-1)$, after a sufficiently short time interval Δt, the probability of the CT-PBMC, as shown in Figure 2.4, remaining in state n is derived as

$$p_n(t+\Delta t) = p_{n-1}(t)\widetilde{\lambda}_{n-1}\Delta t + p_n(t)[1-\widetilde{\lambda}_n\Delta t], \tag{2.16}$$

where $\widetilde{\lambda}_n\Delta t$ is the probability of the CT-PBMC traversing from state n to state $(n+1)$ during the time interval Δt, whereas $\widetilde{\lambda}_{n-1}\Delta t$ holds a similar meaning. After some equivalent transformation applied to Eq.(2.16), we arrive at

$$\frac{d}{dt}p_n(t) = \lim_{\Delta t\to 0}\frac{p_n(t+\Delta t)-p_n(t)}{\Delta t} = \widetilde{\lambda}_{n-1}p_{n-1}(t) - \widetilde{\lambda}_n p_n(t). \tag{2.17}$$

Similarly, we can also derive the corresponding differential equation for the cases of $n=0$ and $n=N$. As a result, the following set of differential equations are obtained

$$\begin{cases} \frac{d}{dt}p_0(t) = -\widetilde{\lambda}_0 p_0(t), & n=0, \\ \frac{d}{dt}p_n(t) = \widetilde{\lambda}_{n-1}p_{n-1}(t) - \widetilde{\lambda}_n p_n(t), & 1\leq n\leq N-1, \\ \frac{d}{dt}p_N(t) = \widetilde{\lambda}_{N-1}p_{N-1}(t), & n=N. \end{cases} \tag{2.18}$$

Since only the BS owns the IoCI at the beginning of the information dissemination, the initial condition is given by $\{p_0(0)=1, p_1(0)=0, \cdots, p_N(0)=0\}$. As a result, applying the Laplace transform to the above differential equations, and taking the aforementioned initial condition into account, we arrive at

$$\begin{cases} sP_0(s) = -\widetilde{\lambda}_0 P_0(s) + 1, & n=0, \\ sP_n(s) = -\widetilde{\lambda}_n P_n(s) + \widetilde{\lambda}_{n-1}P_{n-1}(s), & 1\leq n\leq N-1, \\ sP_N(s) = \widetilde{\lambda}_{N-1}P_{N-1}(s), & n=N, \end{cases} \tag{2.19}$$

from which we obtain

$$P_n(s) = \begin{cases} \frac{1}{s+\widetilde{\lambda}_0}, & n=1 \\ \frac{1}{s+\widetilde{\lambda}_n}\prod_{m=0}^{n-1}\frac{\widetilde{\lambda_m}}{s+\widetilde{\lambda}_m}, & 0<n<N, \\ \frac{1}{s}\prod_{m=0}^{N-1}\frac{\widetilde{\lambda}_m}{s+\widetilde{\lambda}_m}, & n=N. \end{cases} \tag{2.20}$$

Finally, applying the inverse-Laplace-transform to the above equations, we may arrive at the closed-form solutions for $p_n(t)$, as expressed in Eq.(2.14). Hence the theorem has been proved. ■

Chapter 3

Mobile Social Networking Aided Content Dissemination in Cellular Systems Relying on Altruistic Human Behaviour

3.1 Introduction

3.1.1 Background and Related Works

As a combination of social science and mobile networks, Mobile Social Networks (MSNs) [4] are attracting an increasing attention across the research community. Various social characteristics of Mobile Users (MUs) incurred by their mobility patterns are exploited for routing design in Mobile *Ad hoc* NETworks (MANETs). For example, in both [40] and [100], routing protocols are designed by exploiting social centralities of MUs in MANETs and the communities formed by MUs, aiming for finding the best information carrier toward the final destination. The authors of [101] exploit both the users' willingness to forward the information and their opportunistic contact incurred by their mobilities for the sake of improving routing performance.

There are substantial contributions to the performance analysis of epidemic forwarding [93] in MANETs. A two-dimensional Continuous-Time-Pure-Birth-Markov-Chain (CT-PBMC) was proposed in [96] for evaluating the performance of a heterogeneous MANETs. To a further advance, the authors of [102] derived a tight upper bound of the flooding time, which is defined as the number of time-steps required for broadcasting a message from a source node to all nodes. Furthermore, in [103] the end-to-end message delivery delay using an epidemic forwarding protocol was investigated theoretically in a composite twin-layer network, which includes a physical MANET and a virtual social network.

However, epidemic forwarding is often criticised as being an end-to-end routing protocol, because it consumes substantial resources of the intermediate nodes, which might not be interested in the information to be relayed. However, if MUs can form a MSN group and request the content of common interest together, epidemic forwarding becomes an efficient way of cooperatively disseminating the content in the target MSN group[1]. Content dissemination in purely distributed opportunistic networks was investigated in [104] and [105]. Epidemic forwarding aided content dissemination was invoked in [104], where the users share any

[1] Other MUs that do not belong to the target MSN group are not relied upon for assisting the content dissemination process.

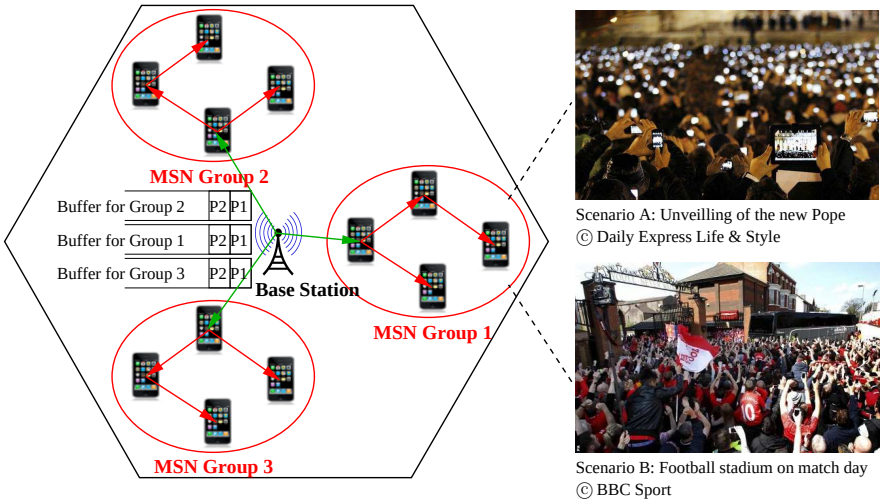

Figure 3.1: MSNs aided content dissemination in cellular systems

content updates with others they meet in order to improve the coverage quality and to increase the capacity. A socially-aware content placement algorithm was proposed in [105] for enhancing the opportunity of MUs to gain access to their contents of interest.

Some researches focused on a hybrid content dissemination approach. In [106] and [43], the authors investigated how the content providers and network operators can interact for the sake of efficiently distributing the contents with the aid of a coalition game. At the time of writing, epidemic forwarding aided content dissemination is widely studied for the sake of off-loading tele-traffic from cellular networks. In [107], the authors proposed a framework for initial content-receiver selection in order to disseminate the content of common interest to as many subscribers as possible before interest in the the content subsides. In [90], mobile users were categorised into 'helpers' as well as 'subscribers' and several algorithms were designed for solving the optimisation problem of off-loading multiple type of contents from the cellular networks.

The above-mentioned contributions focused their attention on user-encounter-based MANETs or 'large-scale MSNs'[2] [59]. In these treatises, the inter-contact duration of MUs is commonly assumed to obey an exponential distribution, which is demonstrated in [79] by synthetic mobility models and in [108] by realistic mobility traces. Due to the underlying long inter-contact duration of MUs, normally in the orders of minutes even hours, user-encounter-based content dissemination is only capable of delivering delay-tolerant services, but cannot deliver delay-sensitive services. There is also substantial interest in dense MANETs. For example, a middleware solution was proposed in [109] for cooperative replication in dense MANETs, while the connectivity probability was analysed in [110] in the context of dense VANETs. However, neither [109] nor [110] provided any closed-form analytical results concerning the content dissemination performance.

3.1.2 Motivations

The conventional method of disseminating the content of common interest relies on Base Station (BS)-aided multicast, where the BS is the sole transmitter. The capacity of multicast channels is predetermined by the worst channel. In this case, due to the uncertainty nature of wireless channels, when the BS multicasts a packet, some MUs may successfully receive it earlier than their less fortunate counterparts. Then, the successful receivers have to remain silent, because the BS would not multicast the second packet, before all the MUs successfully receive the current one. In over-crowded scenarios, as exemplified by the unveiling of new

[2]In large-scale MSNs, mobile nodes are sparsely distributed over a very large area. Only when a pair of nodes enter each other's transmission range, they can communicate. Hence, the system performance is affected by the inter-contact duration of mobile nodes, and by their contact duration.

Pope in Rome or the football stadium on match days, the density of MUs is extremely high, as shown in Figure 3.1. Thus, conventional BS-aided multicast may suffer from a long dissemination delay [55]. If local MUs form a MSN group for requesting the content of common interest from the BS, local communications amongst the MUs, which can be realised by Wi-Fi or Bluetooth, can be exploited for cooperatively multicasting the packets from the packet owners to the hitherto unserved MUs in the target MSN group[3]. The diversity-gain provided by cooperative multicast amongst the MUs might improve the content dissemination performance in the aforementioned over-crowded scenarios.

The size of the area covered by a MSN group should be carefully designed for different scenarios. If the area is as large as a macro-cell, the cooperative content dissemination amongst group members will suffer from a long dissemination delay. This dissemination delay is determined by the inter-contact duration between a pair of MSN users, which is directly influenced by their mobility. This scenario is only suitable for disseminating delay-tolerant information. However, the best option for disseminating delay-sensitive information across a large area is that of classic BS-aided multicast. By contrast, if the area is relatively small, e.g. a circular area with a radius shorter than a hundred meter, which is comparable to the transmission range[4] of the MSN users, cooperative content dissemination is capable of significantly reducing the delay of the conventional BS-aided multicast. This scenario is termed as "small-scale MSNs" [59], where the varying Path-Loss (PL) incurred by MSN users' mobility is often referred to as large-scale fading [112]. As demonstrated by the numerical results of Section 3.6, our approach outperforms the conventional BS-aided multicast, especially when the user density in the area studied is high.

The MSN users' altruistic behaviour has a significant influence on the attainable content dissemination performance. Altruistic MSN users are willing to forward the content that they have received so far to the other hitherto unserved peers and this may accelerate the content dissemination process, enhance the reliability of the content transmission, as well as off-loading the tele-traffic from the congested centralised infrastructure. However, the price paid for these benefits is the increased energy dissipation of the individual MSN users, which might make them reluctant to engage in the content dissemination process.

The MSN users' altruistic behaviour is often affected by many unpredictable factors. During the content dissemination process, a user might immediately switch off his/her device without any particular reason. Moreover, the user might suddenly receive an important call from his/her boss, which may prevent him/her from forwarding the content. Therefore, the user's subjective attitude and a sudden incident make it challenging to find a reasonable approach for modelling the MSN users' altruistic behaviour.

As a result, in this chapter, we simply define a generic Factor of Altruism (FA) for modelling the MSN users' behaviour, which represents the probability of a MSN user forwarding a packet to the hitherto unserved peers.

3.1.3 Novel Contributions

Our novel contributions of this chapter are summarised as follows:

- A hybrid content dissemination approach is proposed, which relies both on BS-aided multicast [113] and on MSN group multicast aided content dissemination. This process is modelled by a *Pure-Birth based Markov Chain (PBMC)*. Various factors that might affect the performance of the content dissemination are accounted for, including the varying PL incurred by users' mobility, the multipath fading and the users' altruistic versus selfish behaviours.
- Considering a specific packet of the commonly interested content, we analyse the statistical properties

[3] A similar idea of improving BS-aided multicast was originally proposed in [111], which was mainly focused on the selection of the initial receivers. However, the authors of [111] ignore the performance analysis of the content dissemination stage.

[4] The new Wi-Fi protocols, such as 802.11n/ac [53], are capable of supporting a transmission range of hundreds of meters.

of the dissemination delay, which is the time from the BS multicasting a packet until all the MSN users receive this packet. We also analyse the individual user-delay, which is the time duration from the BS multicasting packet until a specific MSN user receives this packet, along with the individual transmit time, which is defined as the time duration of a specific MSN user remaining actively operational after it successfully receives the packet until the packet dissemination across the MSN group is completed.

- We analyse the total energy dissipated during exhaustively disseminating a specific packet to all the users in a MSN group, along with the average individual user-energy, namely that is dissipated by a single MSN user during both the packet reception phase and the packet forwarding phase.
- We also evaluate the tele-traffic off-loading ratio, which is defined as the number of packet replicas delivered by the MSN normalised by the total number of packet replicas generated.
- We further evaluate both the above-mentioned delay metrics and energy metrics in the scenario that all the MSN users in the target MSN group move within a bounded circular area by obeying the uniform mobility model and those metrics in the scenario that all the MSN users move in a realistic subway station.

3.1.4 Chapter Organisation

The rest of the chapter is organised as follows:

- In Section 3.2, we introduce our system model from the perspectives of the PHYsical (PHY) layer, the network layer and the Medium-Access-Control (MAC) layer.
- In Section 3.3, we model the process of disseminating a single packet across a MSN group by a PBMC and derive both the average as well as the variance of various delay metrics in closed-form. Furthermore, we also approximate the Tail Distribution Function (TDF) by a Gamma distribution for generic scenarios.
- In Section 3.4, we quantify the total energy consumed by exhaustively disseminating a packet across a MSN group as well as the energy dissipated by an individual user during the packet dissemination process by jointly considering both the transmission energy and signal processing energy.
- In Section 3.5, we evaluate the capability of the MSN group to off-load the tele-traffic from the congested cellular networks.
- In Section 3.6, we present both our analytical and simulation results for the delay and energy metrics as well as the tele-traffic off-loading ratio when the MUs of the MSN group move within a circular area by obeying the uniform mobility model. Furthermore, we evaluate the traffic overhead required for realising our content dissemination scheme.
- In Section 3.7, both the delay and energy metrics of our content dissemination scheme are evaluated in a realistic subway scenario.
- In Section 3.8, we conclude this chapter.

3.2 System Overview

3.2.1 Network Layer

We assume that N users form a MSN group in order to request the content of common interest from a BS, as shown in Figure 3.1. The formation of a MSN group depends on the following conditions:

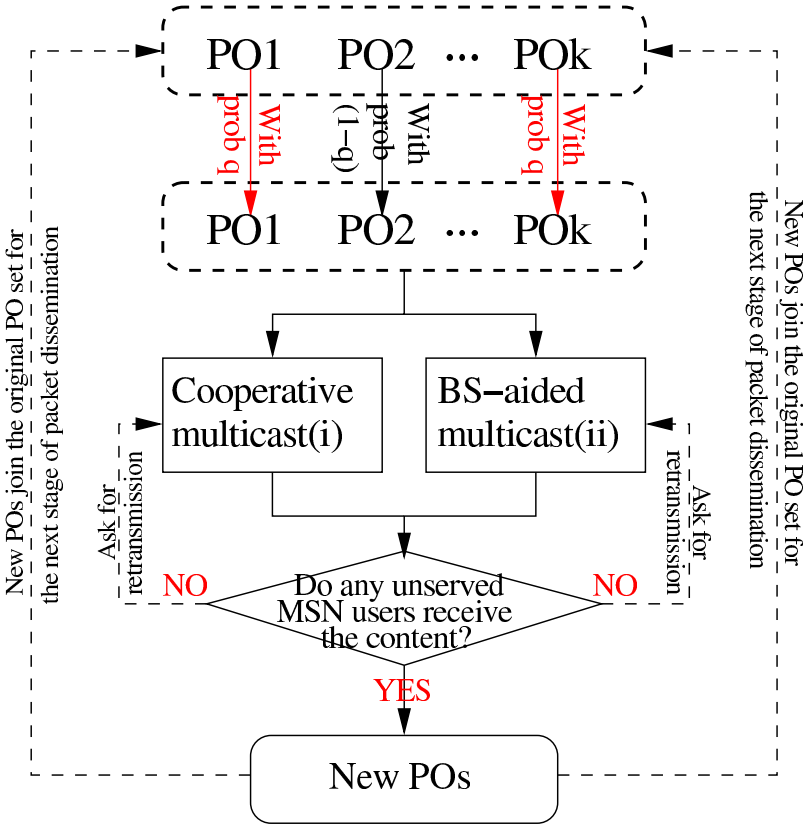

Figure 3.2: Actions of POs during the spontaneous content dissemination

- MUs share the same interest in the content;
- The content of common interest is of delay-sensitive nature;
- MUs roam in a bounded area having a relatively small size.

Then, the BS creates a specific queue for buffering all the packets of the requested content and prepares for disseminating these packets one by one, as described below.

Firstly, the BS is employed for repeatedly multicasting the packet currently at the head of the buffer, until at least one of the MSN users successfully receives it. Then, this packet is cooperatively disseminated across the MSN group using multicast techniques.

During the dissemination process, after successfully receiving the packet, the Packet Owners (POs) may make decisions independently as to whether they would or would not forward the packet during the following stage of the dissemination, as shown in Figure 3.2. Once some POs decide to further forward the packet, they would repeatedly multicast it until at least one unserved MSN user successfully receives it. Afterwards, the new POs join the original PO set. Both the new POs and original POs make the packet forwarding decision again for the subsequent stage of dissemination. The probability of a PO willing to forward the packet is denoted as q ($0 \leq q \leq 1$), which is termed as the Factor of Altruism (FA). At a given instant, there might not be any POs willing to further forward the packet. As a result, the unserved MSN users have to receive the packet directly from the BS. Similarly, the BS repeatedly multicasts the packet until at least one unserved MSN user receives it.

During the content dissemination process, similar to the conventional BS-aided multicast, the BS keeps a specific packet at the head of the buffer, until all the MSN users successfully receive it. Then the packet is dropped from the buffer and the BS is ready to disseminate the subsequent one. Therefore, only a single

packet type exists in the target MSN group. All the control signalling exchange required by our scheme is carried out by the BS. Please refer to Section 6.4 for the details of the control overhead traffic generated by our content dissemination scheme.

3.2.2 Physical Layer

In the PHY layer, the radio propagation between any pair of transmitter and receiver is assumed to experience uncorrelated stationary Rayleigh flat-fading. Hence, the square of the fading amplitudes given by $|h_l(t)|^2$ during the t-th Time Slot (TS) obeys an *exponential distribution* having a unity mean, whose TDF is $P[|h_l(t)|^2 > x] = \mathrm{e}^{-x}$. Given an arbitrary distance y_l in meters, the PL Ω_l is expressed as [114]:

$$\Omega_l(y_l) = \begin{cases} 1, & y_l < d_0, \\ \left(\frac{4\pi f_{l,c}}{c}\right)^{\kappa} y_l^{\kappa}, & y_l \geq d_0, \end{cases} \tag{3.1}$$

where c is the speed of light and $f_{l,c}$ is the carrier frequency, whereas κ is the PL exponent and d_0 is the distance from the transmitter to the 'near-field' edge.

The random distance Y_l is determined by the mobility pattern of the MSN users. The following mobility model is invoked for our performance analysis:

Definition 3.1 (Uniform mobility model)**.** *The position of the i-th MSN user during the t-th time interval is denoted by $\mathbf{P}_i(t)$, which obeys a stationary and ergodic process having a uniform distribution in the area considered. Moreover, the positions of different MSN users are independently and identically distributed (i.i.d.).*

This mobility model has been widely adopted for the performance analysis of MANETs [115] [116]. The Probability Density Function (PDF) of the random distance Y_l is denoted by $f_{Y_l}(y_l)$. Our performance modelling is not only applicable for the uniform mobility model. Any PDF of the random distance incurred by a specific mobility model can be invoked in our analytical model.

Note that, the index l is a generic subscript, which represents 'b' when the BS is the transmitter, while it represents 's' when a MSN user is the transmitter. In the rest of the chapter, 'l', 'b' and 's' hold the same meaning.

3.2.3 Medium-Access-Control Layer

During a TS, a packet of the content is assumed to be successfully received by a MSN user, provided that the instantaneous received Signal-to-Noise-Ratio (SNR) is higher than a predefined threshold γ [117]. In order to avoid collisions amongst multiple transmitters, in the MAC layer, Orthogonal-Frequency-Division-Multiple-Access (OFDMA) or Code-Division-Multiple-Access (CDMA) may be invoked for allocating each transmitter an orthogonal channel. We denote the Successful Packet Reception Probability (SPRP) of a link by $\mu_l(y_l)$. By jointly considering the PHY layer model, the SPRP is derived as

$$\begin{aligned} \mu_l(y_l) &= P\left(P_l^{tx}|h_l(t)|^2 \Big/ \Omega_l(y_l) N_0 W_l > \gamma\right) \\ &= \begin{cases} \mathrm{e}^{-\frac{\gamma N_0 W_l}{P_l^{tx}}}, & y_l < d_0, \\ \mathrm{e}^{-\frac{\gamma N_0 W_l}{P_l^{tx}}\left(\frac{4\pi f_c}{c}\right)^{\kappa} y_l^{\kappa}}, & y_l \geq d_0, \end{cases} \end{aligned} \tag{3.2}$$

where P_l^{tx} is the corresponding transmit power and $N_0 W_l$ is the noise power in a communication bandwidth W_l. Given the PDF $f_{Y_l}(y_l)$ of the random distance Y_l, the average SPRP $\overline{\mu}_l$ of a link is derived as

$$\overline{\mu}_l = \int_0^{d_0} \mathrm{e}^{-\frac{\gamma N_0 W_l}{P_l^{tx}}} f_{Y_l}(y_l) dy_l + \int_{y_l \geq d_0} \mathrm{e}^{-\frac{\gamma N_0 W_l}{P_l^{tx}}\left(\frac{4\pi f_c}{c}\right)^{\kappa} y^{\kappa}} f_{Y_l}(y_l) dy_l. \tag{3.3}$$

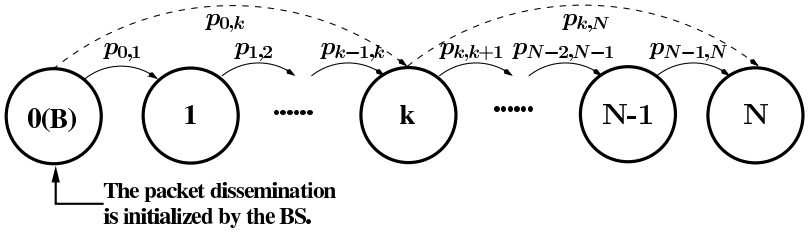

Figure 3.3: A pure-birth based Markov chain having an absorption state

Substituting the corresponding parameters and the PDF of the random distance into Eq.(3.3), we can obtain the average SPRP $\overline{\mu}_s$ between a pair of MSN users and $\overline{\mu}_b$ between the BS and the MSN user. Moreover, the following lemma is proposed for our further analysis:

Lemma 3.1. *Given the average SPRP $\overline{\mu}_l$ of a link during a TS, the average SPRP during a sufficiently short time interval Δt ($\Delta t \ll 1$ TS) is approximately $\overline{\mu}_l \Delta t$.*

Proof. The proof can be found in Appendix A. □

Note that the SPRP also represents the *normalized throughput*, whose unit is packet/TS [117]. In more details, $\overline{\mu}_l$ indicates that $\overline{\mu}_l$ packets in average can be successfully received during a TS. Therefore, during Δt (≤ 1) TS, only $\overline{\mu}_l \Delta t$ packets in average can be successfully received.

3.3 Delay Analysis of the Packet Dissemination Process

3.3.1 Pure-Birth based Markov Chain

During the process of packet dissemination across the target MSN group, the number of POs steadily increases until all the MSN users successfully receive the packet. Hence, the packet dissemination process can be modelled by a discrete-time PBMC, as shown in Figure 3.3. In this PBMC, the states represents the corresponding number of POs having received the packet. State transitions only occur from a lower-indexed state to a higher-indexed one. Specifically, the state transition emerges from state 0, which represents the initial stage of the BS-aided multicast, and terminates in state N, which indicates that all the MSN users in the target MSN group have received the desired packet.

Let us first consider the general state transition probability from state k to state $(k+m)$, where $1 \leq k \leq (N-1)$ and $0 \leq m \leq (N-k)$. In the light of selfish user-behaviour, we assume that only n_k, $1 \leq n_k \leq k$, POs are willing to further disseminate the content in the current stage. Therefore, any unserved MSN user out of the $(N-k)$ unserved ones is connected to the n_k POs by n_k wireless links, and any of these links has the probability of $\overline{\mu}_s \Delta t$ to successfully deliver the packet during the time interval Δt according to *Lemma 1*. As a result, given that n_k POs independently deliver their packets to the same target, the SPRP of an unserved MSN user is expressed as $[1-(1-\overline{\mu}_s \Delta t)^{n_k}]$. Furthermore, the state transition probability $p_{k,k+m|n_k \neq 0}$, which is also the probability of m out of the $(N-k)$ unserved MSN users successfully receiving the packet

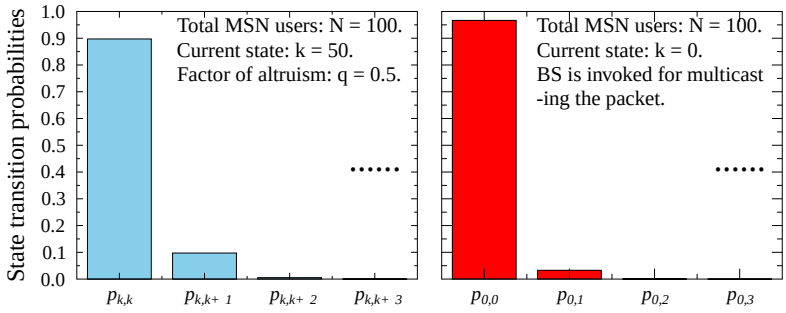

Figure 3.4: State transition probabilities when $\Delta t = 0.001$ TS

during the current time interval Δt, is expressed as

$$\begin{aligned} p_{k,k+m|n_k\neq 0} &= \binom{N-k}{m}\left[1-(1-\overline{\mu}_s\Delta t)^{n_k}\right]^m(1-\overline{\mu}_s\Delta t)^{n_k(N-k-m)} \\ &= \binom{N-k}{m}\left[1-\sum_{i=0}^{n_k}\binom{n_k}{i}(-\overline{\mu}_s\Delta t)^i\right]^m(1-\overline{\mu}_s\Delta t)^{n_k(N-k-m)} \\ &= \binom{N-k}{m}\left[\sum_{i=1}^{n_k}\binom{n_k}{i}(-1)^{i+1}(\overline{\mu}_s\Delta t)^i\right]^m(1-\overline{\mu}_s\Delta t)^{n_k(N-k-m)} \\ &= O(\overline{\mu}_s^m\Delta t^m) \end{aligned} \tag{3.4}$$

where $O(\overline{\mu}_s^m\Delta t^m)$ represents that the state transition probability $p_{k,k+m|n_k\neq 0}$ has the same growth rate as $\overline{\mu}_s^m\Delta t^m$. Therefore, when $m=0$, we obtain the probability of the PBMC retaining in the current state k after Δt, which is $p_{k,k|n_k\neq 0} = (1-\overline{\mu}_s\Delta t)^{n_k(N-k)}$. By contrast, if $m=1$, we can derive from Eq.(3.4) that the adjacent-state transition probability of traversing from state k to state $(k+1)$ is

$$\begin{aligned} p_{k,k+1|n_k\neq 0} &= \binom{N-k}{1}\left[1-(1-\overline{\mu}_s\Delta t)^{n_k}\right](1-\overline{\mu}_s\Delta t)^{n_k(N-k-1)} \\ &= (N-k)\left[(1-\overline{\mu}_s\Delta t)^{n_k(N-k-1)}-(1-\overline{\mu}_s\Delta t)^{n_k(N-k)}\right] \\ &= (N-k)\left[n_k\overline{\mu}_s\Delta t+\sum_{i=2}^{n_k(N-k-1)}\binom{n_k(N-k-1)}{i}(-\overline{\mu}_s\Delta t)^i\right. \\ &\quad \left.-\sum_{j=2}^{n_k(N-k)}\binom{n_k(N-k)}{j}(-\overline{\mu}_s\Delta t)^j\right] \\ &= n_k(N-k)\overline{\mu}_s\Delta t+O(\overline{\mu}_s^2\Delta t^2). \end{aligned} \tag{3.5}$$

As shown in Eq.(3.4) and Eq.(3.5), both $O(\overline{\mu}_s^m\Delta t^m)$ and $O(\overline{\mu}_s^2\Delta t^2)$ are negligibly low, when $\overline{\mu}_s\Delta t$ is sufficiently small, provided that we have $m\geq 2$. As a result, the general state transition probability can be approximated as $p_{k,k+m|n_k\neq 0}\approx 0$ for $m\geq 2$, while the adjacent-state transition probability can be approximated as $p_{k,k+1|n_k\neq 0}\approx n_k(N-k)\overline{\mu}_s\Delta t$. In this case, the state-retention probability can be approximated as $p_{k,k|n_k\neq 0}\approx 1-n_k(N-k)\overline{\mu}_s\Delta t$.

Another scenario is that no POs are willing to forward the packet, indicating $n_k=0$. Then the $(N-k)$ unserved MSN users have to receive the packet directly from the BS. Similarly, we can also demonstrate that $p_{k,k+1|n_k=0}\approx(N-k)\overline{\mu}_b\Delta t$ and $p_{k,k|n_k=0}\approx 1-(N-k)\overline{\mu}_b\Delta t$, while $p_{k,k+m|n_k=0}\approx 0$ for $m\geq 2$, provided that $\overline{\mu}_b\Delta t$ is sufficiently small. Furthermore, it can be shown that $p_{0,1}\approx N\overline{\mu}_b\Delta t$, $p_{0,0}\approx 1-N\overline{\mu}_b\Delta t$ and $p_{0,m}\approx 0$ for $m\geq 2$, provided that $\overline{\mu}_b\Delta t$ is sufficiently small.

According to the PHY layer parameters in Table 3.1 of Section 3.6, we plot the state transition probabilities for state $k=50$ and for state $k=0$, respectively, in Figure 3.4. We observe from Figure 3.4 that the state transition probabilities of $p_{k,k+m}$ and $p_{0,m}$ for $m\geq 2$ are negligibly low, which demonstrates the high accuracy of the above approximations involved.

Therefore, assuming a sufficiently short time interval Δt, only adjacent-state transitions occur during the process modelled by the discrete-time PBMC, as shown in Figure 3.3.

3.3.2 Delay of the State Transition

In order to study the delay statistics of disseminating a specific packet, we first need to know the specific delay that the PBMC spends in a particular state, which is termed as the *state transition delay*. As a result, the following lemma may be formulated:

Lemma 3.2. *Given the state transition probability $\widetilde{\mu}_k\Delta t$ from the current state k to state $(k+1)$, the delay of the transition from state k to state $(k+1)$ obeys the exponential distribution with a mean of $1/\widetilde{\mu}_k$ TS, provided that Δt is sufficiently small. Here, $\widetilde{\mu}_k$ is termed as the transition rate.*

Proof. The proof can be found in Appendix B. □

Based on *Lemma* 3.2, the discrete-time PBMC seen in Figure 3.3 can be further simplified to a continuous-time PBMC, which only has adjacent-state transition. The transition rate of this continuous-time PBMC can be shown to be $p_{k,k+1}/\Delta t$, where $p_{k,k+1}$ is the adjacent-state transition probability derived in Section 3.3.1.

We first consider the delay T_k of the transition from state k to $(k+1)$, when $k \geq 1$. Since each PO has a probability q of forwarding the packet, in the current state k, the number n_k ($0 \leq n_k \leq k$) of POs willing to forward the packet obeys a Binomial distribution having a pair of parameters k and q, whose Probability Mass Function (PMF) is given by [94]

$$\Pr(n_k) = \binom{k}{n_k} q^{n_k}(1-q)^{k-n_k}, n_k = 0, 1, \cdots, k. \tag{3.6}$$

For the case of $n_k \neq 0$, we have $p_{k,k+1|n_k\neq 0} \approx n_k(N-k)\overline{\mu}_s\Delta t$. According to *Lemma* 3.2, the delay T_k of the transition from state k to state $(k+1)$ obeys an exponential distribution having a rate of $n_k(N-k)\overline{\mu}_s = n_k\mu_{s,k}$, where $\mu_{s,k} = (N-k)\overline{\mu}_s$. Hence, when $n_k \neq 0$, the conditional PDF, the mean and the second moment of T_k may be formulated as

$$f_{T_k|n_k}(t_k) = n_k\mu_{s,k} \cdot \mathrm{e}^{-n_k\mu_{s,k}t_k},\ t_k \geq 0 \tag{3.7}$$

$$\mathcal{E}\left[T_k|n_k\right] = \int_0^\infty t_k f_{T_k|n_k}(t_k)dt_k = \frac{1}{n_k\mu_{s,k}}, \tag{3.8}$$

$$\mathcal{E}\left[T_k^2|n_k\right] = \int_0^\infty t_k^2 f_{T_k|n_k}(t_k)dt_k = \frac{2}{(n_k\mu_{s,k})^2}. \tag{3.9}$$

For the case of $n_k = 0$, we have $p_{k,k+1|n_k=0} \approx (N-k)\overline{\mu}_b\Delta t$, as the MSN users have to receive the packet from the BS. According to *Lemma* 3.2, the delay T_k of the transition from state k to $(k+1)$ obeys an exponential distribution having a rate of $\mu_{b,k} = (N-k)\overline{\mu}_b$. Hence, given $n_k = 0$, the conditional PDF, the mean and the second moment of T_k are derived as

$$f_{T_k|n_k=0}(t_k) = \mu_{b,k} \cdot \mathrm{e}^{-\mu_{b,k}t_k},\ t_k \geq 0 \tag{3.10}$$

$$\mathcal{E}\left[T_k|n_k=0\right] = \int_0^\infty t_k f_{T_k|n_k=0}(t_k)dt_k = \frac{1}{\mu_{b,k}}, \tag{3.11}$$

$$\mathcal{E}\left[T_k^2|n_k=0\right] = \int_0^\infty t_k^2 f_{T_k|n_k=0}(t_k)dt_k = \frac{2}{\mu_{b,k}^2}. \tag{3.12}$$

According to the classic Bayesian principle [94], the PDF of T_k may be expressed as

$$\begin{aligned} f_{T_k}(t_k) &= f_{T_k|n_k=0}(t_k)\cdot \Pr(n_k=0) + \sum_{n_k=1}^{k} f_{T_k|n_k}(t_k)\cdot \Pr(n_k) \\ &= (1-q)^k \mu_{b,k} \mathrm{e}^{-\mu_{b,k} t_k} \\ &+ \sum_{n_k=1}^{k} \binom{k}{n_k} q^{n_k}(1-q)^{k-n_k}\cdot n_k \mu_{s,k} \mathrm{e}^{-n_k \mu_{s,k} t_k}. \end{aligned} \tag{3.13}$$

Moreover, the mean and the second moment of T_k are formulated as

$$\begin{aligned} \mathcal{E}\Big[T_k\Big] &= \mathcal{E}\Big[T_k\Big|n_k=0\Big]\Pr(n_k=0) + \sum_{n_k=1}^{k} \mathcal{E}\Big[T_k\Big|n_k\Big]\Pr(n_k) \\ &= \frac{(1-q)^k}{\mu_{b,k}} + \sum_{n_k=1}^{k} \binom{k}{n_k} \frac{q^{n_k}(1-q)^{k-n_k}}{n_k \mu_{s,k}}, \end{aligned} \tag{3.14}$$

$$\begin{aligned} \mathcal{E}\Big[T_k^2\Big] &= \mathcal{E}\Big[T_k^2\Big|n_k=0\Big]\Pr(n_k=0) + \sum_{n_k=1}^{k} \mathcal{E}\Big[T_k^2\Big|n_k\Big]\Pr(n_k) \\ &= \frac{2(1-q)^k}{\mu_{b,k}^2} + \sum_{n_k=1}^{k} \binom{k}{n_k} \frac{2q^{n_k}(1-q)^{k-n_k}}{(n_k \mu_{s,k})^2}. \end{aligned} \tag{3.15}$$

Hence, we can also derive the variance of T_k by using the formula of $Var[T_k] = \mathcal{E}[T_k^2] - \{\mathcal{E}[T_k]\}^2$. Furthermore, we may simply derive the PDF, the mean and the second moment of the transition delay T_0 from state 0 to state 1 by substituting $k=0$ into Eq.(3.10), Eq.(3.11), and Eq.(3.12), respectively.

3.3.3 Dissemination Delay

Since the delay of the transition from a state to its successor is independent of any other state transition's delay, and given that the dissemination delay across the MSN group is defined as $T_D = \sum_{k=0}^{N-1} T_k$, the mean of T_D can be expressed as

$$\mathcal{E}[T_D] = \sum_{k=0}^{N-1} \frac{(1-q)^k}{\mu_{b,k}} + \sum_{k=1}^{N-1} \sum_{n_k=1}^{k} \binom{k}{n_k} \frac{q^{n_k}(1-q)^{k-n_k}}{n_k \mu_{s,k}}, \tag{3.16}$$

while the variance of T_D can be formulated as $Var[T_D] = \sum_{k=0}^{N-1} Var[T_k]$.

Unfortunately, there is no exact closed-form TDF for the dissemination delay T_D in this general case. However, when given its mean and variance, we may approximate it as a variable obeying the *Gamma distribution*, which is usually more accurate than its Gaussian counterpart, when non-negative random variables are concerned [118]. According to the theory of the Gamma distribution [119], it is uniquely and unambiguously described by its *shape parameter* $m = \{\mathcal{E}[T_D]\}^2 / Var[T_D]$ and *scale parameter* $\theta = Var[T_D]/\mathcal{E}[T_D]$. Then, given a delay threshold D_{th}, we may derive the approximate probability of the dissemination delay T_D exceeding D_{th} as

$$P(T_D > D_{th}) \approx \frac{\Gamma\left(m, \frac{D_{th}}{\theta}\right)}{\Gamma(m)} = \frac{\Gamma\left(\frac{\{\mathcal{E}[T_D]\}^2}{Var[T_D]}, \frac{D_{th}\mathcal{E}[T_D]}{Var[T_D]}\right)}{\Gamma\left(\frac{\{\mathcal{E}[T_D]\}^2}{Var[T_D]}\right)}. \tag{3.17}$$

The accuracy of Eq.(3.17) will be verified by our simulation results in Section 3.6. The exact TDFs for two special cases of $q=0$ and $q=1$ are provided in Appendix 3.C.

3.3.4 Individual User-Delay

A specific MSN user $\mathcal{A}$ may receive the packet at any state spanning from 1 to N during the process of state transitions. When considering the transition from state $(k-1)$ to k $(1 \le k \le N)$, any of the $(N-k+1)$

unserved MSN users may successfully receive the packet with a probability of $1/(N-k+1)$, and may not receive it with a probability of $(N-k)/(N-k+1)$. Specifically, the probability of $\mathcal{A}$ receiving the packet in state k, which naturally implies that $\mathcal{A}$ has not received the content at any of the previous states, may be expressed as

$$\Pr_k = \frac{1}{N-k+1} \cdot \prod_{i=1}^{k-1} \frac{N-i}{N-i+1} = \frac{1}{N}, 1 \leq k \leq N. \tag{3.18}$$

Hence, given that $\mathcal{A}$ receives the packet in state k, the individual user-delay of $\mathcal{A}$ is expressed as $T_{\mathcal{A}|k} = \sum_{j=0}^{k-1} T_k$ and the conditional PDF of $T_{\mathcal{A}|k}$ is expressed as $f_{T_{\mathcal{A}}|k}(t_{\mathcal{A}}) = f_{T_0+\cdots+T_{k-1}}(t_{\mathcal{A}})$. According to the Bayesian principle [94], the PDF of the individual user-delay $T_{\mathcal{A}}$ can be expressed as:

$$f_{T_{\mathcal{A}}}(t_{\mathcal{A}}) = \sum_{k=1}^{N} f_{T_{\mathcal{A}}|k}(t_{\mathcal{A}}) \cdot \Pr_k = \sum_{k=1}^{N} \frac{f_{T_0+\cdots+T_{k-1}}(t_{\mathcal{A}})}{N}. \tag{3.19}$$

Furthermore, owing to the fact that $\{T_0, T_1, \cdots, T_{k-1}\}$ are independent of each other, the average of $T_{\mathcal{A}}$ can be obtained as

$$\begin{aligned} \mathcal{E}[T_{\mathcal{A}}] &= \int_0^{\infty} t_{\mathcal{A}} \sum_{k=1}^{N} \frac{f_{T_0+\cdots+T_{k-1}}(t_{\mathcal{A}})}{N} dt_{\mathcal{A}} = \sum_{k=1}^{N} \frac{1}{N} \cdot \sum_{i=0}^{k-1} \mathcal{E}\left[T_i\right] \\ &= \sum_{k=1}^{N} \frac{N-k+1}{N} \mathcal{E}\left[T_{k-1}\right], \end{aligned} \tag{3.20}$$

where $\mathcal{E}\left[T_{k-1}\right]$ is given by Eq.(3.14). Furthermore, the second moment of $T_{\mathcal{A}}$ is given by

$$\begin{aligned} \mathcal{E}[T_{\mathcal{A}}^2] &= \int_0^{\infty} \sum_{k=1}^{N} \frac{t_{\mathcal{A}}^2 f_{T_0+\cdots+T_{k-1}}(t_{\mathcal{A}})}{N} dt_{\mathcal{A}} \\ &= \sum_{k=1}^{N} \frac{\mathcal{E}\left[(T_0+T_1+\cdots+T_{k-1})^2\right]}{N} = \sum_{k=1}^{N} \sum_{i,j=0}^{k-1} \frac{\mathcal{E}[T_i T_j]}{N} \\ &= \sum_{k=1}^{N} \frac{N-k+1}{N} \mathcal{E}[T_{k-1}^2] + \sum_{k=1}^{N} \frac{\boldsymbol{\xi}_k^T \left[\mathbf{H}_k - \mathbf{I}_k\right] \boldsymbol{\xi}_k}{N}, \end{aligned} \tag{3.21}$$

where $\boldsymbol{\xi}_k = (\mathcal{E}[T_0], \mathcal{E}[T_1], \cdots, \mathcal{E}[T_{k-1}])^T$, $\mathbf{H}_k$ is a $k \times k$ matrix, whose elements are all ones, and $\mathbf{I}_k$ is a $k \times k$ identity matrix. Consequently, the variance of $T_{\mathcal{A}}$ can be expressed as $Var(T_{\mathcal{A}}) = \mathcal{E}[T_{\mathcal{A}}^2] - \{\mathcal{E}[T_{\mathcal{A}}]\}^2$. Hence, by substituting $\mathcal{E}[T_{\mathcal{A}}]$ and $Var[T_{\mathcal{A}}]$ into Eq.(3.17), we may obtain the approximate probability of $T_{\mathcal{A}}$ exceeding a delay threshold D_{th}.

3.3.5 Individual Transmit Time

After the specific MSN user $\mathcal{A}$ receives the desired packet, $\mathcal{A}$ might forward the packet to the unserved MSN users during the transition from state j to state $(j+1)$. This event is denoted by a Bernoulli-distributed variable $\mathcal{H}_{\mathcal{A},j} = 1$ having a probability of $\Pr(\mathcal{H}_{\mathcal{A},j} = 1) = q$. Otherwise, $\mathcal{A}$ remains silent during this state transition, which is denoted by the event $\mathcal{H}_{\mathcal{A},j} = 0$ having a probability of $\Pr(\mathcal{H}_{\mathcal{A},j} = 0) = 1-q$. Given that $\mathcal{A}$ actively transmits during the transition from state j to state $(j+1)$, and assuming that we have another n_j' POs who cooperate with $\mathcal{A}$ for forwarding the content, similarly to Eq.(3.8), the average state transition delay is expressed as

$$\mathcal{E}[T_j | \mathcal{H}_{\mathcal{A},j} = 1, n_j'] = \frac{1}{(1+n_j')\mu_{s,j}}. \tag{3.22}$$

Moreover, the probability that we have n_j' POs cooperate with $\mathcal{A}$ for forwarding the packet is given by the PMF of a Binomial distribution, which is formulated as

$$\Pr(n_j') = \binom{j-1}{n_j'} q^{n_j'} (1-q)^{j-1-n_j'}. \tag{3.23}$$

According to the classic Bayesian principle [94], we may derive the average state transition delay T_j given that $\mathcal{A}$ forwards the content during this state transition as

$$\begin{aligned}\mathcal{E}[T_j|\mathcal{H}_{\mathcal{A},j}=1] &= \sum_{n'_j=0}^{j-1}\mathcal{E}[T_j|\mathcal{H}_{\mathcal{A},j}=1,n'_j]\Pr(n'_j)\\ &= \sum_{n'_j=0}^{j-1}\binom{j-1}{n'_j}\frac{q^{n'_j}(1-q)^{j-1-n'_j}}{(1+n'_j)\mu_{s,j}}.\end{aligned} \tag{3.24}$$

Furthermore, the average individual transmit time $T_{W,j}$ of $\mathcal{A}$ during the transition from state j to $(j+1)$ is expressed as

$$\begin{aligned}\mathcal{E}[T_{W,j}] &= \mathcal{E}[T_j|\mathcal{H}_{\mathcal{A},j}=1]\Pr(\mathcal{H}_{\mathcal{A},j}=1)+0\times\Pr(\mathcal{H}_{\mathcal{A},j}=0)\\ &= \sum_{n'_j=0}^{j-1}\binom{j-1}{n'_j}\frac{q^{1+n'_j}(1-q)^{j-1-n'_j}}{(1+n'_j)\mu_{s,j}}.\end{aligned} \tag{3.25}$$

Assuming that $\mathcal{A}$ successfully receives the content in state k ($1\le k\le N-1$), then the average individual transmit time of user $\mathcal{A}$ is expressed as $\mathcal{E}[T_W|k]=\mathcal{E}[T_{W,k}]+\mathcal{E}[T_{W,k+1}]+\cdots+\mathcal{E}[T_{W,N-1}]$. Naturally, if $\mathcal{A}$ receives the packet in state N, we have $\mathcal{E}[T_W|N]=0$. Owing to the Bayesian principle [94] and by exploiting the fact that the probability of $\mathcal{A}$ receiving the packet in state k ($1\le k\le N$) is $\Pr_k=1/N$ as well as the fact that $\{T_{W,j}, j=1,\cdots,N-1\}$ are independent of each other, the average individual transmit time is formulated as

$$\begin{aligned}\mathcal{E}[T_W] &= \sum_{k=1}^{N}\mathcal{E}[T_W|k]\Pr_k\\ &= \sum_{k=1}^{N-1}\frac{1}{N}\sum_{j=k}^{N-1}\mathcal{E}[T_{W,j}]=\sum_{k=1}^{N-1}\frac{k}{N}\mathcal{E}[T_{W,k}],\end{aligned} \tag{3.26}$$

where the second equality is derived since $\mathcal{E}[T_W|N]=0$ and $\mathcal{E}[T_{W,k}]$ is given by Eq.(3.25).

3.4 Energy Dissipation of the Packet Dissemination

Let us assume that, a transmitter assigns P_l^{tx} power to the signal, as discussed in Section 3.2.3, while the receiver consumes P_l^{rx} signal processing power [120] [121] for recovering a received packet, regardless of whether it can or cannot be correctly recovered, which is often much lower than P_l^{tx} in wireless communications.

3.4.1 Total Energy Dissipation

Let us first derive the energy consumed during a transition from state k to state $(k+1)$, as shown in Figure 3.3. Given the current state k, we have $(N-k)$ unserved MSN users waiting for the packet. If there are $n_k(\neq 0)$ POs willing to forward the packet, the total transmit power consumed by these transmitters is $n_kP_s^{tx}$, while $n_kP_s^{rx}$ power is consumed by each receiver during processing the n_k packets sent by these transmitters. Hence the total power consumed by the $(N-k)$ unserved MSN users for processing these packets is $n_k(N-k)P_s^{rx}$. Therefore, given $n_k\neq 0$, the total power consumption of this state transition is $P_{k|n_k}=n_kP_s^{tx}+n_k(N-k)P_s^{rx}$. If no POs are willing to forward the packet, the BS is the sole transmitter of the desired packet and the unserved MSN users only have to process the packet sent by the BS. Therefore, given $n_k=0$, the total power consumption for this state transition is $P_{k|n_k=0}=P_b^{tx}+(N-k)P_s^{rx}$. Then,

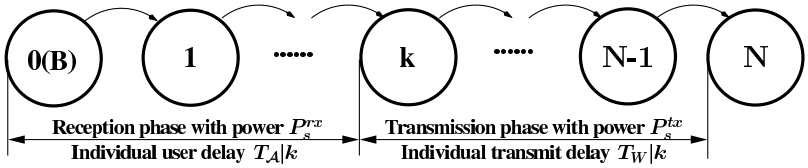

Figure 3.5: Reception/Transmission phases for a MSN user

the average energy dissipation $\mathcal{E}[E_k]$ of the transition from state k to $(k+1)$ can be formulated as

$$\begin{aligned}\mathcal{E}[E_k] &= \sum_{n_k=0}^{k} P_{k|n_k}\mathcal{E}[T_k|n_k]\Pr(n_k) \\ &= \frac{(1-q)^k\left[P_b^{tx}+(N-k)P_s^{rx}\right]}{\mu_{b,k}} \\ &\quad + \sum_{n_k=1}^{k}\binom{k}{n_k}\frac{q^{n_k}(1-q)^{k-n_k}\left[P_s^{tx}+(N-k)P_s^{rx}\right]}{\mu_{s,k}},\end{aligned} \tag{3.27}$$

where the second equality is derived by substituting Eqs.(3.6) (3.8) and (3.11) into the first line of Eq.(3.27). All the metrics related to energy dissipation are quantified in terms of "Watt(W)·TS" or "mW·TS", where TS is the number of time slots.

Since the energy consumption Eq.(3.27) of the transition from a state to its successor is an independent random variable, the average total energy dissipated for disseminating the packet to all the MUs in the MSN group is formulated as

$$\begin{aligned}\mathcal{E}[E_D] = \sum_{k=0}^{N-1}\mathcal{E}[E_k] &= \underbrace{\sum_{k=0}^{N-1}\frac{(1-q)^k P_b^{tx}}{\mu_{b,k}}}_{\mathcal{E}[E_b^{tx}]} + \underbrace{\sum_{k=1}^{N-1}\sum_{n_k=1}^{k}\binom{k}{n_k}\frac{q^{n_k}(1-q)^{k-n_k}P_s^{tx}}{\mu_{s,k}}}_{\mathcal{E}[E_s^{tx}]} \\ &\quad + \underbrace{P_s^{rx}\left\{\sum_{k=0}^{N-1}\frac{(1-q)^k}{\overline{\mu}_b} + \sum_{k=1}^{N-1}\sum_{n_k=1}^{k}\binom{k}{n_k}\frac{q^{n_k}(1-q)^{n_k}}{\overline{\mu}_s}\right\}}_{\mathcal{E}[E_s^{rx}]},\end{aligned} \tag{3.28}$$

where we have $\mu_{b,k} = (N-k)\overline{\mu}_b$ and $\mu_{s,k} = (N-k)\overline{\mu}_s$. Note that in Eq.(3.28), $\mathcal{E}[E_b^{tx}]$ is the average energy dissipated by the BS during the packet dissemination process, $\mathcal{E}[E_s^{tx}]$ is the average energy dissipated by the MSN users during the transmission phase, while $\mathcal{E}[E_s^{rx}]$ is the average energy dissipated by the MSN users during the reception phase.

3.4.2 Individual Energy Dissipation

An individual MSN user $\mathcal{A}$ may experience two phases sequentially during the dissemination of a single packet, namely the packet reception phase and the packet transmission phase, as shown in Figure 3.5. Given the current state k, the power consumed by an individual MSN user during its packet reception phase is $P_{\mathcal{A},k|n_k}^{rx} = n_k P_s^{rx}$, provided that $n_k(\neq 0)$ POs are willing to forward the packet. Otherwise, the power consumption of an individual MSN user during its packet reception phase is $P_{\mathcal{A},k|n_k=0}^{rx} = P_s^{rx}$. As a result, provided that an individual MSN user has not successfully received the desired packet, the individual energy dissipation of packet reception during the transition from state k to state $(k+1)$ is expressed as

$$\begin{aligned}\mathcal{E}[E_{\mathcal{A},k}^{rx}] &= \sum_{n_k=0}^{k} P_{\mathcal{A},k|n_k}^{rx}\mathcal{E}[T_k|n_k]\Pr(n_k) \\ &= \frac{(1-q)^k P_s^{rx}}{\mu_{b,k}} + \sum_{n_k=1}^{k}\binom{k}{n_k}\frac{q^{n_k}(1-q)^{k-n_k}P_s^{rx}}{\mu_{s,k}},\end{aligned} \tag{3.29}$$

where the second equality is derived by substituting Eqs.(3.6) (3.8) and (3.11) into the first line of Eq.(3.29).

Given that $\mathcal{A}$ successfully receives the packet in state k, the energy consumed by $\mathcal{A}$ during the reception phase is $E^{rx}_{\mathcal{A}}|k = \sum_{i=0}^{k-1} E^{rx}_{\mathcal{A},i}$. Since the transmission phase lasts for $T_W|k = \sum_{j=k}^{N-1} T_{W,j}$, the energy consumed by $\mathcal{A}$ during the transmission phase is $E^{tx}_{\mathcal{A}}|k = \sum_{j=k}^{N-1} E^{tx}_{\mathcal{A},j}$, where we have $E^{tx}_{\mathcal{A},j} = P^{tx}_s T_{W,j}$. Hence, the total conditional individual energy dissipation may be expressed as $E_{\mathcal{A}}|k = \sum_{i=0}^{k-1} E^{rx}_{\mathcal{A},i} + \sum_{j=k}^{N-1} E^{tx}_{\mathcal{A},j}$. Since the probability of an MSN user successfully receiving the packet in state k is $\Pr_k = \frac{1}{N}$ for $1 \leq k \leq N$, as shown in Eq.(3.18), the average individual energy dissipation $\mathcal{E}[E_I]$ is expressed as

$$\begin{aligned}\mathcal{E}[E_I] &= \sum_{k=1}^{N} \left\{ \sum_{i=0}^{k-1} \mathcal{E}[E^{rx}_{\mathcal{A},i}] + \sum_{j=k}^{N-1} \mathcal{E}[E^{tx}_{\mathcal{A},j}] \right\} \cdot \Pr_k \\ &= \underbrace{\sum_{k=1}^{N} \frac{N-k+1}{N} \mathcal{E}[E^{rx}_{\mathcal{A},k-1}]}_{\text{Reception phase}} + \underbrace{\sum_{k=1}^{N-1} \frac{k}{N} \mathcal{E}[E^{tx}_{\mathcal{A},k}]}_{\text{Transmission phase}}, \end{aligned} \tag{3.30}$$

where $\mathcal{E}[E^{rx}_{\mathcal{A},k-1}]$ is given by Eq.(3.29) and $\mathcal{E}[E^{tx}_{\mathcal{A},k}] = P^{tx}_s \mathcal{E}[T_{W,k}]$, whereas $\mathcal{E}[T_{W,k}]$ is given by Eq.(3.25).

3.5 Tele-Traffic Off-Loading Ratio

When the process of disseminating a specific packet to N MSN users is completed, N replicas are received by the N MSN users. Some of them might receive the copy from the BS, while others from their peers in the MSN group.

During a transition from state k to state $(k+1)$ $(0 \leq k \leq N-1)$, a single replica is successfully delivered to one of the unserved MSN users either via the POs with a probability of $\Pr(n_k \neq 0)$, or via the BS with a probability of $\Pr(n_k = 0)$. Hence, with the aid of Eq.(3.6), the expected number $\mathcal{R}_k$ of the replicas delivered by the POs during this state transition is expressed as $\mathcal{R}_k = 1 \times \Pr(n_k \neq 0) + 0 \times \Pr(n_k = 0) = 1 - (1-q)^k$. As a result, the expected number $\mathcal{R}_{MSN}$ of replicas off-loaded from the BSs to the MSN group is formulated as

$$\mathcal{R}_{MSN} = \sum_{k=0}^{N-1} \left[1 - (1-q)^k \right] = N - \frac{1-(1-q)^N}{q}, 0 < q \leq 1.$$

Finally, the tele-traffic off-loading ratio r_{MSN} may be defined as the ratio of

$$r_{MSN} = \frac{\mathcal{R}_{MSN}}{N} = 1 - \frac{1}{Nq} + \frac{(1-q)^N}{Nq}, 0 < q \leq 1. \tag{3.31}$$

From Eq.(3.31) we observe that if N tends to infinity, r_{MSN} tends to unity. Furthermore, when no POs are willing to forward the packet, which corresponds to $q = 0$, the tele-traffic off-loading ratio is $r_{MSN} = 0$. Additionally, we have $r_{MSN} = (N-1)/N$ when $q = 1$, since in this case the BS is only invoked during the first state transition.

3.6 Numerical Results For the Uniform Mobility Model

The parameters of the PHY layer are presented in Table 3.1. The specific parameters used for transmissions from the BSs to MSN users are in line with FDD-LTE standard[5], while the transmission parameters between the MSN users are in line with the commonly used 802.11 protocol [53]. Note that the signal processing

[5]We assume a 1.8 GHz carrier frequency in line with the LTE networks operated by the British company EE [122].

Table 3.1: PARAMETERS OF THE PHY LAYER

	BS to Users	Users to Users
Transmit Power	$P_b^{tx} = 31$ dBm	$P_s^{tx} = 0 \sim 10$ dBm
Sig. Pro. Power	N/A	$P_s^{rx} = 0.44mW$
Carrier Freq	$f_{c,b} = 1.8$ GHz	$f_{c,s} = 2.4$ GHz
Bandwidth	$W_b = 10$ MHz	$W_s = 10$ MHz
Noise PSD	$N_0 = -174$ dBm/Hz (20^oC)	
SNR Threshold	$\gamma = 10$ dB	
PL Parameters	Exponent: $\kappa = 3$; Ref Distance: $d_0 = 1$ m	

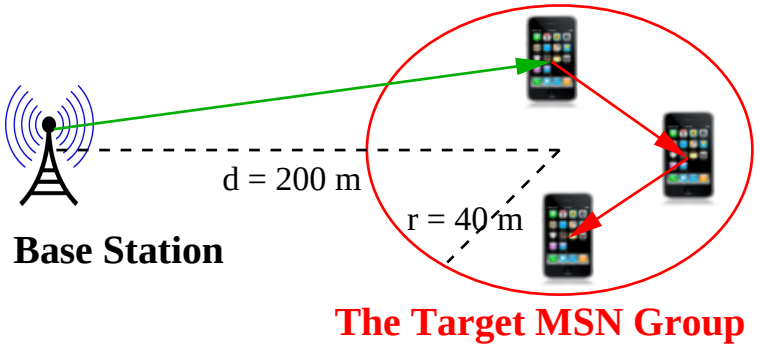

Figure 3.6: Geographic features for obtaining numerical results.

power required for recovering a contaminated packet is $P_s^{rx} = 0.44$ mW, which is in line with [120] and relies on the signal processing power reduction approach proposed in [121].

As shown in Figure 3.6, we assume that all users in the target MSN group roam in a circular area having a radius of $r = 40$ m by obeying the *uniform mobility model* of Section 3.2.2. The BS is $d = 200$ m away from the centre of the circular area. In this scenario, the PDF $f_{Y_s}(y_s)$ of the distance between a pair of MSN users is given by Eq.(23) of [123], and $f_{Y_b}(y_b)$ between the BS and a MSN user can be found in Theorem 6.3 of Chapter 6. Substituting $f_{Y_s}(y_s)$ and $f_{Y_b}(y_b)$ into Eq.(3.3), alongside the parameters offered in Table 3.1, we may obtain the average SPRP $\overline{\mu}_s$ and $\overline{\mu}_b$, which further leads us to the analytical (ana) results for the various metrics. If we let $q = 0$ in our model, the corresponding analytical results are derived for conventional BS-aided multicast.

In the network layer, the number of MSN users is assumed to vary from $N = 1$ to 100. In order to obtain a reliable statistical characterization of the simulation (sim) performance, we repeatedly run simulations 10 000 times and set the time-interval of our system to be $\Delta t = 0.001$ TS, where a TS can be considered as a packet duration. All the delay related metrics are evaluated by the number of TSs.

3.6.1 Delay Metric Evaluation

As shown in Figure 3.7, when FA $\neq 0$, the average dissemination delay firstly increases, as the number of MSN users is increased. When only a few users are in the MSN group, a longer period is required for disseminating the packet to all MSN users due to the increasing content demand of the unserved MSN users. However, by further increasing the number of MSN users, the diversity gain incurred by the cooperation of the multiple transmitters becomes sufficiently high to mitigate the adverse effect of the increasing content demand. As a result, we observe that the average dissemination delay decays after reaching its peak, as the number of MSN users is further increased. For example, for FA $= 0.2$, the delay is reduced by 53.5%, as the number of MSN users is increased from $N = 20$ to 60. Furthermore, a higher FA incurs a lower delay, since more POs are willing to forward the packet after they successfully receive it. For example, for $N = 20$, the average dissemination delay is reduced by 75.4%, as the FA is increased from 0.2 to 1. By contrast, when FA

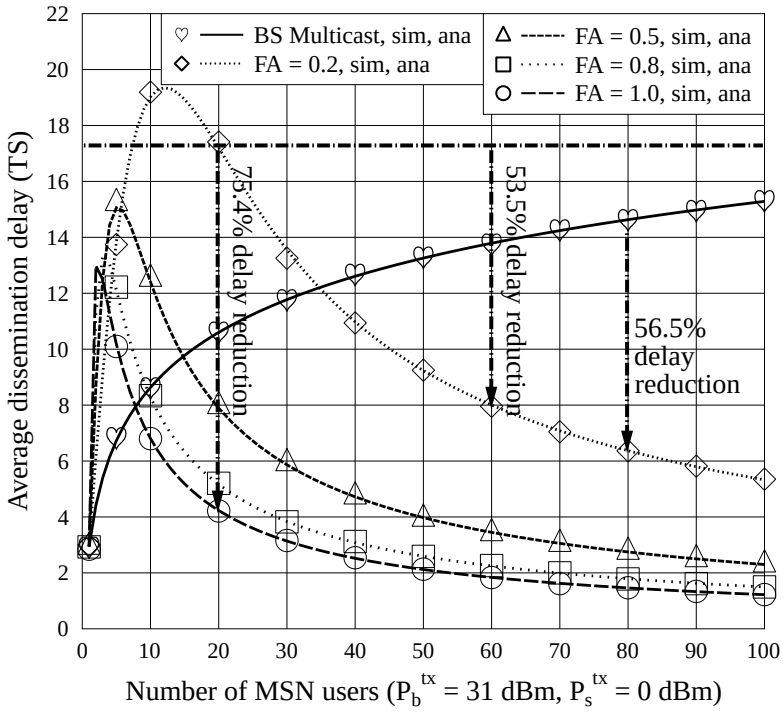

Figure 3.7: Average dissemination delay affected by the number of MSN users, which is parameterized by the FA. The number of the MSN users in the target MSN group varies from 1 to 100, while the FA takes value from $\{0.2, 0.5, 0.8, 1.0\}$. The transmit power of the MUs in the target MSN group is $P_s^{tx} = 0$ dBm and the other parameters related to the physical layer are provided by Table 3.1. The analytical results were evaluated from Eq.(3.16). Furthermore, the BS multicast scheme is used as a benchmark, whose analytical result can be derived by substituting FA $= 0$ into Eq.(3.16).

$= 0$, the conventional BS-aided multicast technique is invoked. However, as the number of the MSN users increases, the average dissemination delay also increases. We observe from Figure 3.7 that our approach is capable of reducing the average dissemination delay of the conventional BS-aided multicast by 56.5% for $N = 80$, when a small FA value of 0.2 is assumed.

As shown in Figure 3.8, when only a few users are in the MSN group and the FA is non-zero, due to the users' selfishness, fewer than two POs are willing to forward the packet during the dissemination process. Therefore, we observe from Figure 3.8 that the average individual user-delay initially increases, because it does not benefit from any diversity gain. However, as we further increase the number of MSN users, an increasing number of POs become willing to forward the packet, which substantially reduces the average individual user-delay, as observed from Figure 3.8. For example, for FA $= 0.2$, the average individual user-delay is reduced by 44.1%, as the number of MSN users is increased from $N = 20$ to 60. Nevertheless, when the conventional BS multicast is invoked, the average individual user-delay, which only relies on the link connecting this specific user to the BS, remains near-constant at 2.95 TS, as the number of MSN users increases. Furthermore, the average individual user-delay is improved, when we increase the value of the FA. For example, given $N = 20$ MSN users, the average individual user-delay is reduced by 60.6%, as the FA is increased from 0.2 to 1.0. Additionally, given $N = 80$ MSN users, the average individual user-delay drops from 2.95 TS to 1.3 TS, comparing the conventional BS multicast to our approach associated with FA$= 0.5$.

Observe in Figure 3.9(a)(b) that the probabilities of both the dissemination delay and individual user-delay exceeding a threshold of $D_{th} = 6$ TS reduce upon increasing the transmit power of each MSN user. Our Gamma-distribution-based approximations match the simulation results.

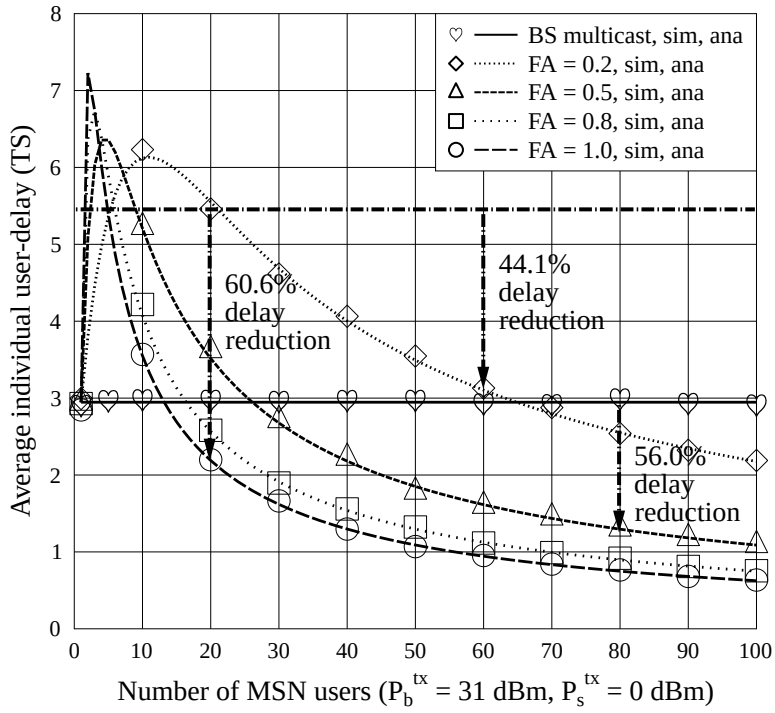

Figure 3.8: Average individual user-delay as a function of the number of MSN users, which is parameterized by the FA. The number of the MSN users in the target MSN group varies from 1 to 100, while the FA takes value from $\{0.2, 0.5, 0.8, 1.0\}$. The transmit power of the MUs in the target MSN group is $P_s^{tx} = 0$ dBm and the other parameters related to the physical layer are provided by Table 3.1. The analytical results were evaluated from Eq.(3.20). Furthermore, the BS multicast scheme is employed as a benchmark, whose analytical result can be derived by substituting FA$= 0$ into Eq.(3.20).

3.6.2 Energy Metric Evaluation

It is observed in Figure 3.10 that the average total energy dissipated by disseminating a packet is substantially reduced, as we increase the number of MSN users, provided that the FA is non-zero. This is because as the number of MSN users increases, a higher portion of the packet dissemination process is completed by the low-power cooperative dissemination amongst the MSN users, while the activation of the high-power BS-aided multicast becomes less frequent. For example, as shown in Figure 3.10, when FA $= 0.2$, we may achieve an 75.8% of energy reduction by increasing the number of MSN users from $N = 10$ to 40. If we further increase the number of MSN users, the total energy consumption becomes slightly higher. In this case, the major portion of the packet dissemination is completed by the MSN users themselves. Therefore, having more MSN users may result in a higher total energy dissipation. Moreover, having more altruistic MSN users results in a reduced total energy dissipation. As presented in Figure 3.10, for $N = 20$, a 77.6% energy reduction is achieved by increasing the FA from 0.2 to 1.0. Furthermore, as portrayed in the sub-figure, the conventional BS-aided multicast consumes a substantially higher amount of energy by multicasting the packet to all the MSN users. For example, for $N = 80$, our content dissemination scheme associated with FA $= 0.2$ may save 96% of the energy.

As shown in Fig.3.11, the average energy dissipated by the BS during the packet dissemination process reduces, as the FA of the MUs increases. As the MUs in the target MSN group becomes more altruistic, more tele-traffic is off-loaded from the congested BS to the local community of MUs. Hence, the high-power BS is less frequently invoked during the packet dissemination process and can be employed for fulfilling other transmission tasks. Compared to the energy dissipated by the BS during the conventional BS-aided multicast, as presented in the inset sub-figure of Fig.3.11, our scheme is capable of reducing the BS's energy dissipation

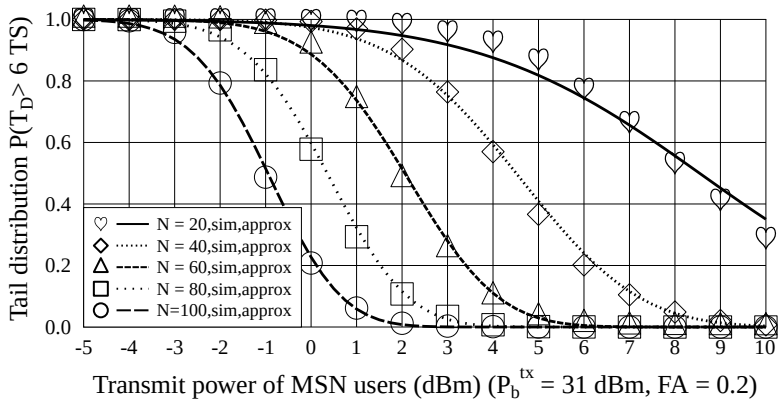

(a) Dissemination delay

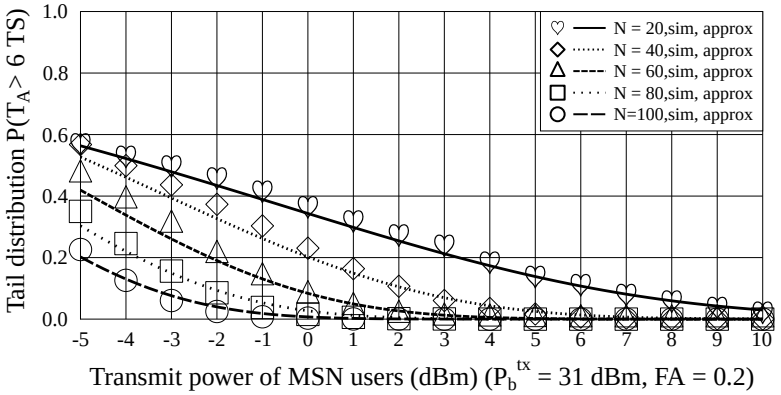

(b) Individual user-delay

Figure 3.9: The tail distribution of the delay versus the transmit power of the MSN users, which is parameterized by the number of MSN users. The transmit power P_s^{tx} of the MSN users varies from -5 dBm to 10 dBm, while the number of these MSN users are $N = \{20, 40, 60, 80, 100\}$. The FA is 0.2, while the other parameters related to the physical layer are provided by Table 3.1. The analytical results were either directly evaluated or derived from Eq.(3.17) by approximating the tail distribution function as Gamma distributions.

by about 90%, when FA increases from 0 to 0.2. Moreover, upon increasing the FA from 0.2 to 1.0, the BS's energy dissipation is reduced by another 86%. By contrast, during the conventional BS-aided multicast, the total energy dissipation of the entire MSN group is dedicated to their packet reception, which is as low as 21% of their dissipation during the MSN-aided dissemination associated with FA $= 0.2$, as shown in the inset sub-figure of Fig.3.11. As we further increase the FA from 0.2 to 1.0, the total energy dissipation of the social group is only increased by 15%.

As shown in Figure 3.12, the average energy dissipated by an individual MSN user during the packet dissemination process firstly increases and then reduces as the number of MSN users increases. Apparently, adopting a more altruistic behaviour, as reflected by a higher FA, results in an increased energy consumption of an individual MSN user. As shown in Figure 3.12, if the FA is increased from 0.2 to 1.0, the individual energy consumed by a MSN user is increased by 17%. However, in this case the total energy consumption observed in Figure 3.10 is reduced by 77.6%, while the individual user-delay of Figure 3.8 is reduced by 60.6%, and finally, the total dissemination delay of Figure 3.7 is reduced by 75.4%. Therefore, it is beneficial for the MSN users to become more altruistic, since a modest sacrifice may pay substantial dividends. Note that in the conventional BS-aided multicast, a MSN user only consumes energy during the reception-phase, which remains near-constant, as the number of MSN users increases.

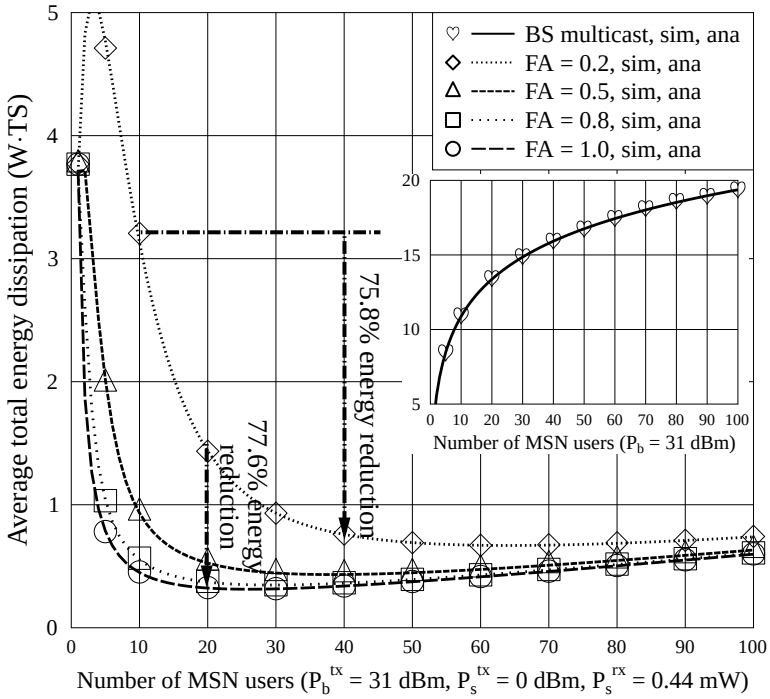

Figure 3.10: Average dissemination energy affected by the number of MSN users, which is parameterized by the FA. The number of the MSN users in the target MSN group varies from 1 to 100, while the FA takes values from $\{0.2, 0.5, 0.8, 1.0\}$. The transmit power of the MSN users, in the target MSN group is $P_s^{tx} = 0$ dBm and the other parameters related to the physical layer are provided by Table 3.1. The analytical results were evaluated from Eq.(3.28). Furthermore, the BS multicast scheme is used as a benchmark, whose analytical performance can be derived by substituting FA$= 0$ into Eq.(3.28).

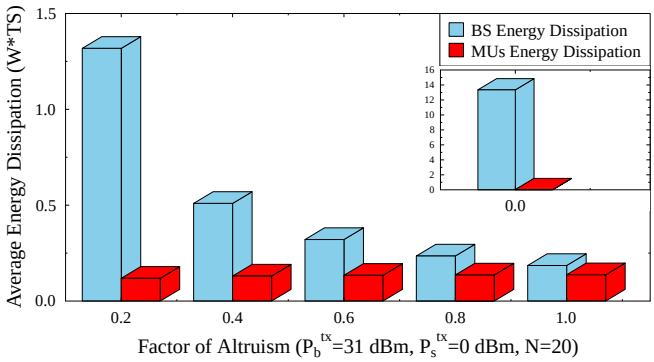

Figure 3.11: Average energy dissipated by the BS and average energy dissipated by all the MSN users in the target MSN group during the packet dissemination process, when different FA is conceived. The number of the MSN users in the target MSN group is 20. The transmit power of the MSN users is $P_s^{tx} = 0$ dBm and the other parameters related to the physical layer are given by Table 3.1. The analytical results can be derived by the first term of Eq.(3.28) and the sum of the second and third term of Eq.(3.28), respectively.

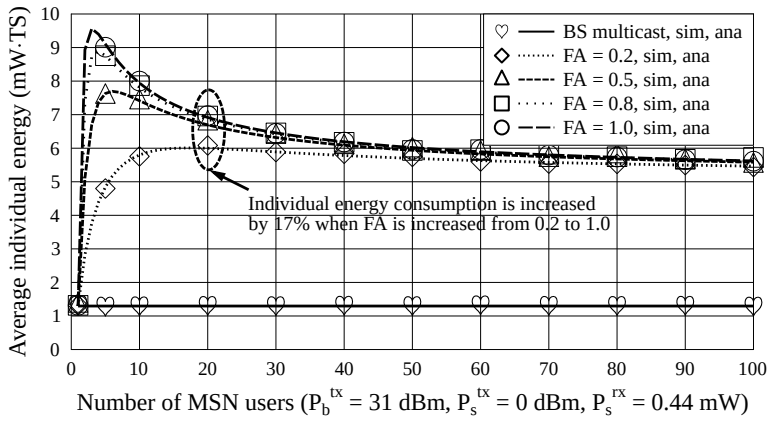

Figure 3.12: Average individual user-energy versus the number of MSN users in the target MSN group, which is parameterised by the FA. The number of these MSN users varies from 1 to 100, while the FA takes values from $\{0.2, 0.5, 0.8, 1.0\}$. The transmit power of the MSN users is $P_s^{tx} = 0$ dBm and the other parameters related to the physical layer are provided by Table 3.1. The analytical results were evaluated from Eq.(3.30). Furthermore, the BS multicast scheme is conceived as a benchmark, whose analytical result can be derived by substituting FA$= 0$ into Eq.(3.30).

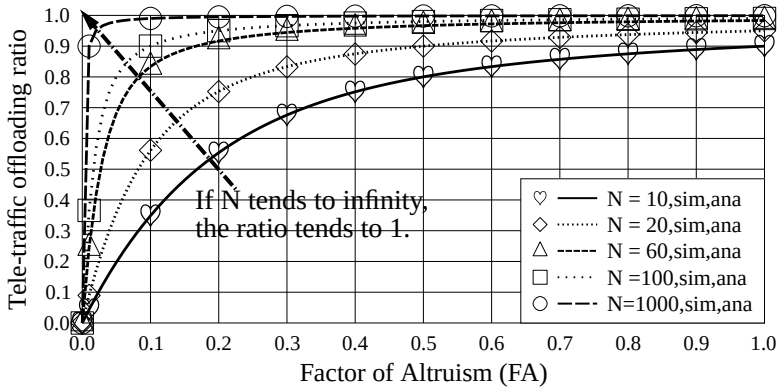

Figure 3.13: Tele-traffic off-loading ratio versus the FA, which is parameterized by the number of MSN users. The FA varies from 0 to 1, while the number of the MSN users is $N = \{10, 20, 60, 100, 1000\}$. Note that the tele-traffic off-loading ratio is uncorrelate to any parameters in the physical layer. The analytical results were evaluated from Eq.(3.31)

3.6.3 Tele-Traffic Off-Loading Ratio

When the FA increases from 0 to 1, the traffic off-loading ratio r_{MSN} also increases from 0 to $(N-1)/N$, as shown in Figure 3.13. For example, if we have $N = 10$ MSN users, whose FAs are all 0.5, 80% of the tele-traffic can be off-loaded from the BSs. Furthermore, it is also observed that when N increases, r_{MSN} also increases and tends to 100%.

3.6.4 Overhead Traffic

The following control overhead traffic is generated in order to realise our content dissemination scheme in a practical scenario:

- The BS holds the content of common interest at the beginning of the content dissemination process. It broadcasts the packet ID as an advertisement across the area using the BroadCast Control Channel (BCCH). The number of bits included in this advertisement message is determined by the total

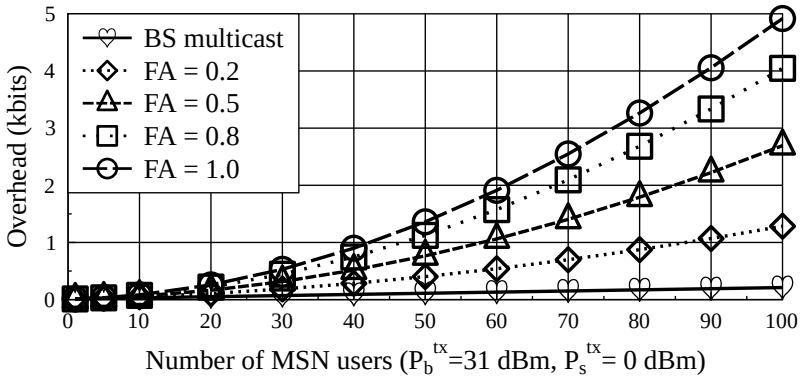

Figure 3.14: Traffic overhead generated during the content dissmination process. The number of the MSN users in the target MSN group varies from 1 to 100, while the FA takes values from $\{0.2, 0.5, 0.8, 1.0\}$. The transmit power of the MSN users is $P_s^{tx} = 0$ dBm and the other physical layer parameters are provided by Table 3.1. We also portray the traffic overhead generated by the conventional BS-aided multicast as a benchmark.

number of packets in the content file. In this section, we assume that there are 1000 packets in this content file. Then the packet ID should be encoded using 10 bits.

- The specific MUs that are interested in this packet report their interest to the BS in the orthogonal Physical Uplink Control CHannel (PUCCH)[6] and form a MSN group for potential cooperative content dissemination. This 'report' message for every MSN user is encoded in a single bit.
- The BS broadcasts the 'task' message using the BCCH in order to find potential helpers. This 'task' message is encoded in a single bit. If no response is received, the BS will multicast the packet.
- Altruistic POs send a single-bit response message to the BS using the PUCCH in order to take over the multicast task. Selfish POs make no response.
- If any unserved MSN users receive the packet, an ACKnowledgement (ACK) encoded in a single bit is returned to the BS using the PUCCH. Then the BS broadcasts the 'task' message again and the same procedure is repeated, until all MSN users receive the packet.
- Finally, the packet is deleted from the head of the buffer at the BS end. The BS is ready for broadcasting the 'advertisement' for disseminating the second packet.

Based on the parameter settings of Table 3.1, we characterise the overhead traffic generated by our scheme in Figure 3.14 for disseminating a specific packet and compare it to the conventional BS-aided multicast. Observe from Figure 3.14 that the overhead traffic increases, as we increase the number of users in the target MSN group. Furthermore, as the MSN users become more altruistic, an increased signalling overhead is generated in order to schedule them for cooperatively disseminating the content of common interest. However, the performance improvement demonstrated in Figures 3.7-3.13 indicates that this is a worthwhile investment.

3.7 Numerical Results For a Realistic Subway Station

Let us now study the content dissemination performance in a densely-populated subway station scenario [124]. The one-hour mobility traces for this scenario can be downloaded from the CRAWDAD database[7].

[6] In mobile cellular communication, each MU is assigned an orthogonal PUCCH (realised by OFDMA or CDMA). As a result, the BS is able to identify different MUs.

[7] http://crawdad.cs.dartmouth.edu/kth/walkers/

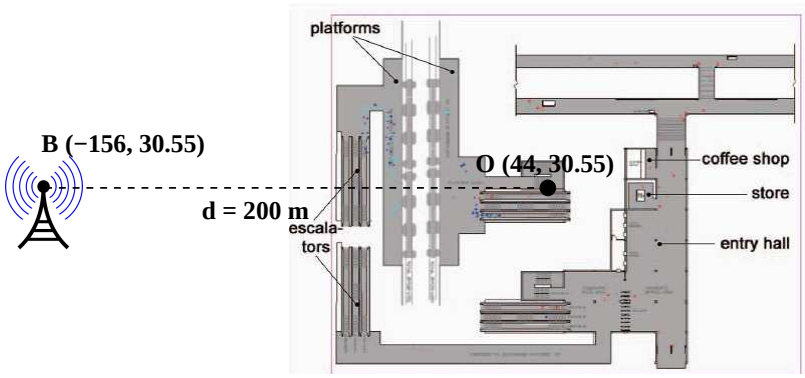

Figure 3.15: A densely popluated subway station

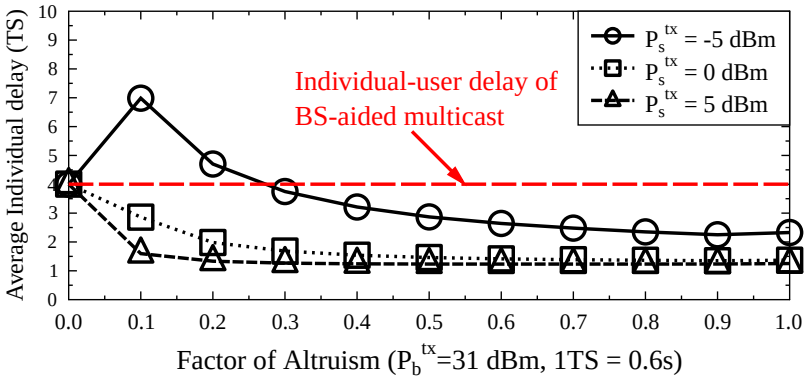

Figure 3.16: Average individual user-delay in a subway station versus the FA. The FA varies from 0 to 1. Different transmit power of the MSN users are conceived, which are $P_s^{tx} = \{-5, 0, 5\}$ dBm. The other physical layer parameters are provided by Table 3.1. The actual duration of a TS is 0.6 s. The average individual user-delay is evaluated in terms of the number of TSs. Note that the average individual user-delay of the BS-aided multicast is attained when the FA is zero.

The active area in this scenario is 1921 m^2. After analysing the mobility traces, the centre O of the active area is found to be at the coordinates of $(44, 30.55)$ m, as shown in Fig.3.15. In our simulations, we placed the BS at the point $(-156, 30.55)$ m, which is 200 m away from the centre of the subway station. During the one-hour period, 3299 MUs appear in the subway station. All these MUs are assumed to form a MSN group in order to download the train schedule of common interest. Since the MUs arrive/depart either through the entrances or during the arrival/departure of trains, the number of MUs dynamically fluctuates during the simulation time. The length of the MUs' period of activity varies from a minimum of 6 seconds(s) to a maximum of 713.4 s. Again, the physical layer parameters are summarised in Table 3.1. Since the positions of the MUs are captured every 0.6 s in this mobility trace, in our simulations we set the basic time interval of $\Delta t = 0.6$ s as a single TS, which can be considered as a packet's duration. Then the delay is evaluated in terms of the number of TSs, while the energy dissipation is evaluated in terms of "Watt(W)*TS" and "mW*TS".

3.7.1 Delay Metric Evaluation

Observe from Figure 3.16 that for the cases of $P_s^{tx} = 0$ dBm and $P_s^{tx} = 5$ dBm, the average individual user-delay is reduced, as we increase the FA from 0.0 to 1.0. For $P_s^{tx} = -5$ dBm, when FA is increased from 0.0 to 0.1, we observe an increasing average individual user-delay. This is because the SPRP between the MSN users is low and also, because fewer POs are willing to forward the packet. As FA becomes higher, more POs may join to assist the packet dissemination process, which significantly reduces the average individual user-delay. Specifically, when FA $= 0$, conventional BS-aided multicast is invoked for disseminating the

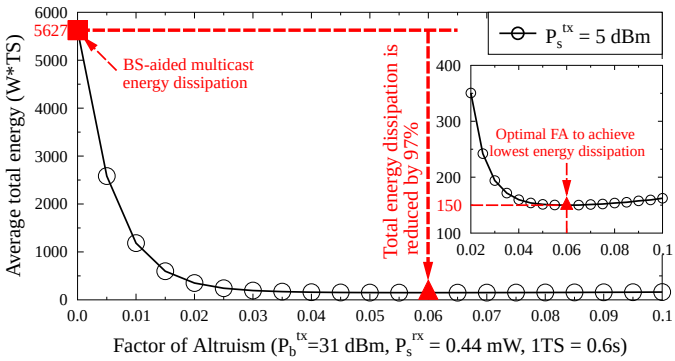

Figure 3.17: Average total energy dissipation for disseminating a packet of common interest in a subway station in the low FA region. The FA vaires from 0 to 0.1. The transmit power of the MSN users is $P_s^{tx} = 5$ dBm. The remaining parameters related to the physical layer are provided by Table 3.1. The energy dissipation is evaluated in terms of "W*TS". Note that the average total energy dissipation of the BS-aided multicast scheme is attained when the FA is zero.

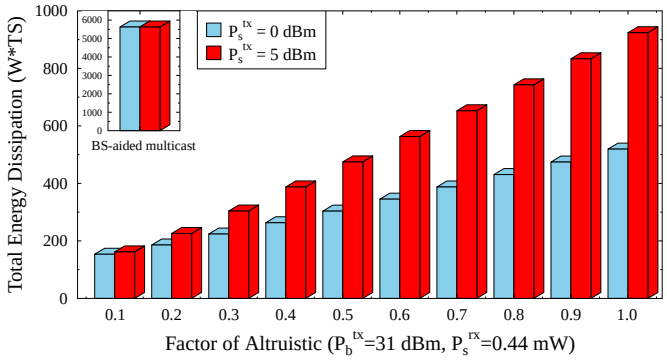

Figure 3.18: Average total energy dissipation for disseminating a packet of common interest in a subway station for the high FA region. The FA vaires from 0.1 to 1.0. The transmit power of the MSN users is $P_s^{tx} = 0$ dBm or $P_s^{tx} = 5$ dBm. The remaining parameters related to the physical layer are provided by Table 3.1. The energy dissipation is evaluated in terms of "W*TS".

packet. For $P_s^{tx} = 0$ or 5 dBm, if the MSN users become only modestly altruistic, say we have FA$= 0.1$, our content dissemination scheme outperforms the conventional BS multicast. For $P_s^{tx} = -5$ dBm, our scheme starts to outperform the classic BS-aided multicast, provided that FA is higher than 0.4.

3.7.2 Energy Metric Evaluation

In Figure 3.17, we portray the average total energy dissipation during exhaustively disseminating a packet of common interest in a subway station for the low FA region. Observe from Figure 3.17 that for $P_s^{tx} = 5$ dBm, the total energy dissipation is dramatically reduced as the FA is increased from 0 to 0.02. Then the total energy dissipation reduces slowly, until the lowest energy dissipation is achieved for FA $= 0.06$. Afterwards, the total energy dissipation slowly increases as the FA is increased from 0.06 to 0.1. Compared to the conventional BS-aided multicast, the total energy dissipation can be reduced by upto 97% when our scheme associated with FA $= 0.06$ is implemented.

Observe from both Figures 3.18 and 3.19 that in the high FA region, as the FA increases, both the total energy dissipation and the individual energy dissipation are gradually increased, since the majority of the packet dissemination process is completed by the local communications amongst the users in the target MSN group and because more MSN users engage in cooperatively multicasting the packet of common interest. For example, as shown in Figure 3.18, when $P_s^{tx} = 5$ dBm, as the FA increases from 0.1 to 1.0,

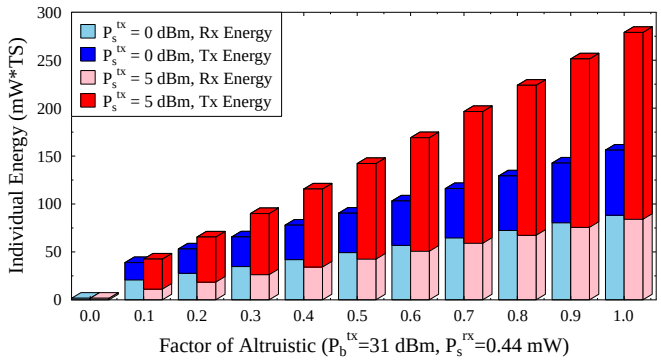

Figure 3.19: Average energy dissipation of an individual user during the packet dissemination process versus the FA. The FA varies from 0 to 1.0. The transmit power of the MSN users is $P_s^{tx} = 0$ dBm or $P_s^{tx} = 5$ dBm. The remaining parameters related to the physical layer are provided by Table 3.1. The energy dissipation is evaluated in terms of "mW*TS".

the total energy dissipation imposed by disseminating a packet of common interest in a subway station is increased by a factor of 4.7, while the energy dissipation of an individual MSN user imposed by assisting the packet dissemination process is increased by a factor of 5.6, as observed from Figure 3.19. However, it is not worth investing extra energy dissipation, because as presented in Figure 3.16, when we have $P_s^{tx} = 5$ dBm, increasing the FA from 0.1 to 1.0 is only capable of reducing the individual user-delay by 0.34 TS. As a result, in the densely populated subway station, the MSN users do not have to have a high FA value.

3.8 Chapter Conclusions

In this chapter, we proposed a MSN-aided content dissemination scheme as a supplement to the conventional cellular system. As introduced in Section 3.2, in our scheme, the MUs form a MSN group in order to request the content of common interest as a group. After receiving the content request, the BS creates a specific queue for buffering all the packets of the content so as to disseminate the packets of the requested content one by one. During the dissemination process of a single packet, the BS firstly multicasts the packet to all the members of the MSN group. If no MSN users successfully receive the packet, the BS would multicast the packet again in the subsequent TS. If at least a single MSN user successfully receives the packet, this packet would be spontaneously disseminated via cooperative multicast amongst the MSN users. However, the packet is still kept at the head of the BS's buffer for the eventuality that no MSN users are willing to forward the packet at any time instant. Once all the members of the MSN group have successfully received the packet, it is removed from the BS's buffer.

In Section 3.2, we elaborated on the various factors that may affect the above-mentioned content dissemination process, such as the altruistic behaviour of the MSN users in the network layer, as well as their mobility and their channel attenuation in the physical layer, plus their successful packet reception in the MAC layer. We initially modelled the hybrid content dissemination process by the DT-PBMC detailed in Section 3.3. With the aid of Theorems 3.1 and 3.2, we converted the DT-PBMC to the CT-PBMC, albeit this is only an approximation. Relying on the approximate CT-PBMC, in Section 3.3, we derived the closed-form expressions for characterising the following delay metrics during the dissemination process of a single packet:

- The dissemination delay, which is the time duration from the BS multicasting a packet until all the members of the MSN group successfully receive the packet of common interest;
- The individual user-delay, which is the time duration from the BS multicasting a packet until a specific MSN user successfully receives this packet;

- The individual transmit time, which is the time duration of a specific MSN user remaining actively operational after it successfully receives the packet until the packet dissemination process is completed across the entire MSN group.

Furthermore, based on the approximate CT-PBMC of Section 3.3, we also derived the closed-form expressions of the following energy metrics in Section 3.4:

- The total energy dissipated during exhaustively disseminating the packet of common interest across the entire MSN group, which consists of the energy dissipated by the BS, the energy dissipated by the MSN users by forwarding the packet during the dissemination process and the energy dissipated by the MSN users during the successful recovery of the packet from the attenuated signal;
- The individual user's energy dissipation, which consists of the energy dissipated by a specific MSN user while successfully recovering the packet during the reception phase plus the energy dissipated upon further forwarding the packet.

In Section 3.5, we analysed the capability of our MSN-aided content dissemination scheme to mitigate the tele-traffic conveyed by the congested cellular networks. This off-loading capability was quantified in terms of the tele-traffic off-loading ratio, which is defined as the ratio of the number of packet replicas delivered by the MSN users themselves to the total number of replicas generated.

In Section 3.6, we then provided numerical results for characterising how our MSN-aided content dissemination scheme performs when the MSN users move within a circular area by obeying the uniform mobility model. Our conclusions are as follows:

- Increasing the number of MSN users in the MSN group may firstly increase both the delay and energy consumption, when our MSN aided content dissemination scheme is implemented, since more MUs may impose a higher traffic load on the system. However, further increasing the number of MUs in the MSN group may significantly reduce both the delay and energy consumption, since having more MSN users in the MSN group provide more frequent cooperative multicast opportunities and the resultant diversity gain may be capable of counteracting the adverse effects incurred by the increased traffic demand. These observations can be made in Figures 3.7-3.10.
- If the MSN users in the MSN group become more altruistic, which is reflected by the increasing value of their FA, both the dissemination delay and the individual delay may be significantly reduced, since more MSN users are willing to assist in the dissemination process of the packet, as observed in Figures 3.7 and 3.8. Furthermore, in this case, the total energy dissipated by disseminating the packet is also significantly reduced, because the high-power BS is rarely invoked during the packet dissemination process and the majority of the tele-traffic load is carried by the low-power transmissions amongst the MSN users themselves, as presneted in Figures 3.10 and 3.11. However, the expense of achieving these performance gains results in the increasing overhead traffic, as shown in Figure 3.14 and in an increased individual energy consumption, as shown in Figure 3.12.
- The accuracy of our mathematical modelling and the corresponding approximation has been validated by the simulation results, as demonstrated in Figures 3.7-3.12. Furthermore, in order to derive closed-form expression for the tail distribution of the dissemination delay and of the individual user-delay, a Gamma distribution based approximation is invoked, whose accuracy is validated by the simulation results as well, as presented in Figure 3.9.
- Increasing both the number of MUs in a MSN group and the FA may improves the MSN group's capability of off-loading the tele-traffic from the congested cellular network, as portrayed in Figure 3.13.

Table 3.2: Comparison between the conventional BS-aided multicast and our MSN-aided content dissemination scheme, when the MSN users move within a circular area by obeying the uniform mobility model.

Perform. metric	Figure	Number of MUs	BS-aided multicast	Our MSN dissemin.	Performance reduction/increase of our scheme over the BS-aided multicast
Dissemination delay	Figure 3.7	80	14.6 TS	6.4 TS (FA=0.2)	Our scheme reduces the average dissemination delay by 56.5%.
Individual user-delay	Figure 3.8	80	3.0 TS	1.3 TS (FA=0.5)	Our scheme reduces the average individual-user delay by 56.0%.
Total energy	Figure 3.10	80	18.6 W*TS	0.7 W*TS (FA=0.2)	Our scheme reduces the average total energy dissipation by 96%.
Tele-traffic on the BS	Figure 3.13	60	60 copies	1.7 copies (FA=0.2)	Our scheme is capable of off-loading 91.7% of the tele-traffic from the BS.
Individual user-energy	Figure 3.12	80	1.3 mW*TS	5.5 mW*TS (FA=0.2)	Our scheme increases the average individual user-energy dissipation by 4.2 mW*TS.
Traffic overhead	Figure 3.14	80	171 bits	873 bits (FA=0.2)	Our scheme increases the average traffic overhead by 702 bits.

- The comparison between our MSN-aided content dissemination scheme and the conventional BS-aided multicast in this specific context is provided by Table 3.2, as observed in Figures 3.7-3.10 and in Figures 3.12-3.14.

Finally, in Section 3.7, we presented how our MSN aided content dissemination scheme performs in the context of a realistic subway station, where the MUs form a MSN group in order to download the information of common interest. Our conclusions are as follows:

- When the MSN users in the subway station become more altruistic, the average individual user-delay is gradually reduced. However, in the scenarios that the transmit power of the MSN users is $P_s^{tx} = 0$ dBm or $P_s^{tx} = 0.5$ dBm, having a higher FA may not result in a significant delay reduction, as observed in Figure 3.16.

- When the MSN users in the subway station become more altruistic, the average total energy dissipation is initially reduced, and then gradually increases as the FA of the MSN users becomes higher. The most beneficial value of the FA, say $q = 0.06$, can be inferred from Figures 3.17 and 3.18, which leads to the most energy efficient content dissemination scheme.

- As the FA increases, the average energy dissipation of an individual MSN user is gradually increased, including the energy dissipation of both its transmission phase as well as its reception phase, as observed in Figure 3.19.

- Our MSN aided content dissemination scheme outperforms the conventional BS-aided multicast in the context of a realistic subway station in terms of the average individual user-delay and the average total energy dissipation, as presented in Figures 3.16-3.18. The quantitative comparison of our scheme and of the conventional BS-aided multicast is provided in Table 3.3.

In this chapter, we only consider the Quality of Service (QoS)-guaranteed packet reception in the MAC layer, while the issues of resource scheduling and interference avoidance aided multiple access are set aside for the following chapters. Moreover, in the network layer, we only consider the altruistic human behaviour. However, in a more realistic scenario, people usually share the content of common interest with their friends during the content dissemination phase. The impact of the specific social relationships amongst the MSN users has to be further investigated.

Furthermore, the mathematical modelling used in this chapter relied on several approximations in order to derive closed-form results. These approximations only hold under some specific conditions. For example, in

Table 3.3: Comparison between the conventional BS-aided multicast and our MSN-aided content dissemination scheme in the context of a realistic subway station.

Perform. metric	Figure	BS-aided multicast	FA	Our MSN dissemin.	Performance reduction/increase of our scheme over the BS-aided multicast
Individual user-delay	Figure 3.16	2.4 TS	0.1	0.96 TS ($P_s^{tx} = 5$ dBm)	Our scheme reduces the average individual-user delay by 60.0%.
Total energy	Figure 3.17	5627 W*TS	0.06	150 W*TS ($P_s^{tx} = 5$ dBm)	Our scheme reduces the average total energy dissipation by 97.3%.
Individual user-energy	Figure 3.19	1.7 mW*TS	0.1	42.6 mW*TS ($P_s^{tx} = 5$ dBm)	Our scheme increases the average individual user-energy dissipation by 40.9 mW*TS.

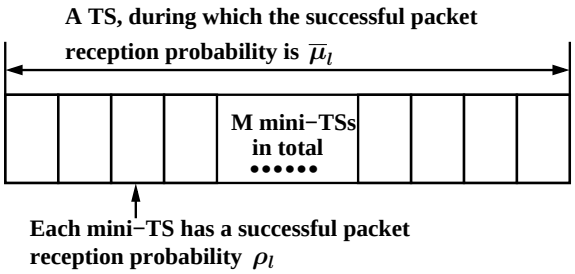

Figure 3.20: The structure of a TS

Section 3.3.1, we only consider the adjacent state transitions in the DT-PBMC, as shown in Figure 3.3, while the other state transitions are ignored. However, this approximation only holds subject to the condition that the basic time interval Δt is far shorter than 1 TS. If this condition is violated, our mathematical modelling cannot produce accurate analytical results.

In order to overcome these drawbacks, in the following chapters, we are going to gradually improve the grade of realism in our mathematical modelling of the content dissemination process by considering a much more realistic MAC layer model, by considering the influence of real-life social relationships, and by pursuing a much more generic mathematical approach.

Appendix

3.A Proof of Lemma 1

As shown in Figure 3.20, a TS is divided into M virtual mini-TSs, each of which has a duration of $\Delta t = 1/M$ TS. We assume that the SPRP in a virtual mini-TS is ρ_l. As a result, given the SPRP $\overline{\mu}_l$ in a TS, we may derive the relation between $\overline{\mu}_l$ and ρ_l, which is expressed as

$$\overline{\mu}_l = \sum_{j=1}^{M} (1-\rho_l)^{j-1}\rho_l = 1-(1-\rho_l)^M. \tag{3.32}$$

Rewriting the above expression, we obtain

$$\rho_l = 1-(1-\overline{\mu}_l)^{1/M} = 1-(1-\overline{\mu}_l)^{\Delta t}, \tag{3.33}$$

where the second equality is derived according to $\Delta t = 1/M$ TS. If we expand $(1-\overline{\mu}_l)^{\Delta t}$ according to the Taylor expansion, we have

$$(1-\overline{\mu}_l)^{\Delta t} = \sum_{n=0}^{\infty} \binom{\Delta t}{n} (-\overline{\mu}_l)^n = 1-\overline{\mu}_l \Delta t + O(\overline{\mu}_l^2), \tag{3.34}$$

where $O(\overline{\mu}_l^2)$ is the infinitesimal by small quantity on the same order as $\overline{\mu}_l^2$. Substituting the above equation into Eq.(3.33), we have

$$\rho_l = \overline{\mu}_l \Delta t + O(\overline{\mu}_l^2) \approx \overline{\mu}_l \Delta t. \tag{3.35}$$

According to our experiments, if we vary $\overline{\mu}_l$ from 0 to 0.8, the Root-Mean-Square-Error (RMSE) between the exact ρ_l given by Eq.(3.33) and the approximated ρ_l given by Eq.(3.35) is 9.45×10^{-4}. As a result, it is reasonable to claim that $\rho_l \approx \overline{\mu}_l \Delta t$.

3.B Proof of Lemma 2

During a time interval Δt, the PBMC may transit from state k to $(k+1)$ with a probability of $\widetilde{\mu}_k \Delta t$. Naturally, the successful state transition first occurring during the $(M_k = m_k)$-th Δt interval obeys a *geometric distribution*. According to the PMF of a geometric distribution having a parameter of $\widetilde{\mu}_k \Delta t$, we arrive at:

$$\Pr\left(M_k \Delta t \leq m_k \Delta t\right) = \sum_{m=1}^{m_k} (1 - \widetilde{\mu}_k \Delta t)^{m-1} \widetilde{\mu}_k \Delta t, \tag{3.36}$$

$$\Pr\left(M_k \Delta t \leq (m_k+1) \Delta t\right) = \sum_{m=1}^{m_k+1} (1 - \widetilde{\mu}_k \Delta t)^{m-1} \widetilde{\mu}_k \Delta t. \tag{3.37}$$

The continuous-valued delay of the adjacent-state transition is denoted as $T_k = M_k \Delta t$, which is associated with a specific value of $t_k = m_k \Delta t$. Hence, we may derive the PDF of T_k as:

$$\begin{aligned} f_{T_k}(t_k) &= \lim_{\Delta t \to 0} \frac{\Pr(T_k \leq t_k + \Delta t) - \Pr(T_k \leq t_k)}{\Delta t} \\ &= \lim_{\Delta t \to 0} \frac{\Pr(M_k \Delta t \leq (m_k+1)\Delta t) - \Pr(M_k \Delta t \leq m_k \Delta t)}{\Delta t} \\ &= \lim_{\Delta t \to 0} \frac{(1 - \widetilde{\mu}_k \Delta t)^{m_k} \widetilde{\mu}_k \Delta t}{\Delta t} = \lim_{\Delta t \to 0} \widetilde{\mu}_k \mathrm{e}^{-m_k \widetilde{\mu}_k \Delta t} \\ &= \widetilde{\mu}_k \cdot \mathrm{e}^{-\widetilde{\mu}_k t_k}, \end{aligned} \tag{3.38}$$

where the last two lines are derived based on $\lim_{\Delta t \to 0} \widetilde{\mu}_k \Delta t = 1 - \mathrm{e}^{-\widetilde{\mu}_k \Delta t}$ and $m_k = t_k / \Delta t$, respectively.

3.C Delay Metrics for Two Special Cases

3.C.1 Case 1: Conventional BS Aided Multicast ($q = 0$)

In this pessimistic case, all the MSN users are selfish during the packet dissemination process. Hence, the BSs have to disseminate the packet to all the MSN users. As a result, in this case, only the dissemination delay and the individual user-delay have to be considered.

3.C.1.1 Dissemination Delay

When FA is $q = 0$, according to Eq.(3.11) in Section 3.3.2, the state transition delays $\{T_k, k = 0, 1, \cdots, (N-1)\}$ are independent exponentially distributed variables associated with the rates of $\{\widetilde{\mu}_k = (N-k)\overline{\mu}_b, k = 0, 1, \ldots, (N-1)\}$. Since the dissemination delay is defined as $T_D = \sum_{k=0}^{N-1} T_k$, T_D obeys the *hypoexponential distribution* [125]. Furthermore, relying on the fact that the rates of $\{T_k, k = 0, 1, \cdots, (N-1)\}$ are different from each other, the PDF of T_D can be expressed as

$$f_{T_D|q=0}(t_D) = \sum_{k=0}^{N-1} \prod_{j=0, j\neq k}^{N-1} \frac{N-j}{k-j} (N-k) \overline{\mu}_b \mathrm{e}^{-(N-k)\overline{\mu}_b t_D}. \tag{3.39}$$

In order to derive the probability of T_D exceeding a given threshold D_{th}, we integrate the above PDF $f_{T_D|q=0}(t_D)$ over the region $[D_{th}, \infty)$, which is expressed as

$$\begin{aligned}\Pr(T_D > D_{th}|q=0) &= \int_{D_{th}}^{\infty} f_{T_D|q=0}(t_D)dt_D \\ &= \sum_{k=0}^{N-1}\prod_{j=0,j\neq k}^{N-1}\frac{N-j}{k-j}\mathrm{e}^{-(N-k)\overline{\mu}_b D_{th}}.\end{aligned} \tag{3.40}$$

3.C.1.2 Individual User-Delay

When the FA is $q = 0$, the individual user-delay is solely determined by the quality of the wireless link connecting the MSN user $\mathcal{A}$ to the BS. As a result, according to *Lemma 2*, the individual user-delay $T_{\mathcal{A}}$ obeys an exponential distribution having a mean of $1/\overline{\mu}_b$. Furthermore, the probability of $T_{\mathcal{A}}$ exceeding a given threshold D_{th} is derived as $\Pr(T_{\mathcal{A}} > D_{th}|q=0) = \exp(-\overline{\mu}_b D_{th})$.

3.C.2 Case 2: Fully Altruistic Behaviour ($q = 1$)

In this optimistic scenario, all the MSN users are completely altruistic. Since there are always some POs willing to forward the packet during the dissemination process, the BS is not invoked for multicasting the packet any more, once some of the MSN users have initially received it from the BS.

3.C.2.1 Dissemination Delay

When the FA is $q = 1$, by substituting $n_k = k$ into Eq.(3.7) in Section 3.3.2, we know that the state transition delays $\{T_k, k = 1, \cdots, (N-1)\}$ are independent exponentially distributed variables associated with the rates of $\{\widetilde{\mu}_k = k(N-k)\overline{\mu}_s, k = 1, 2, \ldots, (N-1)\}$. Furthermore, by substituting $k = 0$ into Eq.(3.10) in Section 3.3.2, the initial state transition delay T_0 is also an exponentially distributed variable associated with a rate of $\widetilde{\mu}_0 = N\overline{\mu}_b$. Note furthermore that T_0 is also independent of $\{T_k, k = 1, \cdots, (N-1)\}$. Since the dissemination delay is defined as $T_D = \sum_{k=0}^{N-1} T_k$, T_D obeys the hypoexponential distribution.

However, the rates of $\{\widetilde{\mu}_k = k(N-k)\overline{\mu}_s, k = 1, 2, \ldots, (N-1)\}$ associated with $\{T_k, k = 1, \cdots, (N-1)\}$ exhibit a symmetric structure. For example, the rates of T_k and T_{N-k} share the same value of $k(N-k)\overline{\mu}_s$. Hence, the closed-form equation for the TDF of T_D may only be expressed in the form of a *continuous phase-type distribution* [95]. As a result, when $q = 1$, the transition rate matrix of the PBMC is expressed as

$$\mathbf{P} = \begin{pmatrix} -\widetilde{\mu}_0 & \widetilde{\mu}_0 & 0 & \cdots & 0 & 0 \\ 0 & -\widetilde{\mu}_1 & \widetilde{\mu}_1 & \ddots & 0 & 0 \\ \vdots & \ddots & -\widetilde{\mu}_k & \widetilde{\mu}_k & \ddots & \vdots \\ 0 & 0 & \ddots & -\widetilde{\mu}_{N-2} & \widetilde{\mu}_{N-2} & 0 \\ 0 & 0 & \cdots & 0 & -\widetilde{\mu}_{N-1} & \widetilde{\mu}_{N-1} \\ 0 & 0 & \cdots & 0 & 0 & 0 \end{pmatrix} = \begin{pmatrix} \mathbf{Q} & \mathbf{Q}_0 \\ \mathbf{0} & 0 \end{pmatrix}, \tag{3.41}$$

where $\mathbf{Q}$ is a $(N \times N)$-element matrix containing all the transition rates between transient states, $\mathbf{Q}_0$ is a $(N \times 1)$ column vector containing all the transition rates from transient states to the absorbing state N, whose last entry is $\widetilde{\mu}_{N-1}$ and finally, the remaining entries are all zeros. As shown in Figure 3.3 of Section 3.3.2, the packet dissemination process starts from the initial state 0. Thus, the probability of T_D exceeding a given threshold D_{th} is expressed as

$$\Pr(T_D \geq D_{th}|q=1) = \boldsymbol{\tau}_1^T \times \mathbf{exp}(D_{th}\mathbf{Q}) \times \mathbf{1}_N. \tag{3.42}$$

We should note that in Eq.(3.42), the $(N \times 1)$ column vector $\boldsymbol{\tau}_{k+1}$ $(0 \leq k \leq N-1)$, whose $(k+1)$th entry is one but all the others are zeros, indicates that the PBMC starts at state k, while the $(N \times 1)$ column

vector $\mathbf{1}_{k+1}$, whose first $(k+1)$ entries are ones and the remaining entries are zeros, indicates that the PBMC process is absorbed at state $(k+1)$. The proof of Eq.(3.42) can be found in [126].

3.C.2.2 Individual User-Delay

Given an event that the MSN user $\mathcal{A}$ successfully receives the packet at state $(k+1)$ $(0 \leq k \leq N-1)$, the PBMC used for modelling the packet dissemination in Figure 3.3 of Section 3.3.2 is considered to be terminated at state $(k+1)$. According to the physical meaning of both $\boldsymbol{\tau}_{k+1}$ and $\mathbf{1}_{k+1}$, similar to Eq.(3.42), the probability of $T_{\mathcal{A}}$ exceeding the threshold D_{th}, given that $\mathcal{A}$ receives the desired packet at state $(k+1)$ for $(0 \leq k \leq N-1)$, is expressed as

$$\Pr(T_{\mathcal{A}} \geq D_{th} | q = 1, k+1) = \boldsymbol{\tau}_1^T \times \mathbf{exp}(D_{th}\mathbf{Q}) \times \mathbf{1}_{k+1}. \tag{3.43}$$

Since we have already derived the probability of $\Pr_{k+1} = 1/N$ that $\mathcal{A}$ receives the packet at state $(k+1)$ in Section 3.3.4, according to the Bayesian principle [94], the probability of $T_{\mathcal{A}}$ exceeding the threshold D_{th} is derived as

$$\begin{aligned}
\Pr(T_{\mathcal{A}} \geq D_{th} | q = 1) &= \sum_{k=0}^{N-1} \Pr(T_{\mathcal{A}} \geq D_{th} | q = 1, k+1) \cdot \Pr_{k+1} \\
&= \sum_{k=0}^{N-1} \frac{\boldsymbol{\tau}_1^T \times \mathbf{exp}(D_{th}\mathbf{Q}) \times \mathbf{1}_{k+1}}{N} = \frac{\boldsymbol{\tau}_1^T \times \mathbf{exp}(D_{th}\mathbf{Q})}{N} \times \sum_{k=0}^{N-1} \mathbf{1}_{k+1} \\
&= \frac{\boldsymbol{\tau}_1^T \times \mathbf{exp}(D_{th}\mathbf{Q}) \times \boldsymbol{\eta}}{N},
\end{aligned} \tag{3.44}$$

where $\boldsymbol{\eta} = (N, N-1, \cdots, 1)^T$ is a $(N \times 1)$ column vector.

3.C.2.3 Individual Transmit Time

The *continuous phase-type* distribution [95] is also invoked for deriving the TDF of the individual transmit time when $q = 1$. Given the event that a specific MSN user $\mathcal{A}$ successfully receives the packet at state k $(1 \leq k \leq N-1)$, the PBMC is considered to commence at state k and to terminate at state N. As a result, given a threshold D_{th}, the conditional TDF of T_W for $(1 \leq k \leq N-1)$ is expressed as

$$\Pr(T_W \geq D_{th} | q = 1, k) = \boldsymbol{\tau}_{k+1}^T \times \mathbf{exp}(D_{th}\mathbf{Q}) \times \mathbf{1}_N. \tag{3.45}$$

Specifically, if $\mathcal{A}$ receives the packet at state N, the individual transmit time is 0, which results in $\Pr(T_W \geq D_{th} | q = 1, k = N) = 0$. Since the probability $\Pr_k = 1/N$ that $\mathcal{A}$ receives the packet at state k has been derived in Section 3.3.4, the TDF of T_W is derived as

$$\begin{aligned}
\Pr(T_W \geq D_{th} | q = 1) &= \sum_{k=1}^{N} \Pr(T_W \geq D_{th} | q = 1, k) \cdot \Pr_k \\
&= \sum_{k=1}^{N-1} \frac{\boldsymbol{\tau}_{k+1}^T \times \mathbf{exp}(D_{th}\mathbf{Q}) \times \mathbf{1}_N}{N} = \left(\sum_{k=1}^{N-1} \boldsymbol{\tau}_{k+1}^T \right) \times \frac{\mathbf{exp}(D_{th}\mathbf{Q}) \times \mathbf{1}_N}{N} \\
&= \frac{(\mathbf{1}_N - \mathbf{1}_1)^T \times \mathbf{exp}(D_{th}\mathbf{Q}) \times \mathbf{1}_N}{N}.
\end{aligned} \tag{3.46}$$

Chapter 4

Distributed Multi-Stage Cooperative Social Multicast Aided Content Dissemination in Random Mobile Networks

4.1 Introduction

4.1.1 Background

In densely populated areas, such as a football stadium and open air festivals, mobile users (MUs) always find it difficult to rely on the data services supported by the Centralised Infrastructure (CI), such as Wi-Fi access points and Base Stations (BSs). For instance, in a circular area having a radius of 25 meters in one of these scenarios, there may be hundreds of Mobile Users (MUs), which may impose a heavy traffic load on the CI. However, the MUs of these particular scenarios usually share the common interest in some of the contents. Based on their multi-functional mobile devices, an *ad hoc* network can be organised in order to disseminate the content of common interest via short-range communication techniques, such as Wi-Fi or bluetooth. As a result, a large fraction of the tele-traffic can be off-loaded from the CI to the *ad hoc* network. This promising approach requires us to design a novel distributed approach for efficiently disseminating the contents of common interest.

As the demand for the broadband wireless multimedia services grows, multicast [54] techniques may be invoked in order to more efficiently disseminate the content of common interest to numerous MUs. Three main types of wireless multicast techniques have attracted attention across the research community [2]-[8]. The first type is the direct wireless multicast [127], where a single node, such as a BS, solely transmits the same content to multiple destinations. In [55], the authors theoretically derived both the achievable multicast throughput as well as delay and then characterised the associated trade-off between these conflicting performance metrics, while using hybrid-ARQ protocols. In order to increase the successful content delivery probability, while simultaneously enhancing the coverage area of direct wireless multicast, multi-hop wireless multicast may be invoked. In this multicast technique, the source node first multicasts the content to all the targets. Then a specific node is randomly selected from the set of targets, which have successfully received the content, for the sake of further multicasting it to the other hitherto unserved targets. In [128], the

authors derived both the outage probability and the multicast transmission capacity for both the direct and multi-hop multicast scenarios. For the sake of further exploiting the diversity gain provided by multiple multicasters, cooperative multicast is proposed for further enhancing the attainable system performance [129]. Given its appealing benefits, substantial efforts have been devoted to the development of two-stage cooperative multicast, especially to its power allocation [130] as well as relay selection problems [131]. In two-stage cooperative multicast, the BS firstly multicasts the content to all the targets. Then the specific targets which have successfully received the content may further multicast it. As a result, the receiver may benefit from a substantial diversity gain, which leads to an improved performance [132]. In [133], the authors analysed the outage performance and find the optimal power allocation for both distributed cooperative multicast[1] and for 'geni-aided' cooperative multicast[2]. In [111], a social group-casting algorithm was proposed for a social networking group, so that they become capable of cooperatively downloading the same content in a heterogeneous network. Unfortunately, the authors mainly focused on the scheduling of the content download from the BSs without considering the details of the content dissemination in local *ad hoc* networks.

However, the above research efforts ignore the delay analysis of multi-stage cooperative multicast. Moreover, in self-organised *ad hoc* networks, the multicasting tasks are carried out by multifunctional mobile handsets, such as smart phones and tablets. Instead of broadcasting the content to all the MUs, they usually multicast it to the genuinely interested subset of MUs, who are simultaneously their social contacts. These social characteristics of hand-held mobile devices are to a large extent ignored by the operational wireless systems. Therefore, as argued in [134], it is necessary for us to consider the impact of social networking on the wireless network's performance.

For video sharing in wireless mobile networks, community-based solutions were proposed in [135] and [136], respectively, both of which operated by jointly considering the users' viewing behaviours as well as their mobility patterns. There is also a growing number of contribution on the content dissemination in Mobile Social Networks (MSNs) [137] [138] [139] [140]. However, these treatises mainly concentrated on large-scale MSNs [59], where the system performance is determined by the encounter properties of mobile nodes. For example, in [141], the continuous-time Markov chain was invoked for analysing the relevant delay performance, where the state transition rate is determined by the inter-contact time between a pair of mobile nodes. This approach cannot be used in the small-scale MSNs [59], where the system performance is determined by the wireless channel attenuation as well as social selection of the targets[3].

4.1.2 Novel Contribution

In Chapter 3, we have presented the philosophy of analysing the content dissemination performance across a MSN group, where we approximate the original Discrete-Time-Pure-Birth-Markov-Chain (DT-PBMC) by the Continuous-Time-Pure-Birth-Markov-Chain (CT-PBMC). However, some idealised simplifying assumptions[4] have been made for the sake of deriving the closed-form expressions of the various performance metrics. In this chapter, we will relax these idealised assumptions, but still manage to obtain the closed-form expressions of the content dissemination delay based on the original DT-PBMC.

Furthermore, during the content dissemination process of Chapter 3, all the MUs in the target MSN group were considered to have the same behaviour. Hence the MU's specific preference in selecting the content receivers, when he/she decided to multicast the content, was not considered in the mathematical modelling.

[1]The second stage of multicast is carried out by MUs who successfully receive the content during the first stage of multicast.

[2]The second stage of multicast is carried out by fixed relay stations.

[3]In large-scale MSNs, mobile nodes are sparsely distributed over a very large area. Only when a pair of nodes enters each other's transmission range, they can communicate. Hence, the system performance is substantially affected by the encounter rate (or the encounter probability) of mobile nodes, by their inter-contact duration and by their contact duration. By contrast, in small-scale MSNs, the mobile nodes are densely distributed in a small area, where all pairs of nodes tend to be within each other's transmission range. Hence, the system's performance is mainly affected by wireless channel, by the interference as well as the resource allocation and etc.

[4]Please refer to Section 3.8 for more details.

By contrast, in this chapter, the specific impact of real-life social relationships amongst the MUs will be taken into account.

Apart from the packet reception mechanism proposed in Chapter 3, we will introduce a Time-Division-Multiple-Access (TDMA) scheme into the Medium-Access-Control (MAC) layer so as to mitigate the adverse effects of the interference and packet collisions, when multiple MUs simultaneously multicast their content.

The novel contributions of this chapter are summarised as follows:

- We propose a novel content dissemination scheme based on a multi-stage cooperative social multicast protocol conceived for delivering the content of common interest to all the interested MUs in densely populated areas. The scheme considered falls into the category of small-scale MSNs [59].
- After receiving the content of common interest during the content dissemination process, a MU may only multicast the content to his/her social contacts rather than multicasting it to all the other hitherto unserved MUs. The social contacts of a MU are categorized into regular contacts and opportunistic contacts based on their geographic social relationships.
- A TDMA based multiple access scheme is invoked for the sake of readily implementing our content dissemination scheme in a practical scenario. Apart from the specific Time Slots (TSs) reserved for the MUs' multicast of the content, several TSs are reserved at the beginning of each transmission frame for the relevant control signalling exchange.
- Based on the geographic social relationships, the probability of a pair of MUs becoming each other's social contact is derived in closed-form. Furthermore, the achievable social unicast throughput is determined by jointly exploiting both the social relationships as well as the wireless links and the closed-form expression of the average social unicast throughput is derived.
- We model the multi-stage cooperative social multicast protocol aided content dissemination process by a DT-PBMC and derive closed-form expressions for characterising the statistical properties of the content dissemination delay, which is the time duration spanning from the initial Content Owners (COs) multicasting of the content until all the MUs successfully receive it.
- We compare the multi-stage cooperative multicast protocol conceived to a range of benchmark that have been widely adopted in previous studies of the content dissemination, such as non-cooperative direct social multicast, single-stage cooperative social multicast and non-cooperative gossip based social unicast protocols. The numerical results demonstrate the remarkable advantage of the multi-stage cooperative social multicast over the other protocols in terms of the average content dissemination delay.

4.1.3 Chapter Organisation

The rest of the chapter is organised as follows:

- In Section 4.2, we characterise the main features of our multi-stage cooperative social multicast aided content dissemination scheme.
- In Section 4.3, we introduce both the geographic social relationships in the social domain and the physical layer model of our wireless transmission scheme. We further investigate the specific impact of the social relationships and derive the achievable social unicast throughput.

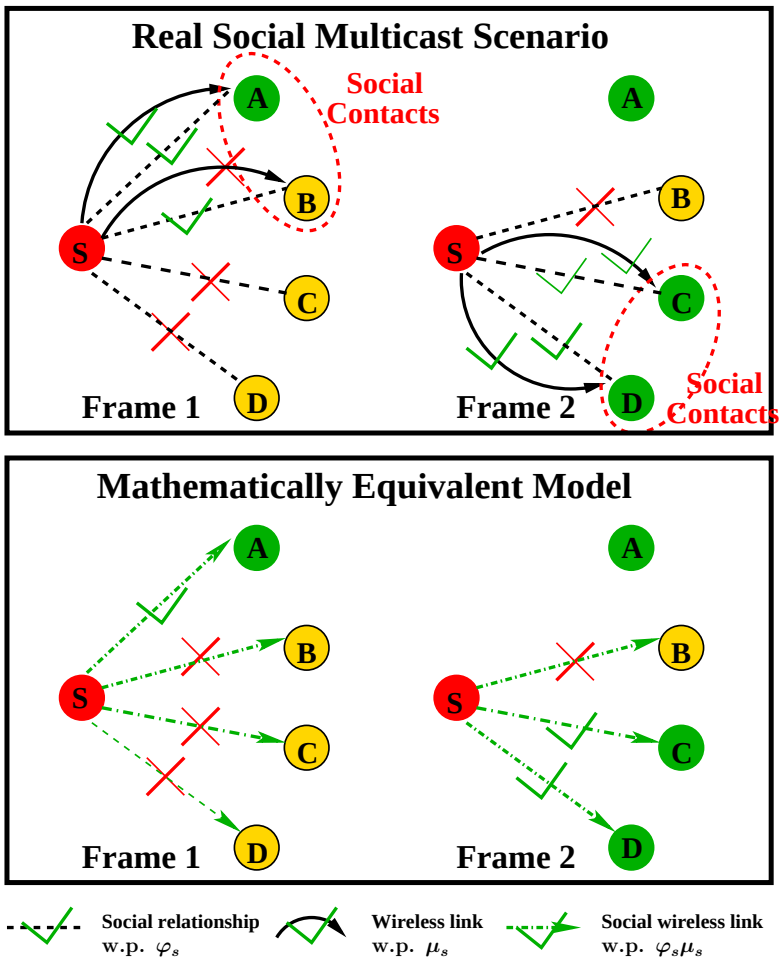

Figure 4.1: An example of the social multicast

- In Section 4.4, our content dissemination scheme is modelled by a DT-PBMC, whose state transition rates can be represented by a random matrix. Based on a set of four theorems, we characterise the statistical properties of the content dissemination delay in closed-form.
- In Section 4.5, the simulation based and the analytical performance of the content dissemination process are compared. We demonstrate that our multi-stage cooperative social multicast protocol aided content dissemination regime outperforms the benchmark schemes in terms of its average content dissemination delay.
- In Section 4.6, we conclude this chapter.

4.2 System Overview

In this section, we first introduce the social multicast model, based on which a distributed cooperative social multicast aided content dissemination protocol is proposed. Furthermore, other existing protocols that can be used for content dissemination are introduced. At last, a TDMA approach is invoked for solving the implementation concern of our protocol.

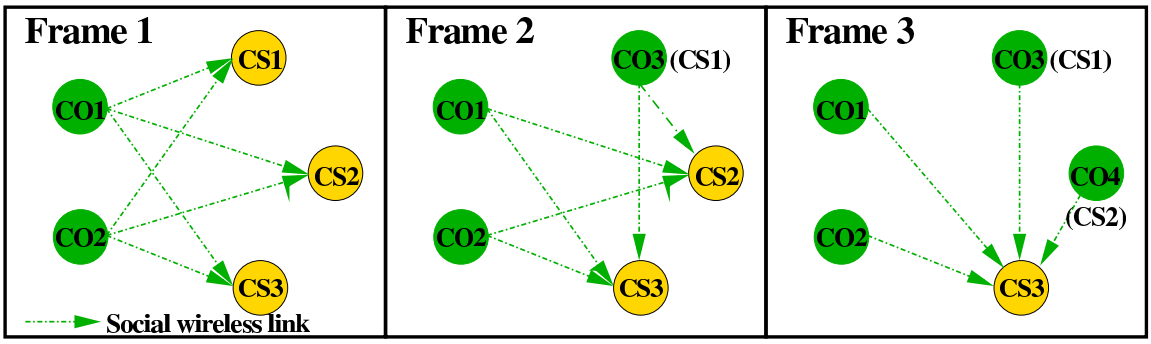

Figure 4.2: Multi-stage cooperative social multicast protocol

4.2.1 Social Multicast

The basic time unit of our discrete-time system is defined as the duration of a transmission frame. Different from the conventional multicast technique studied in [55]- [133], in this chapter, a CO only multicasts the content to the Content Seekers (CSs) who are simultaneously the CO's social contacts during the current frame.

The upper half of Figure 4.1 portrays a social multicast model in two consecutive transmission frames, where node S represents the CO, while node A to D represent the CSs. We assume that a CS may be one of the CO's social contacts with a probability of φ_s. As shown in Figure 4.1, during the first transmission frame, node A and B are node S's social contacts. Thus, the required physical wireless links are established between S and A as well as between S and B. However, due to the wireless propagation-induced degradation, a packet is only delivered successfully by a wireless link with a probability of μ_s. As shown in the upper half of Figure 4.1, during the first transmission frame, only the wireless link SA is capable of successfully delivering the content to the target, while SB fails. As a result, after the first frame, only node A has received the content successfully. Instead of A and B, node C and D become S's social contacts during the second transmission frame. Thus, the required wireless links are established between S and C as well as between S and D. Fortunately, both of these wireless links have successfully delivered the content to the targets. Then, at the end of the second transmission frame, node A, C and D have successfully received the content.

As a result, we observe that the successful packet delivery depends on the following two events: (1) The target is indeed the source's social contact, which occurs with a probability of φ_s; (2) The physical wireless link successfully delivers the packet from the source to the target, which has a probability of μ_s. These two independent random events are encountered simultaneously with a probability of $\varphi_s\mu_s$. As seen in Figure 4.1, in order to theoretically analyse the content dissemination delay, we may mathematically transform the upper 'Real social multicast scenario' of Figure 4.1 into an equivalent model.

Note that in the original social multicast model, S only multicasts the content to its social contacts during each transmission frame. However, in the mathematically equivalent model, S multicasts the content to all the interested CSs via the 'social wireless links', which are constituted by a combination of the social relationships and the physical wireless links, as shown in the bottom half of Figure 4.1. Moreover, the probability of a social wireless link successfully delivering a packet of the content to the target is $\varphi_s\mu_s$ during a transmission frame. This probability is termed here as the **social unicast throughput**, whose average is derived in Section 4.3.

4.2.2 Multi-Stage Cooperative Social Multicast Protocol for Content Dissemination

In this chapter, we conceive a multi-stage cooperative social multicast protocol for disseminating the content of common interest to N MUs, which roam within a bounded circular area. Before the commencement of content dissemination, some MUs actively acquire the content from the Centralised Infrastructure (CI). These MUs forms the initial CO set and cooperatively multicast the content to the other hitherto unserved CSs. The size of this initial CO set is assumed to be U. Once a CS successfully receives the content, it joins the CO set and cooperatively multicasts the content to the other hitherto unserved CSs with the aid of other COs, until all the CSs successfully receive this content. During the content dissemination process, we observe that the size of CO set continually increases as more and more served CSs join the CO set. If we consider the cooperative action within a specific CO set as a single stage of cooperative social multicast, then we typically need multiple stages of the cooperative social multicast for the sake of completely disseminating the content of common interest to all the CSs.

Figure 4.2 portrays an example of the multi-stage cooperative social multicast aided content dissemination process. During Frame 1, the CO set $\{CO1, CO2\}$ cooperatively multicasts the content to the unserved CS set $\{CS1, CS2, CS3\}$. At the end of Frame 1, $CS1$ successfully receives the content and joins the CO set as $CO3$. Thus, during Frame 2, the new CO set $\{CO1, CO2, CO3\}$ cooperatively multicasts the content to the unserved CS set $\{CS2, CS3\}$. By the end of Frame 2, $CS2$ successfully receives the content and joins the CO set as $CO4$. Finally, during Frame 3, the new CO set $\{CO1, CO2, CO3, CO4\}$ carries out the last stage of cooperative social multicast, and successfully delivers the content to the last unserved $CS3$.

4.2.3 Other Protocols for Content Dissemination

There are other protocols for content dissemination in literatures, which are portrayed in Figure 4.3. In order to implement these protocols in our model, we should impose the social constraints that a transmitter is only willing to unicast/multicast the content to its social contacts on these existing protocols.

4.2.3.1 Non-Cooperative Direct Social Multicast

This protocol originates from the conventional direct multicast, which was studied in [55]. Although we may have multiple COs at the beginning, in this protocol, we assume that there is only a single CO, who continually multicasts the content of common interest to its social contacts, until all the other unserved CSs successfully receive it, as detailed in Section 4.2.1. The social multicast delay of this protocol has been characterised in our previous work [61].

As shown in Figure 4.3(a), we have a pair of COs before the first transmission frame of the content dissemination process. However, only $CO1$ is enabled to continually multicast the content of common interest to the remaining unserved CSs via its social wireless links[5], while $CO2$ remains silent. After successfully receiving the content from $CO1$, the unserved $CS1$ becomes $CO3$. For the second transmission frame, we still have $CO1$ as the sole multicaster, while both $CO2$ and $CO3$ remain silent. Then the unserved $CS2$ becomes $CO4$ after it successfully receives the content from $CO1$ at the end of the transmission frame. However, $CO2$, $CO3$ and $CO4$ remain silent during the third transmission frame. Only $CO1$ multicasts the content towards the unserved $CS3$.

4.2.3.2 Single-Stage Cooperative Social Multicast

This protocol originates from the widely studied cooperative multicast model of [129]- [133], where only those specific COs that initially own the content would cooperatively multicast the content to their social

[5]Please refer to Section 4.2.1 for the definition of the social wireless link.

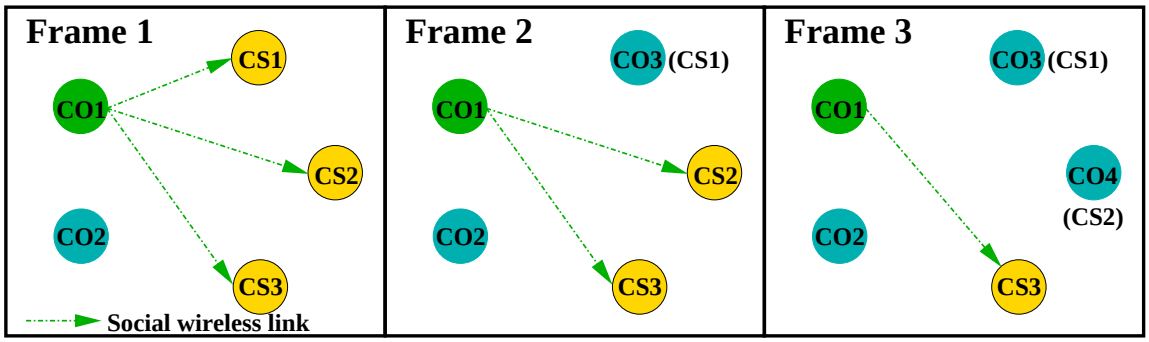

(a) Non−cooperative direct social multicast protocol

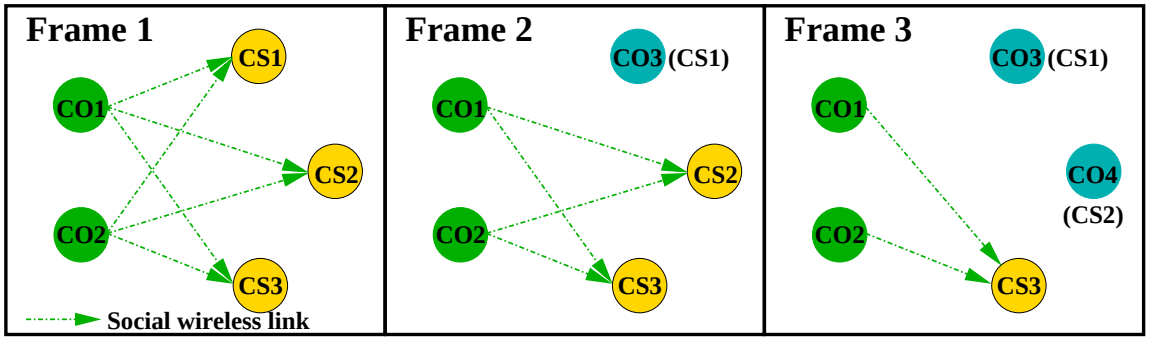

(b) Single−stage cooperative social multicast protocol

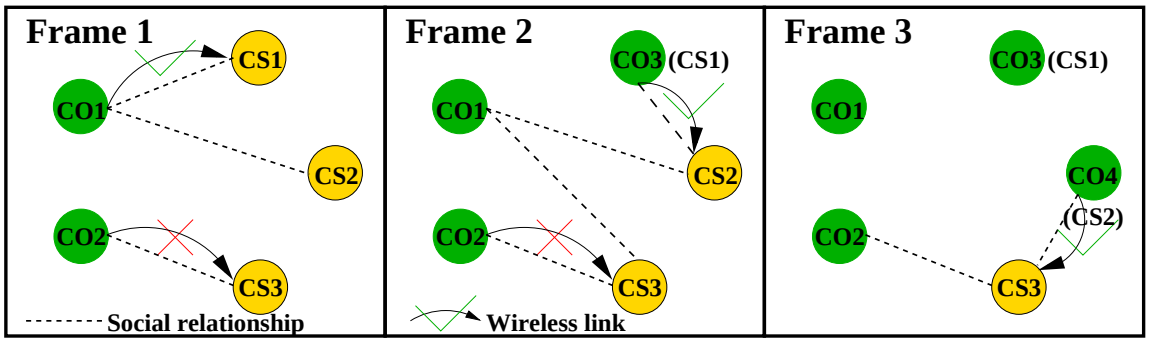

(c) Non−cooperative gossip based social unicast social multicast protocol

Figure 4.3: Other protocols adopted for disseminating the conent of common interest

contacts.

As shown in Figure 4.3(b), we have a pair of active COs, $CO1$ and $CO2$, before the content dissemination process commences. During the first transmission frame, $CO1$ and $CO2$ cooperatively multicast the content of common interest to the remaining unserved CSs. After this transmission frame, $CS1$ successfully receives the content and becomes $CO3$. During the second transmission frame, $CO1$ and $CO2$ continually multicast the content to other unserved CSs, but $CO3$ remains silent. After this transmission frame, $CS2$ successfully receives the content and becomes $CO4$. During the third transmission frame, $CO1$ and $CO2$ still cooperatively multicast the content to the unserved $CS3$, but both $CO3$ and $CO4$ remain silent.

4.2.3.3 Non-Cooperative Gossip based Social Unicast

This protocol originates from [142] and was further invoked for information dissemination in [115]. When we implement this protocol in our scenario, we made a few changes in comparison to the protocol studied

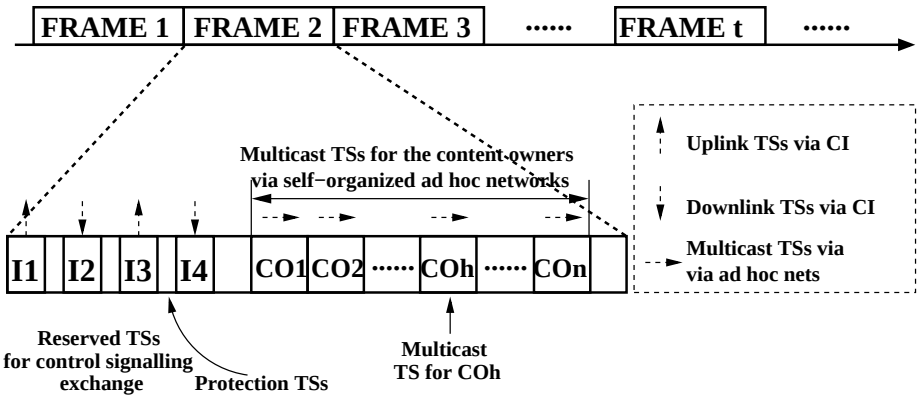

Figure 4.4: The frame structure

in [115]. During a transmission frame, a CO may have several social contacts and it has to select a single one from its social contacts in order to form a CO and CS pair for further disseminating the content. If a CS has already been selected by one of the COs, it cannot be selected by other COs. According to [115], for the sake of forming this CO and CS pair, the CS should be randomly selected from the CO's social contacts. However, in order to form as many CO and CS pairs as possible, in our algorithm, a CO that has fewer social contacts during a transmission frame has a higher priority to select a CS, who is simultaneously one of the CO's social contact. After the CS successfully receives the content, it may join the set of COs for futher disseminating the content.

As shown in Figure 4.3(c), we have a pair of active COs, namely $CO1$ and $CO2$, before the content dissemination process commences. During the first transmission frame, we observe from Figure 4.3(b) that $CO1$ has two social contacts, namely $CS1$ and $CS2$. Then $CO1$ chooses $CS1$ as its gossiping partner and establishes a wireless unicast link towards it. Meanwhile, $CO2$ only has a single social contact, namely $CS3$. Consequently they form another gossiping pair and a wireless unicast link is established between them. Then these two gossiping pairs start transmitting the content from the COs to the unserved CSs. However, due to the channel's attenuation, only $CS1$ receives the content successfully from its gossiping partner $CO1$. During the second transmission frame, $CO1$ has both $CS2$ and $CS3$ as its social contacts, while $CO3$ only has $CS2$ and $CO2$ only has $CS3$ as their social contacts, respectively. Hence, $CO2$ and $CO3$ have higher priorities to select their gossiping partners than $CO1$ does. As a result, two gossiping pairs are formed, which includes the pair of $CO3$ and $CS2$ and the pair of $CO2$ and $CS3$. The corresponding wireless unicast links are established as well. However, only $CS2$ succeeds in receiving the content from its gossiping partner $CO3$ at the end of this transmission frame. $CO1$ remains silent during the current frame, since it is not in any gossiping pairs. During the third transmission frame, $CO2$ and $CO4$ have a common social contact, namely $CS3$. However, only $CO4$ chooses $CS3$ to form a gossiping pair and establishes a wireless unicast link towards $CS3$. At the end of this frame, $CS3$ successfully received the content from $CO4$. The other COs, say $CO1$, $CO2$ and $CO3$ remain silent during the current transmission frame, since they do not belong to any gossiping pairs.

4.2.4 Time-Division-Multiple-Access Approach for Implementation

According to the protocol introduced in Section 4.2.2, multiple COs simultaneously multicast the content of common interest during a transmission frame. In order to avoid any collisions incurred by these multiple COs, each CO should be allocated an orthogonal channel. Here, we invoke a TDMA-based approach for

implementing our content dissemination scheme[6]. An Information Controller (IC)[7] is appointed in order to reduce the overhead of information exchange between COs and CSs. The structure of a transmission frame is seen in Figure 4.4.

As shown in Figure 4.4, the first four TSs are reserved for the control signalling exchange between the IC and the COs/CSs. Specifically, the TS 'I1' of Figure 4.4 is allocated to the COs for reporting their willingness to disseminate the content. The TS 'I2' of Figure 4.4 is dedicated to the IC for broadcasting both the resource scheduling information as well as the COs' identities to the potential CSs. The TS 'I3' of Figure 4.4 is assigned to the active CSs for the sake of reporting their interests to the IC. Moreover, the TS 'I4' of Figure 4.4 is allocated to the IC for informing the COs of both the active CSs' identities as well as of the resource allocation scheme employed.

Following the control signalling exchange phase, the *ad hoc* network is ready for content dissemination. As shown in Figure 4.4, each CO is allocated a TS for multicasting the content of common interest to its social contacts.

The frame structure portrayed in Figure 4.4 is similar to the TDMA scheme proposed in [143] for Wi-Fi mesh networks, where a frame consists of 'control slots', 'contention slots' as well as 'data slots'. The so-called 'control slots' of [143] are used both for time synchronisation and for explicitly conveying the resource allocation scheme's features and the identities of the mobile nodes. We can see that these 'control slots' of [143] have similar functions to those of the TSs reserved for information exchange in our proposed frame structure, as introduced above. Furthermore, as demonstrated in [143], time synchronisation can also be achieved with the aid of 'control slots' at a high timing accuracy. Nevertheless, thanks to the IC, accurate time synchronisation can be more readily realised in our TDMA approach than in the distributed approach of [143]. Moreover, as reported in [143], the control overhead is less than 10% for a purely self-organised *ad hoc* network operating without any ICs. Hence, with the aid of the IC, we impose an even lower control overhead in our scheme.

4.3 Social Strength and Social Unicast Throughput

In this section, we will firstly define the probability φ_s that a CS becomes a CO's social contact, while deriving the successful packet reception probability μ_s of a physical wireless link. Then, we derive the closed-form formula for the average social unicast throughput $\overline{v}_s$.

4.3.1 PDF of the Random Geographic Distance

4.3.1.1 Mobility and Connectivity

We assume that all MUs roam in a bounded circular area having a radius of R. The position of the i-th MU during the frame t is denoted by $\mathbf{P}_i(t)$, which obeys a stationary and ergodic process with a stationary uniform distribution in the circular area [116]. Moreover, the positions of different MUs are independently and identically distributed (i.i.d.). This mobility model has been widely used for analysing the performance of mobile networks [115].

Moreover, the range of Wi-Fi in outdoor scenarios can be up to 100 m. If the diameter of the studied circular area is comparable to this range, our content dissemination model belongs to the scenario of small-scale MSNs [59], where the system performance is dominated by the wireless channel's attenuation as well

[6]Other approaches that are capable of providing orthogonal channels can also be implemented, such as Carrier-Sense-Multiple-Access (CSMA), Orthogonal-Frequency-Division-Multiple-Access (OFDMA), and Code-Division-Multiple-Access (CDMA).

[7]Centralised infrastructure, such as a BS and a Wi-Fi access point, is a nature-born information controller, since all the MUs in the same area regularly exchange control signalling with it.

as by the specific social contact selection.

4.3.1.2 PDF of the Geographic Distance

We may derive the Probability Density Function (PDF) of the geographic distance Y_s between a pair of MUs by exploiting the following methodology. Given that the source is currently located at a point $\mathbf{P} = \mathbf{p}$, we may derive the conditional probability $P(Y_s \leq y_s|\mathbf{P} = \mathbf{p})$ by computing the intersection area of two circles, one of which is the circular area considered and the other is a circle centred at the point $\mathbf{P} = \mathbf{p}$ having a radius of y_s. Integrating $P(Y_s \leq y_s|\mathbf{P} = \mathbf{p})$ over all possible points gives us the Cumulative Distribution Function (CDF) of Y_s, whose derivative gives the PDF of Y_s between a pair of MUs [123]:

$$f_{Y_s}(y_s) = \frac{8}{\pi R}\frac{y_s}{2R}\left[\arccos\left(\frac{y_s}{2R}\right) - \frac{y_s}{2R}\sqrt{1-\left(\frac{y_s}{2R}\right)^2}\right], \tag{4.1}$$

for $0 \leq y_s \leq 2R$, and 0, otherwise. Note that we can also arrive at the PDF $f_{Y_s}(y_s)$ of Eq.(4.1) by exploiting Crofton's famous fixed-point theorem [144], the derivation process relying on this method is detailed in Theorem 6.9 of Chapter 6.

However, due to its complexity, further integration over $f_{Y_s}(y_s)$ may not produce a closed-form expression. Hence, we may need an approximate alternative expression for $f_{Y_s}(y_s)$. Given the following two Taylor expansion based expressions:

$$\arccos(z) = \frac{\pi}{2} - \sum_{n=0}^{\infty}\frac{(2n)!}{4^n(n!)^2(2n+1)}\cdot z^{2n+1}, \tag{4.2}$$

$$\sqrt{1-z^2} = 1 + \sum_{n=1}^{\infty}\prod_{m=1}^{n}(2m-3)\frac{z^{2n+1}}{n!2^n}, \tag{4.3}$$

by replacing z in Eqs.(4.2) and (4.3) by $y_s/2R$ and substituting them into Eq.(4.1), we arrive at an alternative expression for Eq.(4.1):

$$f_{Y_s}(y_s) = \frac{8}{\pi R}\left[\frac{\pi}{2}\frac{y_s}{2R} + \sum_{n=0}^{\infty}C_n\left(\frac{y_s}{2R}\right)^{2n+2}\right], \tag{4.4}$$

$$\text{where } C_n = \frac{2\cdot(2n)!}{4^n(n!)^2(2n+1)(2n-1)} \tag{4.5}$$

for $0 \leq y_s \leq 2R$, and 0, otherwise.

If we limit the maximum number of terms in the summation to $n_{\max}$, we arrive at an approximate version of Eq.(4.4):

$$\widetilde{f_{Y_s}}(y_s) = C_{Y_s}\cdot\frac{8}{\pi R}\left(\frac{\pi}{2}\frac{y_s}{2R} + \sum_{n=0}^{n_{\max}}C_n\left(\frac{y_s}{2R}\right)^{2n+2}\right), \tag{4.6}$$

$$\text{where } C_{Y_s} = \frac{\pi}{4}\left(\pi + \sum_{n=0}^{n_{\max}}\frac{4C_n}{2n+3}\right)^{-1}, \tag{4.7}$$

for $0 \leq y_s \leq 2R$, and 0, otherwise. The constant C_{Y_s} in Eq.(4.6) is derived for the sake of guaranteeing that $\int_0^{2R}\widetilde{f_{Y_s}}(y_s)dy_s = 1$.

In Figure 4.5, we plot the Root-Mean-Square-Error (RMSE) between $f_{Y_s}(y_s)$ of Eq.(4.1) and $\widetilde{f_{Y_s}}(y_s)$ of Eq.(4.6). As shown in Figure 4.5, when R is higher than 10 m, $n_{\max} = 4$ guarantees that the RMSE becomes lower than 10^{-3}. This sufficiently low RMSE indicates that our approximation is valid for the most practical cases.

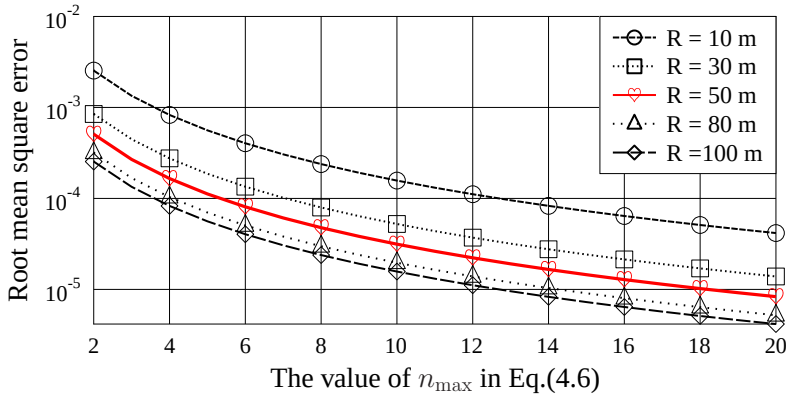

Figure 4.5: The root-mean-square-error (RMSE) between $\widetilde{f_{Y_s}}(y_s)$ and $f_{Y_s}(y_s)$

4.3.2 Geographic Social Relationships

In Milgram's widely known 'small-world' experiment [145], he proved that there was a maximum of six hop separation on average between any pair of people in the U.S.A. Furthermore, Watts and Strogatz claimed that any network obeys a hybrid structure between regular networks and random ones [16]. They also defined the so-called short-range and long-range contacts. The well-known results of Milgram's experiment were theoretically proved in [19] [20].

The authors of [18] studied a two-dimensional grid network obeying the small-world property of [16]. In [18], source node s selects any other node v as its long-range contact with a probability proportional to $y^{-\alpha}(s,v)$, where $y(s,v)$ is the distance between s and v, while α is an social exponent. Here, the 'distance' may indicate either a virtual social distance or an exact geographic distance. This work was extended to wireless *ad hoc* networks in [146] in order to analyse the impact of social groups on the wireless network's capacity, where a node in the wireless *ad hoc* network is selected to be the target with a probability proportional to $y^{-\alpha}(s,v)$, where $y(s,v)$ represents the exact geographic distance.

Furthermore, the authors of [147] found that when the geographic distance is shorter than 1000 km, the probability of a pair of users sharing a social relationship largely depends on the geographic distance between them[8]. This probability is proportional to $y^{-\alpha}$, where the social exponent α is estimated to be 1.2. Similar results were also provided in [148], where the social exponent was estimated for mobile communication. When using the maximum-likelihood method of [149], these exponents were found to be $\alpha \approx 1.58$ for voice ties and $\alpha \approx 1.49$ for text ties.

Based on the aforementioned literature, we assume that if a CS is within the neighbourhood range of a CO, the probability of this CS becoming the CO's social contact is unity, and this CS is termed as the *regular contact* of the CO. If the CS is beyond the neighbourhood range of the CO, the CS may still become the social contact of the CO with a probability that is inversely proportional to the geographic distance between them. This sort of social contact is termed as opportunistic contact. As a result, the probability of a CS becoming a CO's social contact[9], which is also termed as social strength, is defined as:

$$\varphi_s(y_s) = \begin{cases} 1, & 0 \le y_s \le r, \\ \dfrac{1}{(y_s/r)^{\alpha}}, & y_s > r, \end{cases} \tag{4.8}$$

where y_s is the geographic distance between a pair of MUs, r is the neighbourhood range and α is the social exponent in line with [18]- [148].

[8]The data are extracted from an online community–LiveJournal (http://www.livejournal.com)

[9]For the sake of social contact selection, a CO should be aware of the distances from itself to CSs. This distance awareness can be easily realised by the GPS module and the relevant mobile applications (such as WeChat, http://www.wechat.com) installed on the CO's multifunctional mobile devices.

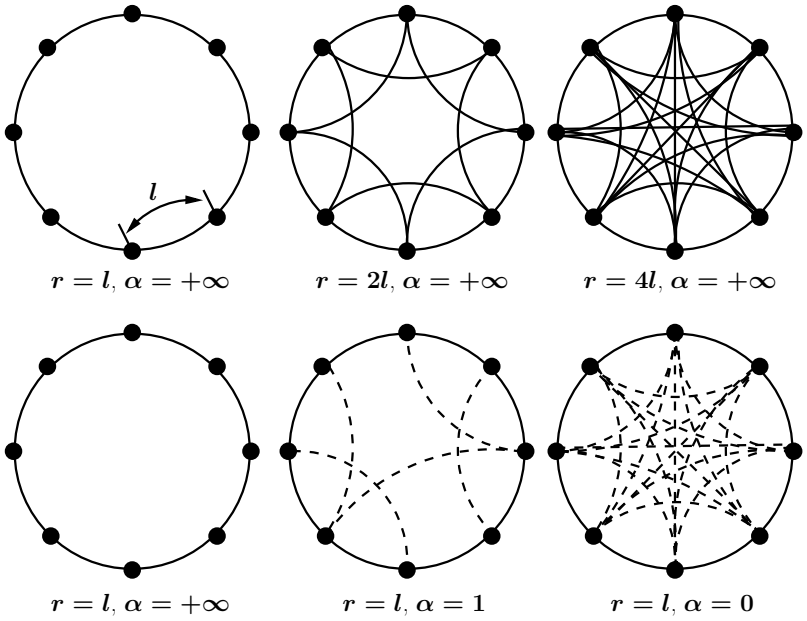

Figure 4.6: Impact of the neighbourhood range and social exponent on geographic social relationships

In Figure 4.6, eight nodes are seen to be uniformly arranged on a circle. If $\alpha = +\infty$, indicating that a node only has regular contacts (solid lines in Figure 4.6), as r increases from l to $4l$, a node may have more regular contacts for potential communications. If we fix r to l, indicating that a node only has the adjacent nodes in its regular contact set, as α reduces from infinity to 0, in line with Eq.(4.8), a node may have more opportunistic contacts (dotted lines in Figure 4.6).

4.3.3 Analysis of the Social Strength

Since the social strength between a pair of MUs is dominated by the distance between them according to Eq.(4.8), it varies from one transmission frame to another, when both of the MUs move within the area studied. The average social strength $\overline{\varphi}_s$ may be derived by integrating $\varphi_s(y_s)$ over all possible values of $Y_s = y_s$, as expressed in the following equation:

$$\overline{\varphi}_s = \int_0^{2R} \varphi_s(y_s) \cdot f_Y(y_s) dy = \underbrace{\int_0^r 1 \cdot f_{Y_s}(y_s) dy_s}_{\overline{\varphi}_{s,reg}} + \underbrace{\int_r^{2R} \frac{1}{(y_s/r)^\alpha} f_{Y_s}(y_s) dy_s}_{\overline{\varphi}_{s,opp}}, \tag{4.9}$$

where $f_{Y_s}(y_s)$ is the PDF of the random distance Y_s between this pair of MUs. The upper integral limit of Eq.(4.9) is determined by the maximum possible distance between a pair of MUs. Since we assume that all the MUs move within a circular area having a radius of R, as introduced in Section 4.3.1, the upper integral limit of Eq.(4.9) is $2R$. The first integral of Eq.(4.9) represents the average probability of this pair of MUs becoming each other's regular contact, while the second represents the average probability of this pair of MUs becoming each other's opportunistic contact.

By substituting the PDF $f_{Y_s}(y_s)$ of Eq.(4.1) into the first integral of Eq.(4.9), we may express the average

probability $\overline{\varphi}_{s,reg}$ as

$$\begin{aligned}\overline{\varphi}_{s,reg} &= \int_0^r \frac{8}{\pi R}\frac{y_s}{2R}\left[\arccos\left(\frac{y_s}{2R}\right) - \frac{y_s}{2R}\sqrt{1-\left(\frac{y_s}{2R}\right)^2}\right]dr \\ &= \frac{2}{\pi}\Bigg\{4\left(\frac{y_s}{2R}\right)^2\arccos\left(\frac{y_s}{2R}\right) + \arcsin\left(\frac{y_s}{2R}\right) \\ &\quad - \left[\frac{y_s}{2R} + 2\left(\frac{y_s}{2R}\right)^3\right]\sqrt{1-\left(\frac{y_s}{2R}\right)^2}\Bigg\}\Bigg|_0^r. \end{aligned} \tag{4.10}$$

However, due to its underlying complexity, it is impossible to derive the closed-form expression for the probability $\overline{\varphi}_{s,opp}$ by substituting the original distance PDF $f_{Y_s}(y_s)$ of Eq.(4.1) into Eq.(4.9). Therefore, we have to substitute the approximate PDF $\widetilde{f}_{Y_s}(y_s)$ of Eq.(4.6) into Eq.(4.9). As a result, the average probability $\overline{\varphi}_{s,opp}$ can be derived as

$$\begin{aligned}\overline{\varphi}_{s,opp} &\approx \int_r^{2R} \frac{C_{Y_s}}{(y_s/r)^\alpha}\frac{8}{\pi R}\left(\frac{\pi}{2}\frac{y_s}{2R} + \sum_{n=0}^{n_{\max}} C_n\left(\frac{y_s}{2R}\right)^{2n+2}\right) \\ &= \frac{8C_{Y_s}r^\alpha}{\pi R}\left(\frac{\pi}{4R}\Psi(y_s|1,\alpha) + \sum_{n=0}^{n_{\max}}\frac{C_n\Psi(y_s|2n+2,\alpha)}{2R^{2n+2}}\right)\Bigg|_r^{2R}, \end{aligned} \tag{4.11}$$

where the expressions of C_n and C_{Y_s} can be found in Eqs.(4.5) and (4.7), respectively. The function $\Psi(y_s|\beta,\alpha)$ in Eq.(4.11) is expressed as

$$\Psi(y_s|\beta,\alpha) = \int y_s^{\beta-\alpha}dy_s = \begin{cases} \dfrac{y_s^{\beta-\alpha+1}}{\beta-\alpha+1}, & \text{if } \beta-\alpha \neq -1, \\ \ln y_s, & \text{if } \beta-\alpha = -1. \end{cases} \tag{4.12}$$

Finally, the average social strength $\overline{\varphi}_s$ can be derived as $\overline{\varphi}_s = \overline{\varphi}_{s,reg} + \overline{\varphi}_{s,opp}$. Given that N MUs move within the circular area studied, the number $\mathcal{N}_{soc}$ of the social contacts that a specific MU has is a binomially distributed random variable, which can be denoted as $\mathcal{N}_{soc} \sim B(N,\overline{\varphi}_s)$. Hence its average number of social contacts can be expressed as $\overline{\mathcal{N}}_{soc} = N\cdot\overline{\varphi}_s$. Similarly, the number of both the regular contacts and of the opportunistic contacts of a specific MU are binomially distributed random variables as well, which are denoted as $\mathcal{N}_{reg} \sim B(N,\overline{\varphi}_{s,reg})$ and $\mathcal{N}_{opp} \sim B(N,\overline{\varphi}_{s,opp})$, respectively.

4.3.4 Successful Packet Delivery Probability of a Physical Wireless Link

4.3.4.1 Small-Scale Fading

The small-scale fading is modelled by uncorrelated stationary flat Rayleigh fading [114]. The fading magnitude $|h_s(t)|$ during the t-th TS, which varies from one TS to another, is a Rayleigh distributed random variable. Since each CO is assigned a single TS during a transmission frame according to Section II-B, t can also be interpreted as the index of the transmission frame. Consequently, the square of the channel's magnitude $|h_s(t)|^2$ obeys the exponential distribution associated with $\mathcal{E}[|h_s(t)|^2] = 1$. The PDF and CDF of $X = |h_s(t)|^2$ are $f_X(x) = \exp(-x)$, $F_X(x) = 1-\exp(-x)$, $x > 0$, respectively.

4.3.4.2 Path-Loss

According to [114], the Path-Loss (PL) equation is invalid for calculating the attenuation in the near-field of the transmit antennas. We assume that the PL only imposes attenuation on a wireless link, when its length

y_s is longer than a reference threshold d_0. Then the PL model is formulated as

$$\frac{P_{s,r}}{P_{s,0}} = \begin{cases} 1, & 0 \leq y_s \leq d_0, \\ \dfrac{1}{(y_s/d_0)^{\kappa}}, & y_s > d_0, \end{cases} \tag{4.13}$$

where $P_{s,0}$ is the received power at the point that is d_0 meters away from the transmitter, $P_{s,r}$ is the average power received after experiencing PL at a CS, while κ is the PL exponent.

4.3.4.3 Successful Packet Delivery

In the MAC layer, we assume that a packet of the content is transmitted successfully during a TS from a CO to a CS, only when the instantaneous received Signal-to-Noise-Ratio (SNR) is above a predefined threshold γ [117]. As a result, when jointly considering the small-scale fading and the PL, the successful packet delivery probability of a physical wireless link is given by

$$\mu_s(y_s) = \begin{cases} P(|h_s|^2 > Ad_0^{\kappa}) = e^{-Ad_0^{\kappa}}, & 0 \leq y_s \leq d_0, \\ P(|h_s|^2 > Ay_s^{\kappa}) = e^{-Ay_s^{\kappa}}, & y_s > d_0, \end{cases} \tag{4.14}$$

where we have $A = (\gamma N_0 W_s)/(P_{s,0} d_0^{\kappa})$ and y_s is the distance between a CO and CS pair, while $N_0 W_s$ is the noise power. Naturally, $\mu_s(y_s)$ is equivalent to the throughput of the physical wireless link expressed in packets/frame [150].

4.3.5 Analysis of the Social Unicast Throughput

Given a specific distance of $Y_s = y_s$, we denote the social unicast throughput as $\nu_s(y_s) = \varphi_s(y_s) \cdot \mu_s(y_s)$. Then, we may derive the average social unicast throughput by integrating $\nu_s(y_s)$ over all possible values of $Y_s = y_s$. However, we may have different expressions for $\nu_s(y_s)$, given the different values of the neighbourhood range r and PL reference distance d_0:

Case 1: If $d_0 \leq r$, then we have the following expression for $\nu_{s,(1)}(y_s)$:

$$\nu_{s,(1)}(y_s) = \begin{cases} e^{-Ad_0^{\kappa}}, & 0 \leq y_s \leq d_0, \\ e^{-Ay_s^{\kappa}}, & d_0 < y_s \leq r, \\ e^{-Ay_s^{\kappa}} \cdot \left(\dfrac{y_s}{r}\right)^{-\alpha}, & r < y_s \leq 2R. \end{cases} \tag{4.15}$$

Therefore, the average social unicast throughput can be formulated as

$$\begin{aligned} \mathcal{E}[\nu_{s,(1)}] = & \underbrace{\int_0^{d_0} e^{-Ad_0^{\kappa}} f_{Y_s}(y_s) dy}_{I_1^{(1)}} + \underbrace{\int_{d_0}^{r} e^{-Ay_s^{\kappa}} f_{Y_s}(y_s) dy}_{I_2^{(1)}} \\ & + \underbrace{\int_r^{2R} e^{-Ay_s^{\kappa}} \left(\frac{r}{y_s}\right)^{\alpha} f_{Y_s}(y_s) dy_s}_{I_3^{(1)}}. \end{aligned} \tag{4.16}$$

Let us now substitute $f_{Y_s}(y_s)$ of Eq.(4.1) into the first integral $I_1^{(1)}$ of Eq.(4.16). Hence, $I_1^{(1)}$ can be formulated as

$$\begin{aligned} I_1^{(1)} &= \int_0^{d_0} e^{-Ad_0^{\kappa}} f_{Y_s}(y_s) dy_s \\ &= e^{-Ad_0^{\kappa}} \cdot \frac{2}{\pi} \left\{ 4 \left(\frac{y_s}{2R}\right)^2 \arccos\left(\frac{y_s}{2R}\right) + \arcsin\left(\frac{y_s}{2R}\right) \right. \\ &\quad \left. - \left[\frac{y_s}{2R} + 2\left(\frac{y_s}{2R}\right)^3\right] \sqrt{1 - \left(\frac{y_s}{2R}\right)^2} \right\} \Bigg|_0^{d_0}, \end{aligned} \tag{4.17}$$

Given the inherent complexity of Eq.(4.1), we have to substitute the approximate PDF $\widetilde{f_{Y_s}}(y_s)$ of Eq.(4.6) into $I_2^{(1)}$ of Eq.(4.16), we have

$$\begin{aligned} I_2^{(1)} &\approx \int_{d_0}^{r} e^{-Ay_s^\kappa} \widetilde{f}_{Y_s}(y_s) dy_s \\ &= \int_{d_0}^{r} e^{-Ay_s^\kappa} \cdot \frac{8C_{Y_s}}{\pi R} \left(\frac{\pi}{2} \frac{y_s}{2R} + \sum_{n=0}^{n_{\max}} C_n \left(\frac{y_s}{2R} \right)^{2n+2} \right) dy_s \\ &= \frac{8C_{Y_s}}{\pi R} \left[\frac{\pi}{4R} \int_{d_0}^{r} e^{-Ay_s^\kappa} y_s dy_s + \sum_{n=0}^{n_{\max}} \frac{C_n}{(2R)^{2n+2}} \int_{d_0}^{r} e^{-Ay_s^\kappa} y_s^{2n+2} dy_s \right] \\ &= \frac{8C_{Y_s}}{\pi R} \left[\frac{\pi}{4R} \Phi(y_s|1,0,A) + \sum_{n=0}^{n_{\max}} \frac{C_n \Phi(y_s|2n+2,0,A)}{(2R)^{2n+2}} \right] \Big|_{d_0}^{r}, \end{aligned} \tag{4.18}$$

where the function $\Phi(y_s|\beta,\alpha,A)$ is defined as

$$\begin{aligned} \Phi(y_s|\beta,\alpha,A) &= \int y_s^{\beta-\alpha} e^{-Ay_s^\kappa} dy_s \\ &= \begin{cases} -\dfrac{A^{z_1}\Gamma(-z_1, Ay_s^\kappa)}{\kappa}, & z_1 = \dfrac{\alpha-\beta-1}{\kappa}, \text{ if } \beta < \alpha, \\ -\dfrac{\Gamma(z_2, Ay_s^\kappa)}{\kappa A^{z_2}}, & z_2 = \dfrac{\beta-\alpha+1}{\kappa}, \text{ if } \beta \geq \alpha, \end{cases} \end{aligned} \tag{4.19}$$

while the functions $\Gamma(-z_1, Ay_s^\kappa)$ and $\Gamma(z_2, Ay_s^\kappa)$ are given by the following two equations [151]:

$$\Gamma(-z_1, Ay_s^\kappa) = \int_{Ay_s^\kappa}^{\infty} \frac{1}{t^{z_1+1}} e^{-t} dt, \ \Gamma(z_2, Ay_s^\kappa) = \int_{Ay_s^\kappa}^{\infty} t^{z_2-1} e^{-t} dt.$$

Furthermore, the closed-form expression for the third integral $I_3^{(1)}$ of Eq.(4.16) can also be derived by substituting $\widetilde{f_{Y_s}}(y_s)$ of Eq.(4.6) into $I_3^{(1)}$, which is expressed as

$$\begin{aligned} I_3^{(1)} &\approx \int_{r}^{2R} e^{-Ay_s^\kappa} \left(\frac{r}{y_s} \right)^\alpha \widetilde{f_{Y_s}}(y_s) dy_s \\ &= \int_{r}^{2R} e^{-Ay_s^\kappa} \left(\frac{r}{y_s} \right)^\alpha \frac{8C_{Y_s}}{\pi R} \left(\frac{\pi}{2} \frac{y_s}{2R} + \sum_{n=0}^{n_{\max}} C_n \left(\frac{y_s}{2R} \right)^{2n+2} \right) dy \\ &= \frac{8C_{Y_s} r^\alpha}{\pi R} \left[\frac{\pi}{4R} \Phi(y_s|1,\alpha,A) + \sum_{n=0}^{n_{\max}} \frac{C_n \Phi(y_s|2n+2,\alpha,A)}{(2R)^{2n+2}} \right] \Big|_{r}^{2R}, \end{aligned} \tag{4.20}$$

where the function $\Phi(y_s|\beta,\alpha,A)$ has been defined in Eq.(4.19).

Case 2: If $d_0 > r$, then we have the following expression for $\nu_{s,(2)}(y_s)$:

$$\nu_{s,(2)}(y_s) = \begin{cases} e^{-Ad_0^\kappa}, & 0 \leq y_s \leq r, \\ e^{-Ad_0^\kappa} \cdot \left(\dfrac{y_s}{r} \right)^{-\alpha}, & r < y_s \leq d_0, \\ e^{-Ay_s^\kappa} \cdot \left(\dfrac{y_s}{r} \right)^{-\alpha}, & d_0 < y_s \leq 2R. \end{cases} \tag{4.21}$$

Similarly to Eq.(4.16), we may express the average social unicast throughput as

$$\begin{aligned} \mathcal{E}[\nu_{s,(2)}] = &\underbrace{\int_0^r e^{-Ad_0^\kappa} f_{Y_s}(y_s) dy_s}_{I_1^{(2)}} + \underbrace{\int_r^{d_0} e^{-Ad_0^\kappa} \left(\frac{r}{y_s} \right)^\alpha f_{Y_s}(y_s) dy_s}_{I_2^{(2)}} \\ &+ \underbrace{\int_{d_0}^{2R} e^{-Ay_s^\kappa} \left(\frac{r}{y_s} \right)^\alpha f_{Y_s}(y_s) dy_s}_{I_3^{(2)}}. \end{aligned} \tag{4.22}$$

Substituting the integration limits of $[0, d_0]$ in Eq.(4.17) by $[0, r]$, we are now capable of deriving the closed-form formula for $I_1^{(2)}$. Similarly, substituting the integration limits of $[r, 2R]$ in Eq.(4.20) by $[d_0, 2R]$, we

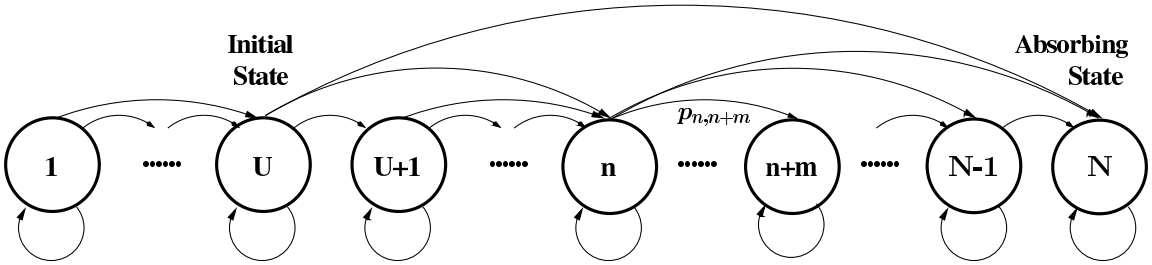

Figure 4.7: Discrete-Time-Pure-Birth-Markov-Chain

arrive at the closed-form formula for $I_3^{(2)}$. However, we have to derive the integral $I_2^{(2)}$ specifically. Substituting $\widetilde{f_{Y_s}}(y_s)$ of Eq.(4.6) into $I_2^{(2)}$ of Eq.(4.22), $I_2^{(2)}$ is expressed as

$$\begin{aligned} I_2^{(2)} &\approx \int_r^{d_0} e^{-Ad_0^\kappa} \left(\frac{r}{y_s}\right)^\alpha \widetilde{f_{Y_s}}(y_s) dy_s \\ &= \int_r^{d_0} e^{-Ad_0^\kappa} \left(\frac{r}{y_s}\right)^\alpha \frac{8C_{Y_s}}{\pi R} \left(\frac{\pi}{2}\frac{y_s}{2R} + \sum_{n=0}^{n_{\max}} C_n \left(\frac{y_s}{2R}\right)^{2n+2}\right) dy_s \\ &= e^{-Ad_0^\kappa} \cdot \frac{8C_{Y_s} r^\alpha}{\pi R} \left[\frac{\pi}{4R}\int_r^{d_0} y_s^{1-\alpha} dy + \sum_{n=0}^{n_{\max}} \frac{C_n}{(2R)^{2n+2}} \int_r^{d_0} y_s^{2n+2-\alpha} dy_s\right] \\ &= e^{-Ad_0^\kappa} \cdot \frac{8C_{Y_s} r^\alpha}{\pi R} \left[\frac{\pi}{4R}\Psi(y_s|1,\alpha) + \sum_{n=0}^{n_{\max}} \frac{C_n}{(2R)^{2n+2}} \Psi(y_s|2n+2,\alpha)\right]\Bigg|_r^{d_0}, \end{aligned} \tag{4.23}$$

where the function $\Psi(y_s|\beta,\alpha)$ has been defined by Eq.(4.12).

In a nutshell, the average social unicast throughput is obtained as

$$\overline{\nu}_s = \mathcal{E}[\nu_s] = \begin{cases} I_1^{(1)} + I_2^{(1)} + I_3^{(1)}, & \text{if } d_0 \le r, \\ I_1^{(2)} + I_2^{(2)} + I_3^{(2)}, & \text{if } d_0 > r. \end{cases} \tag{4.24}$$

4.4 Delay Analysis of the Content Dissemination Process

Let us now analyse the delay characteristics of the multi-stage cooperative social multicast protocol aided content dissemination.

4.4.1 Discrete-Time-Pure-Birth Based Markov Chain

According to Section 4.2.2, all the CSs become the COs upon successfully receiving the content of common interest. Hence, the number of the COs increases, until all the N MUs in this area receive the content. Hence, we model this multi-stage cooperative social multicast protocol aided content dissemination process by a DT-PBMC, as shown in Figure 4.7.

State n of the DT-PBMC represents the number of COs during the current transmission frame, while the number of unserved CSs is $(N-n)$. Observe in Figure 4.7 that $p_{n,n+m}$ $(m \ge 0)$ represents the probability of the DT-PBMC's transition from state n to state $(n+m)$ during this transmission frame, which also indicates the probability of m unserved CSs out of $(N-n)$ successfully receiving the content. When we have $m=0$, the state transition probability $p_{n,n}$ represents that no unserved CS receives the content during the current frame. As shown in Figure 4.7, the state transitions emerge from the initial state U $(1 \le U < N)$, where U represents the number of initial COs before the commencement of the content dissemination according to Section 4.2.1, and terminate at the absorbing state N, which is the total number of MUs in the area studied. All the other states between the initial state U and the absorbing state N are termed as transient states. Since

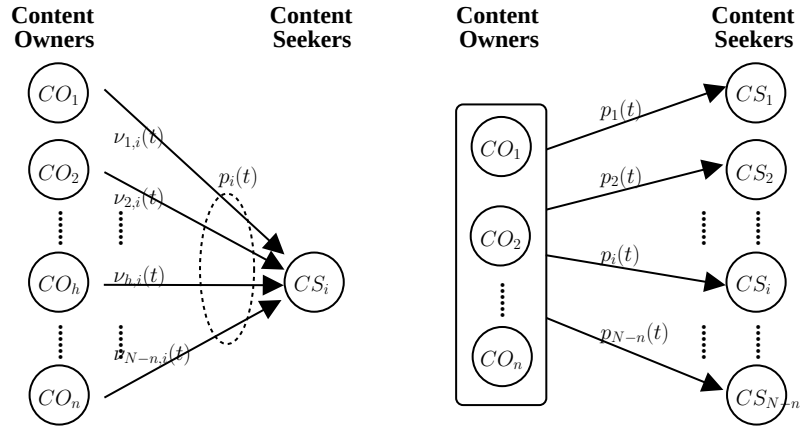

(a) Packet reception at a CS **(b) Equivalent social multicast**

Figure 4.8: The content dissemination in a frame

the content dissemination is a discrete-time process[10], the content dissemination delay K is equivalent to the number of transmission frames, when the absorbing state N is reached after emerging from the initial state U.

Before delving into the statistical properties of the random content dissemination delay K, we first have to derive the state transition probability $p_{n,n+m}$ and the state transition matrix $\mathbb{P}$.

4.4.2 State Transition Matrix

4.4.2.1 Successful Packet Reception Probability of a CS

According to the frame structure of Figure 4.4, at the beginning of the t-th transmission frame, n TSs are allocated to COs, if there are n COs willing to multicast the content to the $(N-n)$ unserved CSs. Specifically, the h-th TS during the t-th transmission frame is allocated to CO_h ($1 \leq h \leq n$). As seen in Figure 4.8(a), CS_i ($1 \leq i \leq N-n$) is connected to all the COs via the 'social wireless link' defined in Section 4.2.1. Moreover, the successful packet delivery probability of the 'social wireless link' connecting CO_h and CS_i is equivalent to the social unicast throughput $\nu_{h,i}(t)$.

According to Figure 4.4 and Figure 4.8(a), the packet detection process of CS_i is characterised as follows. In each transmission frame, CS_i detects the signal of the n multicast TSs one by one in order to successfully receive a packet. If the packet is indeed successfully detected during the h-th TS, the detection process is terminated. By contrast, if the packet cannot be detected in any of the n multicast TSs, the detection process is terminated and the unserved CS_i will request the content again during the next transmission frame. As a result, during the transmission of the t-th frame, the probability of CS_i successfully detecting a packet within the h-th multicast TS, which implies that the packet's detection failed during the first $(h-1)$ TSs, is expressed as

$$p_i^{(h)}(t) = \prod_{j=1}^{h-1}[1-\nu_{j,i}(t)] \cdot \nu_{h,i}(t), \tag{4.25}$$

where $\nu_{j,i}(t)$ is the social unicast throughput of the 'social wireless link' connecting CO_j and CS_i during the dissemination of the t-th frame. Since the social unicast throughput $\nu_{j,i}(t)$ is determined by the time-varying geographic distance as well as by the small-scale fading, they may be assumed to remain constant during the t-th frame, but they vary independently from one frame to another.

[10] As defined at the beginning of Section II-A, the basic time unit in this discrete-time system is the duration of a transmission frame

As a result, the probability of CS_i successfully receiving a packet during the t-th frame is formulated as

$$p_i(t) = \sum_{h=1}^{n} p_i^{(h)}(t) = \sum_{h=1}^{n} \prod_{j=1}^{h-1} [1 - \nu_{j,i}(t)] \cdot \nu_{h,i}(t)$$
$$= 1 - \prod_{h=1}^{n} [1 - \nu_{h,i}(t)]. \tag{4.26}$$

According to the mobility model introduced in Section 4.3.3, the geographic positions of different MUs are i.i.d. random variables, thus, the distances between any CO and CS pair are also i.i.d. random variables. Hence, according to Eq.(4.15) and Eq.(4.21), $\{\nu_{h,i}(t), h = 1, 2, \cdots, n\}$ are also i.i.d. random variables. As a result, the expected value of $p_i(t)$ may be expressed as

$$\overline{p} = \mathcal{E}[p_i(t)] = 1 - \prod_{h=1}^{n} (1 - \mathcal{E}[\nu_{h,i}(t)]) = 1 - (1 - \overline{\nu}_s)^n, \tag{4.27}$$

where $\overline{\nu}_s$ is the average social unicast throughput that is derived in Section 4.3.4.

4.4.2.2 State Transition Probability

Figure 4.8(b) portrays the cooperative multicast aided content dissemination process during the t-th transmission frame, given n COs and $(N-n)$ CSs, where $p_i(t)$ of Eq.(4.26) is the probability of CS_i successfully receiving a packet of the content during this transmission frame.

Let us assume that m CSs having the indices of $\mathcal{I} = \{i_g | 1 \leq g \leq m\}$ receive the packet at the end of the current transmission frame associated with the successful packet reception probabilities of $\mathcal{P}_\mathcal{I} = \{p_{i_g}(t) | i_g \in \mathcal{I}\}$, whilst the remaining $(N-n-m)$ CSs having the indices of $\mathcal{J} = \{j_h | 1 \leq h \leq (N-n-m)\}$ do not receive any packet. The latter event is associated with the unsuccessful packet reception probabilities of $\mathcal{P}_\mathcal{J} = \{1 - p_{j_h}(t) | j_h \in \mathcal{J}\}$. We should note that $\mathcal{I} \bigcap \mathcal{J} = \phi$, while $\mathcal{I} \bigcup \mathcal{J}$ is the full set of $(N-n)$ unserved CSs at the beginning of the current transmission frame. Furthermore, $\mathcal{P}_\mathcal{I}$ and $\mathcal{P}_\mathcal{J}$ are independent of each other. Thus the state transition probability $p_{n,n+m}(t)$ may be expressed as

$$p_{n,n+m}(t) = \sum_{\text{All possible combinations for } \mathcal{I}} \left[\prod_{i_g \in \mathcal{I}} p_{i_g}(t) \prod_{j_h \in \mathcal{J}} (1 - p_{j_h}(t)) \right]. \tag{4.28}$$

As a result, the $(N \times N)$-element state-transition matrix $\mathbb{P}(t)$ of the DT-PBMC during the t-th frame is expressed as

$$\mathbb{P}(t) = \begin{pmatrix} p_{1,1}(t) & p_{1,2}(t) & p_{1,3}(t) & p_{1,4}(t) & \cdots & p_{1,N-1}(t) & p_{1,N}(t) \\ 0 & p_{2,2}(t) & p_{2,3}(t) & p_{2,4}(t) & \cdots & p_{2,N-1}(t) & p_{2,N}(t) \\ \vdots & \vdots & \ddots & \vdots & & \vdots & \vdots \\ 0 & 0 & \cdots & p_{U,U}(t) & \cdots & p_{U,N-1}(t) & p_{U,N}(t) \\ \vdots & \vdots & & & \ddots & \vdots & \vdots \\ 0 & 0 & \cdots & 0 & \cdots & p_{N-1,N-1}(t) & p_{N-1,N}(t) \\ 0 & 0 & \cdots & 0 & \cdots & 0 & p_{N,N}(t) \end{pmatrix}$$
$$= \begin{pmatrix} \mathbf{Q}(t) & \mathbf{Q_0}(t) \\ \mathbf{0} & 1 \end{pmatrix}, \tag{4.29}$$

where $\mathbf{Q}(t)$ is the $(N-1) \times (N-1)$-element transition matrix for the $(N-1)$ transient states of the DT-PBMC, and $\mathbf{Q_0}(t)$ is the $(N-1) \times 1$-element vector consisting of the probabilities of the transient states being absorbed.

Since the entries of $\mathbb{P}(t)$ are random variables, $\mathbb{P}(t)$ is a random matrix. Taking the expected value of every entry in $\mathbb{P}(t)$, the expected matrix of $\mathbb{P}(t)$ is formulated as

$$\overline{\mathbb{P}} = \mathcal{E}[\mathbb{P}(t)] = \begin{pmatrix} \overline{\mathbf{Q}} & \overline{\mathbf{Q}}_0 \\ \mathbf{0} & 1 \end{pmatrix}. \tag{4.30}$$

Given $p_{n,n+m}(t)$ derived in Eq.(4.28), and that all the elements in $\mathcal{P}_{\mathcal{I}}$ are i.i.d. random variables having an identical mean of $\overline{p}$ as well as that all the elements in $\mathcal{P}_{\mathcal{J}}$ are i.i.d. random variables having an identical mean of $(1-\overline{p})$, the associated entry $\overline{p}_{n,n+m}$ of $\overline{\mathbb{P}}$ becomes

$$\begin{aligned} \overline{p}_{n,n+m} &= \sum_{\text{All possible combination for } \mathcal{I}} \left[\prod_{i_g \in \mathcal{I}} \mathcal{E}[p_{i_g}(t)] \prod_{j_h \in \mathcal{J}} \mathcal{E}[1-p_{j_h}(t)] \right] \\ &= \binom{N-n}{m} \overline{p}^m (1-\overline{p})^{N-n-m} \\ &= \binom{N-n}{m} \left(1-(1-\overline{v}_s)^n\right)^m (1-\overline{v}_s)^{n(N-n-m)}, \end{aligned} \tag{4.31}$$

where the third equality is obtained by substituting Eq.(4.27) into Eq.(4.31).

4.4.3 Statistical Properties of the Content Dissemination Delay

In order to derive the Tail Distribution Function (TDF) of the content dissemination delay as well as its average value, we only have to consider the transition matrix of the transient states, which is denoted by $\mathbf{Q}(t)$ in Eq.(4.29). Specifically, we have $\mathbf{Q}(0) = \mathbf{I}$, indicating that the DT-PBMC has a unity probability of staying in its current state.

Theorem 4.1. *The entry $q_{i,j}(k)$ of the matrix $\mathbb{Q}(k) = \prod_{t=0}^{k} \mathbf{Q}(t)$ represents the probability of state j being reached after k frames, given that the initial state is state i.*

Proof. Please refer to Appendix 4.A. □

Before deriving the statistical properties of the content dissemination delay, we must firstly study the convergence of the matrix $\mathbb{Q}(k)$. As a result, Theorem 4.2 is formulated.

Theorem 4.2. *Given $\mathbb{Q}(k) = \prod_{t=0}^{k} \mathbf{Q}(t)$, when k tends to infinity, we have $\mathbb{Q}(k) \to \mathbf{0}$, as well as $E[\mathbb{Q}(k)] = \overline{\mathbf{Q}}^k \to \mathbf{0}$.*

Proof. Please refer to Appendix 4.B. □

With the aid of Theorem 4.1 and Theorem 4.2, we obtain the matrix $\mathbb{Q}(k)$ containing the probabilities of any transient states being reached from any initial states after k frames.

Given the initial state i, the probability of the DT-PBMC not being terminated after k frames is the sum of the entries in row i of the matrix $\mathbb{Q}(k)$, which is also the probability of the random content dissemination delay K being larger than k. The initial state of content dissemination is set to U, according to Section 4.4.1. Hence, the conditional TDF of the content dissemination delay is formulated as

$$\Pr[K > k | \mathbb{Q}(k)] = \overrightarrow{\boldsymbol{\tau}} \mathbb{Q}(k) \overrightarrow{\mathbf{1}}, \tag{4.32}$$

where $\overrightarrow{\boldsymbol{\tau}}$ is a $1 \times (N-1)$-element row vector, whose U-th entry is one and all the other entries are zeros, $\overrightarrow{\mathbf{1}}$ is a $(N-1) \times 1$-element column vector, whose entries are all ones. According to Bayesian principle

and Theorem 4.2, the TDF of the content dissemination delay can be expressed as

$$\begin{aligned}\Pr(K>k) &= \int_{\mathbb{Q}(k)} \Pr[K>k|\mathbb{Q}(k)]f[\mathbb{Q}(k)]d\mathbb{Q}(k)\\ &= \overrightarrow{\tau}\times\int_{\mathbb{Q}(k)}\mathbb{Q}(k)f[\mathbb{Q}(k)]d\mathbb{Q}(k)\times\overrightarrow{\mathbf{1}}\\ &= \overrightarrow{\tau}\mathcal{E}[\mathbb{Q}(k)]\overrightarrow{\mathbf{1}} = \overrightarrow{\tau}\overline{\mathbf{Q}}^{k}\overrightarrow{\mathbf{1}},\end{aligned} \tag{4.33}$$

where $f[\mathbb{Q}(k)]$ is the PDF of the random matrix $\mathbb{Q}(k)$, and the second equality is derived by substituting Eq.(4.32) into Eq.(4.33). Furthermore, the Probability Mass Function (PMF) $\Pr(K=k)$ is derived as

$$\begin{aligned}\Pr(K=k) &= \Pr(K>k-1)-\Pr(K>k) = \overrightarrow{\tau}\overline{\mathbf{Q}}^{k-1}\overrightarrow{\mathbf{1}} - \overrightarrow{\tau}\overline{\mathbf{Q}}^{k}\overrightarrow{\mathbf{1}}\\ &= \overrightarrow{\tau}\left(\overline{\mathbf{Q}}^{k-1}-\overline{\mathbf{Q}}^{k}\right)\overrightarrow{\mathbf{1}} = \overrightarrow{\tau}\overline{\mathbf{Q}}^{k-1}\left(\mathbf{I}-\overline{\mathbf{Q}}\right)\overrightarrow{\mathbf{1}}\\ &= \overrightarrow{\tau}\overline{\mathbf{Q}}^{k-1}\overline{\mathbf{Q}}_0,\end{aligned} \tag{4.34}$$

where $\overline{\mathbf{Q}}_0$ is the expected vector of $\mathbf{Q}_0(t)$ defined in Eq.(4.29).

In order to obtain the expected value of the random content dissemination delay K, Theorem 4.3 is formulated as:

Theorem 4.3. *The ij-th-entry θ_{ij} of the new matrix $\mathbf{\Theta}=\sum_{k=0}^{\infty}\mathbb{Q}(k)$ represents the expected number of frames that the DT-PBMC spends in state j, given the initial state i.*

Proof. Please refer to Appendix 4.C. □

Given Theorem 4.3, after summing up all the entries in row i of the matrix $\mathbf{\Theta}$, we have the expected number of frames that the DT-PBMC spends in the transient states, which is also the expected number of frames before the DT-PBMC is terminated. Therefore, we have

$$\mathcal{E}[K|\{\mathbb{Q}(k)|k=0,1,\cdots,+\infty\}] = \overrightarrow{\tau}\mathbf{\Theta}\overrightarrow{\mathbf{1}} = \overrightarrow{\tau}\sum_{k=0}^{\infty}\mathbb{Q}(k)\overrightarrow{\mathbf{1}}, \tag{4.35}$$

where $\overrightarrow{\tau}$ and $\overrightarrow{\mathbf{1}}$ have already been defined in Eq.(4.32). Furthermore, according to Bayesian principle and Theorem 4.2, we have

$$\begin{aligned}\mathcal{E}[K] &= \overrightarrow{\tau}\left[\sum_{k=0}^{\infty}\int_{\mathbb{Q}(k)}\mathbb{Q}(k)f[\mathbb{Q}(k)]d\mathbb{Q}(k)\right]\overrightarrow{\mathbf{1}}\\ &= \overrightarrow{\tau}\times\sum_{k=0}^{\infty}\mathcal{E}[\mathbb{Q}(k)]\times\overrightarrow{\mathbf{1}} = \overrightarrow{\tau}\times\sum_{k=0}^{\infty}\overline{\mathbf{Q}}^{k}\times\overrightarrow{\mathbf{1}},\end{aligned} \tag{4.36}$$

where $f[\mathbb{Q}(k)]$ is the PDF of the random matrix $\mathbb{Q}(k)$. For the sake of deriving the closed-form expression of $\sum_{k=0}^{\infty}\overline{\mathbf{Q}}^{k}$, the following theorem is formulated:

Theorem 4.4. *The inverse matrix of $(\mathbf{I}-\overline{\mathbf{Q}})$ exists, and $\sum_{k=0}^{\infty}\overline{\mathbf{Q}}^{k}=(\mathbf{I}-\overline{\mathbf{Q}})^{-1}$.*

Proof. Please refer to Appendix 4.D. □

Finally, according to Theorem 4.4, we arrive at the closed-form expression of the expected number of frames that the DT-PBMC encountered before being terminated, which is also the average content dissemination delay of:

$$\mathcal{E}[K] = \overrightarrow{\tau}\times\sum_{k=0}^{\infty}\overline{\mathbf{Q}}^{k}\times\overrightarrow{\mathbf{1}} = \overrightarrow{\tau}\left(\mathbf{I}-\overline{\mathbf{Q}}\right)^{-1}\overrightarrow{\mathbf{1}}. \tag{4.37}$$

Table 4.1: Parameters of the physical layer

Parameter	Value
Reference received power	$P_{s,0} = -34$ dBm
Reference distance	$d_0 = 1$ m
Path loss exponent	$\kappa = 3$
Carrier frequency	$f_{s,c} = 3.6$ GHz
Transmission bandwidth	$W_s = 10$ MHz
Noise power spectral density	$N_0 = -174$ dBm/Hz
Packet reception SNR threshold	$\gamma = 10$ dB
Radius of the circular area	$R = 50$ m

4.5 Numerical Results

The power spectral density of the noise is $N_0 = -174$ dBm/Hz, and the bandwidth for the COs' social multicast is $W_s = 10$ MHz. Hence, the noise power is $N_0 W_s = -104$ dBm. If the transmission from a CO to CSs takes place at the carrier frequency of 3.6 GHz, the PL at the reference point stipulated to be $d_0 = 1$ m away from the transmitter is 44 dB, according to the free space PL equation [114], while the PL exponent for the receiver beyond d_0 is set to be $\kappa = 3$. Furthermore, we generally set the received power at the reference point to be $P_{s,0} = -34$ dBm. This setting indicates that the actual transmit power is 10 dBm ($= -34$ dBm $+ 44$ dB). We also set the successful packet reception SNR threshold to be $\gamma = 10$ dB, which guarantees that the BER of the Quadrature Phase-Shift Keying (QPSK) modulation at the receiver is below 10^{-2} without channel coding [152]. All these physical layer related parameter settings are in line with the 802.11 protocol [53]. All the MUs roam in the bounded circular area having a radius of $R = 50$m by obeying the mobility model introduced in Section 4.3.3. In order to accurately characterise the statistical properties of the system, we repeated the content dissemination process corresponding to the model introduced in Section 4.2 100 000 times. The above-mentioned parameters are summarised in Table 4.1.

In order to obtain accurate analytical results, we set $n_{\max}$ in $\widetilde{f_{Y_s}}(y_s)$ of Eq.(4.6) to be $n_{\max} = 10$. According to Figure 4.5, when $R = 50$ m, the RMSE between $\widetilde{f_{Y_s}}(y_s)$ of Eq.(4.6) and $f_{Y_s}(y_s)$ of Eq.(4.1) is 3×10^{-5}.

4.5.1 Social Strength and Social Contacts

Let us first investigate the average social strength and the number of social contacts. Both of them are jointly determined by the social domain parameters, such as the neighbourhood range r and the social exponent α, as well as the geographic positions of the MUs. The parameters of the physical layer provided by Table 4.1 do not affect these two metrics.

We first evaluate the average social strength of the geographic social relationship between a pair of MUs in Figure 4.9, where we vary the neighbourhood range r from 1 m to 100 m and increase the social exponent α from 0 to 100. As shown in Figure 4.9, when $\alpha = 0$, the average social strength remains one, regardless of what value the neighbourhood range r may take. This is because when $\alpha = 0$, according to Eq.(4.8), the MU may become its counterpart's opportunistic contact with a unity probability, even if their distance is longer than the neighbourhood range. By contrast, when $\alpha > 0$, the average social strength increases as we increase r, because a longer neighbourhood range r indicates that a MU has a high probability of becoming its counterpart's regular contact. Furthermore, increasing the social exponent α results in a lower social strength, since a higher α reduces the chance that a pair of MUs become each other's opportunistic contact, when their distance is longer than the neighbourhood range r. The simulation results of Figure 4.9 demonstrate the accuracy of our analysis in Section 4.3.3 .

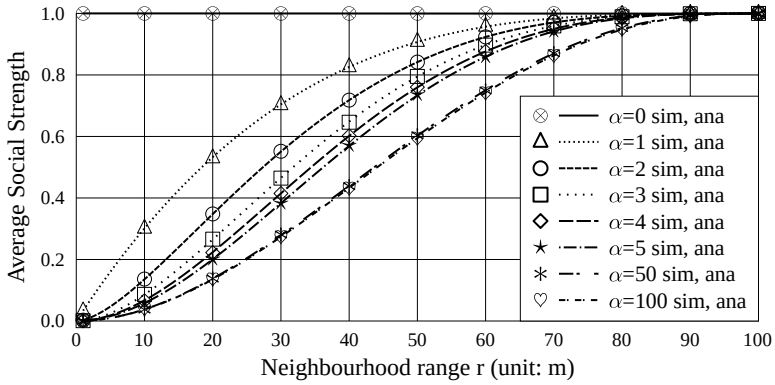

Figure 4.9: The average social strength versus the neighbourhood range, which is parameterised by the social exponent. A pair of MUs move within a circular area having a radius of $R = 50$ m. The neighbourhood range r of a MU varies from 1 m to 100 m, while the social exponent α takes a value from the set $\{0, 1, 2, 3, 4, 5, 50, 100\}$. The analytical results are evaluated by Eq.(4.9).

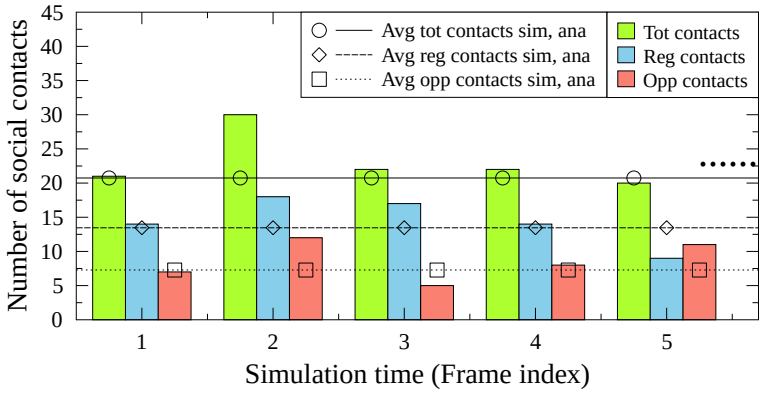

Figure 4.10: The instantaneous number of social contacts of a MU for five transmission frames. There are $N = 50$ MUs moving within a circular area having a radius of $R = 50$ m. The neighbourhood range is $r = 30$ m, while the social exponent is $\alpha = 4$. The analytical results for the average numbers of total (tot) social contacts and regular (reg) contacts as well as opportunistic (opp) contacts are derived by $\overline{\mathcal{N}}_{soc} = N \cdot \overline{\varphi}_s$, $\overline{\mathcal{N}}_{reg} = N \cdot \overline{\varphi}_{reg}$ and $\overline{\mathcal{N}}_{opp} = N \cdot \overline{\varphi}_{opp}$, respectively, where $\overline{\varphi}_s$, $\overline{\varphi}_{s,reg}$ and $\overline{\varphi}_{s,opp}$ are provided by Eqs.(4.9), (4.10) and (4.11).

We now proceed to quantify both the average and the instantaneous number of social contacts that a MU may have, as seen in Figure 4.10, when $N = 50$ MUs move within a circular area having a radius of $R = 50$ m. We set the neighbourhood range to $r = 30$ m and set the social exponent to $\alpha = 4$. Since all the MUs change their positions in the circular area during different transmission frames, we can observe from Figure 4.10 that the instantaneous number of social contacts of a MU varies from one transmission frame to another. Based on our parameter settings, this MU normally has more regular contacts than opportunistic ones, which indicates that the potential communications between this MU and his/her social contacts are more often limited to his/her neighbourhood range. Furthermore, Figure 4.10 also provides the average number of social contacts. Observe that the average number of the regular contacts is higher than that of the opportunistic contacts.

4.5.2 Social Unicast Throughput

By jointly considering both the parameters in the social domain as well as those in the wireless domain, we quantify the social unicast throughput in Figures 4.11 and 4.12.

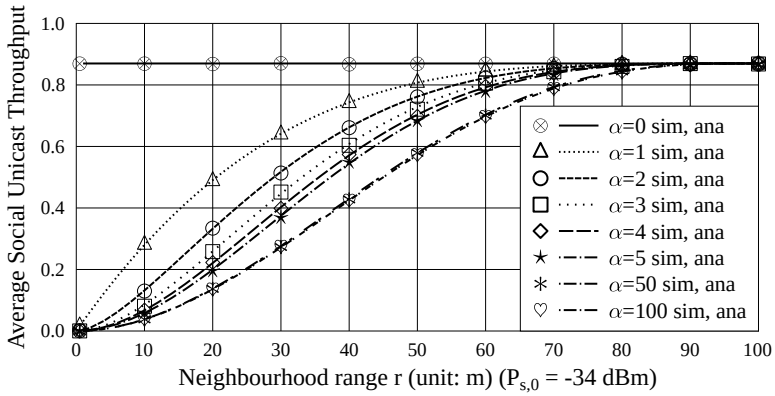

Figure 4.11: The average social unicast throughput versus the neighbourhood range, which is parameterised by various social exponent. A pair of CO and CS move within a circular area having a radius of $R = 50$ m. The neighbourhood range r varies from 1 m to 100 m, while the social exponent α takes a value from the set $\{0, 1, 2, 3, 4, 5, 50, 100\}$. The reference received power is $P_{s,0} = -34$ dBm and the other parameters relate to the physical layer are provided in Table 4.1. The analytical results are derived either by Eq.(4.16) or Eq.(4.22).

We first study the impact of social domain parameters, such as the neighbourhood range r and the social exponent α, on the average social unicast throughput. In Figure 4.11, we observe that as the neighbourhood range r increases, the average social unicast throughput remains constant for $\alpha = 0$. In this case, based on Eq.(4.8), the CS may become the CO's opportunistic contact with a unity probability. As a result, increasing r does not affect the social unicast throughput. However, if $\alpha \neq 0$, we may observe in Figure 4.11 that the average social unicast throughput increases, as we increase the neighbourhood range r. This can be explained by the fact that a higher neighbourhood range increases the probability of the CS becoming one of the CO's social contacts, as shown in Eq.(4.8). Furthermore, if r is equal to the maximum possible distance $2R$ in a circular area, observe in Figure 4.11 that the average throughput achieves its maximum value for $\alpha = 0$, because in this case the destination is always one of the source's regular contacts. Moreover, since a higher α indicates that the CS may become one of the CO's opportunistic contact with a lower probability, it is less likely to establish a physical wireless link between the CO and the CS beyond the CO's neighbourhood range. As a result, a higher α leads to a reduced average throughput. Furthermore, in the case of α tending to infinity, the CO is only willing to share the content with the CSs within his/her neighbourhood range. Hence, we observe in Figure 4.11(a) that if α is high, say 50 or 100, the average social unicast throughput converges to that of the scenario, where communications between a CS and CO pair only occur, if the CS is within the CO's neighbourhood range.

Let us now study the impact of the physical layer parameters on the average social unicast throughput. We set $\alpha = 2$, and vary the reference received power $P_{s,0}$ from -60 dBm to -10 dBm in combination with different neighbourhood ranges r. Observe in Figure 4.12 that the average social unicast throughput increases, as we increase $P_{s,0}$. However, the average social unicast throughput converges to a constant value, as $P_{s,0}$ tends to infinity. According to our analysis in Section 4.3, the social unicast throughput depends both on the successful packet delivery probability $\mu_s(y_s)$ of a physical wireless link, and on the geographic social strength $\varphi_s(y_s)$. When the transmit power tends to infinity, $\mu_s(y_s)$ converges to one, hence, the average social unicast throughput is dominated by the geographic social strength $\varphi_s(y_s)$. As a result, when we have $r = 100$ m, indicating no influence from the geographic social strength, the average throughput converges to one. However, when r is below 100 m, the average social unicast throughput converges to a specific value, which is derived by integrating the social strength $\varphi_s(y_s)$ over the distance PDF $f_{Y_s}(y_s)$.

The simulation results presented in both Figures 4.11 and 4.12 demonstrate the accuracy of our analysis in Section 4.3.5.

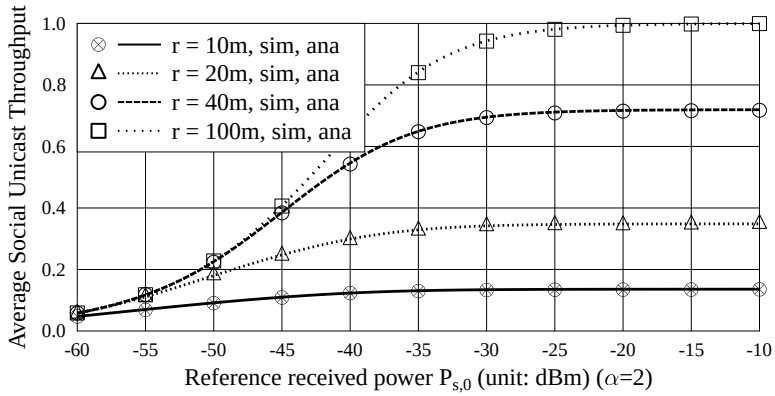

Figure 4.12: The average social unicast throughput versus the reference received power, which is parameterised by various neighbourhood range. A pair of CO and CS move within a circular area having a radius of $R = 50$ m. The reference received power varies from -60 dBm to -10 dBm, while the neighbourhood range r takes a value from the set $\{10, 20, 40, 100\}$ m. The social exponent is $\alpha = 2$. The other parameters relate to the physical layer are provided in Table 4.1. The analytical results are derived either by Eq.(4.16) or Eq.(4.22).

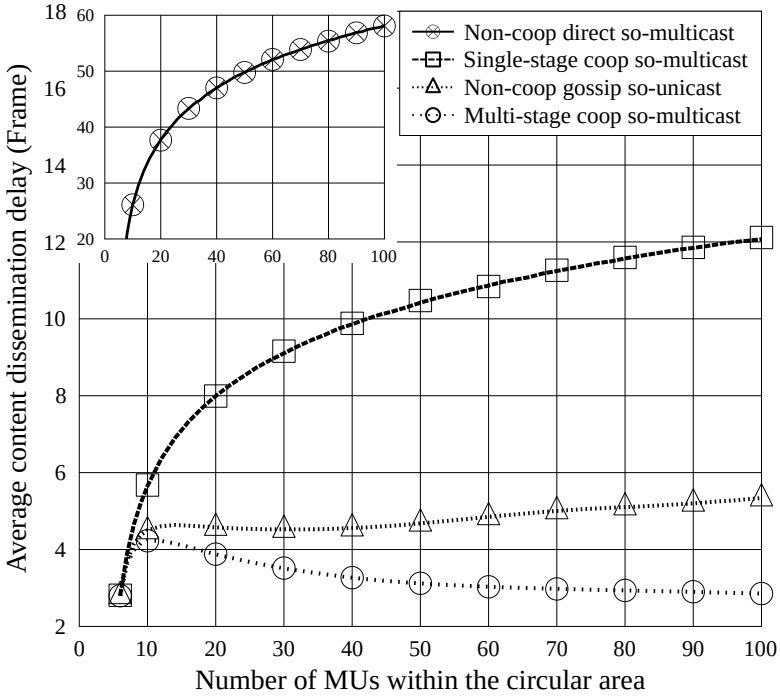

Figure 4.13: Comparison of different protocols in terms of the average content dissemination delay. All the MUs move within a circular area having a radius of $R = 50$ m. The total number N of these MUs varies from 6 to 100. Amongst these MUs, we have $U = 5$ COs initially. The neighbourhood range is $r = 10$ m, while the social exponent is $\alpha = 3$. All the parameters related to the physical layer are provided in Table 4.1. Four protocols are compared, including the non-cooperative direct social multicast, the single-stage cooperative social multicast, the non-cooperative gossip based social unicast and the multi-stage cooperative social multicast protocols, as introduced in Sections 4.2.2 and 4.2.3. Only simulation results are presented in this figure.

4.5.3 Content Dissemination Delay

In Figure 4.13, we evaluate the average content dissemination delay of four different protocols. We observe from Figure 4.13 that both the non-cooperative direct social multicast (Non-coop direct so-multicast) and the

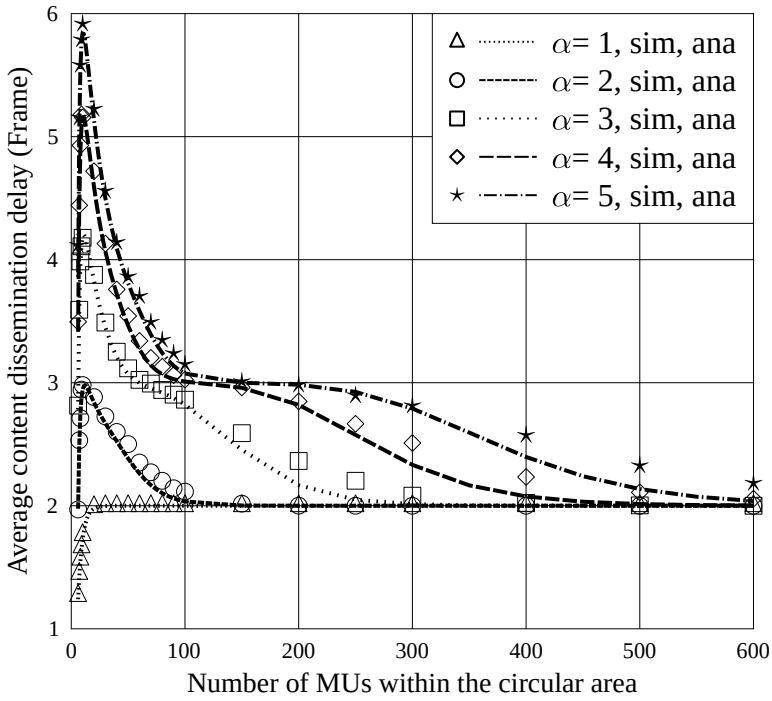

Figure 4.14: Average content dissemination delay versus the number of MUs, which is parameterised by various social exponent. All the MUs move within a circular area having a radius of $R = 50$ m. The total number N of these MUs varies from 6 to 600. Amongst these MUs, we have $U = 5$ COs before the content dissemination commences. The neighbourhood range is $r = 10$ m, while the social exponent takes a value from the set $\{1, 2, 3, 4, 5\}$. All the parameters related to the physical layer are provided in Table 4.1. Our multi-stage cooperative social multicast protocol is invoked for disseminating the content of common interest. The analytical results are derived by Eq.(4.37).

single-stage cooperative social multicast (Single-stage coop so-multicast) protocols exhibit a monotonically increasing trend in terms of the average content dissemination delay, as we increase the number of MUs in the circular area studied. Since the served CSs join the initial group of COs for further forwarding the content of common interest, we observe from Figure 4.13 that the average content dissemination delay is significantly reduced when the non-cooperative gossip based social unicast (Non-coop gossip so-unicast) protocol is invoked. Our multi-stage cooperative social multicast (Multi-stage coop so-multicast) protocol is capable of further reducing the average content dissemination delay, because our social multicast procedure provides more successful content delivery opportunities than social unicast. Based on this comparison, we conclude that our multi-stage cooperative social multicast protocol is significantly faster in disseminating the content of common interest than the other three existing protocols, when imposing social constraint on the wireless transmissions.

As evidenced by Figure 4.14, we observe that the content dissemination delay converges to 2 frames under our multi-stage cooperative social multicast protocol. More explicitly, as we increase the number of MUs to $N = 600$, we observe in Figure 4.14 that both our simulation and analytical results of the average content dissemination delay finally converge to 2 frames, regardless of the value of the social exponent α. This somewhat surprising results suggests that when there are sufficient MUs in the circular area, invoking a two-stage cooperative social multicast is sufficient on average for the sake of guaranteeing that all the interested MUs successfully receive the content. Furthermore, according to our simulations, for $\alpha = 5, 4, 3, 2$, the specific number of MUs, resulting in the highest average content dissemination delay, is 10, 11, 11, 12 frames, respectively. As a result, we may conclude that a higher α results in an early reduction of the content dissemination delay. However, when $\alpha = 1$, the content dissemination delay increases and finally converges

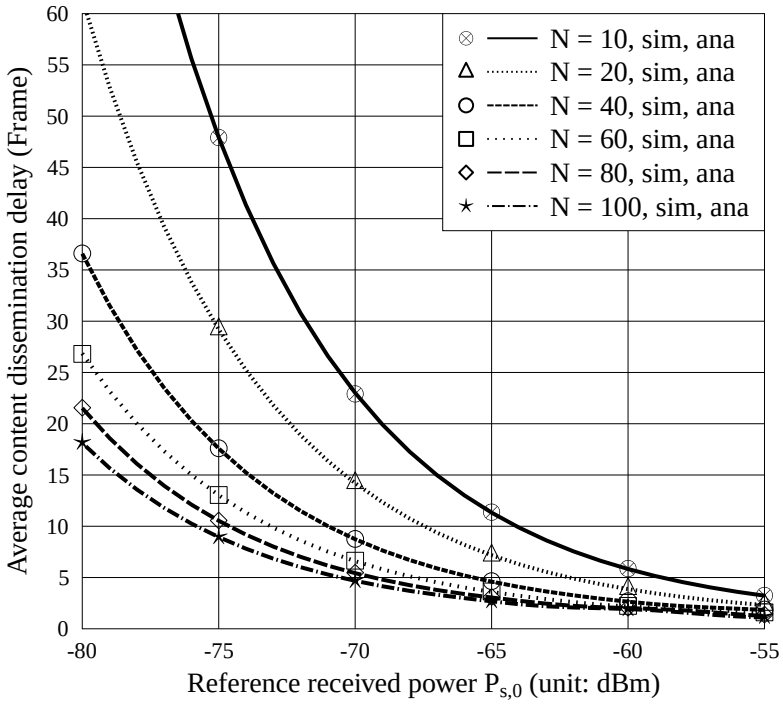

Figure 4.15: Average content dissemination delay versus the reference received power, which is parameterised by the numebr of MUs. The reference received power $P_{s,0}$ varies from -80 dBm to -55 dBm. All the other parameters related to the physical layer are provided in Table 4.1. All the MUs move within a circular area having a radius of $R = 50$ m. The total number N of these MUs takes a value from the set $\{10, 20, 40, 60, 80, 100\}$. Half of these MUs own the content of common interest before the content dissemination process. The social exponent is set to $\alpha = 0$. Our multi-stage cooperative multicast protocol is invoked for disseminating the content of common interest. The analytical results are derived by Eq.(4.37).

to 2 frames, because in contrast to the other scenarios, the delay is lower than 2 frames, when N is small.

Finally, we set the social exponent α to $\alpha = 0$ for the sake of cancelling the impact of the socially-related parameters and vary the reference received power $P_{s,0}$ from -80 dBm to -55 dBm. Half of MUs are assumed to receive the content of common interest before the content dissemination process. During each frame, the COs multicast the content to all CSs rather than only multicast the content to his/her social contacts. As a result, the physical layer parameters dominate the attainable content dissemination performance.

We may observe from Figure 4.15 that the average content dissemination delay substantially reduces, as we increase $P_{s,0}$. For the case of $N = 40$, the average content dissemination delay reduces from 37 frames at $P_{s,0} = -80$ dBm to just 1 frame at $P_{s,0} = -55$ dBm.

Furthermore, in Figure 4.16 we evaluate the probability of the content dissemination delay exceeding a pre-defined threshold of $k_{th} = 5$ frames. Observe in Figure 4.16 that the tail probability of the content dissemination delay decreases, as we increase $P_{s,0}$. The simulation results demonstrate the accuracy of our analysis in Section 4.5.3.

4.6 Chapter Conclusions

In this chapter, we proposed a distributed multi-stage cooperative social multicast protocol aided content dissemination scheme relying on the MUs' common interest in certain content and on the spontaneous dissemination initiated by the smart devices owned by the MUs. In our scheme, the centralised infrastructure is

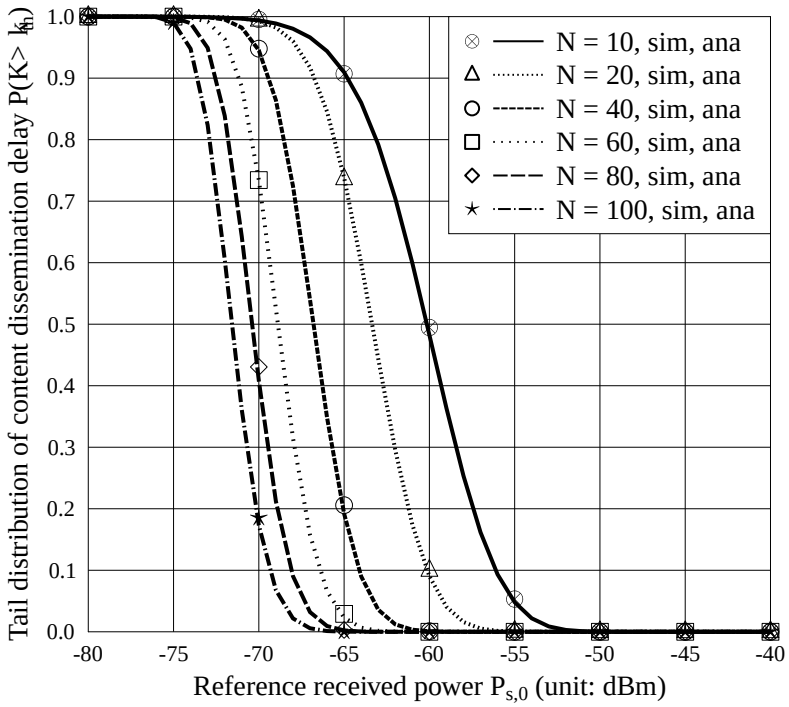

Figure 4.16: Tail probability of the content dissemination delay versus the reference received power, which is parameterised by the numebr of MUs. The reference received power $P_{s,0}$ varies from -80 dBm to -55 dBm. All the other parameters related to the physical layer are provided in Table 4.1. All the MUs move within a circular area having a radius of $R = 50$ m. The total number N of these MUs takes a value from the set $\{10, 20, 40, 60, 80, 100\}$. Half of these MUs own the content of common interest before the content dissemination process. The social exponent is set to $\alpha = 0$. Our multi-stage cooperative multicast protocol is invoked for disseminating the content of common interest. The delay threshold is set to $k_{th} = 5$ frames. The analytical results are derived by Eq.(4.33).

only relied upon as a controller in order to facilitate the relevant control signalling exchange, but it does not directly contribute to the content dissemination process.

In Section 4.2, we considered the impact of the social constraints on the conventional wireless multicast technique. In reality, MUs are only willing to multicast the content of common interest to their social contacts, rather than conventionally multicasting the content to all the MUs who request it. Therefore, communications between a pair of MUs are jointly influenced by their social relationship and by the quality of the wireless link between them. We then described our multi-stage cooperative social multicast protocol. With the aid of this protocol, once a MU successfully receives the content of common interest, he/she may join the CO set and cooperate with other COs so as to multicast the content to the other hitherto unserved CSs. We also briefly introduced a number of other feasible protocols designed for content dissemination, including the non-cooperative direct social multicast, single-stage cooperative social multicast as well as the non-cooperative gossip based social unicast. Furthermore, for the sake of simplifying the implementation issues, we proposed a TDMA approach in the MAC layer, which is capable of coordinating the control signalling exchange, whilst mitigating adverse effects of the interferences and avoiding collisions during the content dissemination process.

In Section 4.3, we first introduced our mobility model and discussed the connectivity of the MUs in a random mobile network. With the aid of Taylor series expansion, we proposed an approximation of the PDF of the random distance between a pair of MUs moving within a circular area. Figure 4.5 demonstrated the accuracy of our approximate PDF. Then the relevant geographic social relationships were exploited for

defining the social contacts of a MU. According to their geographic positions, the social contacts were categorised into regular contacts and opportunistic contacts. Furthermore, we derived the average social strength in closed-form, which was defined as the probability of a pair of MUs becoming each other's social contact. Apart from discussing the social domain, we also introduced the physical layer model of the wireless transmission link between a pair of MUs, such as the PL model and the Rayleigh distributed multipath fading as well as the successful packet delivery probability of a wireless link. By considering the social constraints imposed on the wireless transmission regime, a transmitter is capable of successfully conveying a packet to a receiver in our system, provided that the following two conditions are satisfied:

- During a specific transmission frame, the receiver constitutes a social contact of the transmitter;
- During the same transmission frame, the instantaneous SNR at the receiver end should exceed a predefined SNR threshold.

The probability of both these conditions being satisfied was defined as the social unicast throughput between a transmitter and a receiver pair. Furthermore, the average social unicast throughput was derived in closed-form in this section.

In Section 4.4, we modelled the content dissemination process by a DT-PBMC. The indices of the states in the DT-PBMC represent the numbers of the COs. Specifically, the state transitions emerge from the initial state U, which represents that we have U COs before the content dissemination process commences, and terminate at the absorbing state N, which represents that all the N MUs in the circular area studied have successfully received the content of common interest. Then we obtained all the state transition probabilities and represented them with the aid of a random state transition matrix. Given the average unicast throughput derived in Section 4.3, we then derived the matrix containing the expected values of the original random state transition matrix elements. After formulating a set of four theorems, we finally derived both the average and the tail distribution of the content dissemination delay, which is the time duration spanning from the initial U COs cooperatively multicasting the content until all the N MUs successfully receive it.

In Section 4.5, we provided numerical results for characterising the average social strength, the average social unicast throughput and the average content dissemination delay as well as its tail distribution. Several important conclusions may be drawn:

- We may achieve a higher average social strength both upon increasing the neighbourhood range and upon reducing the social exponent, as shown in Figure 4.9. This is because a higher neighbourhood range increases the probability of a pair of MUs becoming each other's regular contact, whilst a lower social exponent increases the chances of this pair of MUs becoming each other's opportunistic contact. Furthermore, we observe from Figure 4.10 that the social contacts of the MUs change as their geographic positions change from one transmission frame to another.
- Both the social unicast throughput and the content dissemination delay are substantially affected by both the social parameters as well as by the physical layer parameters. A more communicative CO, which is represented by a lower social exponent α and a higher neighbourhood range r, is capable of substantially increasing the social unicast throughput, as shown in Figure 4.11, whilst simultaneously reducing the content dissemination delay, as demonstrated in Figure 4.14. Similarly, a more powerful transceiver, which is represented by a higher reference received power $P_{s,0}$ and a lower successful packet reception SNR threshold γ, has the same beneficial effects, as observed in Figures 4.12 and 4.15 as well as 4.16.
- The content dissemination delay is also heavily affected by the number of interested MUs. An increased number of interested MUs provides more potential COs during the content dissemination process. This diversity gain provided by multiple COs is capable of substantially reducing the content

Table 4.2: The quantitative comparison of our multi-stage cooperative social multicast protocol and the other three protocols, extracted from Figure 4.13. All the parameters related to physical layer is provided in Table 4.1.

Protocol	Non-cooperative direct social multicast	Single-stage cooperative social multicast	Non-cooperative gossip based social unicast	Multi-stage cooperative social multicast
Number of MUs	$N = 100$	$N = 100$	$N = 100$	$N = 100$
Neigh. range	$r = 10$ m	$r = 10$ m	$r = 10$ m	$r = 10$ m
Social exp.	$\alpha = 3$	$\alpha = 3$	$\alpha = 3$	$\alpha = 3$
Dissem. delay	$K = 58.1$ frames	$K = 12.1$ frames	$K = 5.34$ frames	$K = 2.85$ frames
Comp-arison	Our scheme reduces the average content dissemination delay by 95.1%.	Our scheme reduces the average content dissemination delay by 76.5%.	Our scheme reduces the average content dissemination delay by 46.7%.	N/A

dissemination delay, as demonstrated in Figures 4.14-4.16. When the number of interested MUs is high, using a two-stage cooperative social multicast is sufficient for the sake of guaranteeing that all the MUs successfully receive the content of common interest, as observed in Figure 4.14.

- As demonstrated by the numerical results of Figure 4.13, our multi-stage cooperative social multicast protocol outperforms the other three existing protocols in terms of its average content dissemination delay. Hence our protocol is more beneficial than the other three, when the geographic social relationships are taken into consideration. The quantitative results are provided in Table 4.2.

Furthermore, our analytical model invoked for analysing the content dissemination delay has wide-ranging applications:

- If we set the social exponent to $\alpha = 0$ or set the neighbourhood range to $r = 2R$, the impact of the social parameters is eliminated. Hence, our analytical model can be invoked for analysing both the delay and the throughput of the conventional multi-stage cooperative multicast technique.
- If we set the social exponent to $\alpha = +\infty$ and equate the neighbourhood range to the transmission range, our analytical model can also be used for analysing the delay characteristics of the mobile *ad hoc* networks [153]. In this scenario, a packet can only be received by a CS, when it roams within the CO's transmission range and when the wireless link is capable of successfully delivering the content.
- Our analytical model can also be used for analysing the content dissemination delay for the non-cooperative direct social multicast protocol. Since only a single CO is multicasting the content during a transmission frame, we simply set $n = 1$ in Eq.(4.27) for the sake of characterising the delay performance of this protocol.
- Our analytical model can also be used for analysing the content dissemination delay for the single-stage cooperative social multicast protocol. Given this protocol, only the initial group of COs, whose size is U, cooperatively social multicast the content of common interest. Hence, if we set $n = U$ in Eq.(4.27), we may readily derive the delay metrics of this protocol.

Without affecting the tractability of the closed-form statistical properties of the content dissemination delay, our DT-PBMC based analytical model relaxed the assumptions made in Chapter 3 in the following aspects:

- The duration of a basic time interval Δt, which is a transmission frame in this chapter but a TS in Chapter 3, can be of any length. We do not have to assume a 'sufficiently short' Δt in our analytical model.
- In Chapter 3, since the transition probability $p_{n,n+m}$ associated with $m \geq 2$ from state n to state $(n+m)$ is negligibly low, we ignored all the multiple-step transitions and assumed that only adjacent-state transition may occur. However, in the DT-PBMC based analytical model of this chapter, we dispensed with the above assumption and allowed multiple-step state transitions, which results in more accurate analytical results.

However, the analytical model studied in this chapter still has the following limitations:

- In our system, the content dissemination process amongst the MUs is started by some of the initial COs. Hence, the entire content dissemination process is completed by a homogeneous network, which is organised by the MUs' mobile devices. The centralised infrastructure is not relied upon.
- In our system, a TDMA approach is proposed for mitigating the interference and for avoiding collisions. We assumed that every CO may be allocated a single TS for its own multicast and hence we did not invoke any resource scheduling methods. However, the number of TSs provided by a realistic communication system is quite limited. We have to carefully design an appropriate scheduling algorithm for fully exploiting the precious resources for approaching the optimal content dissemination performance.
- Our DT-PBMC based analytical model only facilitated the derivation of the content dissemination delay, which is the time duration spanning from the initial COs multicasting the content until all the MUs successfully receive it, but ignored som of the other important performance metrics related to the content dissemination process, such as the individual user-delay, the MSN group delay and the energy dissipations.

In order to overcome the above-mentioned limitations, in the next chapter, we will improve our system model by considering the benefits of the centralised infrastructure based communication and those of the distributed communication amongst the MUs, which results in a heterogeneous network constructed for disseminating the content of common interest. Moreover, a more realistic MAC layer model will be taken into account and the impact of resource scheduling on the content dissemination process will be studied. Furthermore, a more generic DT-PBMC analytical model will be introduced for unifying various delay metrics.

Appendix

4.A Proof of Theorem 4.1

This theorem may be proved by using the technique of mathematical induction.

Explicitly, when we have $k = 0$, $\mathbb{Q}(0) = \mathbf{Q}(0) = I$ and the theorem holds, because the system stays at its current state after 0 frames with a unity probability.

When $k = 1$, $\mathbb{Q}(1) = \mathbf{Q}(0)\mathbf{Q}(1) = I \times \mathbf{Q}(1) = \mathbf{Q}(1)$. The ij-th-entry of $\mathbb{Q}(1)$ is $q_{i,j}(1) = p_{i,j}(1)$. Since $p_{i,j}(1)$ is the transition probability from state i to state j during frame 1, it is also the probability of state j being reached after one frame, given the initial state i.

Furthermore, we assume that Theorem 4.1 holds for $\mathbb{Q}(k) = \prod_{t=0}^{k} \mathbf{Q}(t)$, whose ij-th-entry is $q_{i,j}(k)$. Then the probability of the state j being reached after $(k+1)$ frames, given the initial state i, is derived as

$$q_{i,j}(k+1) = \sum_{h=i}^{j} q_{i,h}(k) p_{h,j}(k+1),\ i \leq j. \tag{4.38}$$

Thus, the matrix $\mathbb{Q}(k+1)$ constructed by $q_{i,j}(k+1)$ can be also expressed as $\mathbb{Q}(k+1) = \mathbb{Q}(k)\mathbf{Q}(k+1) = \prod_{t=0}^{k+1} \mathbf{Q}(t)$. Hence, Theorem 4.1 is proved.

4.B Proof of Theorem 4.2

Given the initial state i and the ij-th-entry $q_{i,j}(k+1)$ of $\mathbb{Q}(k+1)$ in Eq.(4.38), the probability of the DT-PBMC not being terminated after $(k+1)$ frames can be expressed as the sum of the i-th row's entries, which is formulated as

$$\begin{aligned} p_{i,unab}(k+1) &= \sum_{j=1}^{N-1} q_{i,j}(k+1) = \sum_{j=i}^{N-1} \sum_{h=i}^{j} q_{i,h}(k) p_{h,j}(k+1) \\ &= \sum_{j=i}^{N-1} q_{i,j}(k) \left[p_{j,1}(k+1) + \cdots + p_{j,N-1}(k+1) \right] \\ &= \sum_{j=i}^{N-1} q_{i,j}(k) [1 - p_{j,N}(k+1)]. \end{aligned} \tag{4.39}$$

Clearly, the probability of the DT-PBMC not being terminated after k frames is expressed as

$$p_{i,unab}(k) = \sum_{j=i}^{N-1} q_{i,j}(k). \tag{4.40}$$

Since $0 \leq p_{j,N} \leq 1$, we have $p_{i,unba}(k+1) < p_{i,unba}(k)$. Obviously, the probability of the DT-PBMC not being terminated is a monotonically decreasing function with respect to the number of frames k. If k tends to infinity, we may have

$$\lim_{k\to\infty} p_{i,unab}(k) = \lim_{k\to\infty} \sum_{j=i}^{N-1} q_{i,j}(k) = 0. \tag{4.41}$$

Thus, the relation of $\lim_{k\to\infty} q_{i,j}(k) = 0$ can be inferred. As a result, we have $\lim_{k\to\infty} \mathbb{Q}(k) = \mathbf{0}$. Furthermore, since the set of $\{\mathbf{Q}(t), t = 0, 1, 2, \cdots\}$ are i.i.d. random matrices, we have

$$\lim_{k\to\infty} \mathcal{E}[\mathbb{Q}(k)] = \lim_{k\to\infty} \prod_{t=0}^{k} \mathcal{E}[\mathbf{Q}(t)] = \lim_{k\to\infty} \overline{\mathbf{Q}}^{k} = 0. \tag{4.42}$$

Hence, Theorem 4.2 is proved.

4.C Proof of Theorem 4.3

According to Theorem 4.3, the ij-th-entry $q_{i,j}(k)$ of $\mathbb{Q}(k)$ represents the probability of transient state j being reached after k frames, given the initial state i. Then, given the initial state i, a new random variable $X(k)$ is defined. It is one if the state j is reached after k frames, and it is zero otherwise. Hence, we have $P[X(k) = 1] = q_{i,j}(k)$ and $P[X(k) = 0] = 1 - q_{i,j}(k)$. Then the expected value of $X(k)$ is $\mathcal{E}[X(k)] = q_{i,j}(k)$.

When considering the transmission of k frames, state j may be reached at any frame index spanning from zero to k. Hence, the total number of times that the state j is reached during these k frames can be expressed

as $X(0)+X(1)+\cdots+X(k)$, whose expected value is

$$\mathcal{E}[X(0)+X(1)+\cdots+X(k)] = q_{i,j}(0)+q_{i,j}(1)+\cdots+q_{i,j}(k).$$

If k tends to infinity, we have

$$\mathcal{E}[X(0)+X(1)+\cdots] = q_{i,j}(0)+q_{i,j}(1)+\cdots = \theta_{i,j}. \tag{4.43}$$

if we expand Eq.(4.43) to a matrix form, we arrive at $\mathbf{\Theta} = \sum_{k=0}^{\infty} \mathbb{Q}(k)$, whose ij-th-entry is $\theta_{i,j}$.

Since the time elapse is measured in terms of the number of transmission frames in the DT-PBMC, given the initial state i, the transient state j is reached $\theta_{i,j}$ times on average, which indicates that the system stays in state j for $\theta_{i,j}$ frames on average. Hence, Theorem 4.3 is proved.

4.D Proof of Theorem 4.4

Let us construct a system of linear equations $(I-\overline{\mathbf{Q}})\overrightarrow{\mathbf{x}} = \mathbf{0}$, where $\overrightarrow{\mathbf{x}}$ is a $1\times(N-1)$-element column vector. Then, iterating this equation k times, we have $\overrightarrow{\mathbf{x}} = \overline{\mathbf{Q}}^k\overrightarrow{\mathbf{x}}$. Upon letting k to tend to infinity, according to Theorem 4.2, we have $\lim_{k\to\infty}\overline{\mathbf{Q}}^k = \mathbf{0}$. Then the equation $(I-\overline{\mathbf{Q}})\overrightarrow{\mathbf{x}} = \mathbf{0}$ has a single solution, which is $\overrightarrow{\mathbf{x}} = \overrightarrow{\mathbf{0}}$. Hence, we may claim that $(\mathbf{I}-\overline{\mathbf{Q}})$ is a full-rank square matrix, whose inverse matrix denoted by $(\mathbf{I}-\overline{\mathbf{Q}})^{-1}$ does exist.

Clearly, the following equation holds

$$\left(\mathbf{I}-\overline{\mathbf{Q}}\right)\times\left(\mathbf{I}+\overline{\mathbf{Q}}+\overline{\mathbf{Q}}^2+\cdots+\overline{\mathbf{Q}}^k\right) = \mathbf{I}-\overline{\mathbf{Q}}^{k+1}. \tag{4.44}$$

Left-multiplying both sides of Eq.(4.44) by $(\mathbf{I}-\overline{\mathbf{Q}})^{-1}$, we arrive at:

$$\mathbf{I}+\overline{\mathbf{Q}}+\overline{\mathbf{Q}}^2+\cdots+\overline{\mathbf{Q}}^k = \left(\mathbf{I}-\overline{\mathbf{Q}}\right)^{-1}\times\left(\mathbf{I}-\overline{\mathbf{Q}}^{k+1}\right). \tag{4.45}$$

Provided that $\lim_{k\to\infty}\overline{\mathbf{Q}}^k = \mathbf{0}$ holds, upon letting k in both sides tend to infinity, we have

$$\sum_{k=0}^{\infty}\overline{\mathbf{Q}}^k = \left(\mathbf{I}-\overline{\mathbf{Q}}\right)^{-1}. \tag{4.46}$$

Hence, Theorem 4.4 is proved.

Chapter 5

Information Dissemination in Integrated Cellular and Small-Scale Opportunistic Networks

5.1 Introduction

5.1.1 Background

In densely populated areas, such as a football stadium and open air festivals, Mobile Users (MUs) always experience limitations, when they rely on the data services supported by Centralised Infrastructure (CI), such as Wi-Fi access points and cellular Base Stations (BSs). For instance, in a circular area having a radius of 50 meters in one of the above-mentioned scenarios, there may be hundreds of MUs, which may impose a heavy tele-traffic load on the CI. Moreover, the range of Wi-Fi [53] in outdoor scenarios can be up to 250 m. If the diameter of the circular area studied is lower than this transmission range, it is reasonable for us to assume that the MUs are always in the transmission range of each other. As a result, in contrast to the integrated cellular and large-scale opportunistic networks, as introduced in Chapter 2, the information dissemination in this densely populated area is no longer dominated by the encounter-properties of the MUs' mobility. However, the varying distance between a pair of MUs incurred by their movement would impose a fluctuating signal strength induced by the Path-Loss (PL) at the receiver end [154]. Apart from the PL induced by the varying distance and the multi-path fading, sophisticated MAC layer protocols are needed for efficiently scheduling the resources so as to minimise the adverse effects of the interference and to optimise the information dissemination performance. All these features differentiate the integrated cellular and small-scale opportunistic networks from their large-scale counterpart.

In an effort to guarantee a high Quality of Service (QoS), the classic BS-aided multicast suffers from long delay in disseminating the Information of Common Interest (IoCI) to all the subscribers in a densely populated area, since the next packet cannot be multicast until all of subscribers successfully received the current one. Due to the PL-, shadowing- and Doppler-dependent channel variations, the specific MUs having higher-quality channels may successfully receive the IoCI earlier than those having lower-quality channels. However, during the BS-aided multicast process, the particular MUs that have already received the IoCI have to remain silent and wait until all their peers have successfully received it. Furthermore, in the classic BS-aided multicast, we only have the high-power BS as the sole transmitter. Hence again, the energy dissipation of disseminating the IoCI towards all the MUs by solely relying on the BS-aided multicast is high.

As a remedy, cooperative multicast techniques may be invoked for improving the attainable performance by relying on a set of information multicasters (IMs) during the information dissemination process. When the transmitted signal arrives at a cooperating receiver, the receiver may recover the original information from the contaminated packet and then it may forward this packet to its unserved peers. By exploiting the common interest shared by the MUs, Peer-to-Peer (P2P) communications amongst the MUs is capable of cooperatively multicasting the packets from the packet owners to the hitherto unserved Mobile Users (uMUs). Due to the reduced PL and the potential diversity gain facilitated by the independent nature of the MUs, the content dissemination delay may be significantly reduced compared to the classic BS-aided multicast. Furthermore, since the cooperative multicast amongst the MUs is realised by low-power mobile devices operating in P2P mode, it may remarkably reduce the total energy dissipation during disseminating the IoCI to all the subscribers.

The cooperative multicast technique has attracted substantial attention from the communication society. In [128], the concept of multi-hop wireless multicast was proposed for the sake of enhancing the achievable multicast coverage, where a node having received the IoCI in a previous hop is randomly selected for further multicast. In order to exploit the diversity gain provided by multiple IMs, a multi-stage cooperative multicast scheme was proposed in [129]. Moreover, it was argued in [132] that the employment of two-stage cooperative multicast is more practical than that of its multi-stage counterpart. Therefore, the attainable performance of two-stage cooperative multicast was analysed in [133], while the associated optimum power allocation was characterised in [130]. Furthermore, in [131] and [155], the authors studied the benefits of relay selection techniques in the context of two-stage cooperative multicast. Specifically, in [131] the best relay was selected for maximizing the end-to-end cooperative multicast capacity. By contrast, in order to avoid unnecessary power wastage, in [155] the relays were activated only if there were unserved nodes within their transmission range.

5.1.2 Novel Contributions

In this chapter, we will introduce an improved mathematical framework for analysing the performance of the information dissemination process of integrated cellular and small-scale opportunistic networks.

The information dissemination model of this chapter constitutes an extension based on the model proposed in Chapter 4. In Chapter 4, the information dissemination process is completed by the local communications amongst the MUs without considering any CI-based transmissions. Additionally, we proposed a Time-Division-Multiple-Access (TDMA) approach in the Medium-Access-Control (MAC) layer in order to mitigate the adverse effects of the interference and contention-induced collisions, where each IM can be guaranteed to have a dedicated Time Slot (TS) for its multicast. However, in reality only a limited amount of resources are provided by a communication system. As a result, we have to study the resource scheduling issues of the information dissemination process, especially when multiple IMs exist but limited resources are provided.

In Chapter 4, relying on a Discrete-Time-Pure-Birth-Markov-Chain (DT-PBMC), we only provided a mathematical framework for analysing the statistical properties of the dissemination delay, which is the time duration spanning from the initial Information Owners (IOs) multicasting the IoCI to the instant of all other MUs successfully receiving it. However, in Chapter 4 a range of other crucial delay metrics and energy dissipation issues remained unsolved. As a result, the following two questions arise:

- Is there a generic mathematical approach of analysing the various delay metrics?
- How much energy will be dissipated, when exhaustively disseminating the IoCI to all of the MUs?

We will find the answers to both of these questions in this chapter. Against this background, the novel contributions of this chapter are summarised as below:

- We propose a hybrid information dissemination scheme for integrated cellular and small-scale opportunistic networks. This scheme consists of two main stages, namely the BS-aided multicast and the cooperative-multicast-aided spontaneous dissemination. In order to avoid any interference amongst multiple IMs, a TDMA scheme is invoked.

- The varying distances between the transmitters and receivers, which are incurred by the MUs' mobility, result in varying PL. By jointly considering the PL and the multipath fading in the physical layer as well as the classic round-robin resource scheduling in the MAC layer, we analyse the average throughput of both the cellular links[1] and of the opportunistic links[2].

- We model the hybrid information dissemination scheme by a DT-PBMC and focus our attention on the delay of a specific group of MUs, which is the time duration spanning from the BS multicasting the IoCI to the instant, when all the members in this group successfully receive it. This group of MUs can be regarded as the target of our hybrid information dissemination scheme. The other MUs, who do not belong to this target group can be regarded as 'helpers', since they are capable of relaying the IoCI towards the target group.

- The group delay can be regarded as a generic terminology subsuming various delay metrics. When the group size is one, it is equivalent to the end-to-end delay of a single source-to-destination path. When the group size is equal to the total number of MUs in the area studied, it is equivalent to the total dissemination delay, which is the time required to serve all of the MUs. Furthermore, the average energy dissipation of disseminating the IoCI is also derived.

- In order to further reduce both the delay and the energy dissipation in the context of our hybrid information dissemination scheme, a number of centrality based resource scheduling approaches are proposed, including the shortest-longest-distance scheduling, the shortest-shortest-distance scheduling, the shortest-sum-distance scheduling and the highest-sum-rate scheduling concepts.

- We observe from the simulation results that a more vigorous social participation of the MUs is capable of reducing both the dissemination delay and the energy dissipation.

These original contributions were disseminated in [58] and [63].

5.1.3 Chapter Organisation

The rest of the chapter is organised as follow:

- In Section 5.2, we characterise the main features of our hybrid information dissemination scheme in both the network layer and the MAC layer.

- In Section 5.3, we describe the physical layer model of our wireless transmission regime, followed by the derivation of the L-th moment of the throughput for both the cellular and opportunistic links during a single TS. Then, we derive the average throughput of an opportunistic link, when multiple TSs are assigned to the transmitter during a transmission frame.

- In Section 5.4, we model our hybrid information dissemination scheme by a DT-PBMC. The statistical properties of various delay and energy metrics are derived in closed-form.

- In Section 5.5, a number of social centrality based resource scheduling approaches are proposed for reducing both the delay and energy dissipation of our hybrid information dissemination scheme.

[1] A wireless link connecting a MU to a BS is regarded as a cellular link

[2] A wireless link connecting a pair of MUs is regarded as a opportunistic link

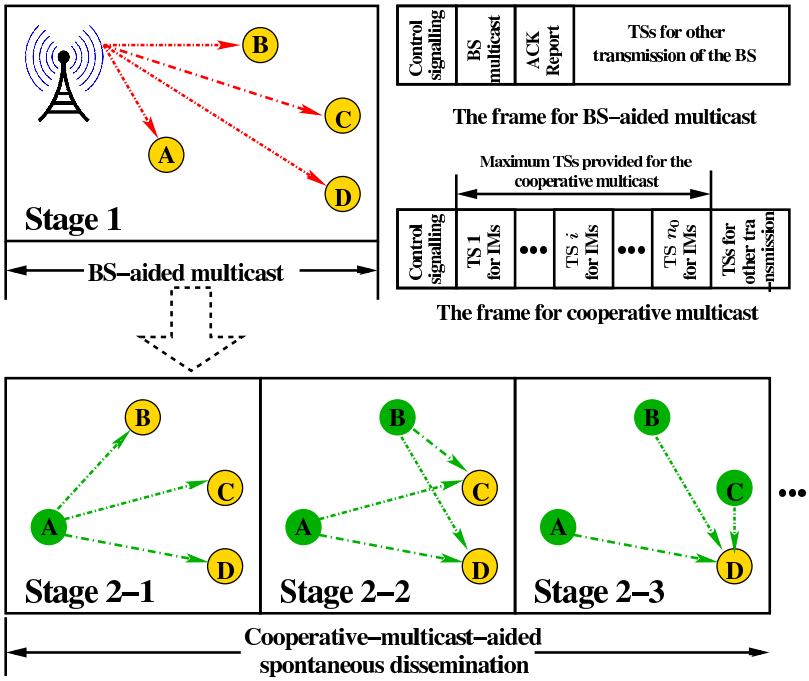

Figure 5.1: Hybrid information dissemination scheme

- In Section 5.6, both our simulation and analytical results related to our hybrid information dissemination scheme are provided. We also evaluate different resource scheduling approaches in terms of both their average total dissemination delay as well as their average total energy dissipation.
- In Section 5.7, we conclude this chapter.

5.2 Hybrid Information Dissemination Scheme

As shown in Figure 5.1, the hybrid information dissemination scheme is comprised of two main stages, which are the BS-aided multicast and the cooperative-multicast-aided spontaneous dissemination, respectively. For the integrated cellular and small-scale networks, the communication system works in a discrete-time manner, where the basic time unit is the duration of a transmission frame. We assume that all the MUs and the BS are synchronously operated at the frame level, which can be readily realised since MUs normally exchange control signalling with the BS.

5.2.1 BS-Aided Multicast

At the first main stage, the cellular BS initially tries to multicast the IoCI to all the MUs in the studied area. The frame structure employed at this stage is portrayed in Figure 5.1. At the beginning of the frame, several TSs are reserved for control signalling exchange between the MUs and the BS. Next, a single TS is invoked by the BS for multicasting the IoCI. Afterwards, several TSs are allocated to the MUs for reporting their feedback. If a MU successfully receives the IoCI, an ACKnowledgement (ACK) message is reported to the BS. The BS repeats multicasting the IoCI in the next frame, until it receives a single ACK at least. In this case, the BS-aided multicast completes.

Algorithm 5.1: Round-robin resource scheduling algorithm

Initialise the set $\mathcal{IM} \leftarrow$ randomly sort the IMs during the current frame;
Set $n \leftarrow |\mathcal{IM}|$, the size of $\mathcal{IM}$;
Set $n_0 \leftarrow$ the size of the available TSs for multicast;
Initialise the available TSs set $\mathcal{TS} \leftarrow \{TS_i | 1 \leq i \leq n_0\}$;
Set $indexTS = 1$; $indexIM = 1$;
for $indexTS = 1$ to n_0 **do**
    $\mathcal{TS}[indexTS]$ is allocated to $\mathcal{IM}[indexIM]$;
    $indexIM \leftarrow indexIM + 1$;
    if $indexIM > n$ **then**
        $indexIM \leftarrow 1$;
    end if
end for

5.2.2 Cooperative-Multicast-Aided Spontaneous Dissemination

During the second main stage, the IoCI is spontaneously disseminated by the IMs to the hitherto uMUs via cooperative multicast techniques, until all the MUs in the studied area successfully receive the information. As shown in Figure 5.1, we have an increasing number of IMs during this stage, and this may substantially speed up the information dissemination process. Furthermore, in order to avoid the interference and contention-induced collisions amongst the multiple IMs, a TDMA scheme is introduced[3].

During this stage, the BS may play the role of a controller. The frame structure of this stage is also portrayed in Figure 5.1, which consists of several TSs for the relevant control signalling exchange between the MUs and the controller as well as n_0 TSs for IMs' multicast. During the TSs for the control signalling exchange, the following tasks are completed:

- The IMs report to the controller their willingness of sharing the IoCI;
- The uMUs send requests to the controller for the IoCI;
- The controller schedules the available resources of n_0 TSs to the IMs, and then broadcasts the resource scheduling scheme to all the IMs and uMUs. The detail of the resource scheduling scheme invoked in our model is introduced in Section 5.2.3 and Section 5.5.

Following the control signalling exchange, IMs multicast the IoCI to uMUs during the allocated TSs. Finally, if the controller does not receive any requests from the uMUs at the beginning of a transmission frame, it will inform all the IMs that the information dissemination process is completed.

5.2.3 Round-Robin Resource Scheduling for the Spontaneous Dissemination

In order to fully exploit the n_0 TSs provided by the TDMA system for the cooperative-multicast-aided spontaneous dissemination, the classic round-robin scheme is invoked for scheduling the n_0 TSs of the current transmission frame to the IMs. After collecting the IMs' willingness of sharing the IoCI at the beginning of the transmission frame, the controller randomly sorts the IMs into a set of $\mathcal{IM}$, whose size is $|\mathcal{IM}| = n$. Each TS in the available TS set $\mathcal{TS} = \{TS_i | 1 \leq i \leq n_0\}$ is allocated to a IM belonging to the $\mathcal{IM}$ set. If the size of $\mathcal{IM}$ is larger than n_0, only the first n_0 IMs of $\mathcal{IM}$ are assigned with a single TS for their own multicast. If the size of $\mathcal{IM}$ is smaller than n_0, the controller continues to allocate the remaining

[3]TDMA is one of the possible solutions that are capable of providing orthogonal channel access. The TDMA scheme in distributed Wi-Fi system has already been thoroughly studied in [143] in terms of synchronisation, control overhead, which makes it an available solution for our model. Other solutions, e.g. Orthogonal-Frequency-Division-Multiple-Access (OFDMA), Code-Division-Multiple-Access (CDMA), and Carrier-Sense-Multiple-Access (CSMA) can be invoked as well.

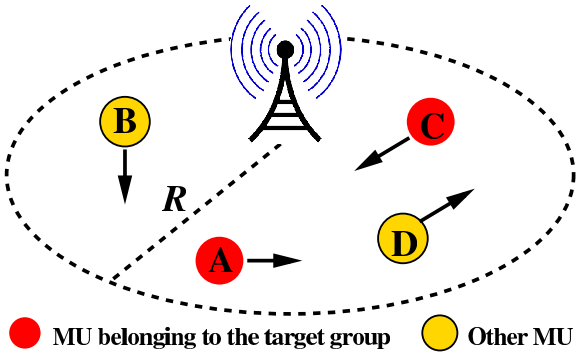

Figure 5.3: random mobile networks

TSs to the IMs belonging to $\mathcal{IM}$ in the same order for another round after every IM in $\mathcal{IM}$ set has already been assigned with a single TS in the first round of scheduling. This process continues until all the TSs in the $\mathcal{TS}$ set are assigned. The details of the round-robin scheduling algorithm are shown in Algorithm 5.1.

According to this algorithm, there are $mod(n_0, n)$ IMs receiving $\lceil n_0/n \rceil$ TSs for each of them, while there are $[n - mod(n_0, n)]$ IMs receiving $\lfloor n_0/n \rfloor$ TSs for each of them. Here, $mod(n_0, n)$ represents the remainder after the division of n_0 by n, $\lceil n_0/n \rceil$ represents the first integer that is higher than the real value n_0/n, while $\lfloor n_0/n \rfloor$ represents the first integer that is lower than the real value n_0/n. These results will be exploited in the derivation of the state transition probabilities in Section 5.4.1.

5.2.4 Random Mobile Networks

We assume that N MUs roam in a cell, which is a circular area having a radius of R, as shown in Fig.5.3. Naturally, the BS is assumed to be located at the center of the circular area. In line with the mobility model introduced in [116] [115], the position of the i-th MU during frame t is denoted by $\mathbf{P}_i(t)$, which represents a stationary and ergodic process having a stationary uniform distribution in the circular area. In other words, $\mathbf{P}_i(t)$ *is unchanged during a transmission frame but varies from one frame to another.* Moreover, the positions of the different MUs are independently and identically distributed (i.i.d.). As a result, the Cumulative Distribution Function (CDF) and the Probability Density Function (PDF) of the distance Y_b between the BS and a MU can be formulated as

$$F_{Y_b}(y_b) = \frac{y_b^2}{R^2},\ f_{Y_b}(y_b) = \frac{dF_{Y_b}(y_b)}{dy_b} = \frac{2y_b}{R^2},\ 0 \le y_b \le R. \tag{5.1}$$

The detailed derivation process of Eq.(5.1) can be found in Theorem 6.1 of Chapter 6. By contrast, the CDF of the distance Y_s between a pair of MUs can be expressed as

$$F_{Y_s}(y_s) = \frac{2}{\pi}\left\{4\left(\frac{y_s}{2R}\right)^2 \arccos\left(\frac{y_s}{2R}\right) + \arcsin\left(\frac{y_s}{2R}\right) - \left[\frac{y_s}{2R} + 2\left(\frac{y_s}{2R}\right)^3\right]\sqrt{1-\left(\frac{y_s}{2R}\right)^2}\right\}, \tag{5.2}$$

while the corresponding PDF can be derived as

$$f_{Y_s}(y_s) = \frac{8}{\pi R}\frac{y_s}{2R}\left[\arccos\left(\frac{y_s}{2R}\right) - \frac{y_s}{2R}\sqrt{1-\left(\frac{y_s}{2R}\right)^2}\right] \tag{5.3}$$

for $0 \le y_s \le 2R$, according to Theorem 6.9 of Chapter 6. However, in order to make our following analysis tractable, we use the approximated PDF derived in Section 4.3.1 of Chapter 4 for Eq.(5.3), which is expressed

as

$$\widetilde{f_{Y_s}}(y_s) = C_{Y_s} \cdot \frac{8}{\pi R}\left(\frac{\pi}{2}\frac{y_s}{2R} + \sum_{n=0}^{n_{\max}} C_n \left(\frac{y_s}{2R}\right)^{2n+2}\right), \tag{5.4}$$

where we have

$$C_{Y_s} = \frac{\pi}{4}\left(\pi + \sum_{n=0}^{n_{\max}} \frac{4C_n}{2n+3}\right)^{-1},\ C_n = \frac{2\cdot(2n)!}{4^n(n!)^2(2n+1)(2n-1)}.$$

5.3 Throughput Analysis of Wireless Links

5.3.1 Physical Layer Model

5.3.1.1 Path-Loss

Given the distance y_l between a transmitter-receiver pair, which is assumed to be longer than the reference distance d_0 determining the edge of the near-field, the PL model is defined by the following equation

$$\Omega_l(y_l) = \frac{P_{l,0}}{P_{l,r}} = \left(\frac{y_l}{d_0}\right)^{\kappa},\ y_l \geq d_0, \tag{5.5}$$

where $P_{l,r}$ is the power received at the receiver, $P_{l,0}$ is the power received at the reference point that is d_0 m away from the transmitter and κ is the PL exponent. The free-space PL model [114] is exploited for calculating the PL from the transmitter to the reference point, which is expressed as

$$\Omega_{l,0} = \frac{P_{l,t}}{P_{l,0}} = \frac{(4\pi)^2 d_0^2}{\lambda_l^2} = \left(\frac{4\pi d_0}{c/f_{l,c}}\right)^2, \tag{5.6}$$

where $\lambda_l = c/f_{l,c}$ is the wave-length, c is the speed of light, $f_{l,c}$ is the carrier frequency, and $P_{l,t}$ is the transmit power. Thus, the received reference power $P_{l,0}$ is obtained as $P_{l,0} = P_{l,t}/\Omega_{l,0}$. Unfortunately, Eq.(5.6) is invalid for calculating the PL in the near-field of the transmit antenna. As a result, we assume that, when the distance y_l between the transmitter and receiver is shorter than d_0, the received power $P_{l,r}$ is equal to the transmit power $P_{l,t}$. In a nutshell, given an arbitrary distance y_l, the PL model in our system is defined as

$$\Omega_l(y_l) = \frac{P_{l,0}}{P_{l,r}} = \begin{cases} 1/\Omega_{l,0}, & 0 \leq y_l < d_0, \\ (y_l/d_0)^{\kappa}, & y_l \geq d_0. \end{cases} \tag{5.7}$$

5.3.1.2 Small-Scale fading

The small-scale fading is modelled by uncorrelated stationary Rayleigh flat-fading. *The channel's amplitude $|h_l(t)|$ during the t-th TS, which varies from one TS to another, is a Rayleigh distributed random variable.* Consequently, the square of the channel amplitude $|h_l(t)|^2$ obeys an exponential distribution associated with $\mathcal{E}[|h_l(t)|^2] = 1$. The PDF and CDF of $X = |h_l(t)|^2$ are $f_X(x) = \exp(-x)$, $F_X(x) = 1 - \exp(-x)$, $x > 0$, respectively.

5.3.2 Throughput Analysis of Wireless Links

We assume that a packet can only be successfully received during a TS, if the instantaneously received Signal-to-Noise-Ratio (SNR) exceeds a pre-defined SNR threshold γ. Given the distance y_l between a

transmitter-receiver pair, the successful packet delivery probability μ_l during a single TS is derived as

$$\mu_l(y_l) = \mathrm{P}\left[\frac{P_{l,0}|h_l(t)|^2}{N_0 W_l \cdot \Omega_l(y_l)} \geq \gamma\right] = \begin{cases} \exp(-B_l),\ 0 \leq y_l < d_0, \\ \\ \exp(-A_l y_l^{\kappa}),\ y_l \geq d_0, \end{cases} \tag{5.8}$$

where $A_l = (\gamma N_0 W_l)/(P_{l,0} d_0^{\kappa})$, $B_l = (\gamma N_0 W_l)/P_{l,t}$, N_0 is the noise Power Spectrum Density (PSD), W_l is the available bandwidth, $P_{l,t}$ is the transmit power and $P_{l,0}$ is the associated received reference power. According to [117], $\mu_l(y_l)$ is also equivalent to the normalized throughput of the link connecting the transmitter and receiver, whose unit is 'packets/frame'. We should note that the generic subscript 'l' appearing throughout this chapter represents 'b' for the transmission between the BS and MUs, while it represents 's' for the transmission between a pair of MUs.

5.3.2.1 *L*-th Moment of Throughput Between the BS and a MU During a Time Slot

Integrating the L-th power of $\mu_b(y_b)$, provided by Eq.(5.8), over the PDF of Eq.(5.1), we can derive the L-th moment of the link throughput between the BS and a MU as

$$\begin{aligned} \mathcal{E}[\mu_b^L] &= \int_0^R \mu_b^l(y_b) f_{Y_b}(y_b) dy_b \\ &= \int_0^{d_0} \exp(-LB_b)\frac{2y_b}{R^2} dy_b + \int_{d_0}^R \exp(-LA_b y_b^{\kappa})\frac{2y_b}{R^2} dy_b \\ &= \exp(-LB_b)\frac{d_0^2}{R^2} + \frac{2}{R^2}\left[\frac{\Gamma(LA_b d_0^{\kappa}, 2/\kappa)}{\kappa(LA_b)^{2/\kappa}} - \frac{\Gamma(LA_b R^{\kappa}, 2/\kappa)}{\kappa(LA_b)^{2/\kappa}}\right], \end{aligned} \tag{5.9}$$

where $\Gamma(\cdot,\cdot)$ is the upper incomplete Gamma function. By letting $L = 1$, we obtain the average link throughput $\overline{\mu}_b$ between the BS and a MU, which is also the upper bound of the average social unicast throughput derived in [61].

5.3.2.2 *L*-th Moment of Throughput Between a Pair of MUs During a Time Slot

Integrating the L-th power of $\mu_s(y_s)$, provided by Eq.(5.8), over the PDF of Eq.(5.3) as well as its approximate version of Eq.(5.4), we can derive the L-th moment of the link throughput between a pair of MUs as

$$\begin{aligned} \mathcal{E}[\mu_s^L] &= \int_0^{2R} \mu_s^L(y_s) f_{Y_s}(y_s) dy_s \\ &= \underbrace{\int_0^{d_0} \exp(-LB_s) f_{Y_s}(y_s) dy_b}_{I_1} + \underbrace{\int_{d_0}^{2R} \exp(-LA_s y_s^{\kappa}) \widetilde{f}_{Y_s}(y_s) dy_s}_{I_2} \end{aligned} \tag{5.10}$$

The first integral I_1 of Eq.(5.10) may be expressed as

$$I_1 = \exp(-LB_s)\int_0^{d_0} f_{Y_s}(y_s) dy_s = \exp(-LB_s) \cdot F_{Y_s}(d_0),$$

while the second integral I_2 of Eq.(5.10) may be derived as

$$\begin{aligned} I_2 &= \int_{d_0}^{2R} \exp(-LA_s y_s^{\kappa}) C_{Y_s} \cdot \frac{8}{\pi R}\left(\frac{\pi}{2}\frac{y_s}{2R} + \sum_{n=0}^{n_{\max}} C_n \left(\frac{y_s}{2R}\right)^{2n+2}\right) dy_s \\ &= \frac{8C_{Y_s}}{\pi R}\left[\frac{\pi}{4R}\frac{\Gamma(LA_s d_0^{\kappa}, 2/\kappa) - \Gamma(LA_s(2R)^{\kappa}, 2/\kappa)}{\kappa(LA_s)^{2/\kappa}}\right. \\ &\left. + \sum_{n=0}^{n_{\max}} \frac{C_n(\Gamma(LA_s d_0^{\kappa}, (2n+3)/\kappa) - \Gamma(LA_s(2R)^{\kappa}, (2n+3)/\kappa)}{\kappa(2R)^{2n+2}(LA_s)^{(2n+3)/\kappa}}\right]. \end{aligned}$$

By letting $L = 1$, we obtain the average link throughput $\overline{\mu}_s$ between a pair of MUs during a TS, which is also the upper bound of the average social unicast throughput derived in derived in Section 4.3.5 of Chapter 4.

5.3.2.3 Average Throughput During a Transmission Frame

In the first stage of BS-aided multicast, as detailed in Section 5.2.1, only a single TS is invoked by the BS for the sake of multicasting the IoCI. As a result, the link throughput during a transmission frame between the BS and a MU is the same as that during a single TS, which is given by substituting $L = 1$ into Eq.(5.9).

By contrast, in the second stage of cooperative-multicast-aided spontaneous dissemination, a single IM may be assigned with multiple TSs, say $\mathcal{L}$, for its own multicast. Let us consider an IM and uMU pair as an example. Recalling the mobility model introduced in Section 5.2.4, the distance y_s is unchanged during the transmission frame. Given the $\mathcal{L}$ TSs for the IM's multicast, the packet fails to be conveyed to the uMU only when all the transmission attempts in these $\mathcal{L}$ TSs fail. Since the small-scale fading varies independently from one TS to another, the successful packet delivery probability during a transmission frame may be expressed as

$$\lambda_s(y_s, \mathcal{L}) = 1 - [1 - \mu_s(y_s)]^{\mathcal{L}} = 1 - \sum_{L=0}^{\mathcal{L}} \binom{\mathcal{L}}{L} (-1)^L [\mu_s(y_s)]^L. \tag{5.11}$$

Integrating $\lambda_s(y_s, \mathcal{L})$ over the PDF $f_{Y_s}(y_s)$ given by Eq.(5.3), the average link throughput during a transmission frame is formulated as

$$\begin{aligned} \overline{\lambda}_s(\mathcal{L}) &= \int \left[1 - \sum_{L=0}^{\mathcal{L}} \binom{\mathcal{L}}{L} (-1)^L [\mu_s(y_s)]^L \right] f_{Y_s}(y_s) dy_s \\ &= 1 - \sum_{L=0}^{\mathcal{L}} \binom{\mathcal{L}}{L} (-1)^L \mathcal{E}[\mu_s^L], \end{aligned} \tag{5.12}$$

where $\mathcal{L}$ is the number of TSs that is allocated to the IM for the multicast during the current transmission frame, and $\mathcal{E}[\mu_s^L]$ is the L-th moment of the link throughput during a single TS that has been derived in Eq.(5.10). Specifically, when no TS is allocated to the IM, namely $\mathcal{L} = 0$, we have $\overline{\lambda}_s(\mathcal{L}) = 0$.

5.4 Discrete-Time-Pure-Birth-Markov-Chain Aided Analysis

In contrast to its large-scale counterpart, the integrated cellular and small-scale opportunistic network is a discrete transmission system, where the basic time unit is the duration of a transmission frame. Since the number of IMs always increases during the information dissemination process, we may model this process as a DT-PBMC, whose states are defined by the number of IMs. Moreover, the BS may also be considerd as a special IM. For example, the state $(1+n)$ represents that both the BS and n MUs own the IoCI. In the DT-PBMC, the transition from a lower numbered state to a higher numbered one can only occur once during a single transmission frame. Consequently, $p_{1+n,1+n+m}(t)$ represents the probability of a transition traversing from state $(1+n)$ to state $(1+n+m)$ during a given frame t. As portrayed in Figure 5.4, there are two special states in the DT-PBMC, which are the initial state $1(B)$, representing that only the BS owns the IoCI at the beginning of the information dissemination process, and the absorbing state $(1+N)$, representing that all the MUs have obtained the IoCI. Except for state $(1+N)$, the other states are referred to as the transient states.

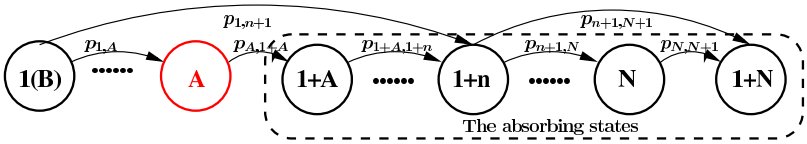

(a) Group $\mathcal{A}$ receive the information after the transient boundary A.

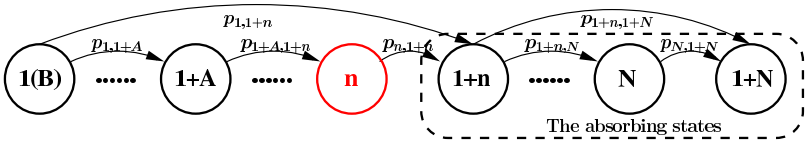

(b) Group $\mathcal{A}$ receive the information after the transient boundary n.

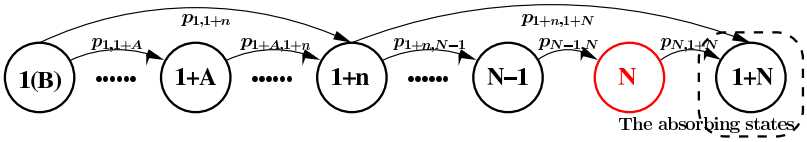

(c) Group $\mathcal{A}$ receive the information after the transient boundary N.

Figure 5.4: The DT-PBMC for the information dissemination in integrated cellular and small-scale opportunistic networks

5.4.1 State Transition Matrix

We can collect the state transition probabilities $\{p_{1+n,1+n+m}(t)|0 \leq n \leq N, 0 \leq m \leq (N-n)\}$ into a state transition matrix $\mathbb{P}(t)$, which is expressed as

$$\mathbb{P}(t) = \begin{pmatrix} p_{1,1}(t) & p_{1,2}(t) & p_{1,3}(t) & p_{1,4}(t) & \cdots & p_{1,N}(t) & p_{1,N+1}(t) \\ 0 & p_{2,2}(t) & p_{2,3}(t) & p_{2,4}(t) & \cdots & p_{2,N}(t) & p_{2,N+1}(t) \\ \vdots & \vdots & \ddots & \vdots & & \vdots & \vdots \\ 0 & 0 & \cdots & p_{n+1,n+1}(t) & \cdots & p_{n+1,N}(t) & p_{n+1,N+1} \\ \vdots & \vdots & & & \ddots & \vdots & \vdots \\ 0 & 0 & \cdots & 0 & \cdots & p_{N,N}(t) & p_{N,N+1} \\ 0 & 0 & \cdots & 0 & \cdots & 0 & p_{N+1,N+1} \end{pmatrix} = \begin{pmatrix} \mathbf{Q}(t) & \mathbf{Q_0}(t) \\ \mathbf{0} & 1 \end{pmatrix}, \tag{5.13}$$

where the $(N \times N)$-element matrix $\mathbf{Q}(t)$ contains all the state transition probabilities between any pairs of transient states. Hence $\mathbf{Q}(t)$ is referred to as the *transient transition matrix*, while $\mathbf{Q_0}(t)$ is an N-length vector, containing the transition probabilities of traversing from any of the N transient states to the absorbing state $(1+N)$. We note that both the matrix $\mathbb{P}(t)$ and $\mathbf{Q}(t)$ are random matrices, varying from one frame to another. The expectation matrix $\overline{\mathbb{P}}$ is derived by computing the expectation of every entry in $\mathbb{P}(t)$. The elements of the expectation matrix $\overline{\mathbb{P}}$ are denoted as $\{\overline{p}_{1+n,1+n+m},\ 0 \leq n \leq N, 0 \leq m \leq (N-n)\}$, which are given by the following lemma:

Lemma 5.1. *Due to the independent mobilities of the MUs, the state transition probability $p_{1+n,1+n+m}(t)$ is an independent time-varying random variable. Its expected value is given by the following formulas:*

i) When $n = 0$ and $0 \leq m \leq N$, the expected value of $p_{1,1+m}(t)$ is expressed as

$$\overline{p}_{1,1+m} = \binom{N}{m} \overline{\mu}_b^m (1-\overline{\mu}_b)^{N-m}, \tag{5.14}$$

where $\overline{\mu}_b$ can been derived by letting $L = 1$ in Eq.(5.9).

ii) When $0 < n \leq N$ and $0 \leq m \leq (N-n)$, the expected value of $p_{1+n,1+n+m}(t)$ is expressed as

$$\overline{p}_{1+n,1+n+m} = \binom{N-n}{m} \overline{p}_i^m (1-\overline{p}_i)^{N-n-m}, \tag{5.15}$$

where $\overline{p}_i$ is the expected probability of an arbitrary uMU successfully receiving the IoCI, which is formulated as

$$\overline{p}_i = 1 - \left[1 - \overline{\lambda}_s \left(\lceil \frac{n_0}{n} \rceil\right)\right]^{mod(n_0,n)} \cdot \left[1 - \overline{\lambda}_s \left(\lfloor \frac{n_0}{n} \rfloor\right)\right]^{n-mod(n_0,n)}. \tag{5.16}$$

Proof. Please refer to Appendix 5.A for the proof. □

Furthermore, the expectation $\overline{\mathbf{Q}}$ of the transient-state transition matrix $\mathbf{Q}(t)$ contains the entries in the first N rows and first N columns of the general state transition matrix $\overline{\mathbb{P}}$.

Various delay metrics can be derived with the aid of the DT-PBMC of Figure 5.4, which are listed as follow:

- The *group delay* K_G, which is defined as the delay when the entire group $\mathcal{A}$ of MUs has successfully received the IoCI;
- The *individual delay* K_I, namely the delay of a specific MU receiving the information;
- The *dissemination delay* K_D, which represents the delay when all the N MUs in the cell have successfully received the information;
- The *BS-aided multicast delay* K_b, which is the delay of the BS-aided first stage of information dissemination.

In this section, the *BS-aided-single-hop-multicast delay* K^{bm} is also derived and used as a benchmark.

5.4.2 Transient Boundary

As shown in Figure 5.4, multiple-step state transitions may occur during a single frame's transmission. For example, the transition can emerge from state $1(B)$ directly to any of the states $(1+n)$ $(0 \leq n \leq N)$. Consequently, we cannot exactly tell at which state the specific group $\mathcal{A}$ of MUs have first successfully received the IoCI as we dealt with the Continuous-Time-Pure-Birth-Markov-Chain (CT-PBMC) in Chapter 2 and the approximate CT-PBMC in Chapter 3, because within a sample trace of the state transitions traversing from the initial state $1(B)$ to the absorbing state N, certain states might be skipped. However, we may ascertain that this group of MUs must successfully receive the IoCI after a certain state n, which also indicates that not all the MUs belonging to the group $\mathcal{A}$ have successfully received the information during the previous states. As a result, the states emanating from state $(1+n)$ to $(1+N)$ can be equivalently considered together as an absorbing state for the event that all the MUs belonging to the group $\mathcal{A}$ have successfully received the information after state n, as shown in Figure 5.4(b). Corresponding to the above event, state n may be referred to as the *transient boundary*.

Lemma 5.2. *Let the size of the group $\mathcal{A}$ be defined as $|\mathcal{A}| = A$. The legitimate transient boundary may be any of the states spanning from state A to state N, as shown in Figure 5.4. The probability Pr_n that the transient boundary is at state n $(A \leq n \leq N)$ is given by the following equation:*

$$Pr_n = \binom{n-1}{A-1} \Big/ \binom{N}{A},\ A \leq n \leq N. \tag{5.17}$$

Proof. Please refer to Appendix 5.B for the proof. □

5.4.3 Group Delay Analysis

Given that the transient boundary is at state n ($A \leq n \leq N$), all the MUs belonging to the target group $\mathcal{A}$ receive the IoCI right after state n. Correspondingly, we represent the *group delay* as K_n frames. As shown in Figure 5.4(b), in this case, the absorbing states for the group $\mathcal{A}$ are comprised of the states $\{n+1, n+2, \cdots, N, N+1\}$. As a result, transition matrix $\mathbf{Q}_n(t)$ of the new DT-PBMC of Fig.5.4(b) is a sub-matrix of $\mathbf{Q}(t)$ containing its entries in the first n rows and n columns, which is expressed as

$$\mathbf{Q}_n(t) = \begin{pmatrix} p_{1,1}(t) & p_{1,2}(t) & \cdots & p_{1,n}(t) \\ 0 & p_{2,2}(t) & \cdots & p_{2,n}(t) \\ \vdots & \vdots & \ddots & \vdots \\ 0 & 0 & \cdots & p_{n,n}(t) \end{pmatrix}, \ A \leq n \leq N. \tag{5.18}$$

According to Eq.(5.18), for different values of n, $\mathbf{Q}_n$ has different size. In order to unify the size of the matrices $\{\mathbf{Q}_n, n = 1, 2, \cdots, N\}$, we may redefine $\mathbf{Q}_n$ without affecting the result of the matrix product as

$$\widetilde{\mathbf{Q}}_n(t) = \begin{pmatrix} \mathbf{Q}_n(t) & \mathbf{0}_{n,N-n} \\ \mathbf{0}_{N-n,n} & \mathbf{0}_{N-n,N-n} \end{pmatrix}, \tag{5.19}$$

where $\mathbf{0}_{m,n}$ is a $(m \times n)$-element matrix whose entries are all zeros. Particularly, the expected matrix of $\widetilde{\mathbf{Q}}_n(t)$ is denoted as $\widehat{\mathbf{Q}}_n$, while the entries of $\widehat{\mathbf{Q}}_n$ are defined in Eq.(5.14) and Eq.(5.15).

According to Theorem 4.1 in Chapter 4, the ij-entry $q_{i,j}$ of the matrix $\widetilde{\mathbb{Q}}_n(k_G) = \prod_{t=1}^{k_G} \widetilde{\mathbf{Q}}_n(t)$ is the probability of state j being reached after k_G frames from the initial state i. Since the information dissemination starts at state $1(B)$, as shown in Figure 5.4, given a series of the i.i.d. transition matrices $\{\widetilde{\mathbf{Q}}_n(t), t = 1, \cdots, k_G\}$, the sum of the entries in the first row of the matrix $\widetilde{\mathbb{Q}}_n(k_G)$ is the probability of $K_n > k_G$, which is expressed as

$$\Pr(K_n > k_G | \widetilde{\mathbf{Q}}_n(1), \cdots, \widetilde{\mathbf{Q}}_n(k_G)) = \boldsymbol{\tau}^T \widetilde{\mathbb{Q}}_n(k_G)\mathbf{1} = \boldsymbol{\tau}^T \prod_{t=1}^{k_G} \widetilde{\mathbf{Q}}_n(t)\mathbf{1},$$

where $\boldsymbol{\tau}$ is a $(N \times 1)$-element column vector, whose first entry is one and all the other entries are zeros, while $\mathbf{1}$ is a $(N \times 1)$-element column vector, whose entries are all ones. According to the Bayesian principle [94], given n as the transient boundary, the tail distribution of the group delay K_n is derived as

$$\begin{aligned} &\Pr(K_n > k_G) \\ &= \int_{\widetilde{\mathbf{Q}}_n(1)} \cdots \int_{\widetilde{\mathbf{Q}}_n(k_G)} \Pr(K_n > k_G | \widetilde{\mathbf{Q}}_n(1), ..., \widetilde{\mathbf{Q}}_n(k_G)) f[\widetilde{\mathbf{Q}}_n(1), ..., \widetilde{\mathbf{Q}}_n(k_G)] d\widetilde{\mathbf{Q}}_n(1) \cdots d\widetilde{\mathbf{Q}}_n(k_G) \\ &= \int_{\widetilde{\mathbf{Q}}_n(1)} \cdots \int_{\widetilde{\mathbf{Q}}_n(k_G)} \left(\boldsymbol{\tau}^T \prod_{t=1}^{k_G} \widetilde{\mathbf{Q}}_n(t)\mathbf{1} \right) f[\widetilde{\mathbf{Q}}_n(1), ..., \widetilde{\mathbf{Q}}_n(k_G)] d\widetilde{\mathbf{Q}}_n(1) ... d\widetilde{\mathbf{Q}}_n(k_G) \\ &= \boldsymbol{\tau}^T \left(\prod_{t=1}^{k_G} \int_{\widetilde{\mathbf{Q}}_n(t)} \widetilde{\mathbf{Q}}_n(t) f[\widetilde{\mathbf{Q}}_n(t)] d\widetilde{\mathbf{Q}}_n(t) \right) \mathbf{1} = \boldsymbol{\tau}^T \left(\prod_{t=1}^{k_G} \mathcal{E}[\widetilde{\mathbf{Q}}(t)] \right) \mathbf{1} = \boldsymbol{\tau}^T \widehat{\mathbf{Q}}_n^{k_G} \mathbf{1}, \end{aligned} \tag{5.20}$$

where $f[\widetilde{\mathbf{Q}}_n(t)]$ denotes the PDF of the random matrix $\widetilde{\mathbf{Q}}_n(t)$.

Since the transient boundary may be at any state spanning from state A to state N with the probabilities of $\left\{ \Pr_n = \binom{n-1}{A-1} \Big/ \binom{N}{A}, n = A, \cdots, N \right\}$, as shown in Lemma 5.2, according to the Bayesian principle [94], we may obtain the tail distribution of the *group delay* K_G as

$$\begin{aligned} \Pr(K_G > k_G) &= \sum_{n=A}^{N} \Pr(K_n > k_G) \cdot \Pr_n = \sum_{n=A}^{N} \boldsymbol{\tau}^T \widehat{\mathbf{Q}}_n^{k_G} \mathbf{1} \cdot \binom{n-1}{A-1} \Big/ \binom{N}{A} \\ &= \boldsymbol{\tau}^T \left(\sum_{n=A}^{N} \frac{\widehat{\mathbf{Q}}_n^{k_G}}{N} \cdot \binom{n-1}{A-1} \Big/ \binom{N}{A} \right) \mathbf{1}. \end{aligned} \tag{5.21}$$

Furthermore, since K_G is a discrete random variable, its average value may be expressed as $\mathcal{E}[K_G] = \sum_{k_G=0}^{+\infty} \Pr(K_G > k_G)$ [94]. As a result, the average *group delay* can be formulated as

$$\begin{aligned}\mathcal{E}[K_G] &= \sum_{k_G=0}^{+\infty} \Pr(K_G > k_G) = \boldsymbol{\tau}^T \left(\sum_{n=1}^{N} \binom{n-1}{A-1} \Big/ \binom{N}{A} \sum_{k_G=0}^{+\infty} \widehat{\mathbf{Q}}_n^{k_G} \right) \mathbf{1} \\ &= \boldsymbol{\tau}^T \left(\sum_{n=A}^{N} \frac{1}{(\mathbf{I} - \widehat{\mathbf{Q}}_n)} \binom{n-1}{A-1} \Big/ \binom{N}{A} \right) \mathbf{1}, \end{aligned} \tag{5.22}$$

where the last equal relation is derived with the aid of Theorem 4.2 and Theorem 4.4 in Chapter 4.

5.4.4 Other Performance Metrics

5.4.4.1 Individual Delay

In order to characterise the statistical properties of the individual delay K_I, we can simply set the size of the target group $\mathcal{A}$ to $|\mathcal{A}| = A = 1$. Consequently, upon substituting $A = 1$ into Eq.(5.21) and Eq.(5.22), the tail distribution of the individual delay K_I can be expressed as

$$\Pr(K_I > k_I) = \boldsymbol{\tau}^T \left(\sum_{n=1}^{N} \frac{\widehat{\mathbf{Q}}_n^{k_I}}{N} \right) \mathbf{1}, \tag{5.23}$$

while its average value can be derived as

$$\mathcal{E}[K_I] = \boldsymbol{\tau}^T \left(\sum_{n=1}^{N} \frac{(\mathbf{I} - \widehat{\mathbf{Q}}_n)^{-1}}{N} \right) \mathbf{1}. \tag{5.24}$$

5.4.4.2 Dissemination Delay

The statistical properties of the dissemination delay K_D can be obtained by setting the size of the target group $\mathcal{A}$ to $|\mathcal{A}| = A = N$. In this case, we have $\widetilde{\mathbf{Q}}_N(t) = \mathbf{Q}(t)$, which has been defined in Eq.(5.13). When substituting $A = N$ into Eq.(5.21) and Eq.(5.22), the tail distribution as well as the average of the dissemination delay K_D can be expressed as

$$\Pr(K_D > k_D) = \boldsymbol{\tau}^T \overline{\mathbf{Q}}^{k_D} \mathbf{1}, \; \mathcal{E}[K_D] = \boldsymbol{\tau}^T (\mathbf{I} - \overline{\mathbf{Q}})^{-1} \mathbf{1}, \tag{5.25}$$

respectively. In Eq.(5.25), $\overline{\mathbf{Q}}$ is the expectation of $\mathbf{Q}(t)$.

5.4.4.3 BS-Aided Multicast Delay in the First Stage

It can be shown that if the transient boundary is at state $1(B)$, the transition matrix $\widetilde{\mathbf{Q}}_1(t)$ only has a single non-zero entry $p_{1,1}(t) = \prod_{\text{All MUs}} (1 - \mu_{b,j}(t))$, whose expected value is $\overline{p}_{1,1} = (1 - \overline{\mu}_b)^N$. In this case, the group delay K_1 is reduced to the multicast delay K_b that only the BS multicasts during the first stage. Corresponding to Eq.(5.20), the tail distribution of K_b is given by

$$\Pr(K_b > k_b) = (1 - \overline{\mu}_b)^{N k_b}, \tag{5.26}$$

while its average value can be expressed as

$$\mathcal{E}[K_b] = \sum_{k_b=0}^{+\infty} \Pr(K_b > k_b) = 1/[1 - (1 - \overline{\mu}_b)^N]. \tag{5.27}$$

As shown in Eq.(5.27), if N tends to infinity, we have $\lim_{N \to \infty} \mathcal{E}[K_b] = 1$ frame, as expected. This explains that on average only one frame is needed by the first stage of our hybrid information dissemination scheme, when a large number of MUs are supported in the integrated network.

5.4.4.4 BS-Aided-Single-Hop Multicast Delay

For the sake of comparison, we also consider the delay of the conventional BS-aided-single-hop multicast. In this case, the BS repeatedly disseminates the IoCI as a sole transmitter until all the MUs have successfully received it. As a result, given the probability $\mu_{b,i}(t)$ of the i-th MU successfully receiving the IoCI during the t-th frame, the probability $p^{(bm)}_{1+n,1+n+m}(t)$ of traversing from state $(1+n)$ to state $(1+n+m)$ is given by

$$p^{(bm)}_{1+n,1+n+m}(t) = \sum_{\text{All } \mathcal{M}} \prod_{uMU_i \in \mathcal{M}} \mu_{b,i}(t) \prod_{uMU_j \notin \mathcal{M}} (1-\mu_{b,j}(t)), \tag{5.28}$$

for $0 \leq n \leq N$ and $0 \leq m \leq N-n$. After taking the expectation, we obtain

$$\overline{p}^{(bm)}_{1+n,1+n+m} = \binom{N-n}{m} \overline{\mu}_b^m (1-\overline{\mu}_b)^{N-n-m}. \tag{5.29}$$

Based on Eq.(5.29), the expectation of the state transition matrix $\overline{\mathbf{Q}}^{(bm)}$ can be formed. Upon replacing $\overline{\mathbf{Q}}$ in Eq.(5.25) by $\overline{\mathbf{Q}}^{(bm)}$, we obtain both the tail distribution and the average of the BS-aided-single-hop multicast delay $K^{(bm)}$.

5.4.4.5 Energy Analysis

Apart from the various delay metrics, we may also analyse the average energy required for disseminating the IoCI to all the N MUs. According to the above analysis, at state $1(B)$, the energy consumed during a single frame is $P_{b,t}$ since the BS only invokes a single TS for multicasting the IoCI. However, at state $(1+n)$, the energy dissipated during a single frame is $n_0 P_{s,t}$, as n_0 TSs are allocated to the IMs for their multicast. Hence, the energy dissipation of different states during a transmission frame is denoted by the N-elements column vector $\boldsymbol{\mathcal{P}}$, whose first element is $P_{b,t}$ and all the other elements are $n_0 P_{s,t}$.

In order to evaluate the average energy dissipation, the number of frames that the system spends in a specific state $(1+n)$ must be known. Thanks to Theorem 4.3 in Chapter 4, the ij-entry θ_{ij} of the matrix $\boldsymbol{\Theta} = \sum_{k_D=0}^{\infty} \mathbb{Q}(k_D) = \sum_{k_D=0}^{\infty} \prod_{t=1}^{k_D} \mathbf{Q}(t)$ represents the average number of frames that the system spend at state j when the initial state is i, where $\mathbf{Q}(t)$ is given by Eq.(5.13). Since in our hybrid information dissemination scheme the system emerges from state $1(B)$, we only consider the first row of the matrix $\boldsymbol{\Theta}$. Given a series of matrices $\{\mathbb{Q}(k_D) = \prod_{t=1}^{k_D} \mathbf{Q}(t), k_D = 0, 1, \cdots, \infty\}$, the average energy dissipation until the information dissemination is completed is derived as

$$\begin{aligned} \mathcal{E}[E_D | \mathbb{Q}(k_D), k_D = 0, 1, \cdots, \infty] &= \boldsymbol{\tau}^T \boldsymbol{\Theta} \boldsymbol{\mathcal{P}} \\ &= \boldsymbol{\tau}^T \times \sum_{k_D=0}^{\infty} \mathbb{Q}(k_D) \times \boldsymbol{\mathcal{P}}. \end{aligned}$$

According to the Bayesian principle [94], we have

$$\begin{aligned} \mathcal{E}[E_D] &= \boldsymbol{\tau}^T \times \left[\sum_{k_D=0}^{\infty} \int_{\mathbb{Q}(k_D)} \mathbb{Q}(k_D) f(\mathbb{Q}(k_D)) d\mathbb{Q}(k_D) \right] \times \boldsymbol{\mathcal{P}} \\ &= \boldsymbol{\tau}^T \times \sum_{k_D=0}^{\infty} \mathcal{E}[\mathbb{Q}(k_D)] \times \boldsymbol{\mathcal{P}} \\ &= \boldsymbol{\tau}^T \times \sum_{k_D=0}^{\infty} \overline{\mathbf{Q}}^{k_D} \times \boldsymbol{\mathcal{P}} = \boldsymbol{\tau}^T \times (\mathbf{I} - \overline{\mathbf{Q}})^{-1} \times \boldsymbol{\mathcal{P}}, \end{aligned} \tag{5.30}$$

where $f[\mathbb{Q}(k_D)]$ is the PDF of $\mathbb{Q}(k_D)$ and the last equal relation is derived with the aid of Theorem 4.2 and Theorem 4.4 in Chapter 4.

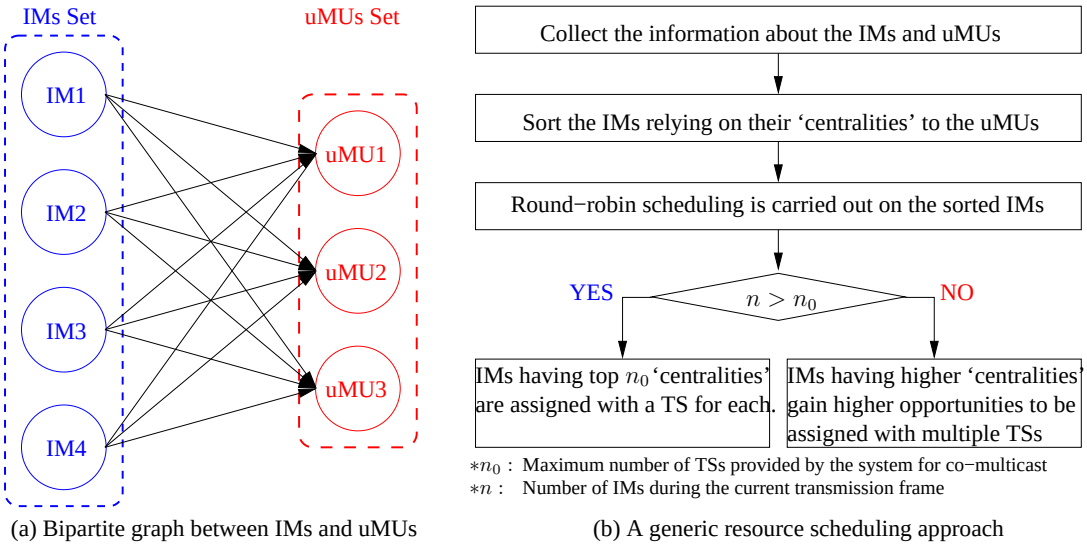

(a) Bipartite graph between IMs and uMUs

(b) A generic resource scheduling approach

Figure 5.5: A biparite graph for characterising the conections between IMs and uMUs during a transmission frame and a flowchart for describing a generic resource scheduling approach.

5.5 Centrality Based Resource Scheduling

Since limited resources are provided for cooperative multicast, we have to choose the best candidates from the set of the IMs for aiding the information dissemination during the current transmission frame. The wireless connections between the IMs and the uMUs can be characterised by a complete bipartite graph, as portrayed in Figure 5.5(a). In this bipartite graph, we have two sets of nodes, namely the set of the IMs and the set of the uMUs. Connections only exist between the nodes belonging to different sets. Each IM has directed connections towards all the uMUs. These connections represent the wireless transmission links between arbitrary IM and uMU pairs. Furthermore, this bipartite graph is a weighted graph. A weight is assigned to a connection for characterising its 'strength'. For instance, in our system, a weight can be represented by the distance between a IM and a uMU pair or the transmission rate of the corresponding wireless link. As a result, different IMs may have different impact on the set of uMUs. In this section, we will provide a number of approaches for evaluating the impact of a IM on the uMUs set, which is inspired by the definition of 'centrality' in social network analysis.

The flowchart of Figure 5.5(b) portrays the procedure of a generic resource scheduling approach. After collecting the relevant information about the IMs and uMUs, we sort the IMs by relying on their 'centralities' with respect to the set of uMUs. Then the round-robin scheduling algorithm is applied to the sorted IMs as presented in Algorithm 5.1. If the size of the IM set is higher than the number n_0 of the total TSs, the IMs having the top n_0 'centralities' can be assigned with a TS for each in order to aid the information dissemination during the current transmission frame. If the size of the IM set is lower than n_0, the IMs having higher centralities may be assigned with more TSs with the aid of Algorithm 5.1.

Note that in the first line of Algorithm 5.1, we randomly sort the IMs during the current transmission frame without considering their different impact on the set of uMUs. This approach may be regarded as *random scheduling*. In the rest of this section, we will propose a range of centrality based resource scheduling approaches in order to optimise the information dissemination performance. However, closed-form performance formulae can only be derived for random scheduling, as elaborated on in Sections 5.3 and 5.4. Unfortunately, the closed-form performance characterisation is intractable for the centrality based resource scheduling approaches.

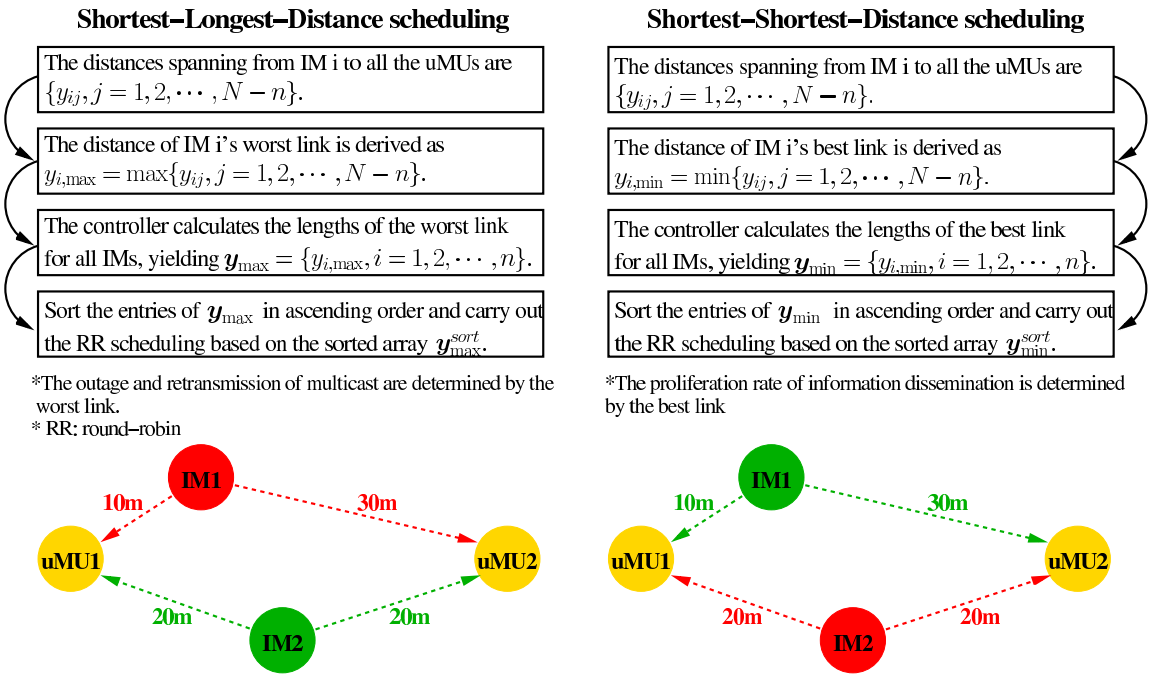

Figure 5.6: The flowcharts and the examples for both the shortest-longest-distance scheduling and the shortest-shortest-distance scheduling. We have n IMs and $(N-n)$ uMUs during the current transmission frame.

5.5.1 Shortest-Longest-Distance Scheduling

As stated in [131], it is plausible that both the outage and the retransmission performance of multicast techniques are dominated by the worst link connecting the target to the source, since the source has to ensure that all of the targets must successfully receive their desired packets with the aid of the multicast technique. During a transmission frame, assuming that we currently have n IMs and $(N-n)$ uMUs, the distances spanning from IM_i to all the uMUs construct an array $\{y_{ij}, j = 1, 2, \cdots, N-n\}$. The worst link of IM_i connects the farthest uMU to IM_i, whose length is expressed as $y_{i,\max} = \max\{y_{ij}, j = 1, 2, \cdots, N-n\}$. At the beginning of the frame, the controller calculates the lengths of the worst link for all the IMs, yielding $\boldsymbol{y}_{\max} = \{y_{i,\max}, i = 1, 2, , \cdots n\}$. Then, it sorts the entries of $\boldsymbol{y}_{\max}$ in ascending order and carries out the round-robin scheduling, as presented in Algorithm 5.1, based on the sorted array $\boldsymbol{y}_{\max}^{sort}$. This scheme is referred to as the shortest-longest-distance scheduling, whose procedure is characterised in the left half of Figure 5.6.

In the example of Figure 5.6, we have two IMs and two uMUs. Given the distances between the IMs and uMUs as shown in Figure 5.6, the length of the IM_1's worst link is $y_{1,\max} = 30$ m, while the length of the IM_2's worst link is $y_{2,\max} = 20$ m. According to the shortest-longest-distance scheduling, we prioritise IM_2 over IM_1. If only a single TS is provided by the system, then it is allocated to IM_2.

5.5.2 Shortest-Shortest-Distance Scheduling

In our information dissemination scheme, the number of IMs increases during the process. Having more potential multicasters may provide more opportunities of successfully delivering the IoCI via cooperative multicast and this significantly reduces the dissemination delay, when all MUs successfully receive the information. Hence, for the sake of reducing the dissemination delay, we have to increase the proliferation rate of IMs. This proliferation rate is dominated by the best links connecting the targets to the sources.

Assuming that we have n IMs and $(N-n)$ uMUs during a specific transmission frame, the distances

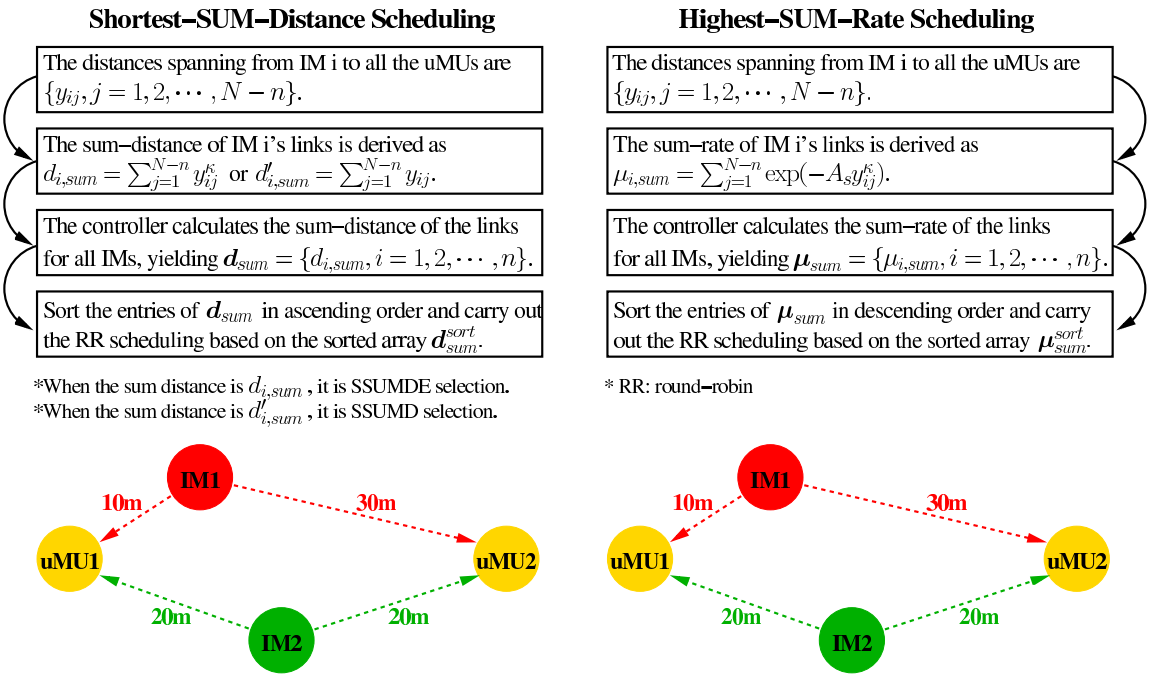

Figure 5.7: The flowcharts and the examples for the shortest-sum-distance and the shortest-sum-distance-exponent as well as the highest-sum-rate schedulings

spanning from IM_i to all the uMUs are collected into an array $\{y_{ij}, j = 1, 2, \cdots, N-n\}$. The best link of IM_i connects the nearest uMU to IM_i, whose length is expressed as $y_{i,\min} = \min\{y_{ij}, j = 1, 2, \cdots, N-n\}$. At the beginning of the transmission frame, the controller calculates the lengths of the best link for all the IMs, yielding $\boldsymbol{y}_{\min} = \{y_{i,\min}, i = 1, 2, , \cdots n\}$. In order to optimally select the IMs, which are likely to result in the highest proliferation rate of the number of IMs, the controller sorts the entries of $\boldsymbol{y}_{\min}$ in ascending order and then carries out the round-robin scheduling, as presented in Algorithm 5.1, based on the sorted array $\boldsymbol{y}_{\min}^{sort}$. This scheme is termed as the shortest-shortest-distance scheduling, whose procedure is characterised in the right half of Figure 5.6.

In the example of Figure 5.6, we have two IMs and two uMUs. Given the distances between the IMs and uMUs as shown in Figure 5.6, the length of the IM_1's best link is $y_{1,\min} = 10$ m, while the length of the IM_2's best link is $y_{2,\min} = 20$ m. According to the shortest-shortest-distance scheduling, we prioritise IM_1 over IM_2. If only a single TS is provided by the system, then it is allocated to IM_1.

5.5.3 Shortest-Sum-Distance Scheduling

Assuming that we have n IMs and $(N-n)$ uMUs during the current transmission frame, given $\{y_{ij}, j = 1, 2, \cdots, N-n\}$, namely all the distances spanning from all the uMUs to IM_i, we define the probability that all the uMUs successfully receive the IoCI, if IM_i has a chance to multicast the IoCI, which is formulated as follows:

$$p_i = \prod_{j=1}^{N-n} \mu_{ij} \approx \prod_{j=1}^{N-n} \exp(-A_s y_{ij}^{\kappa}) = \exp\left(-A_s \sum_{j=1}^{N-n} y_{ij}^{\kappa}\right), \tag{5.31}$$

where μ_{ij} is defined in Eq.(5.8). In a practical scenario of $d_0 = 1$ m and when the radius of the cellular area is $R = 200$ m, the probability of the distance between a pair of roaming MUs being shorter than d_0 is negligible according to the distance CDF derived in Eq.(5.2). Thus, the approximate relationship of Eq.(5.31) holds. Since $\exp(\cdot)$ is a monotonically increasing function, a lower $d_{i,\text{sum}} = \sum_{j=1}^{N-n} y_{ij}^{\kappa}$ leads to a higher p_i and vice versa.

If the PL exponent κ is taken into account by the controller, then at the beginning of a specific transmission frame, the controller calculates $d_{i,\text{sum}}$ for all the IMs, yielding $\boldsymbol{d}_{\text{sum}} = \{d_{i,\text{sum}}, i = 1,2,,\cdots n\}$. In order to optimally select the IMs having the lowest $d_{i,\text{sum}}$, the controller sorts the elements of the array $\boldsymbol{d}_{\text{sum}}$ in ascending order and then carries out the round-robin scheduling, as presented in Algorithm 5.1, based on the sorted array $\boldsymbol{d}^{sort}_{\text{sum}}$. This scheme is referred to as the shortest-sum-distance-exponent scheduling.

If κ is set to one by the controller, instead of $d_{i,\text{sum}} = \sum_{j=1}^{N-n} y_{ij}^{\kappa}$, the controller then calculates $d'_{i,\text{sum}} = \sum_{j=1}^{N-n} y_{ij}$ for all the IMs, yielding $\boldsymbol{d'}_{\text{sum}} = \{d'_{i,\text{sum}}, i = 1,2,,\cdots n\}$. Afterwards, it sorts the elements of the array $\boldsymbol{d'}_{\text{sum}}$ in ascending order and carries out the round-robin scheduling, as presented in Algorithm 5.1, based on the sorted array $\boldsymbol{d'}^{sort}_{\text{sum}}$. This scheme is termed as the shortest-sum-distance scheduling. The procedures of both the shortest-sum-distance-exponent and shortest-sum-distance scheduling are characterised in the left half of Figure 5.7.

In the example of Figure 5.7, we have two IMs and two uMUs. Given the distances between the IMs and uMUs as shown in Figure 5.7, when a PL exponent of $\kappa = 3$ is considered, the sum-product-distance of the IM_1's links is $d_{1,\text{sum}} = (10\text{ m})^3 + (30\text{ m})^3 = 28000\text{ m}^3$, while the sum-product-distance of the IM_2's links is $d_{2,\text{sum}} = (20\text{ m})^3 + (20\text{ m})^3 = 16000\text{ m}^3$. According to the shortest-sum-distance-exponent scheduling, we prioritise IM_2 over IM_1. If only a single TS is provided by the system, then it is allocated to IM_2. Note that the unit 'm^3' is induced by the PL exponent of $\kappa = 3$. However, if we ignore the actual PL exponent, the sum distances of both the IM_1's and IM_2's links are $d'_{1,\text{sum}} = d'_{2,\text{sum}} = 40$ m. According to the shortest-sum-distance scheduling, IM_1 and IM_2 has the same impact on the uMUs. Hence, any of them could be selected for multicasting the IoCI.

5.5.4 Highest-Sum-Rate Scheduling

Assuming that we have n IMs and $(N-n)$ uMUs during the current transmission frame, given $\{y_{ij}, j = 1,2,\cdots,N-n\}$, which is comprised of the distances spanning from all the uMUs to IM_i, we define the sum rate, when IM_i has an opportunity to multicast the IoCI, as follows:

$$\mu_{i,\text{sum}} = \sum_{j=1}^{N-n} \mu_{ij} \approx \sum_{j=1}^{N-n} \exp(-A_s y_{ij}^{\kappa}), \tag{5.32}$$

where μ_{ij} is defined in Eq.(5.8). At the beginning of the transmission frame considered, the controller calculates the above sum rates for all the IMs, yielding $\boldsymbol{\mu}_{\text{sum}} = \{\mu_{i,\text{sum}}, i = 1,2,,\cdots n\}$. In order to optimally select the IMs in the sense of yielding the highest sum rates, the controller sorts the entries of the array $\boldsymbol{\mu}_{\text{sum}}$ in descending order and then carries out the round-robin scheudling, as presented in Algorithm 5.1, based on the sorted array $\boldsymbol{\mu}^{sort}_{\text{sum}}$. This scheme is termed as the highest-sum-rate scheduling. The procedure of the highest-sum-rate scheduling is characterised in the right half of Figure 5.7.

In the example of Figure 5.7, we have two IMs and two uMUs. Given the distances between the IMs and uMUs, as shown in Figure 5.7, the sum rate of the IM_1's links is $\mu_{1,\text{sum}} = 1.89$ packet/TS, while the sum rate of the IM_2's links is $\mu_{2,\text{sum}} = 1.94$ packet/TS. These sum rates are derived relying on the physical layer parameters provided in Table 5.2. According to the highest-sum-rate scheduling, we prioritise IM_2 over IM_1. If only a single TS is provided by the system, then it is allocated to IM_2.

Inspired by social network analysis, in this section, we evaluated the impact of IMs on the uMUs in terms of different centralities, namely using shortest-longest-distance, shortest-shortest-distance, shortest-sum-distance, shortest-sum-distance-exponent and highest-sum-rate regimes. Given the examples in Figures 5.6 and 5.7, we summarise the specific values of different centralities for both the IM_1 and IM_2 in Table 5.1 and provide the required resource scheduling decisions, when IM_1 and IM_2 compete for a single TS.

Table 5.1: Different centralities of IM_1 and IM_2 in the example of Figures 5.6 and 5.7. We also provide the final verdict when IM_1 and IM_2 compete for a single TS. The distances between IM_1 and uMU_1 as well as uMU_2 are 10 m and 30 m, respectively, while the distances between IM_2 and uMU_1 as well as uMU_2 are both 20 m. Specifically, the parameters provided in Table 5.2 are exploited for deriving the HSUMR centralities.

	SLD[1]	SSD[2]	SSUMD[3]	SSUMDE[4]	HSUMR[5]
IM_1	$y_{1,\max} = 30$ m	$y_{1,\min} = 10$ m	$d'_{1,\text{sum}} = 40$ m	$d_{1,\text{sum}} = 28000$ m^3	$\mu_{1,\text{sum}} = 1.89$ packet/TS
IM_2	$y_{2,\max} = 20$ m	$y_{2,\min} = 20$ m	$d'_{2,\text{sum}} = 40$ m	$d_{2,\text{sum}} = 16000$ m^3	$\mu_{2,\text{sum}} = 1.94$ packet/TS
Verdict	IM_2 wins	IM_1 wins	No winners	IM_2 wins	IM_2 wins

[1]SLD: shortest-longest-distance scheduling; [2]SSD: shortest-shortest-distance scheduling; [3]SSUMD: shortest-sum-distance scheduling; [4]SSUMDE: shortest-sum-distance-exponent scheduling; [5]HSUMR: highest-sum-rate scheduling.

Table 5.2: Parameters of the PHY layer

	BS to MUs	MUs to MUs
Transmit Power	$P_{b,t} = 0 \sim 23$ dBm	$P_{t,s} = 0 \sim 20$ dBm
Carrier Freq.	$f_{b,c} = 2$ GHz	$f_{s,c} = 2.4$ GHz
Bandwidth	$W_b = 100$ MHz	$W_s = 10$ MHz
Noise PSD[a]	$N_0 = -174$ dBm/Hz (20^oC)	
SNR Threshold	$\gamma = 10$ dB	
PL Model	$d_0 = 1$ m, $\kappa = 3$	
Studied Area	A circular area having a radius of 200 m	
Mobility Model	Introduced in Section 4.2.4	

[a]PSD: Power Spectrum Density

5.6 Numerical Results

The parameters of the PHY layer are presented in Table 5.2. For the transmissions from the MUs to MUs, the parameters are in line with the 802.11 protocol [53], while for the transmission from the BSs to MUs, the parameters are in line with the Long-Term-Evolution-Advanced (LTE-A) standard [156]. The radius of the cellular system is set to $R = 200$ m and all the N MUs roam in this circular area. The BS is located at the center of the circular area. The classic round-robin scheduling is invoked during the information dissemination process.

The performance metrics of our hybrid information dissemination scheme are evaluated by both the analytical (ana) results as well as by the simulation (sim) results, including the average link throughput during a transmission frame, and various delay metrics as well as the average energy required for disseminating the IoCI. All the delay metrics are quantified in terms of the number of frames, while the energy dissipation is quantified in terms of 'mW*TS'. In order to obtain reliable statistical results, we repeatedly run the Monte-Carlo simulation in MATLAB 10 000 times. The performance of the conventional BS-aided-single-hop multicast is also presented as a benchmarker.

5.6.1 Average Link Throughput During a Transmission Frame

We portray the average link throughput during a transmission frame between a IM and uMU pair associated with different number of TSs allocated to the IM in Figure 5.8. As the transmit power of the IM increases, we observe an increasing trend for the average link throughput. Furthermore, we also observe that the average link throughput during a transmission frame increases, as more TSs are allocated to the IM. The analytical results derived in Eq.(5.12) perfectly match the simulation results.

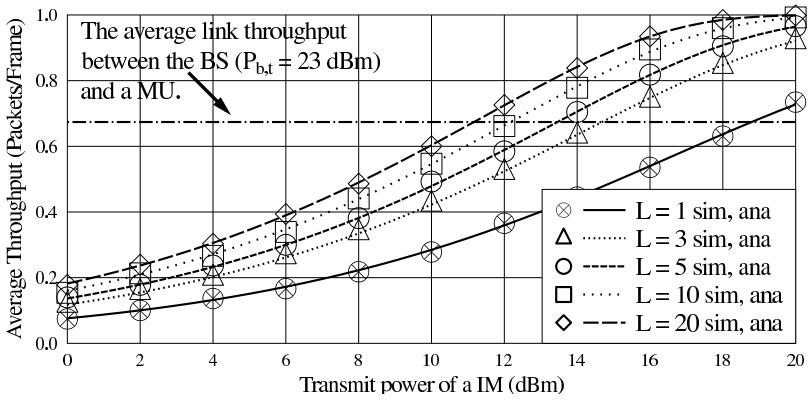

Figure 5.8: The average link throughput during a transmission frame between a IM and uMU pair. The transmit power of the IM varies from 0 dBm to 20 dBm. The number of TSs allocated to the IM for its multicast takes a value from the set $\{1, 3, 5, 10, 20\}$. As a benchmarker, we also portray the average throughput between the BS and a MU when the transmit power of the BS is 23 dBm. All the other parameters are listed in Table 5.2. The analytical results are derived by evaluating Eq.(5.12).

5.6.2 Various Delay Metrics

The average individual delay is depicted in Figure 5.9. The transmit power of the BS is set to $P_{b,t} = 23$ dBm, which is a typical value for picocellular systems, while that of the MUs is $P_{s,t} = 4$ dBm, which is a typical value for 802.11 based transmitters. As shown in Figure 5.9, by invoking the BS-aided-single-hop multicast, the average individual delay of a specific MU receiving the IoCI remains near-constant at about 1.5 frames, as the number N of MUs increases from 1 to 100. The reason for this trend is that the average individual delay in the case of BS-aided-single-hop multicast is only affected by the wireless link connecting the MU to the BS rather than being related to N. If only a single TS is provided for the second stage of the cooperative-multicast-aided spontaneous dissemination, which indicates that only a single IM is scheduled for multicasting the IoCI each frame, the average individual delay firstly increases and then tends to about 3.5 frames as N increases. By contrast, the curves of the average individual delay associated with $n_0 = \{5, 10, 20\}$ firstly increases until reaching their peaks, before they start to decay and tend to constant values. Moreover, if more TSs are provided for the spontaneous dissemination, as reflected by higher values of n_0, the average individual delay may be reduced. Furthermore, compared to the BS-aided-single-hop multicast, our hybrid information dissemination scheme associated with $n_0 = 20$ TSs may reduce the average individual delay by 9% when there are more than 30 MUs.

We then portray the average dissemination delay in Figure 5.10. The transmit power of the MUs is set to $P_{s,t} = 4$ dBm, while that of the BS for the first stage of the information dissemination is varied from 0 dBm to 23 dBm. As the benchmarker, the transmit power of the BS used for the BS-aided-single-hop multicast is set to $P_{b,t} = 23$ dBm. We assume that $n_0 = 20$ TSs are provided for the cooperative-multicast-aided spontaneous dissemination amongst the MUs. As shown in Figure 5.10, the BS-aided-single-hop multicast delay associated with $P_{b,t} = 23$ dBm increases steadily as we increase the number N of the MUs. For our hybrid information dissemination scheme associated with $P_{b,t} = \{12, 23\}$ dBm, the average dissemination delay first increases until reaching its peak, beyond which it decays. However, for the cases of $P_{b,t} = \{0, 6\}$ dBm, the average dissemination delay continuously decreases. Specifically, our hybrid information dissemination scheme associated with the most economical scenario of $P_{b,t} = 0$ dBm, outperforms the BS-aided-single-hop multicast associated with $P_{b,t} = 23$ dBm, when the number of MUs is higher than 50. Furthermore, when $N = 100$, our hybrid information dissemination scheme associated with $P_{b,t} = 23$ dBm may reduce the average dissemination delay by 40.6%, compared to the BS-aided-single-hop multicast.

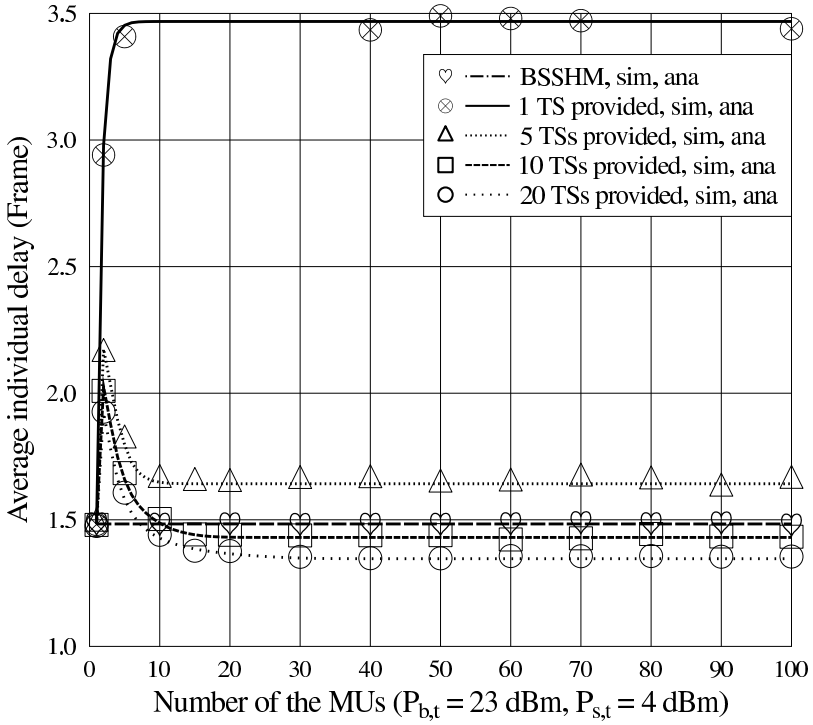

Figure 5.9: Average individual delay versus number of the MUs, which is parameterised by the number of the TSs for the cooperative-multicast-aided spontaneous dissemination. The number of the MUs varies from 1 to 100, while the number n_0 of TSs takes a value from the set $\{1, 5, 10, 20\}$. The transmit power of the BS is $P_{b,t} = 23$ dBm and that of a IM is $P_{s,t} = 4$ dBm. All other parameters are listed in Table 5.2. Random round-robin resource scheduling is invoked, as presented in Algorithm 5.1. The analytical results of our hybrid scheme are derived by Eq.(5.24). The average individual delay of the BS-aided-Single-Hop Multicast (BSSHM) is also evaluated as a benchmarker.

Let us now study the average group delay, as depicted in Figure 5.11. The transmit power of the BS is still set to $P_{b,t} = 23$ dBm, while the transmit power of the MU takes values from the set $\{0, 4, 8, 12, 20\}$ dBm. The maximum number of TSs provided for cooperative multicast is $n_0 = 5$. The total number of MUs is set to $N = 100$, but the size $|\mathcal{A}| = A$ of the target group $\mathcal{A}$ increases from 1 to 100. Observe in Figure 5.11 that the average group delay of all the members in the target group $\mathcal{A}$ receiving the IoCI steadily increases as the group size increases. Moreover, the increased transmit power $P_{s,t}$ of the MUs may significantly reduce the average group delay. According to Figure 5.11, if $P_{s,t}$ is higher than 8 dBm, our hybrid information dissemination scheme may achieve a lower average group delay than the BS-aided-single-hop multicast. Specifically, when $P_{s,t} = 12$ dBm and the group size is $A = 50$, compared to the BS-aided-single-hop multicast, our hybrid information dissemination scheme may reduce the average group delay by 33%. Moreover, the analytical results derived from Eq.(5.22) perfectly match the simulation results.

In order to study the tail distribution of the group delay, the maximum tolerable delay threshold is set to 2 frames, As shown in Figure 5.12, the probabilities of the group delay exceeding 2 frames increases as the size of the target group increases. A higher $P_{s,t}$ leads to a lower 'threshold-violation' probability. Similarly, our hybrid information dissemination scheme associated with $P_{s,t} = 8$ dBm outperforms the conventional BS-aided-single-hop multicast. Furthermore, the analytical results derived from Eq.(5.21) match the simulation results.

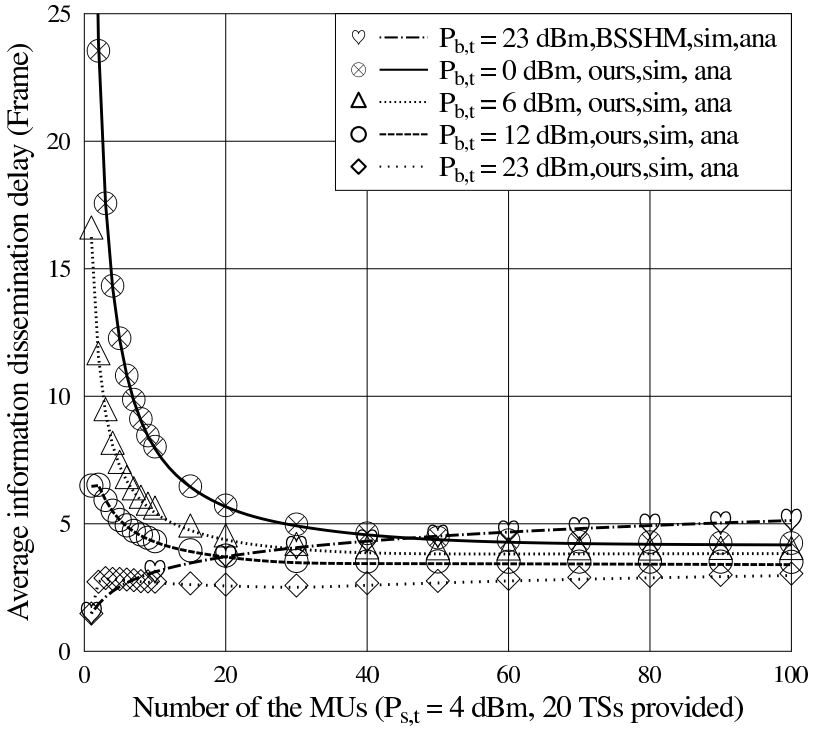

Figure 5.10: Average dissemination delay versus number of the MUs, which is parameterised by the transmit power of the BS. The number of the MUs varies from 1 to 100, while the transmit power $P_{b,t}$ of the BS takes a value from the set $\{0, 6, 12, 23\}$ dBm. The transmit power of IMs is $P_{s,t} = 4$ dBm. The number of TSs provided for cooperative-multicast-aided spontaneous dissemination is $n_0 = 20$. All other parameters are listed in Table 5.2. Random round-robin resource scheduling is invoked, as presented in Algorithm 5.1. The analytical results of our hybrid scheme are derived by Eq.(5.25). The average dissemination delay of BS-aided-Single-Hop Multicast (BSSHM) is also evaluated as a benchmarker.

5.6.3 Average Energy Dissipation

Figure 5.13 portrays the average energy required for disseminating the IoCI to all the MUs, where we have $P_{b,t} = 23$ dBm and $P_{s,t} = 4$ dBm. The average energy dissipation first decays, as we initially increase N, and then it steadily increases, as we further increase N. As presented in Figure 5.13, if we provide more TSs for the cooperative multicast of the IMs, which is represented by a higher n_0 value, more energy is dissipated, but it still remains significantly lower than that of the BS-aided-single-hop multicast benchmarker. For example, when $N = 100$ and $n_0 = 20$ TSs are provided for cooperative multicast, our scheme may reduce the average energy dissipation by about 70%, compared to the BS-aided-single-hop multicast, as evidenced by Figure 5.13.

5.6.4 Comparison Between Different Resource Scheduling Approaches

We first compare the average dissemination delays of the different resource scheduling approaches in Figure 5.14. The number of MUs increases from 1 to 100. The transmit power of the BS is $P_{b,t} = 23$ dBm, while that of a IM is $P_{s,t} = 0$ dBm. The number of TSs is $n_0 = 5$, which is provided for cooperative-multicast-aided spontaneous dissemination. As shown in Figure 5.14, compared to the random scheduling, a significantly improved performance is achieved, when the various centrality based scheduling approaches are chosen. Since the IMs associated with the best links are scheduled for further multicasting the IoCI under the shortest-shortest-distance and highest-sum-rate scheduling approaches, these two regimes both achieve the best performance. Compared to the random scheduling, the shortest-shortest-distance scheduling results in

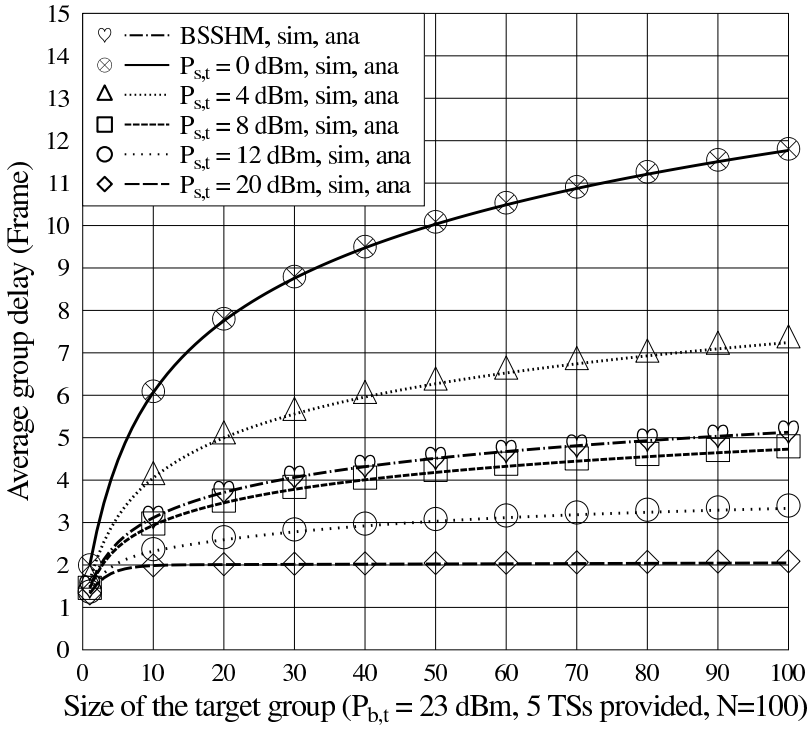

Figure 5.11: Average group delay versus the size of the group studied, which is parameterised by the transmit power of IMs. The size of the group varies from 1 to 100, while the transmit power $P_{s,t}$ of a IM takes a value from the set $\{0, 4, 8, 12, 20\}$ dBm. The transmit power of the BS is $P_{b,t} = 23$ dBm. The number of TSs provided for cooperative-multicast-aided spontaneous dissemination is $n_0 = 5$. The total number of MUs is $N = 100$. All other parameters are listed in Table 5.2. Random round-robin resource scheduling is invoked, as presented in Algorithm 5.1. The analytical results of our hybrid scheme are derived by Eq.(5.22). The average group delay of the BS-aided-Single-Hop Multicast (BSSHM) is also evaluated as a benchmarker.

nearly 50% delay reduction, whilst simultaneously achieving nearly the same delay as the BS-aided-single-hop multicast.

As presented in Figure 5.14, the shortest-sum-distance scheduling outperforms the shortest-sum-distance-exponent regime, because the shortest-sum-distance regime has a higher probability of activating the IMs associated with the best links. Let us consider a simple example, supporting two uMUs with the aid of two IMs. The distances spanning from IM_1 to both the uMUs are $\{1, 90\}$ m, while those from IM_2 to both the uMUs are $\{50, 50\}$ m. According to the shortest-sum-distance-exponent approach, IM_2 has a higher priority to be scheduled, while the shortest-sum-distance approach prefers IM_1. Since IM_1 has the best link, the information may be disseminated more promptly, if IM_1 is scheduled for further multicasting the IoCI. Compared to the shortest-longest distance scheduling, the shortest-sum-distance-exponent scheduling has a higher probability of activating IMs associated with the best link. Let us assume that the distances spanning from IM_1 to both the uMUs are $\{1, 90\}$ m, whilst those from IM_2 to both the uMUs are $\{50, 85\}$ m. Then the shortest-sum-distance-exponent approach awards IM_1 with a higher priority to be scheduled, while the shortest-longest-distance approach prefers IM_2. Hence, as demonstrated in Figure 5.14, the shortest-sum-distance-exponent approach outperforms the shortest-longest-distance scheduling.

We can observe from Figure 5.15 that the shortest-shortest-distance scheduling approach saves the most energy. Compared to the random scheduling, if we have $N = 100$ MUs in total, the average energy dissipation is reduced by 12.3%, when the shortest-shortest-distance scheduling is invoked. Furthermore, compared to the BS-aided-single-hop multicast, the shortest-shortest-distance scheduling approach is capable of reducing the average energy dissipation by 75%.

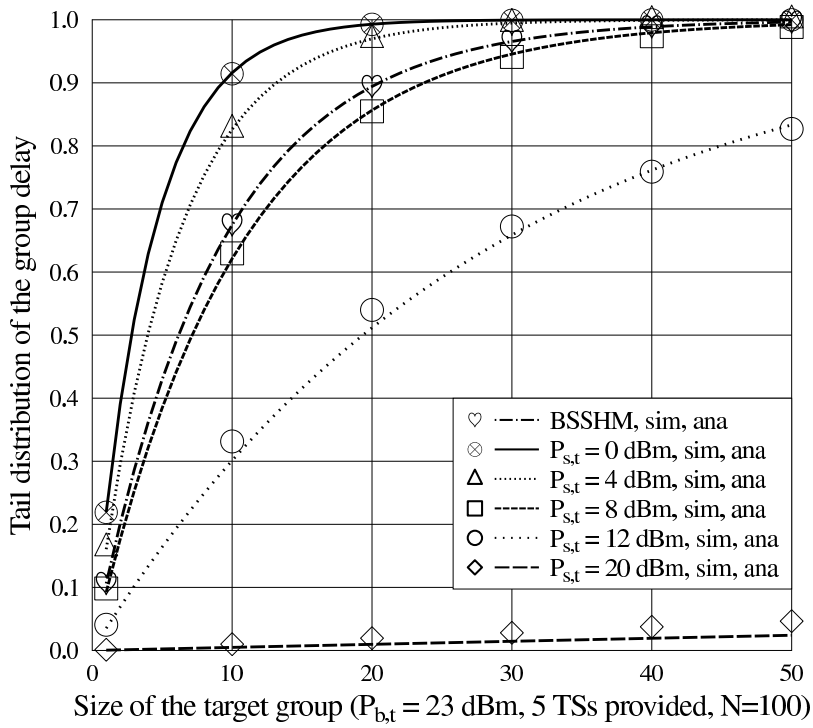

Figure 5.12: Tail distribution of the group delay versus the group size, which is parameterised by the transmit power of IMs. The size of the group varies from 1 to 100, while the transmit power $P_{s,t}$ of IMs takes a value from the set $\{0, 4, 8, 12, 20\}$ dBm. The transmit power of the BS is $P_{b,t} = 23$ dBm. The number of TSs provided for cooperative-multicast-aided spontaneous dissemination is $n_0 = 5$. The total number of MUs is $N = 100$. The delay threshold is 2 frames. All other parameters are listed in Table 5.2. Random round-robin resource scheduling is invoked, as presented in Algorithm 5.1. The analytical results of our hybrid scheme are derived by Eq.(5.21). The tail distribution of the group delay, when the BS-aided-Single-Hop Multicast (BSSHM) is invoked, is also evaluated as a benchmarker.

5.7 Chapter Conclusions

In this chapter, we studied a hybrid information dissemination scheme designed for an integrated cellular and small-scale opportunistic network. The information dissemination process is completed by both the centralised infrastructure based multicast and the distributed information dissemination.

In Section 5.2, we introduced our hybrid information dissemination scheme in the network layer. The information dissemination process was initiated by the BS-aided multicast. If there was at least a single MU successfully receiving the IoCI, the BS-aided multicast was completed and the cooperative multicast amongst the MUs took over the task of disseminating the IoCI across the integrated cellular and opportunistic network. We then provided the detailed description of our hybrid scheme in the MAC layer. In order to avoid the adverse effects of the interferences and collisions, a TDMA approach was invoked in the MAC layer. A round-robin resource scheduling method was implemented for the sake of efficiently exploiting the limited number of TSs during the cooperative-multicast-aided spontaneous dissemination. Finally, both the CDF and the PDF of the random distance between a pair of MUs were characterised, when the positions of the MUs were modelled by a stationary and ergodic process having a stationary uniform distribution in the circular area of Figure 5.3.

In Section 5.3, we assumed that the PL would attenuate the signal if and only if the distance between a pair of transmitter and receiver was higher than a predefined reference distance d_0. The multipath fading was modelled by an uncorrelated Rayleigh distributed signal magnitude. The successful packet reception event

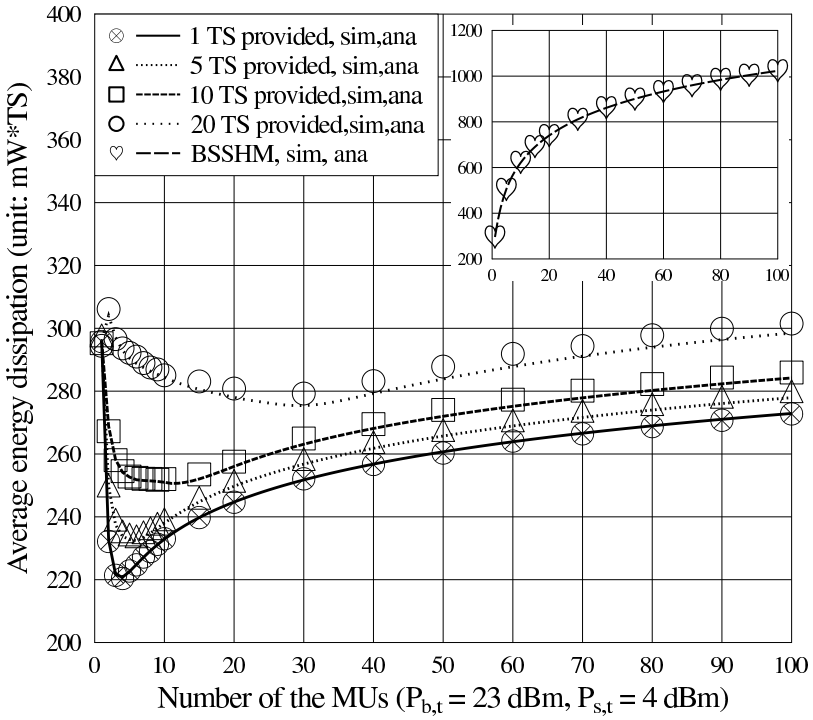

Figure 5.13: The average energy dissipation during exhaustively disseminating the IoCI to all the MUs versus the number of MUs. The transmit power of the BS is $P_{b,t} = 23$ dBm, while the transmit power of IMs is $P_{s,t} = 4$ dBm. The number of the MUs in the area studied varies from 1 to 100, while the number of TSs provided by the TDMA system takes a value from the set $\{1, 5, 10, 20\}$. Other parameters are listed in Table 5.2. Random round-robin resource scheduling is invoked, as presented in Algorithm 5.1. The analytical results of our hybrid scheme are derived by Eq.(5.30). The average total energy dissipation of the BS-aided-Single-Hop Multicast (BSSHM) is also evaluated as a benchmarker.

was defined as the event, when the instantaneous SNR exceeded a predefined threshold. Accordingly, we then derived the closed-form L-moment of the throughput for both the cellular links and opportunistic links during a single TS. When multiple TSs were allocated to a specific opportunistic link during a transmission frame, the average throughput was derived in a closed-form.

In Section 5.4, we modelled the hybrid information dissemination process by a DT-PBMC and focused our attention on characterising the statistical properties of the group delay in closed-form, which was defined as the time duration between the BS multicasting the IoCI and all the members of a specific group successfully receiving it. In order to derive the group delay, all the members of a specific group was deemed to successfully receive the IoCI right after the transient boundary of the DT-PBMC. Then Lemma 5.2 was proposed for characterising the probability of the transient boundary being at a specific state. We also proved that the group delay is a generic metric, which predetermines a range of other delay metrics. If we let the group size to be one, the group delay represented the individual delay of a MU, namely the delay of a specific MU successfully receiving the IoCI, which was initially multicast by the BS. If we let the group size to be equal to the total number of MUs in the area studied, the group delay may be interpreted as the dissemination delay associated with all the MUs in the area successfully receiving the IoCI. Furthermore, other performance metrics were also derived in closed-form, including the BS-aided multicast delay of the first stage, the conventional BS-aided-single-hop multicast delay as well as the average total energy dissipation.

In Section 5.5, we proposed a range of centrality based resource scheduling approaches, including the shortest-longest-distance scheduling, the shortest-shortest-distance scheduling, the shortest-sum-distance and the shortest-sum-distance-exponent scheduling as well as the highest-sum-rate scheduling, so as to further reduce both the dissemination delay and the total energy dissipation. The initial step in these resource

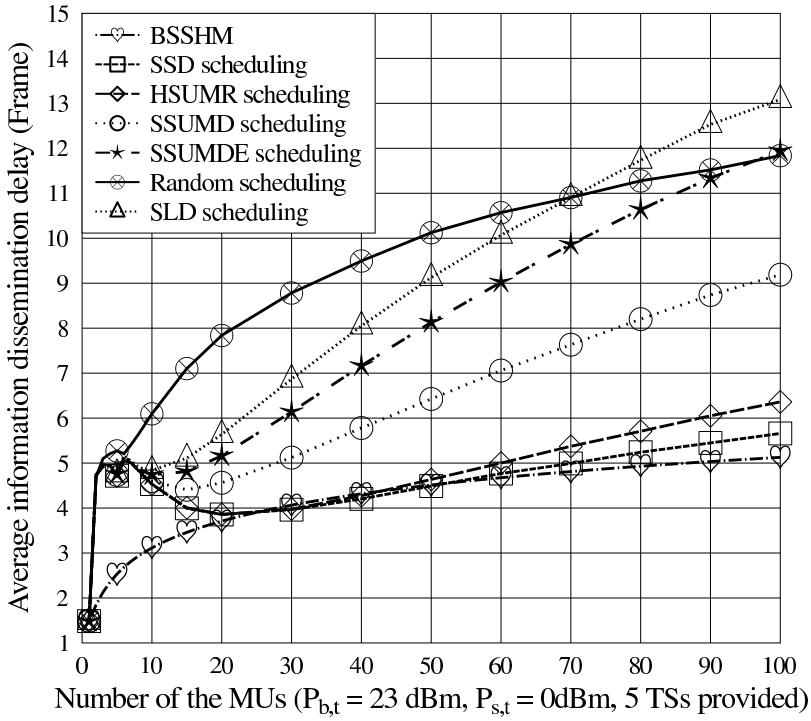

Figure 5.14: Average dissemination delay versus the number of the MUs, when different resource scheduling approaches are implemented. The number of the MUs varies from 1 to 100. The transmit power of the BS is $P_{b,t} = 23$ dBm, while that of IMs is $P_{s,t} = 0$ dBm. The number of TSs provided for cooperative-multicast-aided spontaneous dissemination is $n_0 = 5$. Other parameters are in line with Table 5.2. Six different resource shceduling approaches are considered, as introduced in Section 5.5. The average dissemination delay of BS-aided-Single-Hop Multicast (BSSHM) is also evaluated as a benchmarker. The acronyms in this figure correspond to those in Tables 5.1 and 5.4.

scheduling approaches was to sort the IMs according to their impact on the uMUs during a transmission frame, which was inspired by the centrality concept of social network analysis. As a result, the IMs having a higher impact on the uMUs were capable of gaining higher probability to be scheduled for the cooperative-multicast-aided spontaneous dissemination. Unfortunately, the closed-form delay and energy metrics of these centrality based resource scheduling schemes were intractable.

In Section 5.6, we provided numerical results for characterising the throughput, the various delay metrics and the average total energy dissipation. The following important conclusions may be drawn:

- Increasing the transmit power of IMs substantially increased the average throughput of an opportunistic link, as shown in Figure 5.8. Consequently, it significantly reduced the delay metrics, such as the average group delay and the probability of the group delay exceeding a predefined threshold, as demonstrated in both Figures 5.11 and 5.12.

- Increasing the number of TSs that were assigned to an IM directly increased the probability of this IM successfully multicasting the IoCI, which resulted in an increased average throughput of the corresponding opportunistic link, as shown in Figure 5.8. Furthermore, if we increased the total number of TSs that were provided by the system for the cooperative-multicast-aided spontaneous dissemination, we were capable of reducing the average individual delay, because the IMs secured more opportunities for multicasting the IoCI, as demonstrated in Figure 5.9. However, since the IMs multicast the IoCI more frequently, the total energy dissipation of exhaustively disseminating the IoCI to all the MUs was increased, as depicted in Figure 5.13.

- Increasing the transmit power of the BS during the first stage of BS-aided multicast reduced the average

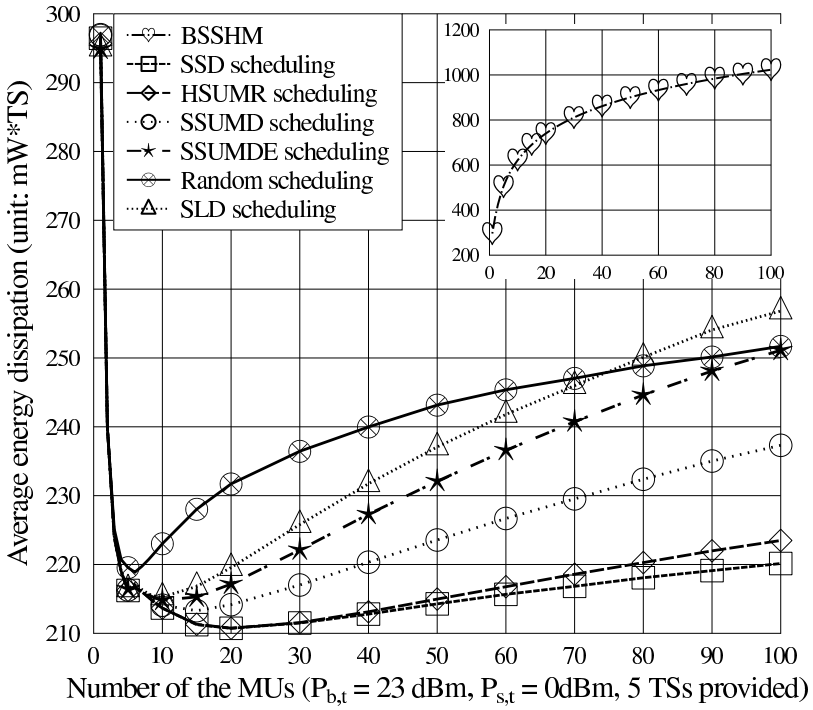

Figure 5.15: Average total energy dissipation versus the number of the MUs, when different resource scheduling approaches are implemented. The number of the MUs varies from 1 to 100. The transmit power of the BS is $P_{b,t} = 23$ dBm, while that of IMs is $P_{s,t} = 0$ dBm. The number of TSs provided for cooperative-multicast-aided spontaneous dissemination is $n_0 = 5$. Other parameters are in line with Table 5.2. Six different resource shceduling approaches are considered, as introduced in Section 5.5. The average total energy dissipation of the BS-aided-Single-Hop Multicast (BSSHM) is also evaluated as a benchmarker. The acronyms in this figure correspond to those in Tables 5.1 and 5.4

dissemination delay of Figure 5.10. Furthermore, we observed from Figure 5.10 that when we had a more active social participation of the MUs, increasing the transmit power of the BS no longer resulted in substantial average dissemination delay reduction.

- Increasing the active social participation of the MUs reduced both the average individual delay of Figure 5.9 and the average dissemination delay of Figure 5.10. Although having more MUs participating in the information dissemination process increased the total traffic demand, the substantial diversity gain achieved by the cooperative multicast amongst more MUs was capable of counteracting the increased traffic demand. Nevertheless, as shown in Figure 5.13, we had to tolerate an increased energy dissipation.

- When the total number of MUs in the area was fixed, the group delay was increased upon increasing the group size, which was observed from Figures 5.11 and 5.12. The reason for this trend was twofold. Firstly, increasing the group size increased the traffic demand generated by the group of the MUs. Secondly, increasing the group size reduced the number of 'helpers', namely the number of MUs not belonging to the group.

- Our hybrid information dissemination scheme outperformed the conventional BS-aided-single-hop multicast scheme in terms of the individual delay, the dissemination delay, the group delay and the energy dissipation. The key quantitative results are summarised in Table 5.3.

- We compared the different resource scheduling schemes in terms of the average dissemination delay and the average energy dissipation. The numerical results, as depicted in both Figures 5.14 and 5.15, demonstrated that the shortest-shortest-distance scheduling performed best amongst its counterparts.

Table 5.3: Quantitative comparison of our hybrid scheme and the BS-aided-Single-Hop Multicast (BSSHM) scheme when $N = 100$ MUs move within the circular area having a radius of $R = 200$ m. The transmit power of the BS is $P_{b,t} = 23$ dBm. For the parameters not mentioned in this table, please refer to the captions of the corresponding figures.

Performance metric	Figure	Number of TSs	TxPower of IMs	Hybrid scheme	BSSHM[1] scheme	Performance reduction/increase of our scheme over the conventional BSSHM
Individual delay	Figure 5.9	10 TSs	4 dBm	1.43 frames	1.48 frames	Our hybrid scheme reduces the average individual delay by 3.4%.
Dissemination delay	Figure 5.10	20 TSs	4 dBm	3.04 frames	5.13 frames	Our hybrid scheme reduces the average dissemination delay by 40.7%.
Group delay ($\|\mathcal{A}\| = 50$)	Figure 5.11	5 TSs	12 dBm	3.08 frames	4.50 frames	Our hybrid scheme reduces the average group delay by 31.6%
Total energy	Figure 5.13	5 TSs	4 dBm	279 mW*TS	1024 mW*TS	Our hybrid scheme reduces the average total energy dissipation by 72.8%

[1] BSSHM: BS-aided-single-hop multicast.

We summarise the salient quantitative results in Table 5.4. For example, we may observe from Table 5.4 that the shortest-shortest-distance scheduling is capable of reducing the average dissemination delay by 56% and reducing the average total energy dissipation by 11.9%, compared to the random scheduling. Furthermore, the shortest-shortest-distance scheduling may achieve the same average dissemination delay as the BS-aided-single-hop multicast scheme, while reducing the energy dissipation by as much as 76.2%.

In our hybrid dissemination scheme, we only invoked BS-aided multicast during the first stage of information dissemination, as depicted in Figure 5.16(a). Once some MUs successfully received the IoCI, the cooperative-multicast-aided spontaneous dissemination amongst the MUs takes over the task of disseminating the IoCI and the BS-aided multicast is no longer enabled, as shown in Figure 5.16(b). However, this hybrid dissemination scheme may not be efficient in the scenario, when the MUs move within a large area. When the IMs cooperatively multicast the IoCI, only their geographic neighbours have high probabilities of successfully receiving the IoCI. As a result, due to the limited mobilities of both the IMs and uMUs, the IMs may become geographically clustered, as shown in Figure 5.16(c). This clustering effect may result in weak wireless links between these IMs and the distant uMUs, which hence become unable to successfully deliver the IoCI. Consequently, the distant uMUs have to wait for a long period, until their distances to the IMs are significantly reduced.

In Section 5.5, several resource scheduling approaches were invented. These approaches were all based on the evaluation of the opportunistic links connecting the IMs and the uMUs. In order to overcome the above-mentioned inefficiency in our hybrid information dissemination scheme, we have to design a hybrid scheduling approach by jointly considering the qualities of the opportunistic links and those of the cellular links connecting the uMUs to the BS. As a result, after the first stage of the BS-aided multicast in our hybrid scheme, the BS can be regarded as a special IM during the second stage of the cooperative-multicast-aided spontaneous dissemination. If the above-mentioned clustering effect appears, the BS can be scheduled for multicasting the IoCI again in order to expedite the information dissemination process, as exemplified in Figure 5.16(d). This concept will be investigated in our future research.

Appendix

Table 5.4: Quantitative comparison of different resource scheduling approaches when $N = 50$ MUs move within the circular area having a radius of $R = 200$ m. The transmit power of the BS is $P_{b,t} = 23$ dBm. The transmit power of IMs is $P_{s,t} = 0$ dBm. The number of TSs provided for cooperative multicast is $n_0 = 5$ TSs. Other parameters are in line with Table 5.2. The quantitative results correspond to Figures 5.14 and 5.15.

Perform. Metric	Hybrid scheme when different resource scheduling approaches are implemented						BSSHM[7] scheme
	SSD[1]	HSUMR[2]	SSUMD[3]	SSUMDE[4]	SLD[5]	Random[6]	
Dissem. delay	4.49 frames	4.64 frames	6.43 frames	8.13 frames	9.13 frames	10.12 frames	4.51 frames
Compared to random	Reduced by 56%	Reduced by 54%	Reduced by 36%	Reduced by 20%	Reduced by 10%	Not applicable	Reduced by 55%
Compared to BSSHM	Almost the same	Increased by 3%	Increased by 43%	Increased by 80%	Increased by 102%	Increased by 124%	Not applicable
Total energy	214.3 mW * TS	215.0 mW * TS	223.6 mW * TS	232.1 mW * TS	237.1 mW * TS	243.2 mW * TS	900.0 mW * TS
Compared to random	Reduced by 11.9%	Reduced by 11.6%	Reduced by 8.1%	Reduced by 4.6%	Reduced by 2.5%	Not applicable	Increased by 270%
Compared to BSSHM	Reduced by 76.2%	Reduced by 76.1%	Reduced by 75.2%	Reduced by 74.2%	Reduced by 73.7%	Reduced by 73.0%	Not applicable

[1]SSD: shortest-shortest-distance scheduling; [2]HSUMR: highest-sum-rate scheduling; [3]SSUMD: shortest-sum-distance scheduling; [4]SSUMDE: shortest-sum-distance-exponent scheduling; [5]SLD: shortest-longest-distance scheduling; [6]Random: random scheduling; [7]BSSHM: BS-aided-single-hop multicast.

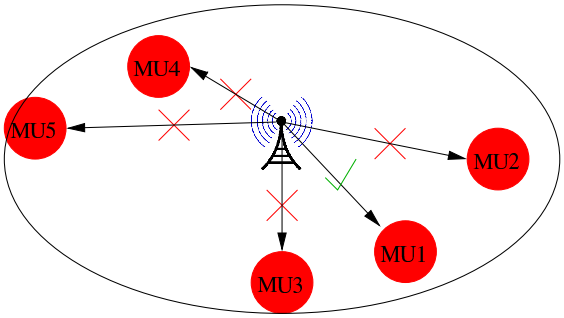

(a) The stage of BS–aided multicast. Only MU1 successfully receives the IoCI from the BS.

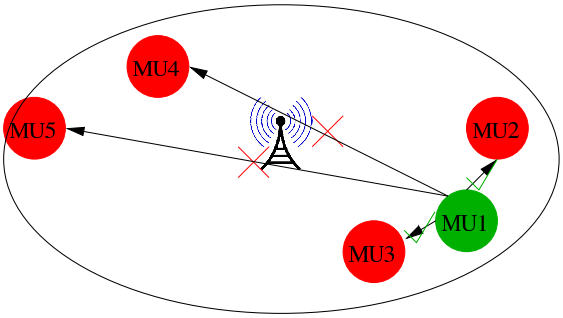

(b) The second stage of cooperative–multicast–aided spontaneous dissemination. MU1 successfully delivers the IoCI towards MU2 and MU3 but fails to deliver it to MU4 and MU5.

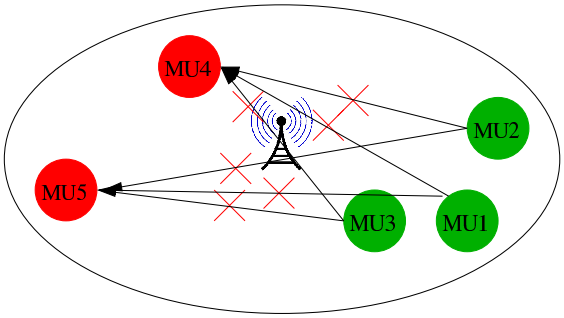

(c) The second stage of cooperative–multicast–aided spontaneous dissemination. Cluster effect appears. MU1, MU2 and MU3 fail to multicast the IoCI to MU4 and MU5.

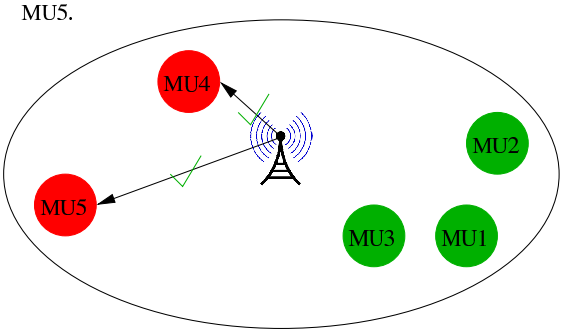

(d) A hybrid scheduling approach. The BS–aided multicast is invoked again in order to overcome the cluster effect if the cellular links to MU4 and MU5 outperform the opportunistic ones.

Figure 5.16: An example to present the cluster effect appearing in our hybrid dissmination scheme and how the hybrid scheduling approach may mitigate the cluster effect.

5.A Proof of Lemma 5.1

5.A.1 Expected State Transition Probability $\overline{p}_{1,1+m}$

Since the first main stage of our hybrid information dissemination scheme is the BS-aided multicast, we first derive the state transition probability $p_{1,1+m}(t)$ during the t-th frame for $0 \leq m \leq N$. A series of successful packet delivery probabilities $\{\mu_{b,i}(t), i = 1, \cdots, N\}$ are provided during the t-th transmission frame, where $\mu_{b,i}(t)$ is the successful packet delivery probability of the link connecting the i-th MU to the BS. Assuming that the group $\mathcal{M}$ of MUs, whose size is $|\mathcal{M}| = m$, successfully receives the IoCI, while the others fail to do so, $p_{1,1+m}(t)$ can be derived as

$$p_{1,1+m}(t) = \sum_{\text{All } \mathcal{M}} \prod_{MU_i \in \mathcal{M}} \mu_{b,i}(t) \prod_{MU_j \notin \mathcal{M}} (1 - \mu_{b,j}(t)), \tag{5.33}$$

for $0 \leq |\mathcal{M}| = m \leq N$, where 'ALL $\mathcal{M}$' represents all the possible combinations for construction of $\mathcal{M}$. Since the geographic positions of the MUs are i.i.d., which also lead to i.i.d. random variables $\{\mu_{b,i}(t), i = 1, \cdots, N\}$, the expected value of $p_{1,1+m}(t)$ is derived as

$$\begin{aligned}\overline{p}_{1,1+m} &= \sum_{\text{All } \mathcal{M}} \prod_{MU_i \in \mathcal{M}} \mathcal{E}[\mu_{b,i}(t)] \prod_{MU_j \notin \mathcal{M}} (1 - \mathcal{E}[\mu_{b,j}(t)]) \\ &= \binom{N}{m} \overline{\mu}_b^m (1 - \overline{\mu}_b)^{N-m},\ 0 \leq m \leq N,\end{aligned} \tag{5.34}$$

where $\overline{\mu}_b$ can be obtained by letting $L = 1$ in Eq.(5.9). The first part of Lemma 5.1 is proved.■

5.A.2 Expected State Transition Probability $\overline{p}_{1+n,1+n+m}$

Let us now derive the state transition probability $p_{1+n,1+n+m}(t)$ during the t-th transmission frame for the stage of cooperative-multicast-aided spontaneous dissemination, where $0 < n \leq N$ and $0 \leq m \leq (N-n)$. In this case, there are n IMs at state $(1+n)$ and hence we have $(N-n)$ uMUs. The IMs are partitioned into two sets $\mathcal{R}_1 = \{IM_{r_1}, 1 \leq r_1 \leq mod(n_0, n)\}$ and $\mathcal{R}_2 \{IM_{r_2}, 1 \leq r_2 \leq (n - mod(n_0, n))\}$ according to the number of TDMA TSs that are allocated to them after the round-robin scheduling. As introduced in Section 4.2.3, each IM of $\mathcal{R}_1$ is allocated $\lceil n_0/n \rceil$ TDMA TSs, while each IM of $\mathcal{R}_2$ is allocated $\lfloor n_0/n \rfloor$ TDMA TSs. The set of uMUs at state $(1+n)$ is denoted as $\mathcal{M} = \{uMU_i | 1 \leq i \leq (N-n)\}$.

Let us consider a single uMU denoted as uMU_i. The successful packet delivery probabilities from the IMs in $\mathcal{R}_1$ to uMU_i are denoted as $\boldsymbol{\lambda}_{\mathcal{R}_1,i} = \left\{\lambda_{r_1,i}\left(t, \lceil \frac{n_0}{n} \rceil\right), 1 \leq r_1 \leq mod(n_0, n)\right\}$, while those from the IMs in $\mathcal{R}_2$ to uMU_i are denoted as $\boldsymbol{\lambda}_{\mathcal{R}_2,i} = \left\{\lambda_{r_2,i}\left(t, \lfloor \frac{n_0}{n} \rfloor\right), 1 \leq r_2 \leq mod(n_0, n)\right\}$. Since the positions of different IMs are i.i.d. random variables, all the elements in both $\boldsymbol{\lambda}_{\mathcal{R}_1,i}$ and $\boldsymbol{\lambda}_{\mathcal{R}_2,i}$ are independent of each other. As a result, as long as at least one IM from $\mathcal{R}_1$ or $\mathcal{R}_2$ successfully delivers the packet to uMU_i, the packet can be successfully received. Therefore, the successful packet reception probability $p_i(t)$ of uMU_i is derived as

$$p_i(t) = 1 - \prod_{IM_{r_1} \in \mathcal{R}_1} \left[1 - \lambda_{r_1,i}\left(t, \lceil \frac{n_0}{n} \rceil\right)\right] \prod_{IM_{r_2} \in \mathcal{R}_2} \left[1 - \lambda_{r_2,i}\left(t, \lfloor \frac{n_0}{n} \rfloor\right)\right]. \tag{5.35}$$

The expectation of $p_i(t)$ is derived as

$$\begin{aligned}\overline{p}_i &= 1 - \prod_{IM_{r_1} \in \mathcal{R}_1} \left\{1 - \mathcal{E}\left[\lambda_{r_1,i}\left(t, \lceil \frac{n_0}{n} \rceil\right)\right]\right\} \\ &\quad \cdot \prod_{IM_{r_2} \in \mathcal{R}_2} \left\{1 - \mathcal{E}\left[\lambda_{r_2,i}\left(t, \lfloor \frac{n_0}{n} \rfloor\right)\right]\right\} \\ &= 1 - \left[1 - \overline{\lambda}_s\left(\lceil \frac{n_0}{n} \rceil\right)\right]^{mod(n_0,n)} \cdot \left[1 - \overline{\lambda}_s\left(\lfloor \frac{n_0}{n} \rfloor\right)\right]^{n - mod(n_0,n)}.\end{aligned} \tag{5.36}$$

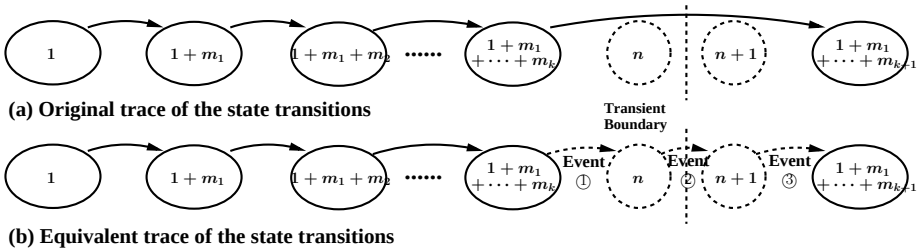

Figure 5.17: A possible trace of the state transitions

Furthermore, we assume that a set $\mathcal{M}$ of uMUs, whose size is $|\mathcal{M}| = m$, successfully receive the IoCI during the t-th frame, while the rest of uMUs fail to do so. As a result, the state transition probability $p_{1+n,1+n+m}(t)$ can be expressed as

$$p_{1+n,1+n+m}(t) = \sum_{\text{All } \mathcal{M}} \prod_{uMU_i \in \mathcal{M}} p_i(t) \prod_{uMU_j \notin \mathcal{M}} (1 - p_j(t)). \tag{5.37}$$

Since the positions of different uMUs are i.i.d. random variables, $\{p_i(t), uMU_i \in \mathcal{M}\}$ are i.i.d. random variables as well. Hence, the expectation of $p_{1+n,1+n+m}(t)$ is derived as

$$\overline{p}_{1+n,1+n+m} = \binom{N-n}{m} \overline{p}_i^m (1 - \overline{p}_i)^{N-n-m}, \tag{5.38}$$

where $\overline{p}_i$ is given by Eq.(5.36). The second part of Lemma 5.1 is proved. ■

5.B Proof of Lemma 5.2

Assuming that the *transient boundary* is at state n, we portray in Fig.5.17(a) a sample trace of the state transitions emerging from the initial state 1 to state $(1 + m_1 + \cdots + m_{k+1})$, which is the first state after crossing the *transient boundary* n. Naturally, when state n is the *transient boundary*, according to the above assumption, we have $(1 + \sum_{i=1}^{k} m_i) \leq n$ and $(1 + \sum_{i=1}^{k+1} m_i) \geq (n+1)$. Let us denote the set of the uMUs whose members have successfully received the IoCI during the i-th frame as $\mathcal{M}_i$, with its cardinality $|\mathcal{M}_i| = m_i$, where $1 \leq i \leq (k+1)$. Let us denote the MUs simultaneously belonging to $\mathcal{M}_i$ and to the target group $\mathcal{A}$ as the set $\mathcal{A}_i$ with a cardinality of $|\mathcal{A}_i|$. As shown in Figure 5.17(a), since all the members of the target group $\mathcal{A}$ have successfully received the IoCI until the $(k+1)$-th frame, we have $\mathcal{A} = \bigcup_{i=1}^{k+1} \mathcal{A}_i$, and $\{\mathcal{A}_i \bigcap \mathcal{A}_j = \phi | i \neq j\}$. Note that the cardinality $|\mathcal{A}_i|$ of the group $\mathcal{A}_i$ is a random integer assuming a value in $[0, m_i]$ subject to the constraint of $\sum_{i=1}^{k+1} |\mathcal{A}_i| = A$. As a specific case during the i-th frame, we have $|\mathcal{A}_i| = a_i$, where a_i is a possible sample for the random integer $|\mathcal{A}_i|$ and $a_i \in [0, m_i]$. As a result, a vector, which reflects the number of newly served MUs belonging to the target group $\mathcal{A}$ from the first frame to the $(k+1)$-th frame, is constructed as $\boldsymbol{a} = (a_1, a_2, \cdots, a_{k+1})^T$, subject to the constraints of $\sum_{i=1}^{k+1} a_i = A$.

Based on the above discussions, we know that before the transition from state $(1 + m_1 + \cdots + m_{i-1})$ to state $(1 + m_1 \cdots + m_i)$, we have $(N - m_1 - \cdots - m_{i-1})$ uMUs, amongst which $(A - a_1 - \cdots - a_{i-1})$ uMUs belong to the group $\mathcal{A}$. After the state transition, $|\mathcal{M}_i| = m_i$ uMUs have successfully received the information, amongst which $|\mathcal{A}_i| = a_i$ uMUs belong to the target group $\mathcal{A}$. Hence, the joint event of $(\mathcal{A}_i \subseteq \mathcal{M}_i, \boldsymbol{a})$ occurs during the i-th frame with the probability, which is expressed as

$$\Pr(\mathcal{A}_i \subseteq \mathcal{M}_i, \boldsymbol{a}) = \frac{\binom{A - a_1 - \cdots - a_{i-1}}{a_i} \binom{N - m_1 - \cdots - m_{i-1} - A + a_1 + \cdots + a_{i-1}}{m_i - a_i}}{\binom{N - m_1 - \cdots - m_{i-1}}{m_i}}. \tag{5.39}$$

As a result, the probability that, after the k-th frame, $(m_1 + m_2 + \cdots + m_k)$ uMUs have successfully received the IoCI, amongst which $(a_1 + a_2 + \cdots + a_k)$ uMUs belong to the target group $\mathcal{A}$, can be expressed

as

$$\begin{aligned}\Pr\left(\bigcap_{i=1}^{k}\left(\mathcal{A}_i \subseteq \mathcal{M}_i\right), \boldsymbol{a}\right) &= \prod_{i=1}^{k}\Pr\left(\mathcal{A}_i \subseteq \mathcal{M}_i, \boldsymbol{a}\right) \\ &= \frac{A!(N-A)!}{N!}\cdot\prod_{i=1}^{k}\frac{m_i!}{a_i!(m_i-a_i)!} \\ &\quad\cdot\frac{(N-m_1-\cdots-m_k)!}{(A-a_1-\cdots-a_k)!(N-m_1-\cdots-m_k-A+a_1+\cdots+a_k)!}.\end{aligned} \tag{5.40}$$

As shown in Figure 5.17(b), given that the transient boundary is state n, the last state transition traversing from state $(1+\sum_{i=1}^{k} m_i)$ to state $(1+\sum_{i=1}^{k+1} m_i)$, can be decomposed into three consecutive *virtual events* as follows.

Event ①: Firstly, let us consider the virtual transition traversing from state $(1+\sum_{i=1}^{k} m_i)$ to state n. Before this state transition, there are $(N-m_1-\cdots-m_k)$ uMUs, which include $(A-a_1-\cdots-a_k)$ uMUs belonging to the target group $\mathcal{A}$. After the state transition, a set $\mathcal{M}_{k+1}^{(1)}$ of uMUs satisfying $|\mathcal{M}_{k+1}^{(1)}| = m_{k+1}^{(1)} = n-1-\sum_{i=1}^{k} m_i$ have successfully received the IoCI. Here $\mathcal{M}_{k+1}^{(1)}$ includes a set $\mathcal{A}_{i+1}^{(1)}$ of uMUs belonging to $\mathcal{A}$, and we have $|\mathcal{A}_{i+1}^{(1)}| = a_{i+1}^{(1)} = a_{k+1}-1 = A-1-\sum_{i=1}^{k} a_i$. In other words, after this transition, there is only a single uMU in $\mathcal{A}$ who has not received the information. The probability of the above event occurring is derived as

$$\begin{aligned}\Pr\left(\mathcal{A}_{i+1}^{(1)} \subseteq \mathcal{M}_{i+1}^{(1)}, \boldsymbol{a}\right) &= \frac{\binom{A-a_1-\cdots-a_k}{a_{k+1}^{(1)}}\binom{N-m_1-\cdots-m_k-A+a_1+\cdots+a_k}{m_{k+1}^{(1)}-a_{k+1}^{(1)}}}{\binom{N-m_1-\cdots-m_k}{m_{k+1}^{(1)}}} \\ &= \frac{m_{k+1}^{(1)}!\cdot(A-a_1-\cdots-a_k)!}{(m_{k+1}^{(1)}-a_{k+1}^{(1)})!\cdot a_{k+1}^{(1)}!}\frac{(N-m_1-\cdots-m_k-A+a_1+\cdots+a_k)!}{(N-m_1-\cdots-m_k)!/(N-n+1)}.\end{aligned} \tag{5.41}$$

Event ②: Secondly, let us consider the virtual transition traversing from state n to state $(1+n)$. After Event ①, there are $(N-n+1)$ uMUs, which include a single uMU belonging to the target group $\mathcal{A}$. After the state transition, a set $\mathcal{M}_{k+1}^{(2)}$ of uMUs with $\left|\mathcal{M}_{k+1}^{(2)}\right| = m_{k+1}^{(2)} = 1$ have successfully received the IoCI. Explicitly, we have $|\mathcal{M}_{k+1}^{(2)}| = m_{k+1}^{(2)} = |\mathcal{A}_{i+1}^{(2)}| = a_{i+1}^{(2)} = 1$. As a result, the probability of this event is

$$\Pr\left(\mathcal{A}_{i+1}^{(2)} \subseteq \mathcal{M}_{i+1}^{(2)}, \boldsymbol{a}\right) = \frac{1}{N-n+1}. \tag{5.42}$$

Event ③: Finally, let us consider the virtual transition traversing from state $(1+n)$ to state $(1+\sum_{i=1}^{k+1} m_i)$. After Event ① and ②, among the remaining $(N-n)$ uMUs, a set $\mathcal{M}_{k+1}^{(3)}$ of uMUs satisfying $\left|\mathcal{M}_{k+1}^{(3)}\right| = m_{k+1}^{(3)} = m_{k+1}-m_{k+1}^{(1)}-m_{k+1}^{(2)}$ have successfully received the IoCI during this virtual state transition. Note that in $\mathcal{M}_{k+1}^{(3)}$, there are no uMUs belonging to the target group $\mathcal{A}$, since all the MUs in the target set $\mathcal{A}$ received the IoCI after Event ① and ②. Consequently, the probability that Event ③ occurs is given by

$$P\left(\mathcal{A}\bigcap\mathcal{M}_{k+1}^{(3)} = \phi, \boldsymbol{a}\right) = 1. \tag{5.43}$$

In summary of the above three virtual events of ①, ② and ③, when $\boldsymbol{a}$ is assumed, the joint probability

that the *transient boundary* is located at state n can be expressed as

$$\begin{aligned}
&\Pr(\text{State } n \text{ is the transient boundary}, \boldsymbol{a}) \\
&= \underbrace{\Pr\left(\bigcap_{i=1}^{k} (\mathcal{A}_i \subseteq \mathcal{M}_i), \boldsymbol{a}\right)}_{\text{Eq. (5.40)}} \cdot \underbrace{\Pr\left(\mathcal{A}_{i+1}^{(1)} \subseteq \mathcal{M}_{i+1}^{(1)}, \boldsymbol{a}\right)}_{\text{Eq.(5.41)}} \cdot \underbrace{\Pr\left(\mathcal{A}_{i+1}^{(2)} \subseteq \mathcal{M}_{i+1}^{(2)}, \boldsymbol{a}\right)}_{\text{Eq.(5.42)}} \cdot \underbrace{\Pr\left(\mathcal{A} \bigcap \mathcal{M}_{k+1}^{(3)} = \phi, \boldsymbol{a}\right)}_{\text{Eq.(5.43)}} \\
&= \binom{m_1}{a_1} \cdot \binom{m_2}{a_2} \cdot \cdots \cdot \binom{m_k}{a_k} \binom{m_{k+1}^{(1)}}{a_{k+1}^{(1)}} \Big/ \binom{N}{A}. \qquad (5.44)
\end{aligned}$$

Finally, upon summing up Eq.(5.44) over all possible combinations for the elements in $\boldsymbol{a}$, we obtain the probability $\Pr_n$ that the transient boundary is located at state n, which is given by

$$\begin{aligned}
\Pr_n &= \sum_{\text{All } \boldsymbol{a}} \Pr(\text{State } n \text{ is the transient boundary}, \boldsymbol{a}) \qquad (5.45) \\
&= \sum_{\text{All } \boldsymbol{a}} \binom{m_1}{a_1} \cdot \binom{m_2}{a_2} \cdot \cdots \cdot \binom{m_k}{a_k} \binom{m_{k+1}^{(1)}}{a_{k+1}^{(1)}} \Big/ \binom{N}{A} = \binom{n-1}{A-1} \Big/ \binom{N}{A},
\end{aligned}$$

for $A \le n \le N$. Note that since $m_{k+1}^{(1)} + \sum_{i=1}^{k} m_i = n-1$ and, for all $1 \le i \le k$, the entries of $\boldsymbol{a}$ are subject to $0 \le a_i \le m_i$ as well as $0 \le a_{k+1}^{(1)} \le m_{k+1}^{(1)}$, while $a_{k+1}^{(1)} + \sum_{i=1}^{k} a_k = A-1$, the combinatorial problem described by the numerator of the second line of Eq.(5.45) is equivalent to that of selecting $(A-1)$ MUs out of the total $(n-1)$ ones. As a result, the third equality of Eq.(5.45) holds, and Lemma 5.2 is proved. According to Eq.(5.45), we can see that $\Pr_n$ is not related to any specific value of $\{m_i, i = 1, 2, \cdots, k+1\}$ and $\{a_i, i = 1, 2, \cdots, k+1\}$. ■

Chapter 6

Stochastic Geometry in Cellular Networks

6.1 Introduction

6.1.1 Background and Related Works

At the time of writing, the global communication community pays much attention to the efficient network-level design of cellular systems. In order to convey the escalating tele-traffic, the concept of heterogeneous networks [157] relying on diverse cell-size and standards emerged as one of the key techniques, paving the way for the evolution of cellular 5G systems [158]. More explicitly, heterogeneous networks consist of different sizes of cells, which include macro-cells providing large coverage in rural areas, and pico-cells in urban areas, as well as the femto-cells supporting communications in homes and offices. Furthermore, apart from cellular communications, other communications techniques, which are operated on the unlicensed frequency bands, such as the IEEE 802.11 protocol [159] aided Wi-Fi hotspots, can also be incorporated into the landscape of heterogeneous networks.

There are two key issues attracting substantial attention from both the academic and industrial communities. The first one is related to the user association issues [160] [161], since a user may simultaneously appear within the radio coverage of many Base Stations (BSs). However, the qualities of the channels connecting the user to these BSs are different from each other. Since some BSs might deny access for the user due to tele-traffic congestions, the network operator should jointly schedule the communications of all these BSs, for example under the control of the Mobile Switching Centre (MSC), analyse the qualities of the channels and finally make an optimal decision on which BS the user should be connected to, so as to optimise the attainable communication performance. The second substantial problem is related to the tele-traffic offloading issues [162] [163]. In order to reduce the maintenance costs and increase the profits, network operators might encourage their subscribers to give a higher user association priority to the low-cost IEEE 802.11 networks supported by numerous Wi-Fi hotspots. By exploiting the Wi-Fi hotspots, network operators become capable of offloading a large fraction of the tele-traffic from the congested cellular networks to the IEEE 802.11 networks, which may further improve their profits, while accommodating more tele-traffic.

However, both the user association and the tele-traffic offloading issues are dominated by the geometrical positions of users. When the Path-Loss (PL) is the dominant factor that determines the channel, the specific BS or Wi-Fi hotspot closest to the user, has to be tasked by fulfilling the communications demand of the user. When the stochastic fading factors, such as shadowing and multipath fading are also taken into account, the

closest BS is still more likely to be relied upon than its counterparts. As a result, stochastic geometry has been widely investigated in the context of heterogeneous networks. A popular mathematical abstraction of modelling the geometric positions of the users around a BS is constituted by a Poisson-Point-Process (PPP) [164]. The PPP is characterised by the following properties:

- The number of isolated points falling within the regions A and B are independent random variables, provided that A and B do not intersect each other.
- The expected number of isolated points falling within a region A is an important measure of the region A. This 'measure' is often proportional to the area or volume of A, but some times more elaborate measures have to be used. This measure has to be defined in such a way that the resultant measure of the union of regions that do not intersect each other is simply the sum of their individual measures.

As a result, the probability of the number X of isolated nodes falling into region A is modelled by a Poisson distribution, which is expressed as

$$\Pr(X = x) = \frac{(\mu S_A)^x \mathrm{e}^{-\mu S_A}}{x!}. \tag{6.1}$$

Here, if A is regarded as a two-dimensional region, S_A in Eq.(6.1) is the area of the region A and μ is the density of the points. In the research of heterogeneous networks, the region A is often modelled as a circular area, whose centre is a transmitter (e.g. BS or Wi-Fi hotspot) and whose radius is the transmission range of this transmitter. The number of receivers (e.g. mobile users) in this circular area is modelled by the PPP, while their positions are modelled by the *independent uniform distribution* in the circular area studied. As a result, the statistical properties of the random distance between the BS, which is at the centre of the circular area, and the Mobile User (MU), which roams within the circular area, are exploited for evaluating the downlink transmission performance at the receiver end [165] [166]. Similarly, this model may also be used for quantifying the uplink interference imposed on the transmitter end by these receivers [167] [168]. However, this common assumption in the current research ignores some other realistic scenarios. For example, the movement of MUs does not cover the entire coverage area of the BS. Realistically, their movements are always bounded by a specific region, such as an office or a building, and the BS can be at any arbitrary position either within or beyond these bounded areas. Hence, it is vital for us to study the distance variation between the BS and the MU in these scenarios.

Apart from the specific family of heterogeneous networks, which are based on the Centralised Infrastructure (CI), direct communication amongst the MUs can also be exploited in order to further improve both the quality and the reliability of communication services. Direct communication amongst the MUs can be realised by relying on the distributed IEEE 802.11 radio ports [169], the Bluetooth technique [170] and the LTE-aided device-to-device technique [171]. With the aid of direct communication amongst the MUs, the distance between the transmitter and the receiver is significantly shortened, which remarkably reduces the adverse channel attenuation incurred by the PL. Direct communication amongst the MUs are also capable of offloading the tele-traffic from the congested CI. In order to accurately analyse direct communication amongst the MUs, it is crucial for us to study the distance variation between a pair of MUs, both of which move within a bounded area.

6.1.2 Novel Contributions and Chapter Organisation

In line with the well-known PPP model, the movement of MUs is characterised by the following uniform mobility model in this chapter:

Definition 6.1 (Uniform mobility model)**.** *The position of the i-th MU during the t-th time interval is denoted by $\mathbf{P}_i(t)$, which obeys a stationary and ergodic process with a stationary uniform distribution in a bounded area. Moreover, the positions of different MUs are independently and identically distributed (i.i.d.).*

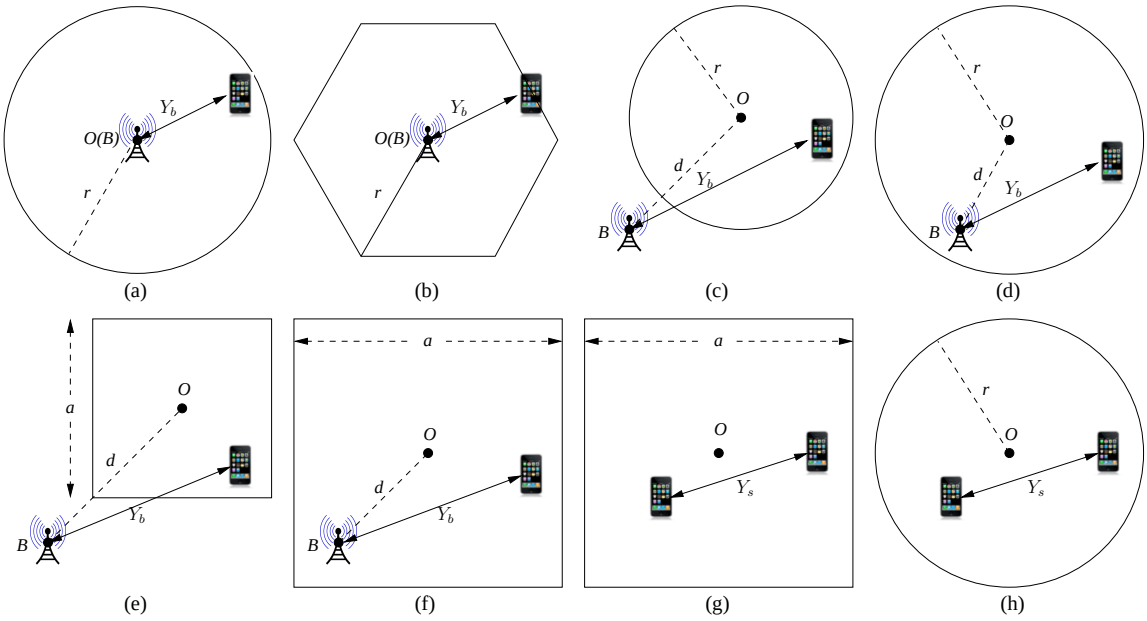

Figure 6.1: Different scenarios for studying the distance distribution between the BS and the MU characterised in subfigures (a) to (f) and that between a pair of MUs in subfigures (g) to (h). Specifically, the BS is either at the centre of a circular cell (a) or of an l-sided regular polygonal cell (b), while the MU roams within the entire cell. We also consider the scenario that the BS is arbitrarily located at any position, either outside a circular/square area (c)/(e) or inside a circular/square area (d)/(f), while the MU roams within the corresponding bounded area. We also study the distance distribution between a pair of MUs, when they roam either within a square area (g) or within a circular area (f).

This mobility model has been widely used for analysing the relevant performance metrics in mobile *ad hoc* networks [172] [173].

The main contributions and the structure of this chapter are summarised as follows:

- In Section 6.2, we will characterise the distance distribution between the BS and the MU, when the BS is at the centre of a circular cell, while the MU roams within the entire circular cell by obeying the uniform mobility model, as shown in Figure 6.1(a). Furthermore, we will also provide the Cumulative Distribution Function (CDF) and the Probability Density Function (PDF) in closed-form for the random distance between the BS and the MU, when the cell is modelled by a l-sided regular polygon, as portrayed in Figure 6.1(b).
- In Section 6.3, we will obtain the CDFs and the PDFs of the random distance between the BS and the MU in closed-form, when the BS is at an arbitrary position, either inside or outside a bounded area, while the MU roams within the bounded area by obeying the uniform mobility model. The bounded area is modelled as either a circular or a square area, as shown in Figures 6.1(c)-(f)
- In Section 6.4, we will analyse both the CDFs and the PDFs of the random distance between a pair of MUs, both of which roam within either a square or a circular area, as portrayed in Figures 6.1(g)(h).
- In Section 6.6, numerical results are provided for validating the accuracy of our theoretical analysis.
- Finally, we conclude in Section 6.7.

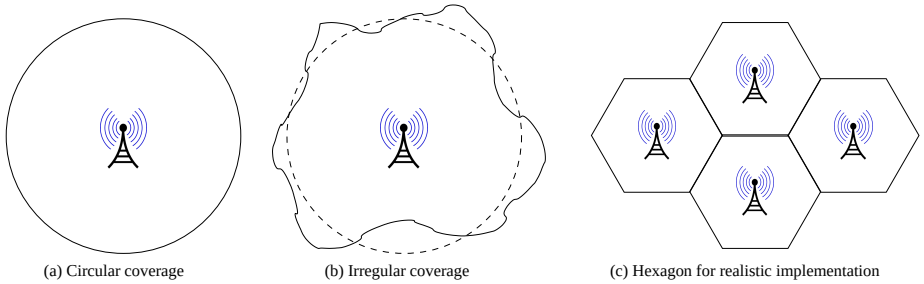

(a) Circular coverage (b) Irregular coverage (c) Hexagon for realistic implementation

Figure 6.2: Various shapes of coverage area of a cell

6.2 Distance Distribution between the BS and MUs Roaming in a Cell

In this scenario, a BS is assumed to be located at the centre of a cell, while the MUs associated with this BS may appear at any arbitrary location of this specific cell with equal probability, as shown in Figures 6.1(a)(b). This distance distribution between the BS and the MU heavily depends on the particular shape of the cellular area. In theory, apart from the maximum affordable transmit power of the BS, both the size and the shape of the cellular area are also determined by the minimum strength of the received signal, which is required by a MU in order to successfully recover the signal contaminated by various channel-effects. When only the PL is considered, the coverage of a cell should be a circular area, as shown in Figure 6.2(a), because there are no uncertainties affecting the coverage range of the BS. However, when uncertainties are introduced by shadowing and multipath fading, the coverage area of a cell becomes an irregular shape, as shown in Figure 6.2(b). Concerning the realistic implementation of cellular networks, a regular hexagon may be invoked for modelling the coverage of a specific cell, as shown in Figure 6.2(c).

In this scenario, the MU obeys the uniform mobility model given by Definition 6.1 within a bounded cell, while the BS is at the centre of the cell studied. Historically, a pair of basic shapes have been used to model the coverage area of a cell, namely a circle and an l-sided regular polygon. The statistical properties of the random distance between the BS and the MU are given by the following theorems:

Theorem 6.1 (Circular cell)**.** *If a cell is modelled by a circular area having a radius of r, the CDF of the random distance Y_b between the centrally-positioned BS and a MU obeying the uniform mobility model is given by*

$$F_{Y_b}(y_b) = \begin{cases} \frac{y_b^2}{r^2}, & 0 \le y_b \le r, \\ 1, & y_b > r. \end{cases} \tag{6.2}$$

Furthermore, the corresponding PDF can be expressed as

$$f_{Y_b}(y_b) = \begin{cases} \frac{2y_b}{r^2}, & 0 \le y_b \le r, \\ 0, & \textit{otherwise}. \end{cases} \tag{6.3}$$

Proof. Please refer to Appendix 6.A.1 for the detailed proof. □

Furthermore, given the PDF of Eq.(6.3), the average distance can be formulated as

$$E[Y_b] = \int_{y_b} y_b f_{Y_b}(y_b) dy_b = \int_0^r y_b \cdot \frac{2y_b}{r^2} dy_b = \frac{2}{3} r. \tag{6.4}$$

The CDF and the PDF given by Theorem 6.1 have already been widely adopted by the communication community for both the PL analysis [174], as well as for the interference analysis [175], and for the outage analysis of wireless multicast/broadcast systems [133].

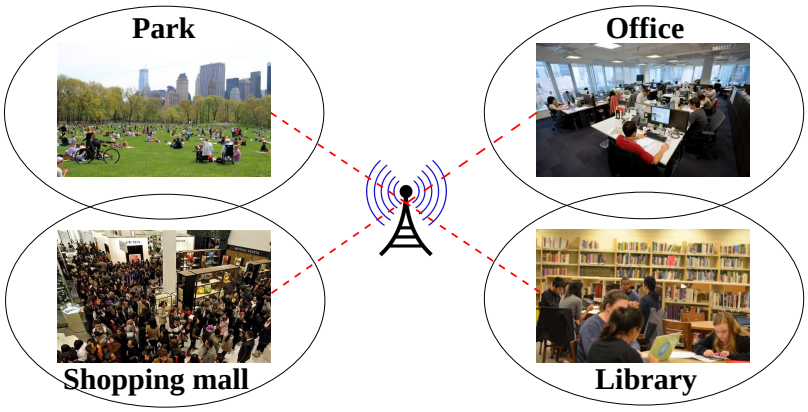

Figure 6.3: MUs move within some bounded areas

Theorem 6.2. *If a cell is modelled by an l-sided ($l \geq 3$) regular polygon having r as its radius*[1]*, the CDF of the random distance Y_b between the centrally-positioned BS and a MU obeying the uniform mobility model is given by*

$$F_{Y_b}(y_b) = \begin{cases} \frac{\pi}{l \tan\theta} \left(\frac{y_b}{r\cos\theta}\right)^2, & 0 \leq y_b \leq r\cos\theta, \\ \frac{1}{l\tan\theta}\left(\frac{y_b}{r\cos\theta}\right)^2 \left(\pi - l\arccos\left(\frac{y_b}{r\cos\theta}\right)^{-1}\right) & \\ \quad + \frac{1}{\tan\theta}\sqrt{\left(\frac{y_b}{r\cos\theta}\right)^2 - 1}, & r\cos\theta < y_b \leq r \\ 1, & \textit{otherwise}. \end{cases} \tag{6.5}$$

Furthermore, the corresponding PDF can be formulated as

$$f_{Y_b}(y_b) = \begin{cases} \frac{2\pi}{lr\sin\theta} \cdot \frac{y_b}{r\cos\theta}, & 0 \leq y_b \leq r\cos\theta, \\ \frac{2}{lr\sin\theta}\frac{y_b}{r\cos\theta}\left(\pi - l\arccos\left(\frac{y_b}{r\cos\theta}\right)^{-1}\right), & r\cos\theta < y_b \leq r, \\ 0, & \textit{otherwise}. \end{cases} \tag{6.6}$$

Proof. Please refer to Appendix 6.A.2 for the detailed proof. □

6.3 Distance Distribution between the BS and MUs Roaming in a Bounded Area

Sometimes the assumption that MUs may appear at any arbitrary positions of the entire cell becomes inaccurate because in some real scenarios, their movement is bounded within a specific area, as seen in Figure 6.3. Families and friends may enjoy the sunshine, have a picnic or do sports in a park on weekends. In this scenario, movements of people are bounded within the park. Employees work in their offices every day, have routine meetings with their colleagues in meeting rooms and enjoy their short break in the coffee room. In this scenario, their movements are bounded within the building of their company. Students walk between shelves of a library in order to find their books, they view multimedia clips or browse the Internet in the coffee bar. In this scenario, the movements of people are bounded within the library building. Before Christmas, people wander in the shopping mall in order to find attractive deals and to spot Christmas gift ideas for their friends and families. In this scenario, their movements are also bounded within the shopping mall. As a result, for the sake of further analysing and predicting the performance of wireless communication between

[1]The radius of a l-sided regular polygon is the distance from the centre to one of the vertices.

a BS and a MU, it is vital for us to characterise the statistical properties of the random distance between a BS and a MU, when the movement of the MU is restricted within a specific area.

Corresponding to the aforementioned realistic scenarios, we assume that a MU roams within a bounded area by following the uniform mobility model. We model the bounded area both as a circular and a square area, and derive the CDFs or PDFs of the random distance Y_b between a BS and a MU for these two scenarios, respectively.

6.3.1 MUs Roam in a Circular Area

First of all, we model the bounded area by a circle having the origin of O and a radius of r meters, as seen in Figures 6.1(c)(d). We denote this circular area as $\odot(O,r)$. A BS is located at the point B, which is d metres away from the centre O of the circular area. A MU roams within the circular area $\odot(O,r)$ by obeying the uniform mobility model. In the following two theorems, we will provide the CDFs and PDFs of the random distance Y_b between the BS and the MU for the scenario that the BS is outside the circular area $\odot(O,r)$ and the scenario that the BS is inside the circular area $\odot(O,r)$, respectively.

Theorem 6.3. *If the BS is outside the studied circular area $\odot(O,r)$ studied, namely we have $d > r$, the CDF of the random distance Y_b between the BS and the MU is expressed as*

$$F_{Y_b}(y_b) = \begin{cases} 0, & 0 \le y_b \le d-r, \\ \frac{1}{\pi}\left[\arccos\left(\frac{r^2+d^2-y_b^2}{2rd}\right) + \frac{y_b^2}{r^2}\arccos\left(\frac{y_b^2+d^2-r^2}{2y_bd}\right)\right. & \\ \quad \left. -\frac{1}{2r^2}\sqrt{4r^2d^2-(r^2+d^2-y_b^2)^2}\right], & d-r < y_b \le d+r, \\ 1, & y_b > d+r. \end{cases} \tag{6.7}$$

Furthermore, the corresponding PDF can be formulated as

$$f_{Y_b}(y_b) = \begin{cases} \frac{2y_b}{\pi r^2}\arccos\left(\frac{y_b^2+d^2-r^2}{2y_bd}\right), & d-r \le y_b \le d+r, \\ 0, & \textit{otherwise}. \end{cases} \tag{6.8}$$

Proof. Please refer to Appendix 6.B.1 for the detailed proof. □

Theorem 6.4. *If the BS is inside the circular area $\odot(O,r)$ studied, namely we have $d \le r$, the CDF of the random distance Y_b between the BS and the MU is expressed as*

$$F_{Y_b}(y_b) = \begin{cases} \frac{y_b^2}{r^2}, & 0 \le y_b \le r-d, \\ \frac{1}{\pi}\left[\arccos\left(\frac{r^2+d^2-y_b^2}{2rd}\right) + \frac{y_b^2}{r^2}\arccos\left(\frac{y_b^2+d^2-r^2}{2y_bd}\right)\right. & \\ \quad \left. -\frac{1}{2r^2}\sqrt{4r^2d^2-(r^2+d^2-y_b^2)^2}\right], & r-d < y_b \le r+d, \\ 1, & y_b > d+r. \end{cases} \tag{6.9}$$

Furthermore, the corresponding PDF can be formulated as

$$f_{Y_b}(y_b) = \begin{cases} \frac{2y_b}{r^2}, & 0 \le y_b \le r-d, \\ \frac{2y_b}{\pi r^2}\arccos\left(\frac{y_b^2+d^2-r^2}{2y_bd}\right), & r-d < y_b \le d+r, \\ 0, & \textit{otherwise}. \end{cases} \tag{6.10}$$

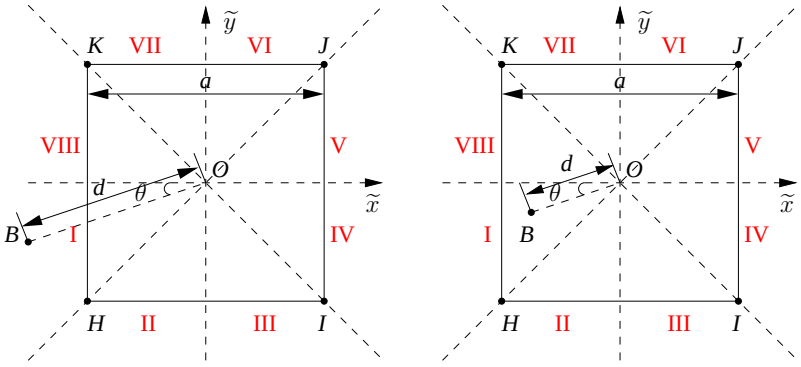

(a) BS is outside the square: $d\cos\theta > \frac{a}{2}$

(b) BS is inside the square: $d\cos\theta \leq \frac{a}{2}$

Figure 6.4: BS is located at an arbitrary position while the MU moves within a square area by obeying the uniform mobility model.

For the special case of $d = 0$, the BS is at the centre of the circular area $\odot(O, r)$ studied. Hence, the CDF and the PDF of the random distance Y_b are the same as in Theorem 6.1.

Proof. Please refer to Appendix 6.B.2 for the detailed proof. □

6.3.2 MUs Roam in a Square Area

Let us model the bounded area as a square having the point O as its centre and having a as its side-length. This square area is denoted by $\square HIJK$, as shown in Figure 6.4. The area of the square is $S_{\square HIJK} = \overline{HI}^2 = a^2$. As shown in Figure 6.4(a)(b), we divide the entire space into eight subspaces indexed as I to VIII. Due to the symmetry of the square area, if the BS is at a specific position in a specific subspace, we can find corresponding symmetric positions within the other subspaces, respectively. The random distances between the roaming MU and these symmetric positions of the BS share the same statistical properties. As a result, we only have to study the scenario that the BS is located in a specific subspace, say in I, as shown in Figure 6.4(a)(b). The CDF or PDF of the random distance Y_b derived is capable of generalising the statistical characteristics of Y_b, regardless of which specific subspace the BS is in.

A BS is located at the point B, as shown in Figure 6.4(a)(b). The position of the point B is determined by a tuple (d, θ), where d is the distance between the point B and the centre O of $\square HIJK$ and θ is the angle between the straight line $\overline{OB}$ and the horizontal line, as shown in Figure 6.4(a)(b). In order to ensure that the BS is located in subspace I, the angle θ should be in the range of $[0, \pi/4]$. Regardless where the BS is, its position can be equivalently converted to a tuple (d, θ) and the corresponding subspace can be converted to subspace I. Let us consider a two-dimensional surface $\widetilde{x}O\widetilde{y}$, as shown in Figure 6.4(a)(b). The centre O of the square $\square HIJK$ is also the origin of the surface $\widetilde{x}O\widetilde{y}$. Given an arbitrary position of the BS, which is denoted by the coordinates $(\widetilde{x}_B, \widetilde{y}_B)$, we can convert the conventional coordinates into a tuple (d, θ) associated with $\theta \in [0, \pi/4]$, which are expressed as follows:

$$d = \sqrt{\widetilde{x}_B^2 + \widetilde{y}_B^2},\ \cos\theta = \frac{\max\{|\widetilde{x}_B|, |\widetilde{y}_B|\}}{\sqrt{\widetilde{x}_B^2 + \widetilde{y}_B^2}},\ \sin\theta = \frac{\min\{|\widetilde{x}_B|, |\widetilde{y}_B|\}}{\sqrt{\widetilde{x}_B^2 + \widetilde{y}_B^2}}. \tag{6.11}$$

Furthermore, the horizontal distance between the point B and the centre O is derived as $d\cos\theta$. If we have $d\cos\theta > \overline{HI}/2 = a/2$, as shown in Figure 6.4(a), the position B of the BS is outside the square area $\square HIJK$ studied. If we have $d\cos\theta \leq \overline{HI}/2 = a/2$, as shown in Figure 6.4(b), the position B of the BS is either inside the square area $\square HIJK$ studied or on its boundary. A MU moves within $\square HIJK$ by obeying the uniform mobility model. In the following sections, we will discuss the statistical properties of the random

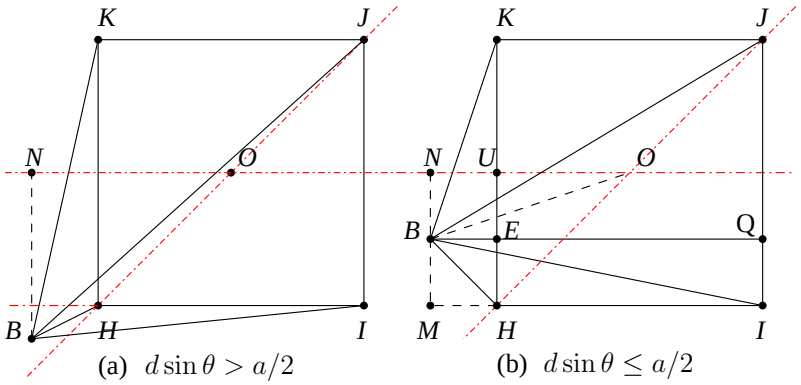

(a) $d\sin\theta > a/2$ (b) $d\sin\theta \leq a/2$

Figure 6.5: BS is outside the bounded square area

distance Y_b between the BS and the MU for the scenarios, when the BS is outside and inside the square area, respectively, as shown in Figures 6.1(e)(f).

6.3.2.1 The BS is outside the Square Area

Let us first consider the scenario that the BS is outside the square area of Figure 6.4(a). In this scenario, the horizontal distance from the point B to the centre O is longer than half of the side-length, i.e. we have $\overline{ON} = d\cos\theta > \overline{HI}/2 = a/2$, as shown in Figure 6.5(a)(b). However, we have to consider two different cases for the vertical distance spanning from the point B to the centre O, which is expressed as $\overline{BN} = d\sin\theta$. If we have $d\sin\theta > a/2$, the position B of the BS is below the horizontal line $\overline{HI}$, as shown in Figure 6.5(a). By contrast, if we have $d\sin\theta \leq a/2$, the position B of the BS is above the horizontal line $\overline{HI}$, as observed in Figure 6.5(b).

In this section, we focus our attention on the derivation of the CDF or the PDF of the random distance Y_b for the scenario of $d\sin\theta \leq a/2$, as shown in Figure 6.5(b). Before taking any further actions, we have to characterise some important distances spanning from the point B to all the vertices as well as to some of the sides of $\square HIJK$, as shown in Figure 6.5(b), which are formulated as follows:

$$\begin{cases} \overline{BE} &= d\cos\theta - a/2, \\ \overline{BH} &= \sqrt{a^2/2 + d^2 - ad(\sin\theta + \cos\theta)}, \\ \overline{BK} &= \sqrt{a^2/2 + d^2 - ad(\cos\theta - \sin\theta)} \\ \overline{BQ} &= d\cos\theta + a/2, \\ \overline{BI} &= \sqrt{a^2/2 + d^2 + ad(\cos\theta - \sin\theta)}, \\ \overline{BJ} &= \sqrt{a^2/2 + d^2 + ad(\cos\theta + \sin\theta)}. \end{cases} \tag{6.12}$$

Note that the formulas derived in Eq.(6.12) for $d\sin\theta \leq a/2$ are also capable of expressing the corresponding distances for $d\sin\theta > a/2$.

Given $d\sin\theta \leq a/2$, we are able to sort the above distances that may affect the derivation of the CDF $F_{Y_b}(y_b)$ in an ascending order, which is expressed as $0 \leq \overline{BE} \leq \overline{BH} \leq \overline{BK} \leq \overline{BQ} \leq \overline{BI} \leq \overline{BJ}$. Then, the CDF $F_{Y_b}(y_b)$ is given by the following theorem:

Theorem 6.5. *If the position B of the BS is outside the square area $\square HIJK$ and is above the horizontal line $\overline{HI}$, namely $d\sin\theta \leq a/2 \leq d\cos\theta$, while the MU roams within $\square HIJK$ by obeying the uniform mobility model, as shown in Figure 6.5(b), the CDF of the random distance Y_b between the BS and the MU*

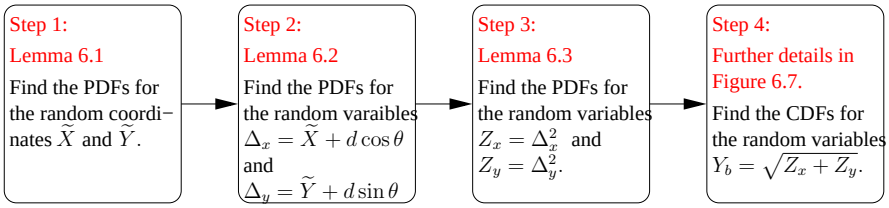

Figure 6.6: Algebraic methodology for deriving the CDF of the random distance Y_b, when the BS is inside the square area.

is expressed by the following equation:

$$F_{Y_b}(y_b) = \begin{cases} F^{I}_{Y_b}(y_b), & 0 \le y_b \le d\cos\theta - \frac{a}{2}, \\ F^{II}_{Y_b}(y_b), & d\cos\theta - \frac{a}{2} < y_b \le \sqrt{a^2/2 + d^2 - ad(\sin\theta + \cos\theta)}, \\ F^{III}_{Y_b}(y_b), & \sqrt{a^2/2 + d^2 - ad(\sin\theta + \cos\theta)} < y_b \le \sqrt{a^2/2 + d^2 - ad(\cos\theta - \sin\theta)}, \\ F^{IV}_{Y_b}(y_b), & \sqrt{a^2/2 + d^2 - ad(\cos\theta - \sin\theta)} < y_b \le d\cos\theta + \frac{a}{2}, \\ F^{V}_{Y_b}(y_b), & d\cos\theta + \frac{a}{2} < y_b \le \sqrt{a^2/2 + d^2 + ad(\cos\theta - \sin\theta)}, \\ F^{VI}_{Y_b}(y_b), & \sqrt{a^2/2 + d^2 + ad(\cos\theta - \sin\theta)} < y_b \le \sqrt{a^2/2 + d^2 + ad(\cos\theta + \sin\theta)}, \\ F^{VII}_{Y_b}(y_b), & y_b > \sqrt{a^2/2 + d^2 + ad(\cos\theta + \sin\theta)}, \end{cases} \tag{6.13}$$

where $F^{I}_{Y_b}(y_b) = 0$ *and* $F^{VII}_{Y_b}(y_b) = 1$, *while* $F^{II}_{Y_b}(y_b)$ *to* $F^{VI}_{Y_b}(y_b)$ *are given by Eqs.*(6.42), (6.44), (6.46), (6.48), *and* (6.50), *respectively. Please refer to Appendix 6.B.3 for the exact expressions.*

Proof. Please refer to Appendix 6.B.3 for the detailed proof. □

After differentiating $F_{Y_b}(y_b)$ given by Eq.(6.13) in each region, we can obtain the PDF of the random distance Y_b. Due to its complexity, here we opt out of presenting the PDF in this chapter.

Moreover, by following the same methodology as presented in Section 6.B.3, we are able to derive the CDF of the random distance Y_b for $d\sin\theta > a/2$. We do not have to consider as many different y_b values as we discussed for $d\sin\theta \le a/2$. If we have $0 \le y_b \le \overline{BH}$, the CDF of Y_b is zero. For $\overline{BH} < y_b \le \overline{BK}$, the CDF of Y_b is given by by $F^{III}_{Y_b}(y_b)$ that is derived in Eq.(6.44) of Section 6.B.3. If we have $\overline{BK} < y_b \le \overline{BI}$, the CDF of Y_b can be expressed by $F^{IV}_{Y_b}(y_b)$ that is derived in Eq.(6.46) of Section 6.B.3. For $\overline{BI} < y_b \le \overline{BJ}$, the CDF of Y_b can be formulated by $F^{VI}_{Y_b}(y_b)$ that is derived in Eq.(6.50) of Section 6.B.3. Finally, if we have $y_b > \overline{BJ}$, the CDF of Y_b is equal to unity.

6.3.2.2 The BS is inside the Square Area

Now, let us consider the scenario that the position B of the BS, which is denoted by the tuple (d, θ), is inside the square area $\square HIJK$. The centre of $\square HIJK$ is located at the origin $(0, 0)$ of the two-dimensional surface $\widetilde{x}O\widetilde{y}$. Without loss of generality, we assume that B is located in subspace I, as shown in Figure 6.4(b). Hence, the coordinate $(\widetilde{x}_B, \widetilde{y}_B)$ of point B can be expressed by the tuple (d, θ), namely $\widetilde{x}_B = -d\cos\theta$ and $\widetilde{y}_B = -d\sin\theta$, where we thus have $\theta \in [0, \frac{\pi}{4}]$ and $d\cos\theta \ge d\sin\theta$ because B is located in subspace I, whereas we also have $d\cos\theta \le \frac{a}{2}$, because the point B is within the square area $\square HIJK$. Given the random position $(\widetilde{X}, \widetilde{Y})$ of a MU, the random distance Y_b between this MU and the BS is derived as

$$Y_b = \sqrt{(\widetilde{X} - \widetilde{x}_B)^2 + (\widetilde{Y} - \widetilde{y}_B)^2} = \sqrt{(\widetilde{X} + d\cos\theta)^2 + (\widetilde{Y} + d\sin\theta)^2}. \tag{6.14}$$

In order to derive the CDF or PDF of the random distance Y_b, we summarise the main steps in Figure 6.6, which rely on Eq.(6.14). Lemmas 6.1-6.3 are proposed for completing the first three steps of Figure 6.6.

Lemma 6.1 (Step 1 of Figure 6.6). *The PDFs of the random coordinates $\widetilde{X}$ and $\widetilde{Y}$ are expressed as*

$$f_{\widetilde{X}}(\widetilde{x}) = \begin{cases} \frac{1}{a}, & -\frac{a}{2} \leq \widetilde{x} \leq \frac{a}{2}, \\ 0, & otherwise, \end{cases} \qquad f_{\widetilde{Y}}(\widetilde{y}) = \begin{cases} \frac{1}{a}, & -\frac{a}{2} \leq \widetilde{x} \leq \frac{a}{2}, \\ 0, & otherwise. \end{cases} \tag{6.15}$$

Proof. Since the MU moves within $\square HIJK$ by obeying the uniform mobility model, $\widetilde{X}$ and $\widetilde{Y}$ are both uniformly distributed random variables in the region $[-\frac{a}{2}, \frac{a}{2}]$. As a result, this lemma is readily proven. □

Lemma 6.2 (Step 2 of Figure 6.6). *Given $\Delta_x = \widetilde{X} + d\cos\theta$, the PDF of the random variable Δ_x is expressed as*

$$f_{\Delta_x}(\delta_x) = \begin{cases} \frac{1}{a}, & -\frac{a}{2} + d\cos\theta \leq \delta_x \leq \frac{a}{2} + d\cos\theta, \\ 0, & otherwise. \end{cases} \tag{6.16}$$

Similarly, given $\Delta_y = \widetilde{Y} + d\sin\theta$, the PDF of the random variable Δ_y is expressed as

$$f_{\Delta_y}(\delta_y) = \begin{cases} \frac{1}{a}, & -\frac{a}{2} + d\sin\theta \leq \delta_y \leq \frac{a}{2} + d\sin\theta, \\ 0, & otherwise. \end{cases} \tag{6.17}$$

Proof. This lemma is readily proven, since the sum of a uniformly distributed random variable and a constant is still uniformly distributed. □

Lemma 6.3 (Step 3 of Figure 6.6). *Given $Z_x = \Delta_x^2$, the PDF of the random variable Z_x is expressed as*

$$f_{Z_x}(z_x) = \begin{cases} \frac{1}{a\sqrt{z_x}}, & 0 < z_x < (\frac{a}{2} - d\cos\theta)^2 \\ \frac{1}{2a\sqrt{z_x}}, & (\frac{a}{2} - d\cos\theta)^2 < z_x < (\frac{a}{2} + d\cos\theta)^2 \\ 0, & otherwise. \end{cases} \tag{6.18}$$

Similarly, given $Z_y = \Delta_y^2$, the PDF of the random variable Z_y is expressed as

$$f_{Z_y}(z_y) = \begin{cases} \frac{1}{a\sqrt{z_y}}, & 0 < z_y < (\frac{a}{2} - d\sin\theta)^2 \\ \frac{1}{2a\sqrt{z_y}}, & (\frac{a}{2} - d\sin\theta)^2 < z_y < (\frac{a}{2} + d\sin\theta)^2 \\ 0, & otherwise. \end{cases} \tag{6.19}$$

Proof. Please refer to Appendix 6.B.4 for the detailed proof. □

More efforts have to be invested in order to finally obtain the CDF of the random variable $Y_b = \sqrt{Z_x + Z_y}$ (Step 4 of Figure 6.6). Specifically, the CDF of Y_b can be expressed as

$$\begin{aligned} F_{Y_b}(y_b) &= \Pr(Y_b \leq y_b) = \Pr(\sqrt{Z_x + Z_y} \leq y_b) = \Pr(Z_x + Z_y \leq y_b^2) \\ &= \iint_{\mathcal{S}} f_{Z_x Z_y}(z_x, z_y) dz_x dz_y, \end{aligned} \tag{6.20}$$

where $f_{Z_x Z_y}(z_x, z_y)$ is the joint PDF of the random variables Z_x and Z_y, while $\mathcal{S}$ is a two-dimensional area jointly determined by the domain of $f_{Z_x Z_y}(z_x, z_y)$ and the straight line $z_x + z_y = y_b^2$. The main steps of solving the double integral of Eq.(6.20) are summarised in Figure 6.7.

According to Eqs.(6.18) and (6.19), the domain of the joint PDF $f_{Z_x Z_y}(z_x, z_y)$ is denoted as the rectangular $\square OBHF$ in Figure 6.8. Furthermore, since Z_x and Z_y are independent random variables, their joint PDF can be expressed as $f_{Z_x Z_y}(z_x, z_y) = f_{Z_x}(z_x) \cdot f_{Z_y}(z_y)$. However, given a pair of values (z_x, z_y) in

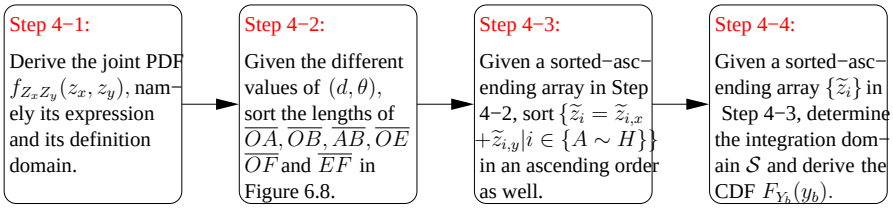

Figure 6.7: Methodology for solving the double integration of Eq.(6.20).

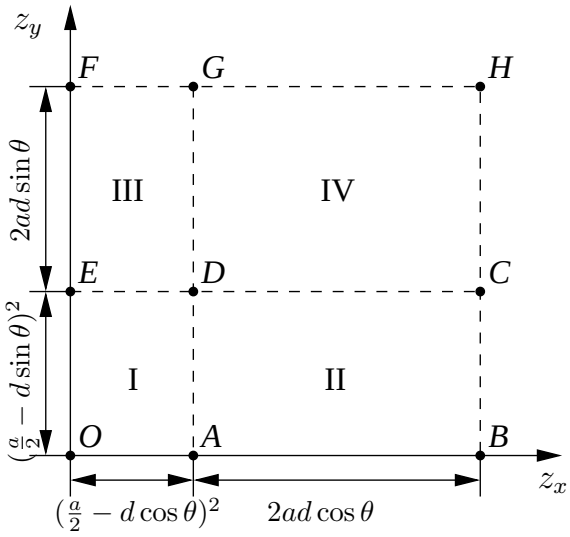

Figure 6.8: The domain of the joint PDF $f_{Z_xZ_y}(z_x, z_y)$.

different regions, namely region I, II, III and IV, as shown in Figure 6.8, we have different expressions for $f_{Z_xZ_y}(z_x, z_y)$, which are presented as the following equations (Step 4-1 of Figure 6.7):

$$f_{Z_xZ_y}(z_x, z_y) = \begin{cases} f^{(I)}_{Z_xZ_y}(z_x, z_y) = \frac{1}{a^2\sqrt{z_xz_y}}, & 0 < z_x < (\frac{a}{2} - d\cos\theta)^2 \\ & 0 < z_y < (\frac{a}{2} - d\sin\theta)^2, \\ f^{(II)}_{Z_xZ_y}(z_x, z_y) = \frac{1}{2a^2\sqrt{z_xz_y}}, & (\frac{a}{2} - d\cos\theta)^2 < z_x < (\frac{a}{2} + d\cos\theta)^2 \\ & 0 < z_y < (\frac{a}{2} - d\sin\theta)^2, \\ f^{(III)}_{Z_xZ_y}(z_x, z_y) = \frac{1}{2a^2\sqrt{z_xz_y}}, & 0 < z_x < (\frac{a}{2} - d\cos\theta)^2 \\ & (\frac{a}{2} - d\sin\theta)^2 < z_y < (\frac{a}{2} + d\sin\theta)^2, \\ f^{(IV)}_{Z_xZ_y}(z_x, z_y) = \frac{1}{4a^2\sqrt{z_xz_y}}, & (\frac{a}{2} - d\cos\theta)^2 < z_x < (\frac{a}{2} + d\cos\theta)^2 \\ & (\frac{a}{2} - d\sin\theta)^2 < z_y < (\frac{a}{2} + d\sin\theta)^2. \end{cases} \tag{6.21}$$

We denote the points on the boundaries between different regions by their corresponding coordinates in axes z_xOz_y, as shown in Figure 6.8. The coordinate of the point A is $((\frac{a}{2} - d\cos\theta)^2, 0)$, and the coordinates of the points B, C, D and E are given by $[(\frac{a}{2} + d\cos\theta)^2, 0]$, $[(\frac{a}{2} + d\cos\theta)^2, (\frac{a}{2} - d\sin\theta)^2]$, $[(\frac{a}{2} - d\cos\theta)^2, (\frac{a}{2} - d\sin\theta)^2]$ and $[0, (\frac{a}{2} - d\sin\theta)^2]$, respectively. Moreover, the coordinates of the points F, G, and H are given by $[0, (\frac{a}{2} + d\sin\theta)^2]$, $[(\frac{a}{2} - d\cos\theta)^2, (\frac{a}{2} + d\sin\theta)^2]$, and $[(\frac{a}{2} + d\cos\theta)^2, (\frac{a}{2} + d\sin\theta)^2]$, respectively.

Given the different values of the tuple (d, θ), which characterise the position of the BS, we have to sort the following array $\{\overline{OA}, \overline{OB}, \overline{AB}, \overline{OE}, \overline{OF}, \overline{EF}\}$ in an ascending order (Step 4-2 of Figure 6.7), where $\overline{OA} = (\frac{a}{2} - d\cos\theta)^2$ is the distance between the points O and A, as shown in Figure 6.8, $\overline{OB} = (\frac{a}{2} + d\cos\theta)^2$ is the distance between the points O and B, while $\overline{AB} = (\frac{a}{2} + d\cos\theta)^2 - (\frac{a}{2} - d\cos\theta)^2 = 2ad\cos\theta$ is the distance between the points A and B, whereas $\overline{OE} = (\frac{a}{2} - d\sin\theta)^2$ is the distance between the points O and E, $\overline{OF} = (\frac{a}{2} + d\sin\theta)^2$ is the distance between the points O and F, and finally, $\overline{EF} =$

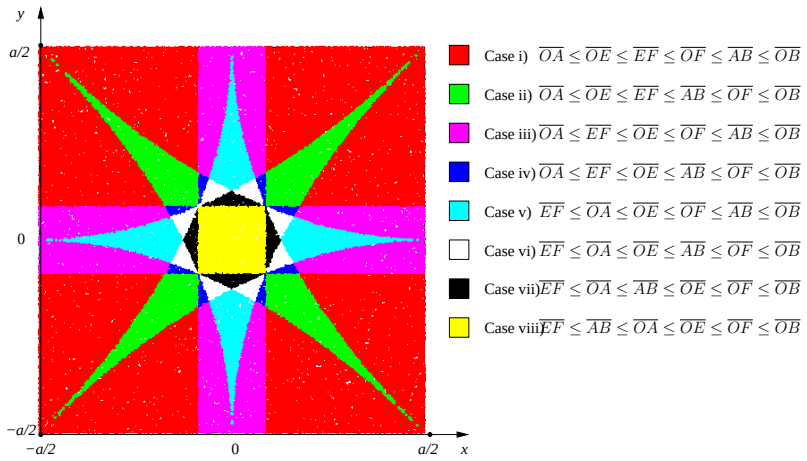

Figure 6.9: Different positions of the BS result in different cases.

$(\frac{a}{2} + d\sin\theta)^2 - (\frac{a}{2} - d\sin\theta)^2 = 2ad\sin\theta$ is the distance between the points E and F. We observe that, since the angle θ is in the region $\theta \in [0, \frac{\pi}{4}]$, we have $d\cos\theta \ge d\sin\theta$. Furthermore, since the BS is located within the square area, we have $d\cos\theta \le \frac{a}{2}$. As a result, we have several apparent inequalities, which are $\overline{OA} \le \overline{OE}$, $\overline{EF} \le \overline{AB}$, $\overline{OA} \le \overline{OB}$ and $\overline{AB} \le \overline{OB}$, as well as $\overline{OE} \le \overline{EF}$, $\overline{EF} \le \overline{OF}$, and $\overline{OF} \le \overline{OB}$. In order to fulfil these inequalities, we might have eight possible ascending-order sorted versions of the array $\{\overline{OA}, \overline{OB}, \overline{AB}, \overline{OE}, \overline{OF}, \overline{EF}\}$, which are given by:

i) $\overline{OA} \le \overline{OE} \le \overline{EF} \le \overline{OF} \le \overline{AB} \le \overline{OB}$, if the BS's location is within the red area of Figure.6.9;

ii)$\overline{OA} \le \overline{OE} \le \overline{EF} \le \overline{AB} \le \overline{OF} \le \overline{OB}$, if the BS's location is within the green area of Figure.6.9;

iii) $\overline{OA} \le \overline{EF} \le \overline{OE} \le \overline{OF} \le \overline{AB} \le \overline{OB}$, if the BS's location is within the magenta area of Figure 6.9;

iv) $\overline{OA} \le \overline{EF} \le \overline{OE} \le \overline{AB} \le \overline{OF} \le \overline{OB}$, if the BS's location is within the blue area of Figure 6.9;

v) $\overline{EF} \le \overline{OA} \le \overline{OE} \le \overline{OF} \le \overline{AB} \le \overline{OB}$, if the BS's location is within the cyan area of Figure 6.9;

vi) $\overline{EF} \le \overline{OA} \le \overline{OE} \le \overline{AB} \le \overline{OF} \le \overline{OB}$, if the BS's location is within the white area of Figure 6.9;

vii) $\overline{EF} \le \overline{OA} \le \overline{AB} \le \overline{OE} \le \overline{OF} \le \overline{OB}$, if the BS's location is within the black area of Figure 6.9;

viii) $\overline{EF} \le \overline{AB} \le \overline{OA} \le \overline{OE} \le \overline{OF} \le \overline{OB}$, if the BS's location is within the yellow area of Figure 6.9.

According to Figure 6.9, we found that if we randomly position a BS into a square area, Case i) $\overline{OA} \le \overline{OE} \le \overline{EF} \le \overline{OF} \le \overline{AB} \le \overline{OB}$ is most likely to happen, which has a probability of 59.5%. As a result, in order to show the methodology of solving the double integral of Eq.(6.20), we will consider Case i as an example in Theorem 6.6.

Furthermore, we have to obtain the sum of each point's z_x-coordinate and z_y-coordinate. For example, we denote the sum of point A's z_x-coordinate and z_y-coordinate as $\widetilde{z}_A = z_{A,x} + z_{A,y} = (\frac{a}{2} - d\cos\theta)^2$. In order to further streamline the double integral of Eq.(6.20), we have to sort the array $\{\widetilde{z}_i = z_{i,x} + z_{i,y} | i \in \{A, B, C, D, E, F, G, H\}\}$ in an ascending order (Step 4-3 of Figure 6.7), which is determined by the order of array $\{\overline{OA}, \overline{OB}, \overline{AB}, \overline{OE}, \overline{OF}, \overline{EF}\}$. For example, as Case i) $\overline{OA} \le \overline{OE} \le \overline{EF} \le \overline{OF} \le \overline{AB} \le \overline{OB}$ is assumed, we have $\widetilde{z}_A \le \widetilde{z}_E \le \widetilde{z}_D \le \widetilde{z}_F \le \widetilde{z}_G \le \widetilde{z}_B \le \widetilde{z}_C \le \widetilde{z}_H$.

Theorem 6.6 (Step 4-4 of Figure 6.7)**.** *Given a specific position of the BS (d, θ), the following inequalities are satisfied $\overline{OA} \le \overline{OE} \le \overline{EF} \le \overline{OF} \le \overline{AB} \le \overline{OB}$. The CDF of the random distance Y_b between the BS*

within the square area and the MU roaming within the same area can be expressed as

$$F_{Y_b}(y_b) = \begin{cases} F^{(1)}_{Y_b}(y_b), & 0 \le y_b \le \frac{a}{2} - d\cos\theta, \\ F^{(2)}_{Y_b}(y_b), & \frac{a}{2} - d\cos\theta < y_b \le \frac{a}{2} - d\sin\theta \\ F^{(3)}_{Y_b}(y_b), & \frac{a}{2} - d\sin\theta < y_b \le \sqrt{a^2/2 + d^2 - ad(\cos\theta + \sin\theta)}, \\ F^{(4)}_{Y_b}(y_b), & \sqrt{a^2/2 + d^2 - ad(\cos\theta + \sin\theta)} < y_b \le \frac{a}{2} + d\sin\theta, \\ F^{(5)}_{Y_b}(y_b), & \frac{a}{2} + d\sin\theta < y_b \le \frac{a}{2} + d\cos\theta, \\ F^{(6)}_{Y_b}(y_b), & \frac{a}{2} + d\cos\theta < y_b \le \sqrt{a^2/2 + d^2 - ad(\cos\theta - \sin\theta)}, \\ F^{(7)}_{Y_b}(y_b), & \sqrt{a^2/2 + d^2 - ad(\cos\theta - \sin\theta)} < y_b \le \sqrt{a^2/2 + d^2 + ad(\cos\theta - \sin\theta)}. \\ F^{(8)}_{Y_b}(y_b), & \sqrt{a^2/2 + d^2 + ad(\cos\theta - \sin\theta)} < y_b \le \sqrt{a^2/2 + d^2 + ad(\cos\theta + \sin\theta)}. \\ F^{(9)}_{Y_b}(y_b), & y_b > \sqrt{a^2/2 + d^2 + ad(\cos\theta + \sin\theta)}, \end{cases} \tag{6.22}$$

where the exact expressions for $F^{(1)}_{Y_b}(y_b)$ *to* $F^{(9)}_{Y_b}(y_b)$ *are provided by Eqs.*(6.56) *to* (6.63) *and* $F^{(9)}_{Y_b}(y_b) = 1$*, as presented in Appendix 6.B.5.*

Proof. Please refer to Appendix 6.B.5 for the detailed proof. □

The calculations of Eq.(6.20) for the remaining seven cases can be completed by following the same methodology, as presented in Section 6.B.5, which are omitted here for reasons of space economy. Another particular case that the position B of the BS is placed at the centre O of the square area $\square HIJK$ needs our further attention. The radius r of $\square HIJK$, which is defined as the distance from the centre O of $\square HIJK$ to any of the four vertices, can be obtained as $r = \overline{HI}/\cos\frac{\pi}{4} = \sqrt{2}a/2$. By substituting r into Eq.(6.5) and Eq.(6.6) in Theorem 6.2 and letting $l = 4$, we may obtain the CDF and the PDF of the random distance Y_b between the BS, which is placed at the centre of the square area $\square HIJK$, and the MU, which moves within $\square HIJK$ by obeying the uniform mobility model.

6.4 Distance Distribution between a Pair of MUs Roaming within a Bounded Area

In Sections 6.2 and 6.3, we discussed the random distance between a BS and a MU in different scenarios, where the BS is a static node and the MU is a mobile node. Generally speaking, various distance distributions derived in the previous sections can be invoked for evaluating the performance of wireless links connecting a static node and a mobile node. In realistic wireless communications, only the CI constituted by the BSs and Wi-Fi hotspots are often modelled as static nodes. As a result, the distance distributions derived in previous sections are only capable of evaluating the performance of centralised wireless links, such as cellular links connecting the MUs to a BS and Wi-Fi links connecting the MUs to a Wi-Fi hotspot.

However, with the rapid development of sophisticated multi-functional mobile devices, direct communications between a pair of MUs have attracted much attention from both the academic and industrial communities. There are several techniques of supporting direct communications between a pair of MUs. Bluetooth and infrared transmission modes have been installed in mobile phones for decades, which would indeed facilitate direct communication between a MU and its neighbour. However, due to their short transmission range, it is impossible for these two techniques to deliver the information to distant receivers. Apart from centralised communication between a MU and an access point, the family of 802.11 protocols [53] is also capable of supporting purely distributed -rather than CI-based- communications between a pair of MUs. From the route establishment in the network layer to the resource allocation in the Medium-Access-Control (MAC) layer, all the actions are completed by the direct or multi-hop communications amongst the MUs equipped with Wi-Fi transmission modules without any aid of the CI. However, a purely distributed way of routing and resource allocation may impose an increased overhead signalling and power dissipation, which might

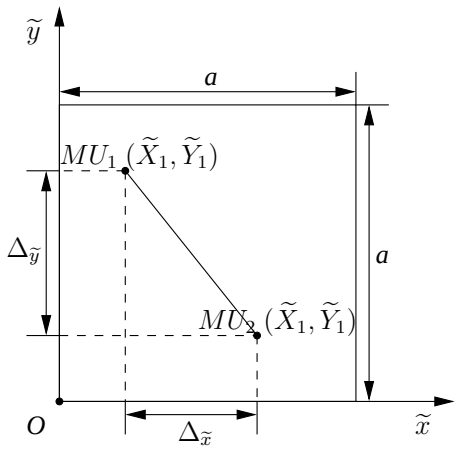

Figure 6.10: The Cartesian coordinate system of calculating the CDF of the random distance Y_s

reduce the efficiency of data transmission. As a result, in order to improve the efficiency of route finding and resource allocation, cellular device-to-device communication [171] has become a more popular choice for realising direct communication between a pair of MUs. In cellular device-to-device communication, all the overhead signalling required for route finding and resource scheduling is carried out by the BS of the cell. Once a pair of MUs have acquired the necessary resources and a direct link between them has been established, the transmitter may directly convey the required data to the receiver.

As a result, the distance distribution between a static node and a mobile node is not suitable for evaluating the performance of a direct link between a pair of MUs due to the mobile nature of both the transmitter and the receiver. Hence, in this section, we will characterise the distance distribution between a pair of MUs in different scenarios in order to provide a more accurate tool for studying the link performance between a pair of mobile nodes.

6.4.1 MUs Roam in a Square Area

In this scenario, as shown in Figure 6.1(g), we assume that a pair of MUs move within a square area by obeying the uniform mobility model, as introduced in Definition 6.1. In order to derive the CDF or the PDF of the random distance Y_s between a pair of MUs roaming in the square area, the two-dimensional Cartesian coordinate system $\widetilde{x}O\widetilde{y}$ is invoked. The left bottom corner of the square area considered is placed at the origin O and the side-length of the square area is a, as shown in Figure 6.10.

Let the Cartesian coordinate of MU_1 be $(\widetilde{X}_1, \widetilde{Y}_1)$ and let that of MU_2 be $(\widetilde{X}_2, \widetilde{Y}_2)$, where all these random variables, namely $\widetilde{X}_1$, $\widetilde{X}_2$, $\widetilde{Y}_1$, $\widetilde{Y}_2$ are independent by obeying an identical uniform distribution defined in the region $[0, a]$ (Step 1 of Figure 6.11). For example, the PDF of the random variable $\widetilde{X}_1$ can be expressed as

$$f_{\widetilde{X}_1}(\widetilde{x}_1) = \begin{cases} \frac{1}{a}, & 0 \leq \widetilde{x}_1 \leq a, \\ 0, & \text{otherwise.} \end{cases} \tag{6.23}$$

Thus, the random distance Y_s between MU_1 and MU_2 can be expressed as

$$Y_s = \sqrt{(\widetilde{X}_1 - \widetilde{X}_2)^2 + (\widetilde{Y}_1 - \widetilde{Y}_2)^2}. \tag{6.24}$$

In order to derive the CDF or PDF of the random distance Y_b, we summarise the main steps in Figure 6.11, which rely on Eq.(6.24). Specifically, the first step of Figure 6.11 has been completed by Eq.(6.23), while the following three steps will be solved by Lemmas 6.4 and 6.5 as well as Theorem 6.7, respectively.

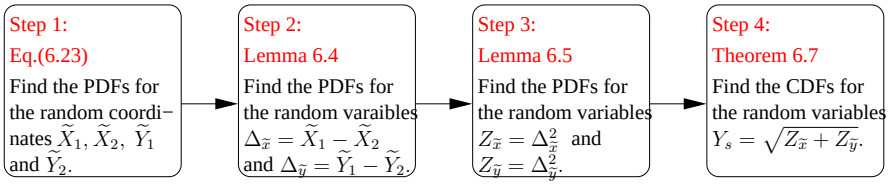

Figure 6.11: Algebraic methodology for deriving the CDF and the PDF of the random distance Y_s, when a pair of MUs roam within in a square area by obeying the uniform mobility model.

Lemma 6.4 (Step 2 of Figure 6.11). *Given that $\Delta_{\widetilde{x}} = \widetilde{X}_1 - \widetilde{X}_2$ and that both $\widetilde{X}_1$ as well as $\widetilde{X}_2$ are i.i.d. random variables, whose PDFs are given by Eq.*(6.23)*, the PDF of the random variable $\Delta_{\widetilde{x}}$ can be expressed as*

$$f_{\Delta_{\widetilde{x}}}(\delta_{\widetilde{x}}) = \begin{cases} \frac{\delta_{\widetilde{x}} + a}{a^2}, & -a \leq \delta_{\widetilde{x}} < 0 \\ \frac{a - \delta_{\widetilde{x}}}{a^2}, & 0 \leq \delta_{\widetilde{x}} \leq a \\ 0, & \text{otherwise.} \end{cases} \tag{6.25}$$

Apparently, $\Delta_{\widetilde{y}} = \widetilde{Y}_1 - \widetilde{Y}_2$ shares an identical PDF with $\Delta_{\widetilde{x}}$.

Proof. Please refer to Appendix 6.C.1 for the detailed proof. □

Lemma 6.5 (Step 3 of Figure 6.11). *Given that $Z_{\widetilde{x}} = \Delta_{\widetilde{x}}^2$, the PDF of the random variable $Z_{\widetilde{x}}$ can be expressed as*

$$f_{Z_{\widetilde{x}}}(z_{\widetilde{x}}) = \begin{cases} \frac{1}{a\sqrt{z_{\widetilde{x}}}} - \frac{1}{a^2}, & 0 \leq z_x \leq a^2 \\ 0, & \text{otherwise.} \end{cases} \tag{6.26}$$

Moreover, the random variable $Z_{\widetilde{y}} = \Delta_{\widetilde{y}}^2$ shares the same PDF with $Z_{\widetilde{x}}$.

Proof. Please refer to Appendix 6.C.2 for the detailed proof. □

Theorem 6.7 (Step 4 of Figure 6.11). *The CDF of the random distance Y_s, which is defined as $Y_s = \sqrt{Z_{\widetilde{x}} + Z_{\widetilde{y}}}$, between a pair of MUs roaming within a square area having a as its side-length can be expressed as*

$$F_{Y_s}(y_s) = \begin{cases} \frac{1}{a^2}\left(\pi y_s^2 - \frac{8y_s^3}{3a} + \frac{y_s^4}{2a^2}\right), & 0 \leq y_s < a \\ \frac{1}{a^2}\left[2y_s^2 \arcsin\frac{2a^2 - y_s^2}{y_s^2} + \left(\frac{4}{3}a + \frac{8}{3a}y_s^2\right)\sqrt{y_s^2 - a^2}\right. & \\ \qquad \left. -2y_s^2 - \frac{y_s^4}{2a^2} + \frac{a^2}{3}\right], & a < y_s \leq \sqrt{2}a \\ 1, & y_s > \sqrt{2}a. \end{cases} \tag{6.27}$$

After differentiating $F_{Y_s}(y_s)$ in each region with respect to y_s, we arrive at the PDF of the random distance Y_s, which is expressed as

$$f_{Y_s}(y_s) = \begin{cases} \frac{1}{a^2}\left(2\pi y_s - \frac{8y_s^2}{a} + \frac{2y_s^3}{a^2}\right), & 0 \leq y_s < a \\ \frac{1}{a^2}\left(4y_s \arcsin\frac{2a^2 - y_s^2}{y_s^2} + \frac{8y_s}{a}\sqrt{y_s^2 - a^2} - 4y_s - \frac{2y_s^3}{a^2}\right), & a < y_s \leq \sqrt{2}a \\ 0, & \text{otherwise.} \end{cases} \tag{6.28}$$

Proof. Please refer to Appendix 6.C.3 for the detailed proof. □

6.4.2 MUs Roam in a Circular Area

Let us first consider the scenario where a pair of MUs move within a circular area $\odot(O,r)$ having a point O as its centre and having a radius of r metres, as shown in Figure 6.1(h). The movements of this MU pair obey the uniform mobility model, as introduced in Definition 6.1. However, it is difficult for us to describe the uniformly-distributed characteristics of MUs within circular area $\odot(O,r)$ in terms of the classic Cartesian coordinates. But the question arises, as to why not try polar coordinates? We will also show the difficulties of deriving the random distance between a pair of MUs, when the polar coordinate system is invoked. The polar coordinates of MU_i are given by (D_i,Θ_i), where D_i is the radial coordinate and Θ_i is the angular coordinate. Then we can convert the polar coordinates into the Cartesian coordinates on the two-dimensional plane $\widetilde{x}O\widetilde{y}$ by invoking the following two relationships: $\widetilde{X}_i = D_i\cos\Theta_i$ and $\widetilde{Y}_i = D_i\sin\Theta_i$. As a result, the Euclidean distance between a pair of MUs is expressed as

$$Y_s = \sqrt{(\widetilde{X}_1-\widetilde{X}_2)^2+(\widetilde{Y}_1-\widetilde{Y}_2)^2} = \sqrt{D_1^2+D_2^2-2D_1D_2\cos(\Theta_1-\Theta_2)}. \tag{6.29}$$

In order to characterise the CDF or PDF of Y_s expressed in Eq.(6.29), apart from the PDF of D_1^2 and D_2^2, we have to obtain the PDF for $2D_1D_2\cos(\Theta_1-\Theta_2)$. Unfortunately, these three random variables are not independent of one another, which makes the CDF derivation of Y_s extremely hard.

However, we may readily derive the CDF or PDF of the random distance Y_s between a pair of MUs with the aid of Crofton's fixed-point theorem [144]. Before introducing this theorem, we firstly provide the definitions of a $\sigma-$algebra and of a specific measure in probability theory.

Definition 6.2 ($\sigma-$algebra)**.** *A $\sigma-$algebra defined over a set $\mathcal{S}$ is a collection of subsets of $\mathcal{S}$ that is closed under a countable-fold applied set of operations (complement, union of countably many sets and intersection of countably many sets).*

Definition 6.3 (measure on a set)**.** *Let $\mathcal{S}$ be a set and let $\Psi_{\mathcal{S}}$ be a $\sigma-$algebra over the set $\mathcal{S}$. A function defined as $\varphi_{\mathcal{S}}:\Psi\rightarrow\mathbb{R}$, where $\mathbb{R}$ is the extended real number system, is termed as a measure, if it satisfies the following properties:*

- *Non-negativity: For any subset $\mathcal{A}$ of $\mathcal{S}$ that belongs to $\Psi_{\mathcal{S}}$, we have $\varphi_{\mathcal{S}}(\mathcal{A})\geq 0$;*
- *Null empty set: For a null set ϕ, we have $\varphi_{\mathcal{S}}(\phi)=0$;*
- *Countable additivity: For all countable collections $\{\mathcal{A}_i, i=1,2,\cdots,N\}$ of pairwise disjoint sets in $\Psi_{\mathcal{S}}$, we have $\varphi_{\mathcal{S}}(\bigcup_{i=1}^{N}\mathcal{A}_i)=\sum_{i=1}^{N}\varphi_{\mathcal{S}}(\mathcal{A}_i)$.*

Let us now define a set $\mathcal{S}$ of points, whose $\sigma-$algebra is denoted as $\Psi_{\mathcal{S}}$. A measure over a subset $\mathcal{A}$ that belongs to $\Psi_{\mathcal{S}}$ is defined as $\varphi_{\mathcal{S}}:\Psi_{\mathcal{S}}\rightarrow\mathbb{R}$. Specifically, if $\mathcal{S}$ is a point sets on the two-dimensional plane, the measure $\varphi_{\mathcal{S}}(\mathcal{A})$ is the area covered by a subset $\mathcal{A}$ of points. If $\mathcal{S}$ is a three-dimensional space set of points, the measure $\varphi_{\mathcal{S}}(\mathcal{A})$ is defined as the volume of a point-subset $\mathcal{A}$. Based on the definition of a measure on a point set, if the probability of an event, which depends on the positions of the points within $\mathcal{A}$, is of interest, Crofton's fixed-point theorem is defined as [144]

Theorem 6.8 (fixed-point theorem)**.** *Given a grand point-set $\mathcal{S}$, whose $\sigma-$algebra is $\Psi_{\mathcal{S}}$, we let n points $\{\epsilon_i, i=1,2,...,n\}$ be randomly distributed in a point-subset $\mathcal{A}$ that belongs to $\Psi_{\mathcal{S}}$. We define $\mathcal{H}$ as an event depending on the positions of these n points. Let $\mathcal{A}'$ be a subset belonging to $\Psi_{\mathcal{S}}$, which is slightly smaller than $\mathcal{A}$ but contained within it, denoted as $\mathcal{A}'\subset\mathcal{A}$. We also let $\delta\mathcal{A}$ be the specific part of $\mathcal{A}$, which is not within $\mathcal{A}'$. Then the following relationship can be invoked for calculating the probability of the event $\mathcal{H}$ occurring:*

$$dPr(\mathcal{H}) = n(Pr(\mathcal{H}|\epsilon_1\in\delta\mathcal{A})-Pr(\mathcal{H}))\left[\varphi_{\mathcal{S}}(\mathcal{A})\right]^{-1}d\varphi_{\mathcal{S}}(\mathcal{A}), \tag{6.30}$$

where $\varphi_{\mathcal{S}}(\mathcal{A})$ is a measure of the point-subset $\mathcal{A}$.

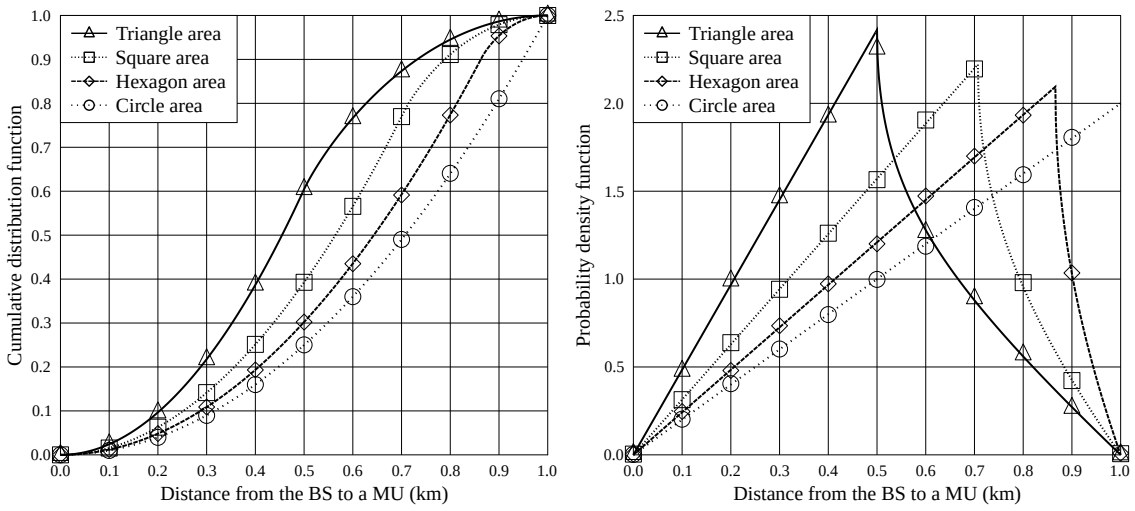

(a) Cumulative distribution function (b) Probability density function

Figure 6.12: The distance distribution between the BS and the MU, when the BS is at the centre of the cell and the MU moves within the entire cell by obeying the uniform mobility model, as shown in Figures 6.1(a)(b). The radius is $r = 1$ km for all the cells having different shapes. The analytical CDFs are given by Eqs.(6.2) and (6.5), while the analytical PDFs are given by Eqs.(6.3) and (6.6).

With the aid of the Crofton's fixed-point theorem [144], we arrive at the following theorem:

Theorem 6.9. *When a pair of MUs roam within a circular area having a radius r by obeying the uniform mobility model, the PDF of the random distance Y_s between this pair of MUs is expressed as*

$$f_{Y_s}(y_s) = \frac{8}{\pi r} \cdot \frac{y_s}{2r} \left[\arccos \frac{y_s}{2r} - \frac{y_s}{2r} \sqrt{1 - \left(\frac{y_s}{2r}\right)^2} \right], \tag{6.31}$$

for $0 \leq y_s \leq 2r$. Furthermore, integrating the above $f_{Y_s}(y_s)$ over the region $[0, y_s]$, we may obtain the CDF $F_{Y_s}(y_s)$ as

$$F_{Y_s}(y_s) = \frac{2}{\pi} \left\{ 4 \left(\frac{y_s}{2r}\right)^2 \arccos\left(\frac{y_s}{2r}\right) + \arcsin\left(\frac{y_s}{2r}\right) - \left[\frac{y_s}{2r} + 2\left(\frac{y_s}{2r}\right)^3 \right] \sqrt{1 - \left(\frac{y_s}{2r}\right)^2} \right\}. \tag{6.32}$$

Proof. Please refer to Appendix 6.C.4 for the detailed proof. □

6.5 Numerical Results

Having provided the associated analytical derivations, we move on to the numerical results of the various distance distributions. Note that in all the numerical results presented in this section, the lines represent the analytical results, which are obtained from the closed-form equations in Sections 6.2–6.4, while the markers represent the simulation results, which are obtained by the Monte-Carlo simulations.

Let us first study the distance distribution between the BS and a specific MU in the typical scenario of cellular communications. In this scenario, as portrayed in Figures 6.1(a)(b), the BS is located at the centre of the cell, while the MUs roam within this cell by obeying the uniform mobility model. In Figures 6.12(a) and (b) we plot both the CDF and the PDF of the random distance for the cells having different shapes. All these cells share the same radius, which is $r = 1$ km. As shown in Figure 6.12(a), the circular cell has the lowest CDF, which indicates that the random distance is more likely to take a higher value than the cells

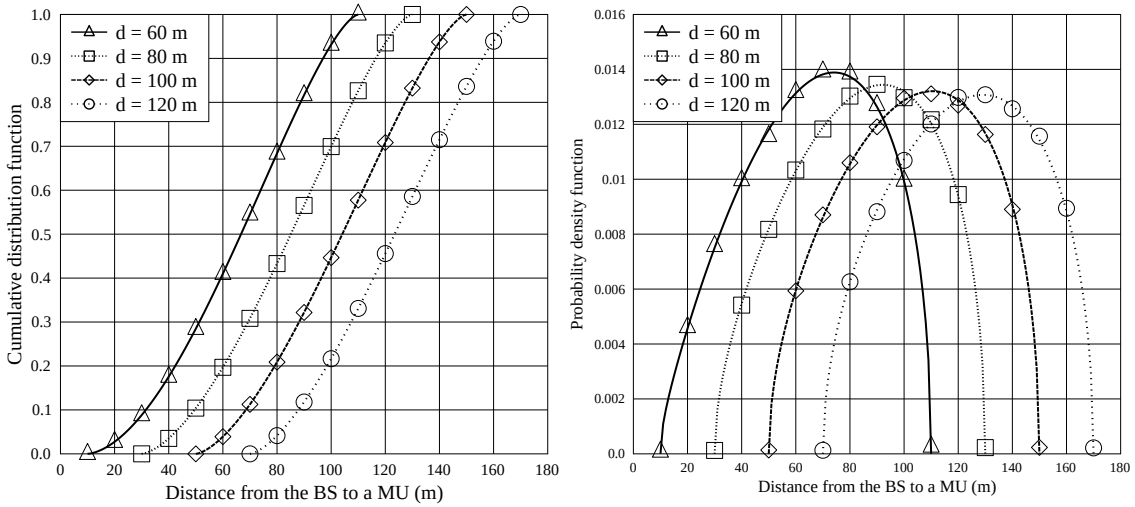

(a) Cumulative distribution function

(b) Probability density function

Figure 6.13: The distance distribution between the BS and the MU, when the BS is outside a circular area and the MU moves within the circular area, as shown in Figure 6.1(c). The radius of the circular area is $r = 50$ m. The distance d between the BS and the centre of the circular area assumes values from the set $\{60, 80, 100, 120\}$ m. The analytical CDFs are given by Eq.(6.7), while the analytical PDFs are given by Eq.(6.8).

obeying other shapes. As shown in Figure 6.12(b), except for the random distance in the circular cell, the random distance in the polygonal cells have PDFs, which linearly increase and then subside after reaching their peaks. Furthermore, the accuracy of the analytical results expressed in Eqs.(6.2) and (6.3), as well as in Eqs.(6.5) and (6.6) is confirmed by the Monte-Carlo simulations, as shown in both Figures 6.12(a) and (b).

Let us now embark on studying the distance distribution between the BS and a specific MU, when the BS is arbitrarily located outside a circular area and the MU roams within the circular area, as portrayed in Figure 6.1(c). The radius of the circular area is $r = 50$ m, while the distance d between the BS and the centre of the circular area varies from 60 m to 120 m. Since the BS is outside the circular area, the distance d from the BS to the centre of the circular area should be longer than the radius r. We observe from both Figures 6.13(a) and (b) that the minimum distance from the BS to the MU is $(d - r)$ m, while the maximum distance is $(d + r)$ m. Furthermore, when the BS is farther away from the centre of the circular area, which indicates a higher value of d, both the CDF and the PDF are shifted to the right hand side. Moreover, the accuracy of the analytical results expressed in Eqs.(6.7) and (6.8) is validated by the Monte-Carlo simulations, as shown in both Figures 6.13(a) and (b).

We next study the distance distribution between the BS and a specific MU, when the BS is located at an arbitrary position inside a circular area and the MU roams within this circular area by following the uniform mobility model, as seen in Figure 6.1(d). The radius of the circular area is $r = 50$ m, while the distance d between the BS and the centre of the circular area varies from $d = 10$ m to $d = 40$ m. In Figures 6.14(a) and (b), we portray the CDF and the PDF of the random distance for this scenario, respectively. As shown in Figure 6.14(a), the minimum value of the random distance is zero for all the different values of d. By contrast, the maximum values depend on the specific values of d and of the radius r. For example, if d takes a value of 40 m, the maximum distance in this case is $d + r = 90$ m. As apparently shown in Figure 6.14(a), if the BS is farther away from the centre of the circular area, which is indicated by a larger value of d, the random distance is more likely to take a higher value. Furthermore, as shown in Figure 6.14(b), the PDFs of the random distance linearly increase first and then subside after reaching their peaks. As the BS is positioned farther away from the centre of the circular area in Figure 6.1(d), the linear parts of the PDFs decay and they become zeros when the BS is located at the circumference of the circular area. Moreover, the accuracy of the

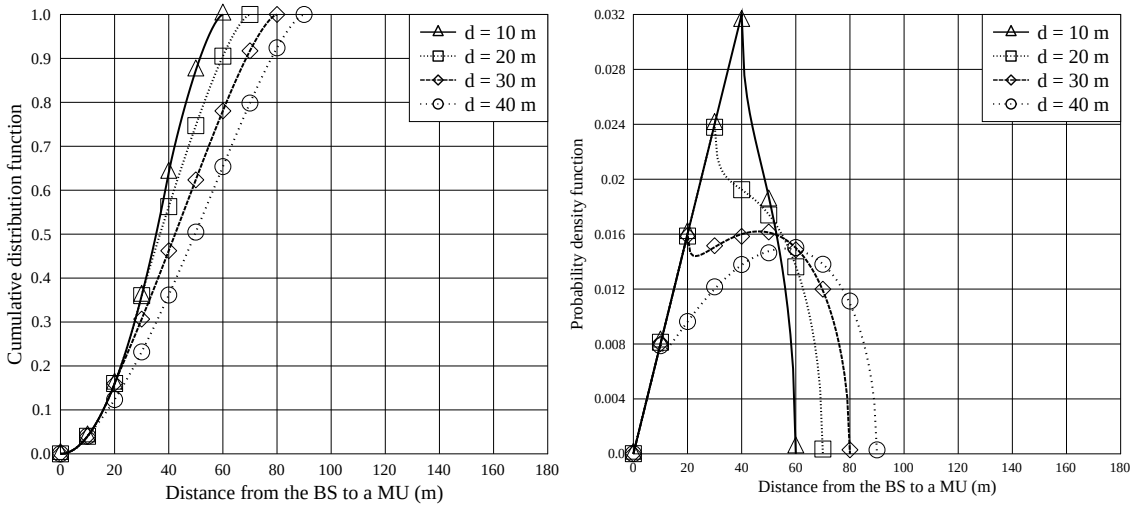

(a) Cumulative distribution function (b) Probability density function

Figure 6.14: The distance distribution between the BS and the MU, when the BS is within a circular area and the MU moves within the circular area, as seen in Figure 6.1(d). The radius of the circular area is $r = 50$ m. The distance d between the BS and the centre of the circular area assumes values from the set $\{10, 20, 30, 40\}$ m. The analytical CDFs are given by Eq.(6.9), while the analytical PDFs are given by Eq.(6.10).

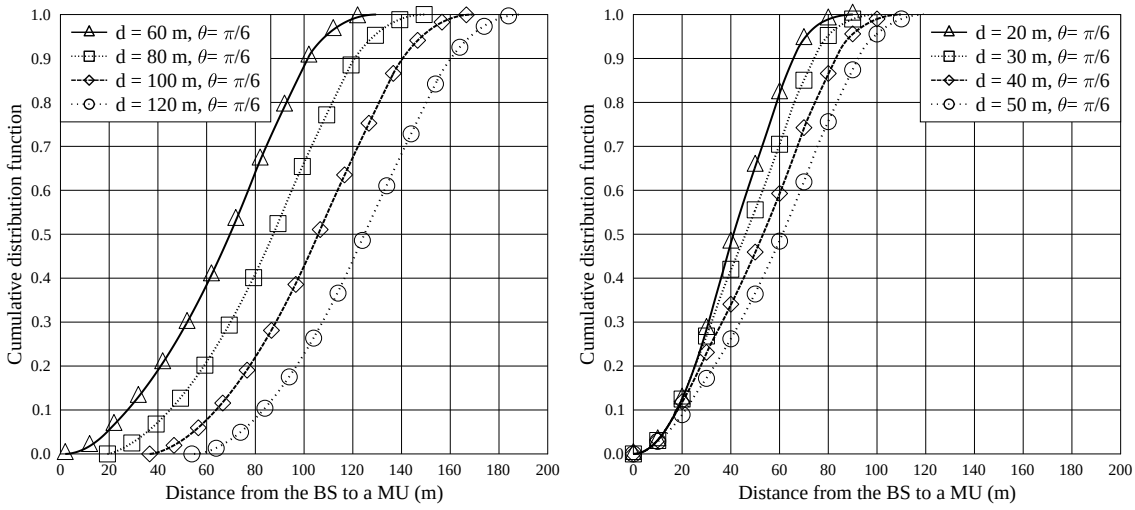

(a) The BS is outside a square area (b) The BS is inside a square area

Figure 6.15: The distance distribution between the BS and the MU, when the BS is outside/inside a square area and the MU moves within the square area by obeying the uniform mobility model, as shown in Figures 6.1(e)/(f). The side-length of the square area is $a = 100$ m. The distance d between the BS and the centre of the square area varies from 20 m to 120 m, while the angle θ defined in Figure 6.4 remains $\pi/6$. The analytical CDFs are given by Eq.(6.13) and Eq.(6.22), respectively.

analytical results expressed in Eqs.(6.9) and (6.10) is validated by the Monte-Carlo simulations, as shown in both Figures 6.14(a) and (b).

Let us now study the CDFs of the random distance between the BS and a specific MU, when the BS is arbitrarily located outside/inside a square area, while the MU roams within the square area by obeying the uniform mobility model, as characterised in Figures 6.1(e)(f). The side-length of the square area is $a = 100$

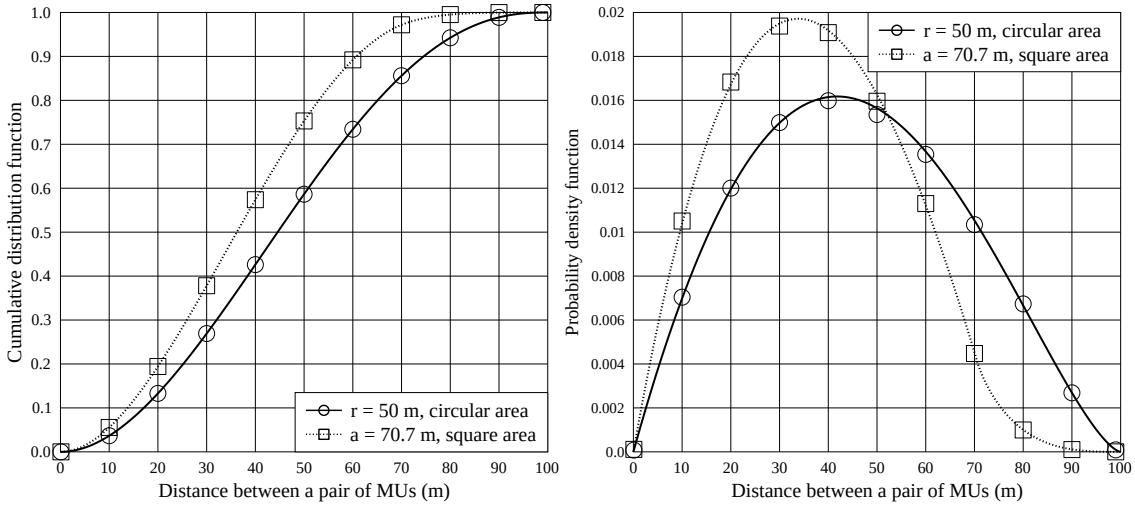

(a) Cumulative distribution function

(b) Probability density function

Figure 6.16: The distance distribution between a pair of MUs, when both of the MUs roam within a square/circle area, as shown in Figures 6.1(g)/(h). The square area and the circular area both have a radius of $r = 50$ m. The analytical CDFs are formulated in Eqs.(6.27) and (6.32), while the analytical PDFs are formulated in Eqs.(6.28) and (6.31).

m. In both Figures 6.15(a) and (b), the same angle of $\theta = \pi/6$ is assumed, while the distance from the BS to the centre of the square varies from 20 m to 120 m. As shown in Figure 6.15(a), when the BS is outside the square area in Figure 6.1(e), both the minimum and maximum achievable distances depend on the distance d. As the BS is positioned farther away from the centre of the square area, the random distance between the BS and the MU may assume higher minimum and maximum values, which results in the CDF shifting towards the right hand side. However, as shown in Figure.6.15(b), only the maximum distance between the BS and the MU depends on d, while the minimum distances are all zeros for different values of d. As the BS is positioned farther away from the centre of the square area of Figure 6.1(f), the random distance between the BS and the MU is distributed across a wider region. Moreover, the accuracy of the analytical results that we derived in Theorems 6.5 and 6.6 is validated by the Monte-Carlo simulations, as shown in both Figures 6.15(a) and (b).

Finally, we evaluate the CDF and the PDF of the random distance between a pair of MUs, both of which roam within a square/circular area by obeying the uniform mobility model, as shown in Figures 6.1(g)(h). The radius of both the circular and square areas is $r = 50$ m. Note that the corresponding side-length of the square area is then $a = 70.7$ m. As shown in Figure.6.16(a), the CDF of the random distance between a pair of MUs for the square area is higher than that for the circular area. As shown in Figure 6.16(b), both of the PDFs in these two scenarios firstly increase and then decay after reaching their peaks. Furthermore, we also observe from Figure 6.16(b) that the random distance for the square area scenario of Figure 6.1(g) is more likely to take a small value than that for the circular area scenario of Figure 6.1(h). Moreover, the accuracy of the analytical results expressed in Eqs.(6.27), (6.28), (6.31) and (6.32) are validated by the Monte-Carlo simulations, as shown in both Figures.6.16(a) and (b).

6.6 Conclusions

In this chapter, we derived the distance distribution between the BS (static transmitter) and the MU (mobile receiver) as well as that between a pair of MUs (mobile transmitter and receiver), when the MUs roam within a bounded area by obeying the uniform mobility model, as introduced in Definition 6.1. Firstly, we studied

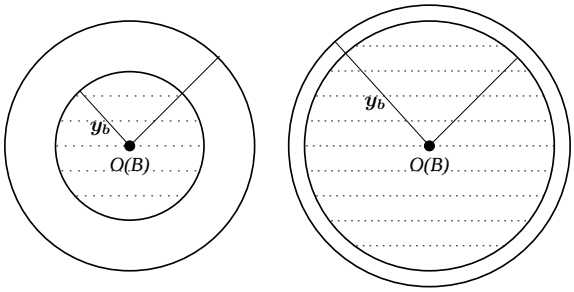

(a) $y_b \leq r$ (b) $y_b > r$

Figure 6.17: An example of a circular cell.

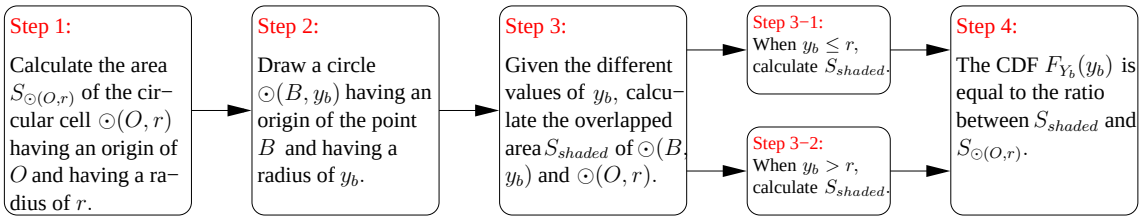

Figure 6.18: The geometric methodology invoked in the proof of Theorem 6.1. Please refer to Figure 6.17 for the definitions of all the geometric notations.

the scenario of the classic cellular communication in Section 6.2, when the BS is located at the centre of the cell while the MU roams within the entire cell by following the uniform mobility model, as shown in Figures 6.1(a)(b). The cell is modelled by either a circular area or by an l-sided regular polygonal area. Both the CDF and the PDF of the random distance between the BS and the MU are derived in closed-form formulas. Then in Section 6.3, we focused our attention on the distance distribution between the BS and the MU, when the MU roams within a bounded area, modelled by either a circular area or a square area, while the BS is located at an arbitrary position either outside or inside the bounded area, as shown in Figures 6.1(c)-(f). At last, in Section 6.4, we further derived the closed-form CDF and PDF of the random distance between a pair of MUs, when both of them roam within a bounded area, which can be modelled by either a square area of Figure 6.1(g) or a circular area of Figure 6.1(h). According to our numerical results, the accuracy of our theoretical analysis is confirmed by the Monte-Carlo simulation results.

By relying on the statistical properties of the random distance between the transmitter (either static or mobile) and the mobile receiver, we are capable of precisely predicting a range of communication metrics at the system level, such as the statistical properties of the PL, the spectral efficiency in both single-hop transmission and multicast transmission, as well as the number of MUs experiencing an outage in the broadcast scenario. Furthermore, the statistical properties of the random distance are also exploited for evaluating the throughput performance of both the cellular link and opportunistic link in Chapters 3–5.

Appendix

6.A Proofs of the Theorems in Section 6.2

6.A.1 Proof of Theorem 6.1

The methodology invoked in this proof is summarised in Figure 6.18.

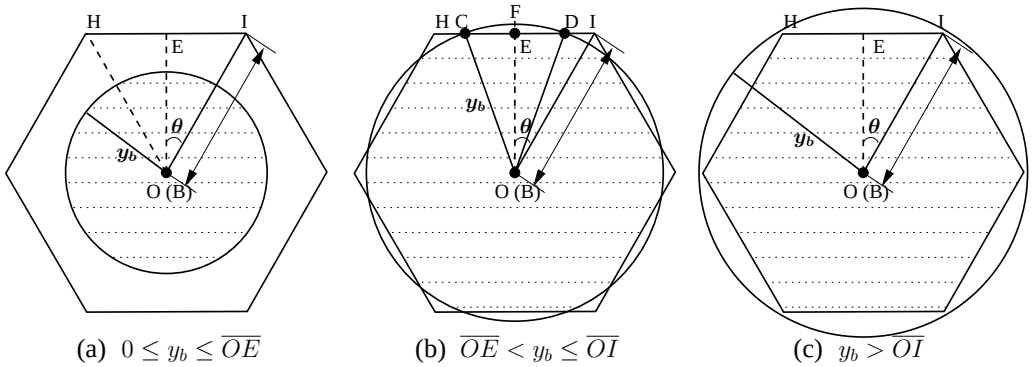

(a) $0 \leq y_b \leq \overline{OE}$ (b) $\overline{OE} < y_b \leq \overline{OI}$ (c) $y_b > \overline{OI}$

Figure 6.19: l-sided regular polygon cell: a regula hexagon example

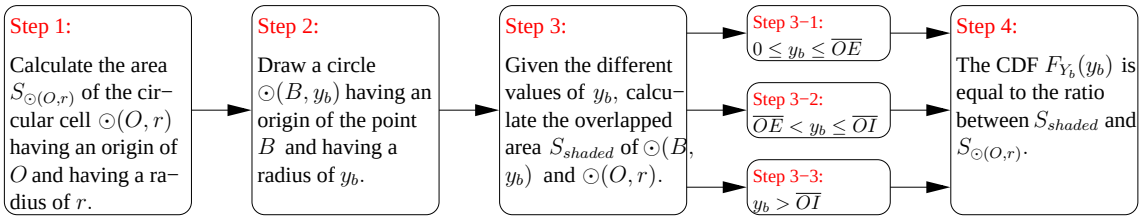

Figure 6.20: The geometric methodology invoked in the proof of Theorem 6.2. Please refer to Figure 6.19 for the definitions of all the geometric notations.

In this scenario, the cell is modelled by a circular area having the point O at its center and having r as its radius, which is denoted as $\odot(O,r)$. The area of $\odot(O,r)$ is expressed as $S_{\odot(O,r)} = \pi r^2$ (Step 1 of Figure 6.18).

The BS is positioned at the centre of this circular area, within which a MU roams by obeying the uniform mobility model, as presented in Definition 6.1. We draw another circle having O as the center and y_b as the radius, which is denoted as $\odot(O,y_b)$ (Step 2 of Figure 6.18), as shown in Figure 6.17.

According to the uniform mobility model, the MU might appear at any position in the circular area with equal probability. Therefore, if the MU appears within $\odot(O,y_b)$, the distance between this MU and the BS is shorter than y_b. Furthermore, since the probability of the MU appearing within $\odot(O,y_b)$ is equal to the ratio between the area $S_{\odot(O,y_b)}$ of $\odot(O,y_b)$ and the area $S_{\odot(O,r)}$ of $\odot(O,r)$, then the CDF $F_{Y_b}(y_b)$ of the random distance Y_b between the BS and the MU is derived as

$$F_{Y_b}(y_b) = \frac{S_{\odot(O,y_b)}}{S_{\odot(O,r)}} = \frac{\pi y_b^2}{\pi r^2} = \frac{y_b^2}{r^2}, \tag{6.33}$$

for $0 \leq y_b \leq r$ (Step 3-1 and Step 4 of Figure 6.18). Since the movement of the MU is bounded within the circular area $\odot(O,r)$ studied, the MU is unlikely to appear within the annulus, when y_b is longer than r, as shown in Figure 6.17(b). As a result, for $y_b > r$, the CDF $F_{Y_b}(y_b)$ is apparently equal to one (Step 3-2 and Step 4 of Figure 6.18).

Summarising the above CDF results, we finally arrive at the CDF of the random distance Y_b between the centrally-positioned BS and the MU obeying the uniform mobility model within a circular cell, as expressed in Eq.(6.2) of Theorem 6.1. Differentiating the CDFs with respect to y_b in different regions, we may obtain the corresponding PDFs, as expressed in Eq.(6.3) of Theorem 6.1. Hence Theorem 6.1 has been proven. □

6.A.2 Proof of Theorem 6.2

The methodology invoked in this proof is summarised in Figure 6.20.

In this scenario, the cell is modelled by a l-sided regular polygon having O as the centre and having r as the radius. The radius of a regular polygon is defined as the length of the straight line connecting the centre to one of the vertices. The coverage of this cell is denoted as a triple $\square(O,r,l)$, where l is the number of sides. As shown in Figure 6.19, we assume $\angle EOI = \theta$. Due to the symmetry of the l-sided regular polygon, the area of $\square(O,r,l)$ can be expressed as (Step 1 of Figure 6.20)

$$\begin{aligned} S_{\square(O,r,l)} &= l \cdot S_{\triangle HOI} = l \cdot \frac{1}{2}\overline{HI} \cdot \overline{OE} \\ &= lr^2 \sin\theta\cos\theta. \end{aligned} \tag{6.34}$$

The angle θ is determined by the number of sides that the regular polygon has, which is formulated as $\theta = \frac{1}{2} \cdot \frac{2\pi}{l} = \frac{\pi}{l}$.

As characterised in Figure 6.1(b), the BS is positioned at the centre of this l-sided regular polygon. A MU roams within this polygon by obeying the uniform mobility model, as defined in Definition 6.1. We draw an circle having O as the centre and y_b as the radius (Step 2 of Figure 6.20). This circular area is denoted by $\odot(O,y_b)$, as shown in Figure 6.19.

According to the uniform mobility model, the MU might appear at any locations within the l-sided polygon with equal probability. Therefore, if the MU appears within the overlapped area of the l-sided regular polygon $\square(O,r,l)$ and the circle $\odot(O,y_b)$, the distance between this MU and the BS is shorter than y_b. Again, this overlapped area is denoted as the shaded part in Figure 6.19. As a result, the CDF $F_{Y_b}(y_b)$ of the random distance Y_b between the BS and the MU is expressed as the ratio between the area of the shaded part and the area of the l-sided regular polygon.

In order to obtain the CDF of the random distance Y_b, we have to derive the overlapped area of the l-sided polygon $\square(O,r,l)$ and of the circle $\odot(O,y_b)$ (Step 3 of Figure 6.20). However, given the different values of y_b, we have to discuss the following cases for calculating the overlapped area and the CDF $F_{Y_b}(y_b)$:

Case I: $0 \leq y_b \leq \overline{OE}$

In this case, the circle $\odot(O,y_b)$ is surrounded by the l-sided regular polygon $\square(O,a)$, as shown in Figure 6.19(a). Hence, the overlapped area is equal to the circular area of $\odot(O,y_b)$, which is shaded in Figure 6.19(a) and given by $S_{shade} = \pi y_b^2$ (Step 3-1 of Figure 6.20). As a result, the CDF of the random distance Y_b in this case is expressed as (Step 4 of Figure 6.20)

$$F_{Y_b}(y_b) = \frac{S_{shade}}{S_{\square(O,r,l)}} = \frac{\pi}{l\tan\theta}\left(\frac{y_b}{r\cos\theta}\right)^2,\ 0 \leq y_b \leq r\cos\theta. \tag{6.35}$$

Case II: $\overline{OE} < y_b \leq \overline{OI}$

In this case, the overlapped area has an irregular shape, which is shaded in Figure 6.19(b). The area of this shaded part is derived by subtracting the number l of identical segments, like the segment $CFDE$ from the area of the circle $\odot(O,y_b)$, which is expressed as (Step 3-2 of Figure 6.20)

$$\begin{aligned} S_{shaded} &= S_{\odot(O,y_b)} - l \cdot S_{CFDE} \\ &= \pi y_b^2 - y_b^2 l \arccos\frac{r\cos\theta}{y_b} + lr\cos\theta\sqrt{y_b^2 - r^2\cos^2\theta}. \\ &= y_b^2\left(\pi - l\arccos\frac{r\cos\theta}{y_b}\right) + lr\cos\theta\sqrt{y_b^2 - r^2\cos^2\theta}. \end{aligned} \tag{6.36}$$

As a result, the CDF of the random distance Y_b in this case is expressed as (Step 4 of Figure 6.20)

$$\begin{aligned} F_{y_b}(y_b) &= \frac{S_{shaded}}{S_{\square(O,r,l)}} \\ &= \frac{1}{l\tan\theta}\left(\frac{y_b}{r\cos\theta}\right)^2\left(\pi - l\arccos\left(\frac{y_b}{r\cos\theta}\right)^{-1}\right) + \frac{1}{\tan\theta}\sqrt{\left(\frac{y_b}{r\cos\theta}\right)^2 - 1} \end{aligned} \tag{6.37}$$

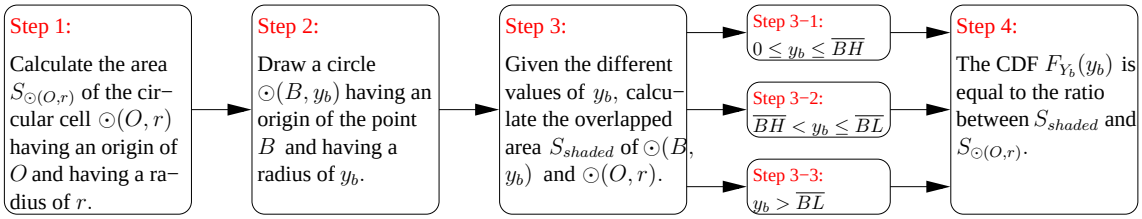

Figure 6.21: The geometric methodology invoked in the proofs of Theorems 6.3 and 6.4. Please refer to Figures 6.22 and 6.23 for the definitions of all the geometric notations.

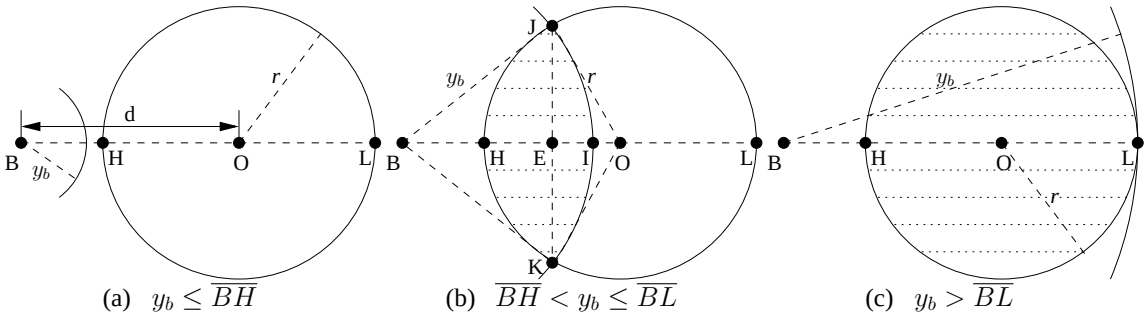

Figure 6.22: The BS is outside the bounded circular area corresponding to the scenario of Figure 6.1(c).

for $r\cos\theta < y_b \le r$.

Case III: $y_b > \overline{OI}$

In this situation, the l-sided regular polygon $\square(O,r,l)$ is completely surrounded by the circle $\odot(O,y_b)$ (Step 3-3 of Figure 6.20). As a result, the random distance between the BS and the MU is definitely shorter than y_b with a unity probability, which indicates that the CDF of the random distance Y_b is $F_{Y_b}(y_b) = 1$ for $y_b > r$ (Step 4 of Figure 6.20).

Summarising the above CDFs derived for the different cases, we arrive at Eq.(6.5) in Theorem 6.2. Differentiating the above CDFs derived for the different cases with respect to y_b, we arrive at the corresponding PDF of the distance Y_b between the centrally-positioned BS and the MU obeying the uniform mobility model within a l-sided regular polygon, as expressed in Eq.(6.6). As a result, Theorem 6.2 has been proven. □

6.B Proofs of the Theorems in Section 6.3

The proofs of Theorems 6.3 and 6.4 share a similar methodology, which is summarised in Figure 6.21.

6.B.1 Proof of Theorem 6.3

The bounded area, which restricts the movement of the MU, is modelled by the circular area $\odot(O,r)$, as shown in Figure 6.22. The area of $\odot(O,r)$ is expressed as $S_{\odot(O,r)} = \pi r^2$ (Step 1 of Figure 6.21).

The BS is at the position B, which is d m away from the centre O. Since the BS is outside $\odot(O,r)$, we have $d > r$. We draw another circle having its centre at the point B and having a radius of y_b. This circle is denoted as $\odot(B,y_b)$ (Step 2 of Figure 6.21).

If the MU is within the overlapped area of $\odot(B,y_b)$ and $\odot(O,r)$, the distance between the MU and the BS is shorter than y_b. Since the MU considered may appear at any positions within the circular area $\odot(O,r)$,

the CDF of the random distance Y_b is the ratio between the overlapped area and the entire area of $\odot(O,r)$. When the BS is outside the circular area, namely we have $d > r$, the following cases have to be specifically considered:

Case I: $0 \leq y_b \leq \overline{BH}$

In this case, as shown in Figure 6.22(a), $\overline{BH} = d - r$ and $\odot(B, y_b)$ does not overlap with $\odot(O,r)$. As a result, the area of the overlapped part is zero (Step 3-1 of Figure 6.21), which indicates that the CDF $F_{Y_b}(y_b)$ is also zero, when $0 \leq y_b \leq d - r$ (Step 4 of Figure 6.21).

Case II: $\overline{BH} < y_b \leq \overline{BL}$

In this case, $\odot(B, y_b)$ intersects $\odot(O,r)$ at the points I and K, as shown in Figure 6.22(b). We connect the points B and O with the straight line $\overline{OB}$, which intersects $\odot(B, y_b)$ and $\odot(O,r)$ at the points H , I and L, respectively. The area of the shaded part of Figure 6.22(b) can be characterised by the following expression (Step 3-2 of Figure 6.21):

$$\begin{aligned} S_{shaded} &= (S_{\widehat{JOKH}} + S_{\widehat{JBKI}}) - S_{\square BJOK} \\ &= r^2 \arccos\left(\frac{r^2 + d^2 - y_b^2}{2rd}\right) + y_b^2 \arccos\left(\frac{y_b^2 + d^2 - r^2}{2y_b d}\right) \\ &\quad - \frac{1}{2}\sqrt{4r^2d^2 - (r^2 + d^2 - y_b^2)^2}, \end{aligned} \tag{6.38}$$

where $S_{\widehat{JOKH}}$ and $S_{\widehat{JBKI}}$ denote the areas of the sectors $\widehat{JOKH}$ and $\widehat{JBKI}$, respectively, while $S_{\square BJOK}$ denotes the area of the polygon $\square BJOK$, as shown in Figure 6.22. Hence, the CDF of Y_b can be obtained as (Step 4 of Figure 6.21)

$$\begin{aligned} F_{Y_b}(y_b) &= S_{shaded}/S_{\odot(O,r)} \\ &= \frac{1}{\pi}\left[\arccos\left(\frac{r^2 + d^2 - y_b^2}{2rd}\right) + \frac{y_b^2}{r^2}\arccos\left(\frac{y_b^2 + d^2 - r^2}{2y_b d}\right)\right. \\ &\quad \left. - \frac{1}{2r^2}\sqrt{4r^2d^2 - (r^2 + d^2 - y_b^2)^2}\right] \end{aligned} \tag{6.39}$$

for $d - r < y_b \leq d + r$.

Case III: $y_b > \overline{BL}$

In this case, as shown in Figure 6.22(c), we have $\overline{BL} = d + r$ and the overlapped part between $\odot(O,r)$ and $\odot(B, y_b)$ is the entire area of $\odot(O,r)$ (Step 3-3 of Figure 6.21). Therefore, the CDF $F_{Y_b}(y_b)$ of the random distance Y_b is expressed as $F_{Y_b}(y_b) = S_{\odot(O,r)}/S_{\odot(O,r)} = 1$ for $y_b > d + r$ (Step 4 of Figure 6.21).

Summarising the above CDFs derived for the different cases, we are able to obtain Eq.(6.7) in Theorem 6.3. Differentiating the above CDFs derived for the different cases with respect to y_b, we may arrive at the corresponding PDFs of the distance Y_b between the BS positioned outside the circular area and the MU obeying the uniform mobility model within the circular area, as expressed in Eq.(6.8). Hence Theorem 6.3 has been proven. □

6.B.2 Proof of Theorem 6.4

Similar to the proof of Theorem 6.3 in the last section, the area of the circle $\odot(O,r)$ is expressed as $S_{\odot(O,r)} = \pi r^2$ (Step 1 of Figure 6.21). Let us now draw another circle, whose centre is at point B and whose radius is y_b, as shown in Figure 6.23. This circle is denoted as $\odot(B, y_b)$ (Step 2 of Figure 6.21). If the MU is within the overlapped area of $\odot(B, y_b)$ and $\odot(O,r)$, the distance between the MU and the BS is shorter than y_b. Since the MU studied may appear at any position within the circular area $\odot(O,r)$, the CDF of the random

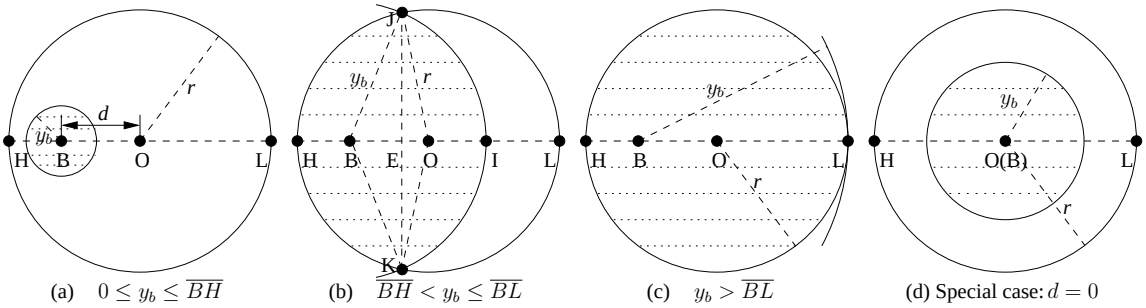

Figure 6.23: The BS is inside the bounded circular area corresponding to the scenario of Figure 6.1(d).

distance Y_b is the ratio between the overlapped area and the whole area of $\odot(O,r)$. When the BS is inside the circular area studied and not at the centre, namely we have $0 < d \le r$, the following cases have to be specifically considered:

Case I: $0 \le y_b \le \overline{BH}$

In this case, as shown in Figure 6.23(a), we have $\overline{BH} = r - d$ and the overlapped area is the entire circular area of $\odot(B, y_b)$ (Step 3-1 of Figure 6.21). Hence, the CDF of the random distance Y_b should be expressed as (Step 4 of Figure 6.21)

$$F_{Y_b}(y_b) = \frac{S_{shaded}}{S_{\odot(O,r)}} = \frac{y_b^2}{r^2} \tag{6.40}$$

for $0 \le y_b \le r - d$.

Case II: $\overline{BH} < y_b \le \overline{BL}$

As shown in Figure 6.23(b), we have $\overline{BH} = r - d$ and $\overline{HL} = r + d$. In this case, the overlapped area is denoted as the shaded part of Figure 6.23, which can be calculated by the same equation as presented in Eq.(6.38) (Step 3-2 of Figure 6.21). Hence, the CDF $F_{Y_b}(y_b)$ can be expressed by Eq.(6.39) for $r - d < y_b \le r + d$ (Step 4 of Figure 6.21).

Case III: $y_b > \overline{BL}$

As shown in Figure 6.23(c), we have $\overline{HL} = r + d$. In this case, the overlapped part between $\odot(O,r)$ and $\odot(B, y_b)$ is the entire area of $\odot(O,r)$ (Step 3-3 of Figure 6.21). Therefore, the CDF $F_{Y_b}(y_b)$ of the random distance Y_b is expressed as $F_{Y_b}(y_b) = S_{\odot(O,r)}/S_{\odot(O,r)} = 1$ (Step 4 of Figure 6.21).

Summarising the above CDFs derived for the different cases, we are able to obtain Eq.(6.9) in Theorem 6.4. Differentiating the above CDFs derived in different cases with respect to y_b, we may arrive at the corresponding PDF of the distance Y_b between the BS positioned inside the circular area and the MU obeying the uniform mobility model within the circular area, as expressed in Eq.(6.10). Therefore Theorem 6.4 has been proven. □

6.B.3 Proof of Theorem 6.5

The methodology invoked in the proof of Theorem 6.5 is summarised in Figure 6.25.

Since the movement of the MU is restricted in a square $\square HIJK$ having its centre at the point O and having a side-length of a, as shown in Figure 6.24, the area of $\square HIJK$ is expressed as $S_{\square HIJK} = a^2$ (Step 1 of Figure 6.25).

We draw a circle having the point B as the centre and having y_b as the radius. This circle is represented as $\odot(B, y_b)$ (Step 2 of Figure 6.25). The overlapped area between $\square HIJK$ and $\odot(B, y_b)$ is shaded in Figure

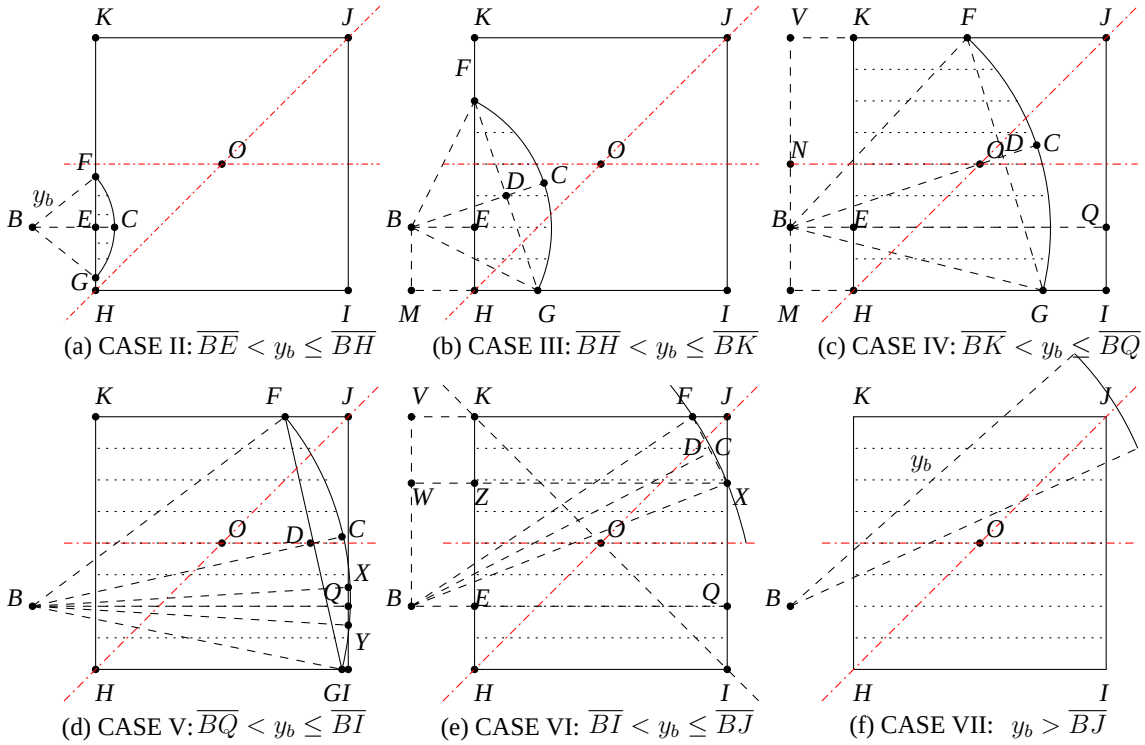

Figure 6.24: The BS is outside the bounded square area

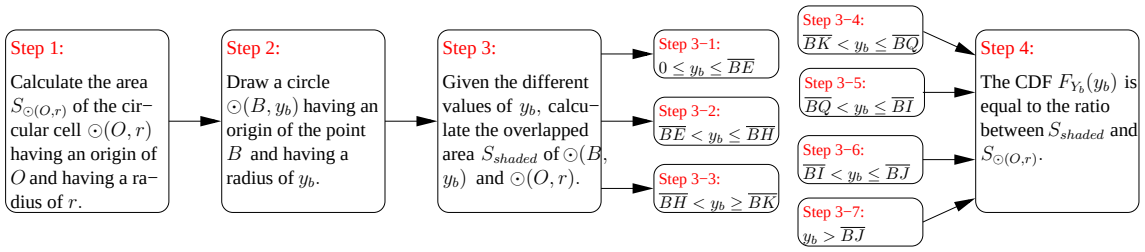

Figure 6.25: The geometric methodology invoked in the proof of Theorems 6.5. Please refer to Figure 6.24 for the definitions of all the geometric notations.

6.24. Since the position of the MU is uniformly distributed within $\square HIJK$ according to the uniform mobility model, the CDF $F_{Y_b}(y_b)$ can be expressed as the ratio of the shaded area to the area of $\square HIJK$. Given the different legitimate values of y_b, the following cases have to be discussed in order to derive the area of the shaded part (Step 3 of Figure 6.25) and hence to derive $F_{Y_b}(y_b)$ (Step 4 of Figure 6.25).

CASE I: $0 \leq y_b \leq \overline{BE}$.

In this case, the circle $\odot(B,y_b)$ does not overlap the square $\square HIJK$. As a result, the area of the overlapped part is zero (Step 3-1 of Figure 6.25), which indicates that the CDF $F^I_{Y_b}(y_b)$ is also zero, when $0 \leq y_b \leq d\cos\theta - a/2$ (Step 4 of Figure 6.25).

CASE II: $\overline{BE} < y_b \leq \overline{BH}$

In this case, as shown in Figure 6.24(a), the circle $\odot(B,y_b)$ intersects the side $\overline{KH}$ at the points F and G. The extension of the straight line $\overline{BE}$ intersects the circle $\odot(B,y_b)$ at the point C. As a result, the overlapped area is a small segment, which is shaded in Figure 6.24(a). Hence this shaded area can be expressed as (Step

3-2 of Figure 6.25)

$$S_{shade}^{II} = S_{\widehat{FBGC}} - S_{\triangle FBG} = y_b^2 \arccos \frac{d\cos\theta - \frac{a}{2}}{y_b} - \left(d\cos\theta - \frac{a}{2}\right)\sqrt{y_b^2 - \left(d\cos\theta - \frac{a}{2}\right)^2}, \tag{6.41}$$

where $S_{\widehat{FBGC}}$ is the area of the sector $\widehat{FBGC}$ and $S_{\triangle FBG}$ is the area of the triangle $\triangle FBG$, as portrayed in Figure 6.24(a).

Finally, in this case, the CDF of the random distance Y_b is given by the ratio between S_{shade}^{II} and $S_{\square HIJK}$, which is presented as (Step 4 of Figure 6.25)

$$F_{Y_b}^{II}(y_b) = \frac{S_{shade}^{II}}{S_{\square HIJK}} = \frac{1}{a^2}\left[y_b^2 \arccos \frac{d\cos\theta - \frac{a}{2}}{y_b} - \left(d\cos\theta - \frac{a}{2}\right)\sqrt{y_b^2 - \left(d\cos\theta - \frac{a}{2}\right)^2}\right] \tag{6.42}$$

for $(d\cos\theta - a/2) < y_b \leq \sqrt{a^2/2 + d^2 - ad(\sin\theta + \cos\theta)}$, where $S_{\square HIJK} = a^2$.

CASE III: $\overline{BH} < y_b \leq \overline{BK}$

In this case, as shown in Figure 6.24(b), the circle $\odot(B, y_b)$ intersects the side $\overline{KH}$ of the square $\square HIJK$ at the point F and intersects the side $\overline{HI}$ of the square $\square HIJK$ at the point G. The line $\overline{BC}$ is perpendicular to $\overline{FG}$ and they intersect at the point D. The overlapped area of $\odot(B, y_b)$ and $\square HIJK$ is denoted as the shaded part in Figure 6.24(b). As a result, this shaded area can be expressed as (Step 3-3 of Figure 6.25)

$$\begin{aligned} S_{shade}^{III} &= S_{\widehat{FBGC}} - S_{\triangle FBG} + S_{\triangle FHG} \\ &= \frac{y_b^2}{2}\left(\arcsin\frac{\frac{a}{2} - d\sin\theta}{y_b} + \arccos\frac{d\cos\theta - \frac{a}{2}}{y_b}\right) \\ &\quad + \frac{1}{2}\left[(\frac{a}{2} - d\sin\theta)\sqrt{y_b^2 - (\frac{a}{2} - d\sin\theta)^2} - (d\cos\theta - \frac{a}{2})\sqrt{y_b^2 - (d\cos\theta - \frac{a}{2})^2}\right. \\ &\quad \left. -2(d\cos\theta - \frac{a}{2})(\frac{a}{2} - d\sin\theta)\right], \end{aligned} \tag{6.43}$$

where $S_{\widehat{FBGC}}$ denotes the area of the sector $\widehat{FBGC}$, $S_{\triangle FBG}$ denotes the area of the triangle $\triangle FBG$ and $S_{\triangle FHG}$ denotes the area of the triangle $\triangle FHG$, as portrayed in Figure 6.24(b).

Finally, in this case, the CDF of the random distance Y_b is the ratio between S_{shade}^{III} and $S_{\square HIJK} = a^2$, which is formulated as (Step 4 of Figure 6.25)

$$\begin{aligned} F_{Y_b}^{III}(y_b) &= \frac{S_{shade}^{III}}{S_{\square HIJK}} \\ &= \frac{y_b^2}{2a^2}\left(\arcsin\frac{\frac{a}{2} - d\sin\theta}{y_b} + \arccos\frac{d\cos\theta - \frac{a}{2}}{y_b}\right) \\ &\quad + \frac{1}{2a^2}\left[(\frac{a}{2} - d\sin\theta)\sqrt{y_b^2 - (\frac{a}{2} - d\sin\theta)^2} - (d\cos\theta - \frac{a}{2})\sqrt{y_b^2 - (d\cos\theta - \frac{a}{2})^2}\right. \\ &\quad \left. -2(d\cos\theta - \frac{a}{2})(\frac{a}{2} - d\sin\theta)\right] \end{aligned} \tag{6.44}$$

for $\sqrt{a^2/2 + d^2 - ad(\sin\theta + \cos\theta)} < y_b \leq \sqrt{a^2/2 + d^2 - ad(\cos\theta - \sin\theta)}$.

CASE IV: $\overline{BK} < y_b \leq \overline{BQ}$

In this case, as shown in Figure 6.24(c), the circle $\odot(B, y_b)$ intersects the side $\overline{JK}$ of the square $\square HIJK$ at the point F and intersects the side $\overline{HI}$ of the square $\square HIJK$ at the point G. Furthermore, $\overline{BC}$ and $\overline{FG}$ are vertical lines and they intersect at the point D. The overlapped area of $\odot(B, y_b)$ and $\square HIJK$ is denoted by

the shaded part in Figure 6.24(c). Then, this shaded area can be expressed as (Step 3-4 of Figure 6.25)

$$\begin{aligned} S^{IV}_{shade} &= S_{\widehat{FBGC}} - S_{\triangle FBG} + S_{\square HGFK} \\ &= \frac{y_b^2}{2}\left(\arcsin\frac{\frac{a}{2}-d\sin\theta}{y_b} + \arcsin\frac{\frac{a}{2}+d\sin\theta}{y_b}\right) \\ &\quad + \frac{1}{2}\left[(\frac{a}{2}-d\sin\theta)\sqrt{y_b^2-(\frac{a}{2}-d\sin\theta)^2} + (\frac{a}{2}+d\sin\theta)\sqrt{y_b^2-(\frac{a}{2}+d\sin\theta)^2}\right. \\ &\qquad \left. -2a(d\cos\theta-\frac{a}{2})\right], \end{aligned} \tag{6.45}$$

where $S_{\widehat{FBGC}}$ denotes the area of the sector $\widehat{FBGC}$, $S_{\triangle FBG}$ denotes the area of the triangle $\triangle FBG$ and $S_{\square HGFK}$ denotes the area of the trapezium $\square HGFK$, as shown in Figure 6.24(c).

Finally, in this case, the CDF of the random distance Y_b is the ratio of S^{IV}_{shade} to $S_{\square HIJK} = a^2$, which is expressed as (Step 4 of Figure 6.25)

$$\begin{aligned} F^{IV}_{Y_b}(y_b) &= \frac{S^{IV}_{shade}}{S_{\square HIJK}} \\ &= \frac{y_b^2}{2a^2}\left(\arcsin\frac{\frac{a}{2}-d\sin\theta}{y_b} + \arcsin\frac{\frac{a}{2}+d\sin\theta}{y_b}\right) \\ &\quad + \frac{1}{2a^2}\left[(\frac{a}{2}-d\sin\theta)\sqrt{y_b^2-(\frac{a}{2}-d\sin\theta)^2} + (\frac{a}{2}+d\sin\theta)\sqrt{y_b^2-(\frac{a}{2}+d\sin\theta)^2}\right. \\ &\qquad \left. -2a(d\cos\theta-\frac{a}{2})\right] \end{aligned} \tag{6.46}$$

for $\sqrt{a^2/2+d^2-ad(\cos\theta-\sin\theta)} < y_b \le (d\cos\theta + a/2)$.

CASE V: $\overline{BQ} < y_b \le \overline{BI}$

In this case, as shown in Figure 6.24(d), the circle $\odot(B, y_b)$ intersects the side $\overline{JK}$ of the square $\square HIJK$ at the point F and intersects the side $\overline{HI}$ at the point G. Moreover, the side $\overline{IJ}$ has two intersection points with the circle $\odot(B, y_b)$, namely the points X and Y, as shown in Figure 6.24(d). The straight line $\overline{BQ}$ is perpendicular to the side $\overline{IJ}$ and intersects $\overline{IJ}$ at the point Q, whose length is $\overline{BQ} = d\cos\theta + a/2$.

The shape of the shaded part in Figure 6.24(d) is slightly different from that in Figure 6.24(c). In order to derive the area S^{V}_{shade} of the shaded part in Figure 6.24(d), we have to subtract the area of a small segment, which is formed by the arc $\widehat{XY}$ and the straight line $\overline{XY}$, from the sum of the area of a trapezium $\square HGFK$ and the area of a segment formed by the arc $\widehat{FCG}$ and the line $\overline{FG}$. As a result, the area of the shaded part of Figure 6.24(d) can be derived as (Step 3-5 of Figure 6.25)

$$\begin{aligned} S^{V}_{shade} &= S^{IV}_{shade} - S_{\widehat{XBY}} + S_{\triangle XBY} \\ &= \frac{y_b^2}{2}\left(\arcsin\frac{\frac{a}{2}-d\sin\theta}{y_b} + \arcsin\frac{\frac{a}{2}+d\sin\theta}{y_b} - 2\arccos\frac{d\cos\theta+\frac{a}{2}}{y_b}\right) \\ &\quad + \frac{1}{2}\left[(\frac{a}{2}-d\sin\theta)\sqrt{y_b^2-(\frac{a}{2}-d\sin\theta)^2} + (\frac{a}{2}+d\sin\theta)\sqrt{y_b^2-(\frac{a}{2}+d\sin\theta)^2}\right. \\ &\qquad \left. +2(d\cos\theta+\frac{a}{2})\sqrt{y_b^2-(d\cos\theta+\frac{a}{2})^2} - 2a(d\cos\theta-\frac{a}{2})\right], \end{aligned} \tag{6.47}$$

where S^{IV}_{shade} is calculated by Eq.(6.45), $S_{\widehat{XBY}}$ denotes the area of the sector $\widehat{XBY}$ and $S_{\triangle XBY}$ denotes the area of the triangle $\triangle XBY$, as shown in Figure 6.24(d).

Finally, in this case, the CDF of the random distance Y_b is the ratio between S^{V}_{shade} and $S_{\square HIJK} = a^2$,

which is presented as (Step 4 of Figure 6.25)

$$\begin{aligned}
F_{Y_b}^{V}(y_b) &= \frac{S_{shade}^{V}}{S_{\square HIJK}} \\
&= \frac{y_b^2}{2a^2}\left(\arcsin\frac{\frac{a}{2}-d\sin\theta}{y_b}+\arcsin\frac{\frac{a}{2}+d\sin\theta}{y_b}-2\arccos\frac{d\cos\theta+\frac{a}{2}}{y_b}\right) \\
&\quad+\frac{1}{2a^2}\left[(\frac{a}{2}-d\sin\theta)\sqrt{y_b^2-(\frac{a}{2}-d\sin\theta)^2}+(\frac{a}{2}+d\sin\theta)\sqrt{y_b^2-(\frac{a}{2}+d\sin\theta)^2}\right. \\
&\qquad\left.+2(d\cos\theta+\frac{a}{2})\sqrt{y_b^2-(d\cos\theta+\frac{a}{2})^2}-2a(d\cos\theta-\frac{a}{2})\right]
\end{aligned} \tag{6.48}$$

for $(d\cos\theta + a/2) < y_b \leq \sqrt{a^2/2 + d^2 + ad(\cos\theta - \sin\theta)}$.

CASE VI: $\overline{BI} < y_b \leq \overline{BJ}$

In this case, as shown in Figure 6.24(e), the circle $\odot(B, y_b)$ intersects the side $\overline{JK}$ at the point F and intersects the side $\overline{IJ}$ at the point X. The straight line $\overline{BC}$ is perpendicular to the line $\overline{FX}$ intersecting $\overline{FX}$ at the point D as well as intersecting the circle $\odot(B, y_b)$ at the point C of Figure 6.24(e). Furthermore, $\overline{WX}$ is a horizontal line, which intersects the side KH of $\square HIJK$ at the point Z. The overlapped area between the circle $\odot(B, y_b)$ and the square $\square HIJK$ is denoted as the shaded part in Figure 6.24(e). Then, the area of this shaded part in Figure 6.5(e) is formulated as (Step 3-6 of Figure 6.25)

$$\begin{aligned}
S_{shade}^{VI} &= S_{\widehat{FBXC}} - S_{\triangle FBX} + S_{\square KFXZ} + S_{\square HIXZ} \\
&= \frac{y^2}{2}\left(\arcsin\frac{\frac{a}{2}+d\sin\theta}{y_b}-\arccos\frac{\frac{a}{2}+d\cos\theta}{y_b}\right) \\
&\quad+\frac{1}{2}\left[(\frac{a}{2}+d\sin\theta)\sqrt{y_b^2-(\frac{a}{2}+d\sin\theta)^2}+(d\cos\theta+\frac{a}{2})\sqrt{y_b^2-(\frac{a}{2}+d\cos\theta)^2}\right. \\
&\qquad\left.+2a(\frac{a}{2}-d\sin\theta)-2(\frac{a}{2}+d\sin\theta)(d\cos\theta-\frac{a}{2})\right],
\end{aligned} \tag{6.49}$$

where $S_{\widehat{FBXC}}$ denotes the area of the sector $\widehat{FBXC}$, $S_{\triangle FBX}$ represents the area of the triangle $\triangle FBX$, $S_{\square KFXZ}$ denotes the area of the trapezium $\square KFXZ$ and $S_{\square HIXZ}$ is the area of the rectangle $\square HIXZ$, as portrayed in Figure 6.5(e).

Finally, in this case, the CDF of the random distance Y_b is the ratio between S_{shade}^{VI} and $S_{\square HIJK} = a^2$, which is expressed as (Step 4 of Figure 6.25)

$$\begin{aligned}
F_{Y_b}^{VI}(y_b) &= \frac{S_{shade}^{VI}}{S_{\square HIJK}} \\
&= \frac{y_b^2}{2a^2}\left(\arcsin\frac{\frac{a}{2}+d\sin\theta}{y_b}-\arccos\frac{\frac{a}{2}+d\cos\theta}{y_b}\right) \\
&\quad+\frac{1}{2a^2}\left[(\frac{a}{2}+d\sin\theta)\sqrt{y_b^2-(\frac{a}{2}+d\sin\theta)^2}+(d\cos\theta+\frac{a}{2})\sqrt{y_b^2-(\frac{a}{2}+d\cos\theta)^2}\right. \\
&\qquad\left.+2a(\frac{a}{2}-d\sin\theta)-2(\frac{a}{2}+d\sin\theta)(d\cos\theta-\frac{a}{2})\right]
\end{aligned} \tag{6.50}$$

for $\sqrt{a^2/2 + d^2 + ad(\cos\theta - \sin\theta)} < y_b \leq \sqrt{a^2/2 + d^2 + ad(\cos\theta + \sin\theta)}$.

CASE VII: $y_b > \overline{BJ}$

In this scenario, as shown in Figure 6.24(f), the entire square area of $\square HIJK$ is completely surrounded by the circle $\odot(B, y_b)$. As a result, the overlapped area, which is denoted as the shaded part in Figure 6.24(f), is equal to the area $S_{\square HIJK} = a^2$ (Step 3-7 of Figure 6.25). In this case, the CDF of the random distance Y_b is the ratio between S_{shade}^{VII} and $S_{\square HIJK}$, which is presented as $F_{Y_b}^{VII}(y_b) = 1$ for $y_b > \sqrt{a^2/2 + d^2 + ad(\cos\theta + \sin\theta)}$ (Step 4 of Figure 6.25). Hence Theorem 6.5 has been proven. □

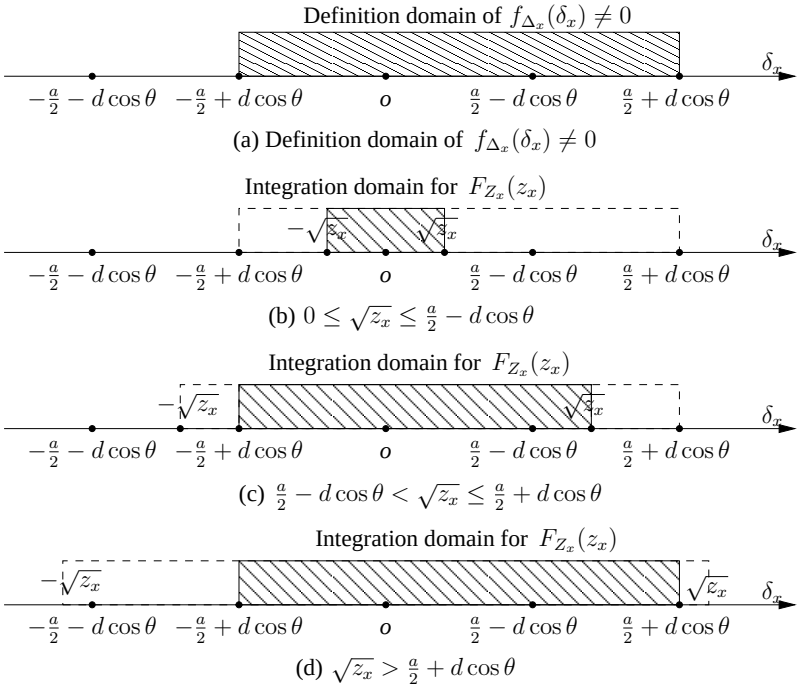

Figure 6.26: The integration domain for different values of $\sqrt{z_x}$.

6.B.4 Proof of Lemma 6.3

Since the random variable Z_x is defined as $Z_x = \Delta_x^2$, the CDF of Z_x should be expressed as

$$\begin{aligned} F_{Z_x}(z_x) &= \Pr(Z_x \leq z_x) = \Pr(\Delta_x^2 \leq z_x) = \Pr(-\sqrt{z_x} \leq \Delta_x \leq \sqrt{z_x}) \\ &= \int_{-\sqrt{z_x}}^{\sqrt{z_x}} f_{\Delta_x}(\delta_x) d\delta_x. \end{aligned} \tag{6.51}$$

Jointly considering Eq.(6.51) and Eq.(6.16), we can see that the integration domain of Eq.(6.51) is determined by the specific value of $\sqrt{z_x}$. When we have $0 \leq \sqrt{z_x} \leq \frac{a}{2} - d\cos\theta$, the integration domain becomes $[-\sqrt{z_x}, \sqrt{z_x}]$, as shown in Figure 6.26(b). As a result, the CDF $F_{Z_x}(z_x)$ can be expressed as

$$F_{Z_x}(z_x) = \int_{-\sqrt{z_x}}^{\sqrt{z_x}} f_{\Delta_x}(\delta_x) d\delta_x = \int_{-\sqrt{z_x}}^{\sqrt{z_x}} \frac{1}{a} \cdot d\delta_x = \frac{2\sqrt{z_x}}{a}. \tag{6.52}$$

When we have $\frac{a}{2} - d\cos\theta < \sqrt{z_x} \leq \frac{a}{2} + d\cos\theta$, the integration domain becomes $[-\frac{a}{2} + d\cos\theta, \sqrt{z_x}]$, as shown in Figure 6.26(c). As a result, the CDF $F_{Z_x}(z_x)$ can be expressed as

$$F_{Z_x}(z_x) = \int_{-\frac{a}{2}+d\cos\theta}^{\sqrt{z_x}} f_{\Delta_x}(\delta_x) d\delta_x = \int_{-\frac{a}{2}+d\cos\theta}^{\sqrt{z_x}} \frac{1}{a} \cdot d\delta_x = \frac{\sqrt{z_x} + \frac{a}{2} - d\cos\theta}{a}. \tag{6.53}$$

When we have $\sqrt{z_x} > \frac{a}{2} + d\cos\theta$, the integration domain becomes $[-\frac{a}{2} + d\cos\theta, \frac{a}{2} + d\cos\theta]$, as shown in Figure 6.26(d). As a result, the CDF $F_{Z_x}(z_x)$ can be expressed as

$$F_{Z_x}(z_x) = \int_{-\frac{a}{2}+d\cos\theta}^{\frac{a}{2}+d\cos\theta} f_{\Delta_x}(\delta_x) d\delta_x = \int_{-\frac{a}{2}+d\cos\theta}^{\frac{a}{2}+d\cos\theta} \frac{1}{a} \cdot d\delta_x = 1. \tag{6.54}$$

Differentiating $F_{Z_x}(z_x)$ formulated in Eqs.(6.52)-(6.54) with respect to z_x, the PDF of Z_x can be expressed as in Eq.(6.18) of Lemma 6.3.

Similarly, by following the same methodology, we may derive the CDF $F_{Z_Y}(z_y)$ of the random variable

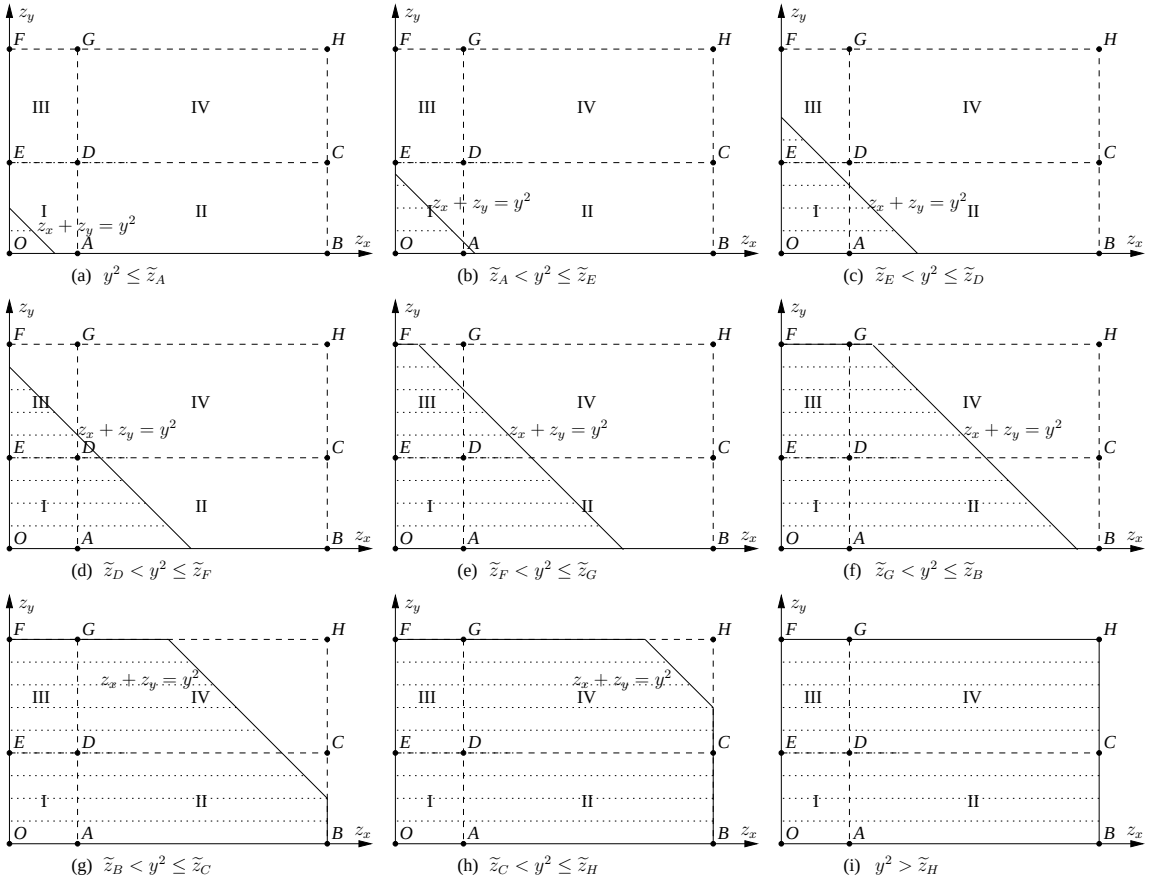

Figure 6.27: The integration domain $\mathcal{S}$, given the different values of y_b^2

$Z_Y = \widetilde{y} + d\sin\theta$, which is expressed as

$$F_{Z_y}(z_y) = \begin{cases} \dfrac{2\sqrt{z_y}}{a}, & 0 \le z_y \le (\dfrac{a}{2} - d\sin\theta)^2, \\ \dfrac{\sqrt{z_y} + \frac{a}{2} - d\sin\theta}{a}, & (\dfrac{a}{2} - d\sin\theta)^2 < z_y \le (\dfrac{a}{2} + d\sin\theta)^2 \\ 1, & z_y > (\dfrac{a}{2} + d\sin\theta)^2. \end{cases} \tag{6.55}$$

Hence, the corresponding PDF of Z_y can be expressed as in Eq.(6.19) of Lemma 6.3. The lemma has hence been proven. □

6.B.5 Proof of Theorem 6.6

The following ascending-order sorting $\overline{OA} \le \overline{OE} \le \overline{EF} \le \overline{OF} \le \overline{AB} \le \overline{OB}$ was assumed in Theorem 6.6, which indicates that $(\frac{a}{2} - d\cos\theta)^2 \le (\frac{a}{2} - d\sin\theta)^2 \le 2ad\sin\theta \le (\frac{a}{2} + d\sin\theta)^2 \le 2ad\cos\theta \le (\frac{a}{2} + d\cos\theta)^2$. As a result, the ascending-order sorting of the array $\{\widetilde{z}_i | i \in \{A, B, C, D, E, F, G, H\}\}$ in this case is given by $\widetilde{z}_A \le \widetilde{z}_E \le \widetilde{z}_D \le \widetilde{z}_F \le \widetilde{z}_G \le \widetilde{z}_B \le \widetilde{z}_C \le \widetilde{z}_H$.

Since the joint PDF $f_{Z_x Z_y}(z_x, z_y)$ has different expressions in different domains, as shown in Eq.(6.21) and Figure 6.8, we have to generally partition the integration domain $\mathcal{S}$ into four parts, namely into $\mathcal{S}_I = \mathcal{S} \cap$ Domain I, $\mathcal{S}_{II} = \mathcal{S} \cap$ Domain II, $\mathcal{S}_{III} = \mathcal{S} \cap$ Domain III and $\mathcal{S}_{IV} = \mathcal{S} \cap$ Domain IV.

When $0 \le y_b^2 \le \widetilde{z}_A$, we have $y_b \le (\frac{a}{2} - d\cos\theta)$ and the integration domain $\mathcal{S}$ is shown by the shaded

part of Figure 6.27(a). As a result, the double integral given by Eq.(6.20) can be further reformulated as

$$F_{Y_b}^{(1)}(y_b) = \int_0^{y_b^2} dz_x \int_0^{y_b^2 - z_x} \frac{1}{a^2\sqrt{z_x z_y}} dz_y = \pi \left(\frac{y_b}{a}\right)^2. \tag{6.56}$$

When $\widetilde{z}_A < y_b^2 \leq \widetilde{z}_E$, we have $(\frac{a}{2} - d\cos\theta) < y_b \leq (\frac{a}{2} - d\sin\theta)$ and the integration domain $\mathcal{S}$ is shown by the shaded part in Figure 6.27(b). As a result, the double integral given by Eq.(6.20) can be further reformulated as

$$F_{Y_b}^{(2)}(y_b) = \frac{1}{a^2}\left[\frac{\pi}{2}y_b^2 + y_b^2 \arcsin\frac{\frac{a}{2} - d\cos\theta}{y_b} + (\frac{a}{2} - d\cos\theta)\sqrt{y_b^2 - (\frac{a}{2} - d\cos\theta)^2}\right]. \tag{6.57}$$

When $\widetilde{z}_E < y_b^2 \leq \widetilde{z}_D$, we have $(\frac{a}{2} - d\sin\theta) < y_b \leq \sqrt{(\frac{a}{2} - d\cos\theta)^2 + (\frac{a}{2} - d\sin\theta)^2}$ and the integration domain $\mathcal{S}$ is shown by the shaded part of Figure 6.27(c). As a result, the double integral given by Eq.(6.20) can be further expressed as

$$\begin{aligned} F_{Y_b}^{(3)}(y_b) = \frac{1}{a^2}\Bigg[&\frac{\pi}{2}y_b^2 + y_b^2 \arcsin\frac{\frac{a}{2} - d\cos\theta}{y_b} - y_b^2 \arcsin\frac{\sqrt{y_b^2 - (\frac{a}{2} - d\sin\theta)^2}}{y_b} \\ &+(\frac{a}{2} - d\sin\theta)\sqrt{y_b^2 - (\frac{a}{2} - d\sin\theta)^2} + (\frac{a}{2} - d\cos\theta)\sqrt{y_b^2 - (\frac{a}{2} - d\cos\theta)^2}\Bigg]. \end{aligned} \tag{6.58}$$

For $\widetilde{z}_D < y_b^2 \leq \widetilde{z}_F$, we have $\sqrt{(\frac{a}{2} - d\cos\theta)^2 + (\frac{a}{2} - d\sin\theta)^2} < y_b \leq (\frac{a}{2} + d\sin\theta)$ and the integration domain $\mathcal{S}$ is shown by the shaded part of Figure 6.27(d). As a result, the double integral given by Eq.(6.20) can be further derived as

$$\begin{aligned} F_{Y_b}^{(4)}(y_b) = \frac{1}{2a^2}\Bigg[&\pi y_b^2 + y_b^2 \arcsin\frac{\frac{a}{2} - d\cos\theta}{y_b} - y_b^2 \arcsin\frac{\sqrt{y_b^2 - (\frac{a}{2} - d\sin\theta)^2)}}{y_b} \\ &+ (\frac{a}{2} - d\sin\theta)\sqrt{y_b^2 - (\frac{a}{2} - d\sin\theta)^2} + (\frac{a}{2} - d\cos\theta)\sqrt{y_b^2 - (\frac{a}{2} - d\cos\theta)^2} \\ &+2(\frac{a}{2} - d\cos\theta)(\frac{a}{2} - d\sin\theta)\Big] \end{aligned} \tag{6.59}$$

In case of $\widetilde{z}_F < y_b^2 \leq \widetilde{z}_G$, we have $(\frac{a}{2} + d\sin\theta) < y_b \leq (\frac{a}{2} + d\cos\theta)$ and the integration domain $\mathcal{S}$ is shown by the shaded part of Figure 6.27(e). As a result, the double integral given by Eq.(6.20) can be further streamlined as

$$\begin{aligned} F_{Y_b}^{(5)}(y_b) = \frac{1}{2a^2}\Bigg[&\pi y_b^2 + y_b^2 \arcsin\frac{\frac{a}{2} - d\cos\theta}{y_b} - y_b^2 \arcsin\frac{\sqrt{y_b^2 - (\frac{a}{2} - d\sin\theta)^2)}}{y_b} \\ &- 2y_b^2 \arcsin\frac{\sqrt{y_b^2 - (\frac{a}{2} + d\sin\theta)^2}}{y_b} + (\frac{a}{2} - d\sin\theta)\sqrt{y_b^2 - (\frac{a}{2} - d\sin\theta)^2} \\ &+ (\frac{a}{2} - d\cos\theta)\sqrt{y_b^2 - (\frac{a}{2} - d\cos\theta)^2} + 2(\frac{a}{2} + d\sin\theta)\sqrt{y_b^2 - (\frac{a}{2} + d\sin\theta)^2} \\ &+2(\frac{a}{2} - d\cos\theta)(\frac{a}{2} - d\sin\theta)\Big]. \end{aligned} \tag{6.60}$$

When $\widetilde{z}_G < y_b^2 \leq \widetilde{z}_B$, we have $(\frac{a}{2} + d\cos\theta) < y_b \leq \sqrt{(\frac{a}{2} + d\sin\theta)^2 + (\frac{a}{2} - d\cos\theta)^2}$ and the integration domain $\mathcal{S}$ is shown by the shaded part of Figure 6.27(f). As a result, the double integral given by

Eq.(6.20) can be further reformulated as

$$F_{Y_b}^{(6)}(y_b) = \frac{1}{2a^2}\Bigg[\pi y_b^2 - y_b^2 \arcsin\frac{\sqrt{y_b^2-(\frac{a}{2}-d\sin\theta)^2}}{y_b} - y_b^2\arcsin\frac{\sqrt{y_b^2-(\frac{a}{2}+d\sin\theta)^2}}{y_b} + (\frac{a}{2}-d\sin\theta)\sqrt{y_b^2-(\frac{a}{2}-d\sin\theta)^2} + (\frac{a}{2}+d\sin\theta)\sqrt{y_b^2-(\frac{a}{2}+d\sin\theta)^2} + 2a(\frac{a}{2}-d\cos\theta)\Bigg]. \tag{6.61}$$

When $\widetilde{z}_B < y_b^2 \le \widetilde{z}_C$, we have

$$\sqrt{(\frac{a}{2}+d\sin\theta)^2+(\frac{a}{2}-d\cos\theta)^2} < y_b \le \sqrt{(\frac{a}{2}-d\sin\theta)^2+(\frac{a}{2}+d\cos\theta)^2},$$

and the integration domain $\mathcal{S}$ is shown by the shaded part of Figure 6.27(g). As a result, the double integral given by Eq.(6.20) can be further streamlined as

$$F_{Y_b}^{(7)}(y_b) = \frac{1}{2a^2}\Bigg[2a(\frac{a}{2}-d\cos\theta) + 2y_b^2\arcsin\frac{\frac{a}{2}+\cos\theta}{y_b} - y_b^2\arcsin\frac{\sqrt{y_b^2-(\frac{a}{2}-d\sin\theta)^2)}}{y_b} - y_b^2\arcsin\frac{\sqrt{y_b^2-(\frac{a}{2}+d\sin\theta)^2}}{y_b} + (\frac{a}{2}-d\sin\theta)\sqrt{y_b^2-(\frac{a}{2}-d\sin\theta)^2} + 2(\frac{a}{2}+d\cos\theta)\sqrt{y_b^2-(\frac{a}{2}+\cos\theta)^2} + (\frac{a}{2}+d\sin\theta)\sqrt{y_b^2-(\frac{a}{2}+d\sin\theta)^2}\Bigg]. \tag{6.62}$$

When $\widetilde{z}_C < y_b^2 \le \widetilde{z}_H$, we have

$$\sqrt{(\frac{a}{2}-d\sin\theta)^2+(\frac{a}{2}+d\cos\theta)^2} < y_b \le \sqrt{(\frac{a}{2}+d\sin\theta)^2+(\frac{a}{2}+d\cos\theta)^2},$$

and the integration domain $\mathcal{S}$ is shown by the shaded part of Figure 6.27(h). As a result, the double integral given by Eq.(6.20) can be further reformulated as

$$F_{Y_b}^{(8)}(y_b) = \frac{1}{2a^2}\Bigg[y_b^2\arcsin\frac{\frac{a}{2}+\cos\theta}{y_b} - y_b^2\arcsin\frac{\sqrt{y_b^2-(\frac{a}{2}+d\sin\theta)^2)}}{y_b} + (\frac{a}{2}+d\cos\theta)\sqrt{y_b^2-(\frac{a}{2}+\cos\theta)^2} + (\frac{a}{2}+d\sin\theta)\sqrt{y_b^2-(\frac{a}{2}+d\sin\theta)^2} + \frac{3}{2}a^2 - ad(\sin\theta+\cos\theta) - 2d^2\sin\theta\cos\theta\Bigg]. \tag{6.63}$$

Finally, when $y_b^2 > \widetilde{z}_H$, we have $y_b > \sqrt{(\frac{a}{2}+d\sin\theta)^2+(\frac{a}{2}+d\cos\theta)^2}$ and the integration domain $\mathcal{S}$ is the entire definition domain of the joint PDF $f_{Z_xZ_y}(z_x,z_y)$, as shown in Figure 6.27(i). As a result, the double integration given by Eq.(6.20) is equal to $F_{Y_b}^{(9)}(y_b) = 1$.

6.C Proofs of the Theorems in Section 6.4

6.C.1 Proof of Lemma 6.4

The CDFs of the random variable $\Delta_{\widetilde{x}} = \widetilde{X}_1 - \widetilde{X}_2$ can be expressed as

$$F_{\Delta_{\widetilde{x}}}(\delta_{\widetilde{x}}) = \Pr(\widetilde{X}_1 - \widetilde{X}_2 \le \delta_{\widetilde{x}}) = \iint_{\mathcal{S}} f_{\widetilde{X}_1\widetilde{X}_2}(\widetilde{x}_1,\widetilde{x}_2)d\widetilde{x}_1 d\widetilde{x}_2, \tag{6.64}$$

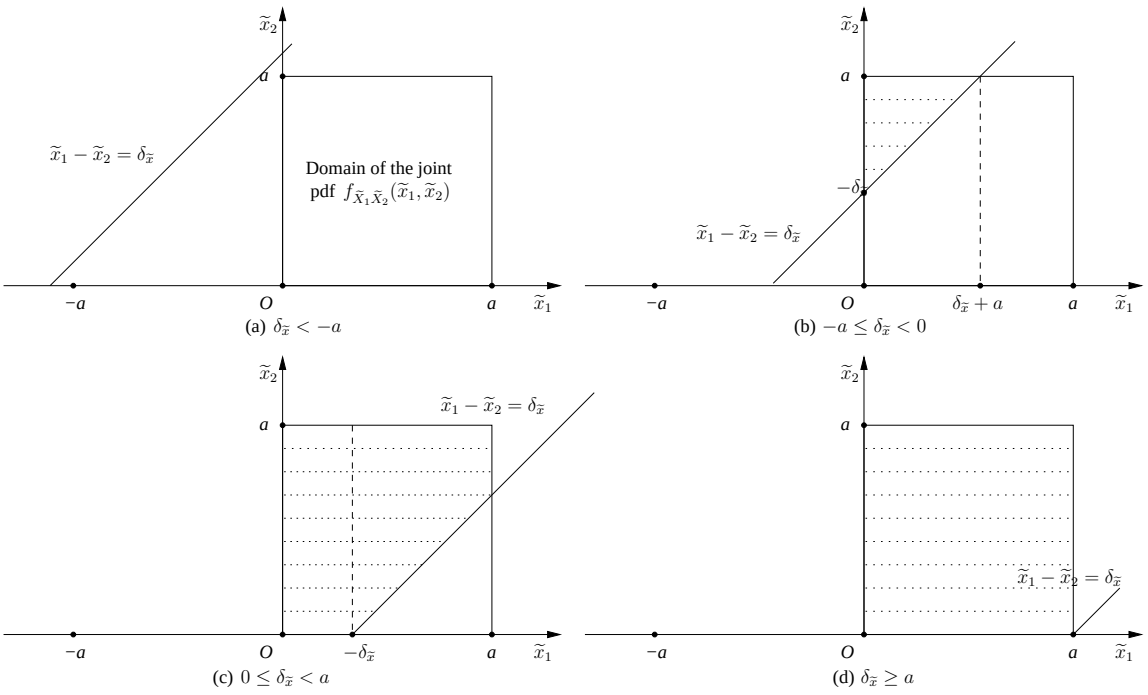

Figure 6.28: Different integration domain $\mathcal{S}$ for the derivation of $F_{\Delta_{\widetilde{x}}}(\delta_{\widetilde{x}})$, given different $\delta_{\widetilde{x}}$.

where $f_{\widetilde{X}_1\widetilde{X}_2}(\widetilde{x}_1, \widetilde{x}_2)$ is the joint PDF of $\widetilde{X}_1$ and $\widetilde{X}_2$, while $\mathcal{S}$ is the integration domain surrounded by the definition domain of $f_{\widetilde{X}_1\widetilde{X}_2}(\widetilde{x}_1, \widetilde{x}_2)$ and the upper part of the straight line $\widetilde{x}_1 - \widetilde{x}_2 = \delta_{\widetilde{x}}$. Since $\widetilde{X}_1$ and $\widetilde{X}_2$ are independent and identical random variables, whose PDFs are both given by Eq.(6.23), $f_{\widetilde{X}_1\widetilde{X}_2}(\widetilde{x}_1, \widetilde{x}_2)$ can be expressed as

$$f_{\widetilde{X}_1\widetilde{X}_2}(\widetilde{x}_1, \widetilde{x}_2) = f_{\widetilde{X}_1}(\widetilde{x}_1) f_{\widetilde{X}_2}(\widetilde{x}_2) = \begin{cases} \dfrac{1}{a^2}, & 0 \le \widetilde{x}_1, \widetilde{x}_2 \le a, \\ 0, & \text{otherwise.} \end{cases} \tag{6.65}$$

Let us now discuss the result of the double integral Eq.(6.64), given different values of $\delta_{\widetilde{x}}$. If we have $\delta_{\widetilde{x}} < -a$, as shown in Figure 6.28(a), the straight line $\widetilde{x}_1 - \widetilde{x}_2 = \delta_{\widetilde{x}}$ does not intersect the square definition domain of the joint PDF $f_{\widetilde{X}_1\widetilde{X}_2}(\widetilde{x}_1, \widetilde{x}_2)$. Therefore, the CDF of $\Delta_{\widetilde{x}}$ is derived as $F_{\Delta_{\widetilde{x}}}(\delta_{\widetilde{x}}) = 0$.

If $-a \le \delta_{\widetilde{x}} < 0$, the integration domain $\mathcal{S}$ is shown as the shaded part in Figure 6.28(b). Hence, the CDF of the random variable $\Delta_{\widetilde{x}}$ can be further expressed from Eq.(6.64) as

$$F_{\Delta_{\widetilde{x}}}(\delta_{\widetilde{x}}) = \int_0^{\delta_{\widetilde{x}}+a} d\widetilde{x}_1 \int_{\widetilde{x}_1-\delta_{\widetilde{x}}}^{a} \frac{1}{a^2} d\widetilde{x}_2 = \frac{(\delta_{\widetilde{x}} + a)^2}{2a^2}. \tag{6.66}$$

If we have $0 \le \delta_{\widetilde{x}} < a$, the integration domain $\mathcal{S}$ is shown as the shaded part in Figure 6.28(c). Hence, the CDF of the random variable $\Delta_{\widetilde{x}}$ can be further derived from Eq.(6.64) as

$$F_{\Delta_{\widetilde{x}}}(\delta_{\widetilde{x}}) = \int_0^{\delta_{\widetilde{x}}} d\widetilde{x}_1 \int_0^{a} \frac{1}{a^2} d\widetilde{x}_2 + \int_{\delta_{\widetilde{x}}}^{a} d\widetilde{x}_1 \int_{\widetilde{x}_1-\delta_{\widetilde{x}}}^{a} \frac{1}{a^2} d\widetilde{x}_2 = \frac{a^2 + 2a\delta_{\widetilde{x}} - \delta_{\widetilde{x}}^2}{2a^2}. \tag{6.67}$$

If $\delta_{\widetilde{x}} \ge a$, the integration domain $\mathcal{S}$ is the entire definition domain of the joint PDF $f_{\widetilde{X}_1\widetilde{X}_2}(\widetilde{x}_1, \widetilde{x}_2)$, as shown in Figure 6.28(d). Hence, the CDF of the random variable $\Delta_{\widetilde{x}}$ can be further expressed as $F_{\Delta_{\widetilde{x}}}(\delta_{\widetilde{x}}) = 1$.

After differentiating both Eqs.(6.66) and (6.67) with respect to $\delta_{\widetilde{x}}$, we arrive at the PDF of the random variable $\Delta_{\widetilde{x}}$, as expressed in Eq.(6.25). Therefore the lemma has been proven. □

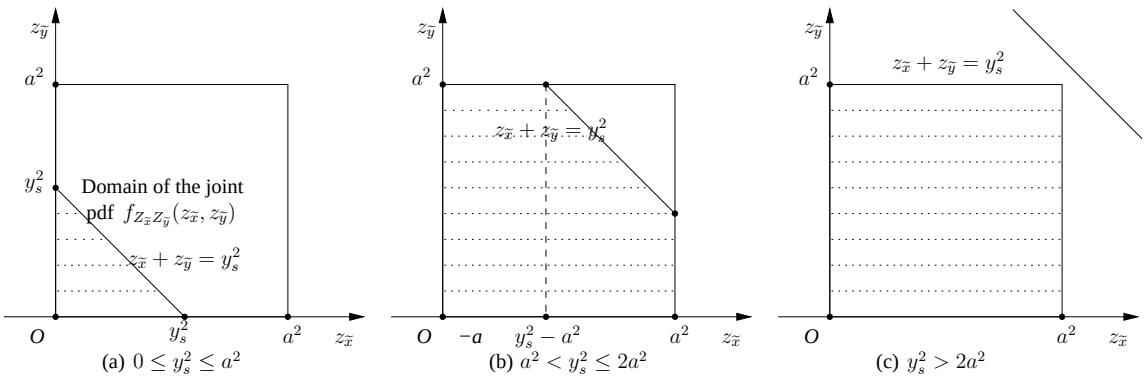

(a) $0 \leq y_s^2 \leq a^2$ (b) $a^2 < y_s^2 \leq 2a^2$ (c) $y_s^2 > 2a^2$

Figure 6.29: Different integral area $\mathcal{S}$ for the derivation of $F_{Y_s}(y_s)$ given different y_s.

6.C.2 Proof of Lemma 6.5

Given that $Z_{\widetilde{x}} = \Delta_{\widetilde{x}}^2$, the CDF of $Z_{\widetilde{x}}$ may be derived as

$$\begin{aligned} F_{Z_{\widetilde{x}}}(z_{\widetilde{x}}) &= \Pr(Z_{\widetilde{x}} \leq z_{\widetilde{x}}) = \Pr(\Delta_{\widetilde{x}}^2 \leq z_{\widetilde{x}}) = \Pr(-\sqrt{z_{\widetilde{x}}} \leq \Delta_{\widetilde{x}} \leq \sqrt{z_{\widetilde{x}}}) \\ &= F_{\Delta_{\widetilde{x}}}(\sqrt{z_{\widetilde{x}}}) - F_{\Delta_{\widetilde{x}}}(-\sqrt{z_{\widetilde{x}}}). \end{aligned} \tag{6.68}$$

If $0 \leq \sqrt{z_{\widetilde{x}}} \leq a$, which also indicates that $-a \leq \sqrt{z_{\widetilde{x}}} \leq 0$, the CDF of the random variable $Z_{\widetilde{x}}$ can be further expressed from Eq.(6.68) as

$$\begin{aligned} F_{Z_{\widetilde{x}}}(z_{\widetilde{x}}) &= F_{\Delta_{\widetilde{x}}}(\sqrt{z_{\widetilde{x}}}) - F_{\Delta_{\widetilde{x}}}(-\sqrt{z_{\widetilde{x}}}) \\ &= \frac{a^2 + 2a\sqrt{z_{\widetilde{x}}} - z_{\widetilde{x}}}{2a^2} - \frac{(a - \sqrt{z_{\widetilde{x}}})^2}{2a^2} = \frac{2\sqrt{z_{\widetilde{x}}}}{a} - \frac{z_{\widetilde{x}}}{a^2}. \end{aligned} \tag{6.69}$$

If $\sqrt{z_{\widetilde{x}}} > a$, which also indicates that $-\sqrt{z_{\widetilde{x}}} < -a$, the CDF of the random variable $Z_{\widetilde{x}}$ can be further derived Eq.(6.68) as

$$F_{Z_{\widetilde{x}}}(z_{\widetilde{x}}) = F_{\Delta_{\widetilde{x}}}(\sqrt{z_{\widetilde{x}}}) - F_{\Delta_{\widetilde{x}}}(-\sqrt{z_{\widetilde{x}}}) = 1 - 0 = 1. \tag{6.70}$$

After differentiating both Eqs.(6.69) and (6.70) with respect to $z_{\widetilde{x}}$, we arrive at the PDF of the random variable $Z_{\widetilde{x}}$, as expressed in Eq.(6.5). Hence the lemma has been proven. □

6.C.3 Proof of Theorem 6.7

Given that $Y_s = \sqrt{Z_{\widetilde{x}} + Z_{\widetilde{y}}}$, its CDF can be formulated as

$$\begin{aligned} F_{Y_s}(y_s) &= \Pr(Y_s \leq y_s) = \Pr(\sqrt{Z_{\widetilde{x}} + Z_{\widetilde{y}}} \leq y_s) = \Pr(Z_{\widetilde{x}} + Z_{\widetilde{y}} \leq y_s^2) \\ &= \iint_{\mathcal{S}} f_{Z_{\widetilde{x}}Z_{\widetilde{y}}}(z_{\widetilde{x}}, z_{\widetilde{y}}) dz_{\widetilde{x}} dz_{\widetilde{y}}, \end{aligned} \tag{6.71}$$

where $f_{Z_{\widetilde{x}}Z_{\widetilde{y}}}(z_{\widetilde{x}}, z_{\widetilde{y}})$ is the joint PDF of the random variables $Z_{\widetilde{x}}$ and $Z_{\widetilde{x}}$, and $\mathcal{S}$ is the integration area surrounded by the domain of $f_{Z_{\widetilde{x}}Z_{\widetilde{y}}}(z_{\widetilde{x}}, z_{\widetilde{y}})$ and the lower part of the straight line $z_{\widetilde{x}} + z_{\widetilde{y}} = y_s$. Since $Z_{\widetilde{x}}$ and $Z_{\widetilde{x}}$ are independent and identical random variables, their joint PDF can be expressed as

$$f_{Z_{\widetilde{x}}Z_{\widetilde{y}}}(z_{\widetilde{x}}, z_{\widetilde{y}}) = \begin{cases} \dfrac{1}{a^2}\left(\dfrac{1}{\sqrt{z_{\widetilde{x}}}} - \dfrac{1}{a}\right)\left(\dfrac{1}{\sqrt{z_{\widetilde{y}}}} - \dfrac{1}{a}\right), & 0 \leq z_{\widetilde{x}}, z_{\widetilde{y}} \leq a^2, \\ 0, & \text{otherwise.} \end{cases} \tag{6.72}$$

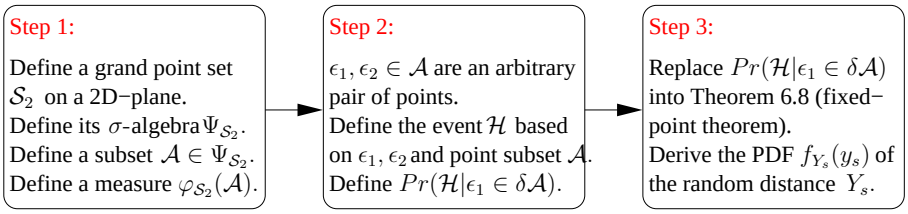

Figure 6.30: Methodology for deriving the PDF of the random distance Y_s when a pair of MUs roam within a circular area by obeying the uniform mobility model.

Given the different values of y_s^2, we have different integration domains $\mathcal{S}$ for calculating the CDF of Y_s. If we have $0 \leq y_s^2 \leq a^2$, as shown in Figure 6.29(a), which indicates that $0 \leq y_s \leq a$, the double integral of Eq.(6.71) can be further expressed as

$$\begin{aligned} F_{Y_s}(y_s) &= \int_0^{y_s^2} dz_{\tilde{x}} \int_0^{y_s^2 - z_{\tilde{x}}} \frac{1}{a^2} \left(\frac{1}{\sqrt{z_{\tilde{x}}}} - \frac{1}{a} \right) \left(\frac{1}{\sqrt{z_{\tilde{y}}}} - \frac{1}{a} \right) dz_{\tilde{y}} \\ &= \frac{1}{a^2} \left(\pi y_s^2 - \frac{8y_s^3}{3a} + \frac{y_s^4}{2a^2} \right). \end{aligned} \tag{6.73}$$

If we have $a^2 < y_s^2 \leq 2a^2$, as shown in Figure 6.29(b), which indicates that $a < y_s \leq \sqrt{2}a$, the double integral of Eq.(6.71) can be further streamlined as

$$\begin{aligned} F_{Y_s}(y_s) &= \int_0^{y_s^2 - a^2} dz_{\tilde{x}} \int_0^{a^2} \frac{1}{a^2} \left(\frac{1}{\sqrt{z_{\tilde{x}}}} - \frac{1}{a} \right) \left(\frac{1}{\sqrt{z_{\tilde{y}}}} - \frac{1}{a} \right) dz_{\tilde{y}} \\ &\quad + \int_{y_s^2 - a^2}^{a^2} dz_{\tilde{x}} \int_0^{y_s^2 - z_{\tilde{x}}} \frac{1}{a^2} \left(\frac{1}{\sqrt{z_{\tilde{x}}}} - \frac{1}{a} \right) \left(\frac{1}{\sqrt{z_{\tilde{y}}}} - \frac{1}{a} \right) dz_{\tilde{y}} \\ &= \frac{1}{a^2} \left[2y^2 \arcsin \frac{2a^2 - y_s^2}{y_s^2} + \left(\frac{4}{3}a + \frac{8}{3a} y_s^2 \right) \sqrt{y_s^2 - a^2} - 2y_s^2 - \frac{y^4}{2a^2} + \frac{a^2}{3} \right]. \end{aligned} \tag{6.74}$$

If we have $y_s^2 > 2a^2$, as shown in Figure 6.29(c), which indicates that $y_s > \sqrt{2}a$, the integration domain is the entire domain of the joint PDF $f_{Z_{\tilde{x}} Z_{\tilde{y}}}(z_{\tilde{x}}, z_{\tilde{y}})$. As a result, the CDF of the random distance Y_s is derived as $F_{Y_s}(y_s) = 1$.

In a nutshell, the CDF of the random distance Y_s between a pair of MUs that move within a square area by obeying the uniform mobility model can be summarised as Eq.(6.27). After differentiating the CDF $F_{Y_s}(y_s)$ of Eq.(6.27) with respect to y_s, we arrive at the PDF of the random distance Y_s, which is expressed as Eq.(6.28). Hence the theorem has been proven. □

6.C.4 Proof of Theorem 6.9

In order to derive the PDF of the random distance Y_s, main steps relying on Theorem 6.8 are summarised in Figure 6.30.

In Step 1 of Figure 6.30, we define the set $\mathcal{S}_2$ as a two-dimensional plane containing all possible points on it, whose $\sigma-$algebra is denoted as $\Psi_{\mathcal{S}_2}$. A measure can be defined over a subset $\mathcal{A}$ that belongs to $\Psi_{\mathcal{S}_2}$ as the area covered by $\mathcal{A}$. For the scenario that a pair of MUs roam within a circular area $\odot(O,r)$, $\mathcal{A}$ is defined as a subset containing all possible points within a circular area $\odot(O,r)$, whose measure should be defined as $\varphi_{\mathcal{S}_2}(\mathcal{A}) = \pi r^2$. As a result, the differential of $\varphi_{\mathcal{S}_2}(\mathcal{A})$ can be expressed as $d\varphi_{\mathcal{S}_2}(\mathcal{A}) = 2\pi r dr$.

Then, in Step 2 of Figure 6.30, we uniformly distribute two points $\{\epsilon_1, \epsilon_2\}$, representing two MUs, within the point-subset $\mathcal{A}$. Furthermore, we let $\delta\mathcal{A}$ be the subset containing all the points on the circumference of $\odot(O,r)$. We define $\mathcal{H}$ as an event that two points are separated by a distance between y_s and $(y_s + dy_s)$. Let us first derive the term of $\Pr(\mathcal{H}|\epsilon_1 \in \delta\mathcal{A})$ in Eq.(6.30).

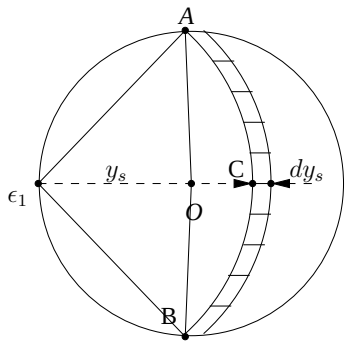

Figure 6.31: Calculate $\Pr(H|\epsilon_1 \in \delta\mathcal{A})$ in the circular area $\odot(O,r)$ considered

Specifically, $\Pr(\mathcal{H}|\epsilon_1 \in \delta\mathcal{A})$ is the probability that when point ϵ_1 is placed on the circumference of $\odot(O,r)$, ϵ_1 and ϵ_2 is separated by a distance between y_s and $(y_s + dy_s)$. As shown in Figure 6.31, we draw a circle $\odot(\epsilon_1, y_s)$ having ϵ_1 as the centre and having y_s as the radius. Then $\odot(\epsilon_1, y_s)$ intersects $\odot(O,r)$ at the points A and B. We draw another circle $\odot(\epsilon_1, y_s + dy_s)$ having ϵ_1 as the centre and having $(y_s + dy_s)$ as the radius. If the point ϵ_2 appears within the shaded annulus of Figure 6.31, the distance separating ϵ_1 from ϵ_2 is between y_s and $(y_s + dy_s)$. Since ϵ_2 is uniformly distributed within $\odot(O,r)$, $\Pr(\mathcal{H}|\epsilon_1 \in \delta\mathcal{A})$ can be derived as the ratio of the area of the annulus to the area of $\odot(O,r)$.

In order to derive the area of the annulus, we have to obtain the length of the arc $\widehat{ACB}$ first. According to the law of cosine, the cosine value of $\angle A\epsilon_1 O$ can be expressed as

$$\cos\angle A\epsilon_1 O = \frac{\overline{\epsilon_1 A}^2 + \overline{\epsilon_1 O}^2 - \overline{AO}^2}{2\overline{\epsilon_1 A}\overline{\epsilon_1 O}} = \frac{y_s^2 + r^2 - r^2}{2y_s r} = \frac{y_s}{2r}. \tag{6.75}$$

Then we can obtain the exact value of the angle $\angle A\epsilon_1 B$ with the aid of the corresponding inverse trigonometric function as $\angle A\epsilon_1 B = 2\angle A\epsilon_1 O = 2\arccos\frac{y_s}{2r}$. Therefore, the length of the arc $\widehat{ACB}$ can be derived as $\widehat{ACB} = y_s \angle A\epsilon_1 B = 2y_s \arccos(y_s/2r)$. Furthermore, the area of the shaded annulus is expressed as $S_{annulus} = \widehat{ACB}dy_s = 2y_s dy_s \cdot \arccos(y_s/2r)$. Thus, $\Pr(H|\epsilon_1 \in \delta\mathcal{A})$ can be expressed as

$$\Pr(H|\epsilon_1 \in \delta\mathcal{A}) = \frac{S_{annulus}}{S_{\odot(O,r)}} = \frac{2y_s dy_s}{\pi r^2}\arccos\frac{y_s}{2r}. \tag{6.76}$$

In Step 3 of Figure 6.30, we substitute $\Pr(H|\epsilon_1 \in \delta\mathcal{A})$, $n = 2$, $\varphi_{\mathcal{S}_2}(\mathcal{A}) = \pi r^2$ and $d\varphi_{\mathcal{S}_2}(\mathcal{A}) = 2\pi r dr$ into Eq.(6.30) of Theorem 6.8. Therefore we may obtain the following differential formula:

$$d\Pr(\mathcal{H}) = 2\left(\frac{2y_s dy_s}{\pi r^2}\arccos\frac{y_s}{2r} - \Pr(\mathcal{H})\right)\cdot\frac{2\pi r dr}{\pi r^2}. \tag{6.77}$$

Upon rearranging the terms in Eq.(6.77), yields:

$$r^4 d\Pr(\mathcal{H}) + 4\Pr(\mathcal{H})r^3 dr = \frac{8y_s dy_s}{\pi}\cdot r\arccos\frac{y_s}{2r}dr. \tag{6.78}$$

Integrating both sides with respect to r, we arrive at

$$\begin{aligned}
r^4\Pr(\mathcal{H}) &= \frac{8y_s dy_s}{\pi}\cdot\int r\arccos\frac{y_s}{2r}dr \\
&= \frac{8y_s dy_s}{\pi}\cdot\frac{y_s^2}{8}\left[\left(\frac{2r}{y_s}\right)^2\arccos\frac{y_s}{2r} - \frac{2r}{y_s}\sqrt{1-\left(\frac{y_s}{2r}\right)^2}\right] \\
&= \frac{8r^3 dy_s}{\pi}\cdot\frac{y_s}{2r}\left[\arccos\frac{y_s}{2r} - \frac{y_s}{2r}\sqrt{1-\left(\frac{y_s}{2r}\right)^2}\right].
\end{aligned} \tag{6.79}$$

Based on the definition of the event $\mathcal{H}$, $\Pr(\mathcal{H})$ can be further formulated as $\Pr(\mathcal{H}) = F_{Y_s}(y_s + dy_s) - F_{Y_s}(y_s)$, where $F_{Y_s}(y_s)$ is the CDF of the random distance Y_s representing the probability of Y_s being shorter

than y_s. As a result, the PDF of the random distance Y_s can be expressed with the aid of Eq.(6.79) as

$$f_{Y_s}(y_s) = \lim_{dy_s \to 0} \frac{F_{Y_s}(y_s + dy_s) - F_{Y_s}(y_s)}{dy_s} = \lim_{dy_s \to 0} \frac{\Pr(\mathcal{H})}{dy_s}$$
$$= \frac{8}{\pi r} \cdot \frac{y_s}{2r} \left[\arccos \frac{y_s}{2r} - \frac{y_s}{2r} \sqrt{1 - \left(\frac{y_s}{2r}\right)^2} \right] \tag{6.80}$$

for $0 \leq y_s \leq 2r$. Hence the theorem has been proven. $\square$

Chapter 7

Conclusions and Future Research

7.1 Main Conclusions

Thanks to the rapid development of the wireless Internet, numerous mobile applications provide platforms for Mobile Users (MUs) to share the Information of Common interest (IoCI) with their friends. For example, mobile applications of Facebook and Twitter enable MUs share information via posts and status update. Similarly, the mobile application of *Wase* (http://www.waze.com/) enables the drivers to share the real-time traffic information collected by themselves. However, at the time of writing, the dissemination process of the IoCI is largely fulfilled by the Centralised Infrastructure (CI) based communication. In order to receive the IoCI, the mobile devices of MUs have to be connected either to a Base Station (BS) or to a Wi-Fi access point. However, the CI-based information dissemination faces the following limitations[1]:

- Intermittent connectivity in rural areas;
- Overloaded CI-based network;
- Inefficient data service in densely populated area.

Due to the rapid development of the powerful mobile devices, it becomes quite common that a mobile device is equipped with large storage capacity, say dozens of Giga Bytes and supports multiple communication standards, such as Infrared, Bluetooth and Wi-Fi modules, so as to readily realise direct peer-to-peer communications. As a result, this treatise contributed towards mitigating some of the above-mentioned design problems in the conventional CI-based information dissemination by seeking assistance both from the opportunistic contacts and opportunistic multicast amongst the MUs, who share common interest in the same information. This results in an integrated cellular and opportunistic network. Since mobile devices are carried by MUs, exploring the social behaviours exhibited by individuals and the social relationships amongst the MUs may assist us in enhancing the communication experience, as discussed in Chapter 1. The important conclusions of this treatise are as follows.

In Chapter 2, we firstly studied an integrated cellular and large-scale opportunistic network, where the MUs were sparsely distributed within a large area. Due to the large size of the area and the sparse distribution of the MUs, the connectivity between a BS and a MU as well as that between a pair of MUs exhibited an intermittent nature. As a result, the information delivery had to be realised by opportunistic contact between a transmitter and receiver pair, when the receiver entered the range of the transmitter. However, a successful information delivery required that the duration of this opportunistic contact had to last longer

[1] Please refer to Chapter 1 for more details.

than the downloading period of the information. This integrated network was relied upon for disseminating delay-tolerant IoCI amongst the MUs. The important conclusions of this chapter are as follows:

- Both the inter-contact duration and the contact duration between a pair of MUs, who moved within a square area by obeying the Random Direction (RD) mobility model, were exponentially distributed random variables. The inter-contact duration between a MU and a BS was also exponentially distributed, when the MU moved within a square area by obeying the RD mobility model and the BS was located at the centre of the area. However, the contact duration between the MU and the BS followed a Gamma distribution.
- Upon modelling the information dissemination by a Continuous-Time-Pure-Birth-Markov-Chain (CT-PBMC), both the analytical results and the simulation results demonstrated that having more MUs participating in the information dissemination process significantly increased the successful delivery ratio of the IoCI before it expired.
- After modelling the contact history of MUs by a social contact graph, several Social Network Analysis (SNA) aided tele-traffic off-loading schemes were conceived for increasing the number of MUs served by the large-scale opportunistic network. Our simulation results demonstrated that with the aid of the large-scale opportunistic network, nearly 58% of the tele-traffic was off-loaded from the congested CI and that the component-based initial receiver selection scheme outperformed its counterparts.

In the densely populated scenario, where numerous MUs can be found within a small area, classic BS-aided multicast is often invoked as a traditional measure of disseminating the IoCI by relying on the broadcast nature of the wireless channels. However, BS-aided multicasting becomes inefficient when the number of MUs is high. If we efficiently exploit the redundant copies of the IoCI held by the already served MUs and activate these IoCI holders as potential relays for the next stage of cooperative multicast, the resultant diversity gain beneficially accelerates the information dissemination process. This approach is normally regarded as opportunistic cooperative multicast, since no deterministic relay selection scheme is required. Its promising advantages experienced during disseminating the delay-sensitive IoCI across the densely populated area considered motivate us to study an integrated cellular and small-scale opportunistic network in Chapters 3–5.

More specifically, in Chapter 3, we studied the Mobile Social Networking (MSN) aided content dissemination in cellular systems relying on altruistic human behaviours. The important conclusions of this chapter are as follows:

- Increasing the number of MUs firstly increased both the delay and energy consumption, when our MSN aided content dissemination scheme was adopted, since having more MUs imposed an increased traffic load on the system. However, increasing the number of MUs in the MSN group beyond a certain density significantly reduced both the delay and the energy consumption, since having more MUs provided more cooperative multicast opportunities and the resultant diversity gain became capable of counteracting the adverse effects incurred by the increased traffic demand.
- When the MUs became more altruistic, the associated delay metrics were substantially improved, since more MUs were willing to assist in the dissemination process. Furthermore, in this case, the total energy dissipated by the content dissemination process was also substantially reduced, because the high-power BS was rarely invoked during the dissemination process and the majority of the tele-traffic load was carried by the low-power transmissions amongst the MUs themselves. However, as the cost of achieving these performance gains, the system suffered from an increased overhead traffic and an increased individual energy dissipation.
- Our MSN aided content dissemination scheme was demonstrated to be capable of off-loading a substantial fraction of the tele-traffic from the potentially congested BS.

- Our MSN aided content dissemination scheme was demonstrated to be more prompt, more efficient and more reliable than the conventional BS-aided multicast in disseminating the content of common interest.

- The accuracy of our approximate CT-PBMC modelling was demonstrated by the simulation results under the assumption of a sufficiently short time interval.

In Chapter 4, we studied the distributed multi-stage cooperative social multicast aided content dissemination process in random mobile networks, where the content owners were only willing to multicast the content of common interest to their social contacts. Furthermore, the content dissemination process was initialised by several content owners and it was completed by the MUs themselves without any assistance from the CI. The salient conclusions of this chapter are as follows:

- After modelling the social strength between any pairs of MUs by taking into account their geographic social relationship, we found that having more 'sociable' MUs expedited the content dissemination in terms of increasing the average social unicast throughput as well as simultaneously reducing the content dissemination delay, since sociable MUs provided more multicasting opportunities to the hitherto unserved MUs.

- The content dissemination delay may be significantly reduced, if more MUs participated in the process. As presented in Chapter 4, if the density of the MUs within the area studied was sufficiently high, two-stage cooperative social multicast was capable of delivering the content of common interest to all the MUs in this extreme case.

- When taking into account the social constraints imposed on the multicast process in Sections 4.2.3 and 4.5.3, we demonstrated that the multi-stage cooperative social multicast protocol was more suitable than other protocols for disseminating the content of common interest.

In Chapter 5, we studied a hybrid information dissemination scheme designed for integrated cellular and small-scale opportunistic networks, which consisted of a BS-aided multicast stage and a cooperative-multicast-aided spontaneous dissemination stage. The main conclusions of this chapter are as follows:

- We found a generic analytical framework for unifying the delay metrics characterising the information dissemination process. One of our main goal was to disseminate the IoCI to a group of MUs. Other MUs not belonging to this group may be regarded as helpers. To this end, the statistical properties of the group delay was derived in closed-form, which was defined as the time duration spanning from the BS multicasting the IoCI until all members of the interest-group successfully received it. Other delay metrics may also be derived and investigated as a function of the interest-group size.

- We considered a realistic scenario, in which only a limited number of Time Slots (TSs) was provided for the spontaneous dissemination stage. In order to efficiently exploit these TSs, a round-robin resource scheduling had to be conceived. When more TSs were assigned to an opportunistic link, its average throughput was increased and its delay metrics were improved, since the MUs were offered more frequent opportunities for multicasting the IoCI. However, for the same reason, the total energy dissipation was increased.

- Centrality-based resource scheduling approaches, namely the shortest-longest-distance scheduling, the shortest-shortest-distance scheduling, the shortest-sum-distance scheduling and the highest-sum-rate scheduling all performed better than the low-complexity random resource scheduling in terms of both the average dissemination delay and the average total energy dissipation. Specifically, the shortest-shortest-distance scheduling performed best amongst all these resource scheduling approaches.

In Chapter 6, we derived the distributions of the random distance between a pair of MUs and that between a BS and a MU for the following scenarios:

- By obeying a uniform mobility model[2], the MU moved right across the entire coverage of a cell, which is in the shape of either a circle or of a regular polygon, while the BS was located at the centre of the cell. The distribution of the random distance derived for this scenario has been adopted for analysing the average throughput of the cellular link between the BS and the MU in Chapter 5.
- By obeying a uniform mobility model, the MU moved within a specific bounded area, which is in the shape of either a circle or a square, while the BS was located at an arbitrary position, either inside or outside the bounded area. The distribution of the random distance derived for this scenario has been borrowed for analysing the average throughput of the cellular link between the BS and the MU in Chapter 3.
- By obeying a uniform mobility model, both of the MUs moved within either a circular or a square area. The distribution of the random distance derived for this scenario has been adopted for analysing the average throughput of the opportunistic link between a pair of MUs in Chapters 3-5.

The closed-form analytical results derived in this chapter may be further exploited for evaluating the path-loss, the spectral efficiency and the outage probability in mobile networks.

Based on our research presented in Chapter 2 to Chapter 6, the above-mentioned three design limitations of the CI-based information dissemination, namely intermittent connectivity in rural areas, overloaded CI-based network and inefficient data service in densely populated areas can be resolved with the aid of opportunistic networks.

7.2 Comparison of the Models Conceived for Small-Scale Opportunistic Networks

The similarities and differences of our contributions in Chapters 3 to 5 are compared in terms of the following aspects:

- *Physical layer model.* Chapters 3 to 5 relied on the classic path loss model and on the uncorrelated Rayleigh distributed multipath fading as our channel model. Furthermore, the MUs in these chapters moved within a bounded area by obeying the uniform mobility model. Additionally, in Chapter 3, we also studied the realistic mobility traces extracted from a subway station.
- *Medium-Access-Control (MAC) layer model.* In Chapter 3, no specific MAC layer model was considered and all the Information Owners (IOs) were assumed to multicast the IoCI on orthogonal non-interfering channels. Both in Chapter 4 and 5, a Time-Division-Multiple-Access (TDMA) scheme was implemented in the MAC layer for carrying out the indispensable overhead exchange and for avoiding the adverse effects of both collisions and interference, when multiple IOs simultaneously multicast the IoCI. However, in Chapter 4, we assumed that each IO was guaranteed a dedicated TS for its own multicast. By contrast, since we realistically assumed a limited number of TSs for the spontaneous dissemination stage in Chapter 5, carefully coordinated resource scheduling approaches had to be considered for assigning these TSs.
- *Network layer model.* Different network layer protocols were invoked in Chapters 3–5. In Chapter 3, the BS-adied multicast was adopted if no IOs were willing to forward the IoCI. Otherwise, the IOs

[2]Please refer to Chapter 6 for the definition.

cooperatively multicast the IoCI to the hitherto unserved MUs after they successfully received it. In Chapter 5, the protocol was slightly different from that of Chapter 3, since the BS-aided multicast was only adopted during the initial stage of the information dissemination. However, in Chapter 4, only the multi-stage cooperative 'social' multicast protocol was invoked without the adoption of BS-aided multicast, where a MU was only willing to multicast the IoCI to its social contacts.

- *Energy model.* In Chapter 3, the energy dissipation of an individual MU during the information dissemination process consists of two parts, namely the signal processing energy required for recovering the contaminated packets and the transmit energy assigned for forwarding the packet. Since we did not evaluate the energy metrics in Chapter 4, no energy model was necessitated. In Chapter 5, we only considered the transmit energy, since the signal processing energy is negligibly low.

- *Social domain factors.* In Chapters 3–5, different design factors borrowed from the social domain were considered. In Chapter 3, the altruistic social behaviour of MUs was considered for characterising the probability of the MUs willing to forward the IoCI in the next stage. This social behaviour depended on whether the MUs have a sufficiently strong motivation to help their peers and also on whether the specific MUs who benefit from the information dissemination process are willing to return the favours by providing relaying services. In Chapter 4, the geographic social relationships were relied upon for defining the social strength between a pair of MUs, which characterised the probability of this pair of MUs becoming each other's social contact. Owing to privacy and security concerns, in Chapter 4 a MU was only willing to convey information to its own social contacts. The model of Chapter 4 can be regarded as that of a twin-layer network [176], where the lower-layer is a physical wireless network and the upper-layer is a virtual social network. The quality of social connection between a pair of MUs heavily affects the information dissemination performance of the physical wireless network. However, we did not consider any social behaviours and social relationships in Chapter 5. In contrast to Chapters 3 and 4, we assumed completely altruistic behaviours for the MUs, who were assumed to be social network partners with each other. However, inspired by the concept of centrality in SNA, we modelled the wireless connections between the IOs and uMUs by a bipartite graph and evaluated the importance of the IOs' relationship with the hitherto uMUs. Finally, we conceived a range of resource scheduling approaches for further improving the information dissemination performance.

- *Analytical tools.* In practice, any communication systems has a discrete-time nature. Any time-related metrics should be evaluated in terms of the number of basic time intervals, such as TSs or transmission frames. However, in Chapter 3, we approximated the discrete-time information process by an approximate CT-PBMC subject to the assumption that the basic time interval was sufficiently short. In this approximate CT-PBMC, we demonstrated that only transitions to the adjacent state occurred, hence multiple-step state transitions were ignored. As a result, closed-form formulas were derived for various delay and energy metrics. In order to more precisely characterise the discrete-time feature of the information dissemination process, we did not impose any constraints on the length of the basic time interval and modelled the information dissemination process by a Discrete-Time-Pure-Birth-Markov-Chain (DT-PBMC) in Chapter 4, where a transition could traverse from any given state to any other higher-indexed state during a single basic time interval. We improved the DT-PBMC model in Chapter 5 by considering both the impact of resource scheduling and of the hybrid structure of the information dissemination process. Moreover, the concept of the *transient boundary* was defined in order to create artificial absorbing states for the sake of deriving the statistical properties of the group delay. The DT-PBMC model based analytical framework of Chapter 5 was suitable for deriving various performance metrics for both our hybrid information dissemination scheme and for the conventional BS-aided-single-hop-multicast protocol.

- *Performance metrics.* The performance metrics studied in Chapter 3 included the dissemination delay, the individual MU's delay, the total energy dissipation, the individual MU's energy dissipation, the

Table 7.1: Comparison of the models conceived for small-scale opportunistic networks

	Chapter 3	**Chapter 4**	**Chapter 5**
Mobility model	Uniform mobility model; Subway station traces.	Uniform mobility model.	Uniform mobility model.
PHY layer model	Two-fold Path loss; Uncorrelated Rayleigh fading.	Two-fold Path loss; Uncorrelated Rayleigh fading.	Two-fold Path loss; Uncorrelated Rayleigh fading.
MAC layer model	No specific MAC layer model.	TDMA scheme for collision and interference avoidance.	TDMA scheme for collision and interference avoidance.
NET layer model	BS-aided multicast when no IOs forward the packet and multi-stage cooperative multicast.	Multi-stage cooperative 'social' multicast. MUs only multicast the IoCI to their social contacts.	BS-aided multicast for the initial stage and cooperative multicast for the subsequent stages.
Resource scheduling	No scheduling. IOs multicast on orthogonal channels.	No scheduling. Each IO is assinged a single TS for its multicast.	Various centrality-based resource scheduling methods are invented.
Energy model	Both transmit energy and signal processing energy.	No energy metrics were evaluated.	Only transmit energy.
Social factors	Altruistic behaviour of MUs.	Geographic social relationships. A twin-layer network model.	SNA aided importance evaluation of IOs to uMUs in a bipartite graph.
Analytical model	Approximate CT-PBMC subject to sufficiently short time interval.	Conventional DT-PBMC model. No extra constraints on it.	DT-PBMC with transient boundary. No extra constraints on it.
Performance metrics	Dissemination delay, individual delay, total energy dissipation individual energy dissipation. tele-traffic offloading ratio.	Average social unicast throughput, average and tail distribution of the dissemination delay.	Average throughput of cellular/opp-tunistic links and group delay,which is a generic form of delay metrics, and total energy dissipation.

amount of the overhead traffic and the tele-traffic offloading ratio. In Chapter 4, we studied both the average social unicast throughput as well as the average dissemination delay and its tail distribution. In Chapter 5, we derived the average throughput for both the cellular links and opportunistic links, when multiple TSs are assigned to them. Furthermore, we focused our attention on formulating the statistical properties of a special interest group's delay in closed-form, which predetermined all the other delay metrics. For example, if the interest-group size is given by the total number of the MUs, the interest-group delay is equal to the dissemination delay; if the interest-group size is one, the interest-group delay is equal to the individual MU's delay; if the transient boundary is fixed at the first state of the DT-PBMC, the group delay is regarded as the delay of the initial BS-aided multicast stage. Please refer to the corresponding chapters for the detailed definitions of the above-mentioned terminologies.

These similarities and differences of our work in Chapters 3–5 are summarised in Table 7.1 for the readers' convenience.

7.3 Large-Scale Versus Small-Scale Opportunistic Networks

We then continued our discourse by comparing the main features of the integrated cellular and large-scale opportunistic networks studied in Chapter 2 to those of its small-scale counterpart of Chapters 3–5, considering the following aspects:

- *Different coverage size.* The area covered by the integrated cellular and large-scale opportunistic network is far larger than the transmission range of MUs. By contrast, its small-scale counterpart only covers an area comparable to the size of the MUs' transmission range.

- *Different MU density.* The MUs in the integrated cellular and large-scale opportunistic network are sparsely distributed across a large area, which results in the intermittent connectivity of the MUs as well as in the intermittent connectivity of the BS and the MUs. By contrast, the MUs moving within the small-scale opportunistic network may be able to reach all their peers in theory, which results in

a fully connected graph for modelling their interactions. Furthermore, in this scenario, the MUs are always capable of maintaining a reliable connectivity with the BSs.

- *Different impact of the MUs' mobility.* The movements of the MUs in the large-scale opportunistic network result in intermittent connectivity amongst these MUs. A reliable wireless link can be established for delivering a file, when a pair of MUs enter each other's transmission range. Furthermore, their wireless link has to remain reliable for a sufficiently long period so as to allow the target MU to download the complete file. As a result, the reliability of the information delivery in the large-scale opportunistic network is dominated by the mobility-related factors, namely by the inter-contact duration and by the contact duration itself. The inter-contact duration between a pair of MUs characterises the relative frequency of the wireless link's establishment, while the contact duration represents the 'life time' of the wireless link. By contrast, the movements of the MUs in the small-scale opportunistic network do not affect their connectivity. However, the mobility-dependent distance results in a fluctuating path loss between a transmitter and receiver pair, which results in a commensurate variation of the signal strength at the receiver end, because there is no power-control in peer-to-peer communications.

- *Different extra factors affecting the information dissemination process.* Apart from the inter-contact as well as contact durations, a range of further factors affect the information dissemination process in the integrated cellular and large-scale opportunistic network. The file size and the transmission rate of a wireless link jointly determine the transmission time required. Furthermore, an IoCI has a specific life time. Once the IoCI has been generated, the MUs maintain their interests in it only for a limited duration. When considering small-scale opportunistic networks, apart from the time-variant distances incurred by the MUs' movements, the information dissemination process is substantially affected by the physical layer parameters. Explicitly, the transmit power, the path loss and the multipath fading jointly determine the received signal strength.

- *Different successful information delivery criteria.* In large-scale opportunistic networks, the IoCI is delivered successfully, when the receiver enters the range of the transmitter, provided that their contact duration is longer than the transmission time required. By contrast, in small-scale opportunistic networks, the success of information delivery fundamentally hinges on the physical layer parameters. The receiver can only recover the original information from the contaminated bits if the received Signal-to-Noise-Ratio (SNR) is higher than a pre-defined threshold. This SNR threshold is determined by the error-correction capability of the receiver.

- *Different resource scheduling requirements.* In large-scale opportunistic networks, resource scheduling may become dispensable, since the sparse distribution of MUs automatically limits the interference, because it rarely occurs that a receiver enters the transmission range of multiple transmitters. By contrast, efficient resource scheduling is indispensable in small-scale opportunistic networks for avoiding the adverse effects of collisions and interferences and for efficiently exploiting the limited resources.

- *Different network layer protocols.* Large-scale opportunistic networks adopt the classic epidemic relaying protocol for disseminating the IoCI, as portrayed in Chapter 2. However, the MUs do not have to rely on a multicast function, since they tend to be sparsely distributed across a large area. Furthermore, the receivers rarely enter the range of multiple transmitters. Even if this rare event occurs, the receiver only selects a single transmitter for downloading the IoCI from. By contrast, in small-scale opportunistic networks, multi-stage cooperative multicasting is adopted for exploiting the broadcast nature of the wireless channel and for benefiting from the potential transmit diversity gain gleaned by exploiting the different channel quality of multiple transmitters.

- *Different latency order.* The latency of information dissemination in large-scale opportunistic networks is on the same order as the inter-contact duration, normally hours. As a result, large-scale

Table 7.2: Comparison between integrated cellular large-scale opportunistic network and its small-scale counterpart

	Cellular+Large-scale opportunistic networks	**Cellular+Small-scale opportunistic networks**
Scale	The size of the area studied is far larger than the transmission range of the MUs.	The size of the area studied is comparable to the transmission range of the MUs.
Density	MUs are sparsely distributed in the area studied.	MUs are densely distributed in the area studied.
Mobility factors	MUs move at a high speed. The inter-contact duration and contact duration dominate the information dissemination.	The path loss between a transmitter and a receiver fluctuates, which affects the information dissemination.
Other factors	File size and transmission rate jointly determine the required transmission time. Information life time decides when the information expires.	Path loss, multi-path fading and transmit power jointly determine the received signal strength. Noise power.
Infomattion delivery	The receiver enters the range of the transmitter, while the contact duration is longer than required transmission time.	The signal-to-noise ratio is higher than a predefined threshold.
Resource Scheduling	Dispensable. Sparse distribution of MUs makes it unlikely that a receiver is in the transmission range of multiple transmitters.	Indispensable in order to avoid interference, when multiple IOs multicast and in order to efficiently exploit the precious resources.
Protocol	Peer-to-peer communication based epidemic relaying protocol.	Multi-stage cooperative multicast protocol.
Latency order	Similar to the inter-contact duration, normally hours, suitable for delivering delay-tolerant services.	Similar to the duration of a transmission frame, normally milli-seconds, suitable for delivering delay-sensitive services.
Math. tool	Conventional CT-PBMC.	Either approximate CT-PBMC or DT-PBMC.
Application Scenarios	Networking in rural areas, emergency communication in large areas, tele-traffic off-loading in macro cellular networks, hybrid vehicular communications.	Networking in densely populated areas, such as shopping malls, football stadiums, open air festivals and small cellular networks.

opportunistic networks are only suitable for delivering delay-tolerant information. By contrast, the information dissemination latency of their small-scale counterparts is on the same order as the duration of a transmission frame, maybe as low as milli-seconds. According to our findings in Chapters 3–5, our small-scale opportunistic network aided information dissemination has a lower latency than traditional BS-aided multicast, which makes small-scale opportunistic networks also suitable for delivering delay-sensitive information.

- *Different mathematical tools.* Owing to its continuous nature, information dissemination in large-scale opportunistic network can be modelled by a CT-PBMC, as argued in Section 2.4. The most distinctive feature of the CT-PBMC is that every single state must be traversed through, before the CT-PBMC reaches the absorbing state. More explicitly, no intermediate state is skipped over. By contrast, due to its discrete nature, the information dissemination in small-scale opportunistic networks can be modelled either by an approximate CT-PBMC or by a DT-PBMC. In contrast to its CT-PBMC counterpart, during a basic time-interval, a state transition of the DT-PBMC may skip over multiple intermediate states. In theory, a transition may occur from any state to any arbitrary higher-indexed state in a single hop.

- *Different application scenarios.* Large-scale opportunistic networks find application in rural area networking, in emergency communications, in tele-traffic offloading etc. By contrast, small-scale opportunistic networks find favour in densely populated areas, with the objective of reducing the information dissemination delay and of relieving the CI from its heavy tele-traffic load etc.

The differences between integrated cellular and large-scale opportunistic networks as well as their small-scale counterparts are summarised in Table 7.2 for the readers' convenience.

7.4 Future Research

At the end of Chapter 5, we have provided our vision on a hybrid resource scheduling approach, where the qualities of both the cellular links and of the opportunistic links should be jointly considered so as to overcome the adverse clustering effects. In this section, we will continue to discuss a range of promising future research in this specific area.

7.4.1 Dissemination of Multiple Content Types

Since we only considered a single type of content, we only had to characterise the MUs' interest in this specific content by a binary variable, say a '1' representing the users having an interest and a '0' representing the users uninterested in this content. Hence, all the MUs reporting '1' form a community of interest in order to cooperatively disseminate this content, while the MUs reporting '0' remain silent and hence do not interfere with the content dissemination process.

However, when we have multiple types of content, this binary variable aided interest modelling approach becomes invalid. In the open literature [177] and [178], the popularity of a range of contents was modelled by a Zipf distribution. To elaborate a little further, if we have a set of content files $\{\mathcal{F}_i | i = 1, \cdots, F\}$, according to the Zipf distribution, the probability of the file $\mathcal{F}_i$ being requested is expressed as

$$\Pr(\mathcal{F}_i) = \frac{\frac{1}{i^{\alpha}}}{\sum_{n=1}^{F} \frac{1}{n^{\alpha}}}, \tag{7.1}$$

where α is a predefined exponent. The MUs requesting the content file $\mathcal{F}_i$ form a community $\mathcal{G}_i$ and hence they may cooperate with each other for the sake of disseminating the content file $\mathcal{F}_i$ of common interest. An important parameter that may influence the content dissemination process is the size $N_{\mathcal{G}_i}$ of the community $\mathcal{G}_i$. If we assume a total of N MUs within the area studied, $N_{\mathcal{G}_i}$ can be modelled by a binomially distributed random variable associated with the pair of parameters N and $\Pr(\mathcal{F}_i)$. Considering the influence of this random variable, we may study the impact of content-popularities on the content dissemination process.

Furthermore, we assume that two communities $\mathcal{G}_i$ and $\mathcal{G}_j$ are formed, where $i \neq j$, for disseminating the content files $\mathcal{F}_i$ and $\mathcal{F}_j$, respectively. If these two communities do not geographically overlap with each other, the corresponding content dissemination processes become independent of each other and we may hence derive their performance metrics separately by relying on the analytical framework proposed in this treatise. However, if this pair of communities geographically overlap with each other, avoiding the collisions and interferences imposes further challenges.

7.4.2 Altruistic Behaviour Modelling

The MUs' altruistic behaviour has a significant influence on the attainable information dissemination performance. However, in order to more precisely model the MUs' altruistic behaviours, the following factors have to be considered by future research:

- *The MUs' altruistic behaviours might be affected by their interest in a specific content.* For example, when the users receive a part of this content, they may find that this content is not quite as good as they expected. Hence, their interest in this content may fade, which also results in the reduction of their willingness to forward it. By contrast, the users might find that the current content is much better than they expected. In this case, their interest in this content may be intensified, which also results in an increased willingness to forward it. However, in order to model the relationship between the user interest and their altruistic behaviour, we have to find a model for quantifying the user interest first. To the best of our knowledge, no commonly accepted mathematical model has been proposed in the open

literature for quantifying the grade of user interest. This mathematical modelling requires joint efforts from the communication community, computer science community and psychology community.

- *The MUs' altruistic behaviour might be affected by their energy concern.* Since the battery lives of mobile devices are often limited, MUs are inclined to reserve energy for their own usage, but might feel reluctant to assist in the information dissemination. Altruistic behaviour is more likely to be the norm in an energy harvesting system [179], where mobile devices are capable of harvesting the energy from the environment. In this system typically, an energy buffer is conceived for a mobile device. The energy harvested by the solar cell enters the energy buffer and it is dissipated from the buffer, when the mobile device carries out any of its tasks. Consequently, the energy saved in this buffer fluctuates dynamically. The willingness of a MU can be modelled based on the probability of having a certain level of residual energy in the battery, which has to be higher than the amount of energy required for transmitting a single packet. The combination of our mobile social networking aided content dissemination and energy harvesting system provides a prolific direction for future work.

7.4.3 Non-cooperative Game Modelling

In game theory [180], a non-cooperative game is defined as one, where players formulate their own strategies independently in order to maximise their own benefits. This technique has been widely adopted in the research of wireless communication systems. For example, the authors of [181] proposed a power control scheme for heterogeneous networks with the aid of a non-cooperative game and the authors of [182] studied a non-cooperative game assisted feedback rate control for providing the transmitter with channel state information in wireless networks.

This effective tool may be further exploited in our content dissemination model. The essence of a non-cooperative game relies on the fact that players are always inclined to choose particular strategies, which may increase their own profits. In our model, the strategies of MUs are represented by their probabilities of aiding the content dissemination process. According to our model, when a MU acts by obeying a specific strategy, the benefit may for example be the reduction of the information acquisition delay, which is achieved at an additional energy dissipated by this MU. As a result, the total cost function $\mathcal{C}(q)$ can be defined as

$$\mathcal{C}(q) = \underbrace{a \cdot T_I(q)}_{\text{Delay-related term}} + \underbrace{b \cdot E_I(q)}_{\text{Energy-related term}} , \tag{7.2}$$

where q denotes the probability of this MU actively assisting the content dissemination process, $T_I(q)$ is the individual MU's information acquisition delay function with respect to q, while $E_I(q)$ is the individual MU's energy function with respect to q. We also have a pair of positive coefficients, namely a and b, in Eq.(7.2), which are adjustable for assigning different weights to the corresponding terms. Increasing q may reduce the delay-related term in Eq.(7.2), which may hence reduce the cost function $\mathcal{C}(q)$. By contrast, a higher q also results in an increased energy-related term in Eq.(7.2), which may consequently increase the cost function $\mathcal{C}(q)$. A trade-off obviously exist between the delay- and energy-related terms. Hence, invoking a non-cooperative game may assist the MUs in minimising their individual costs by achieving Nash-equilibrium.

7.4.4 SNA Aided Cellular Video Caching

In order to accommodate the dramatically increasing tele-traffic demands, small cells, such as pico-cells and femto-cells, may be deployed alongside the conventional macro-cellular system [183]. Small cells are eminently suitable for off-loading huge amounts of tele-traffic from the congested macro-cells and for further enhancing the quality of the MUs' communication experience. However, due to the associated high cost, network operators cannot afford connecting all the BSs of the small cells to the core network via optical fibre.

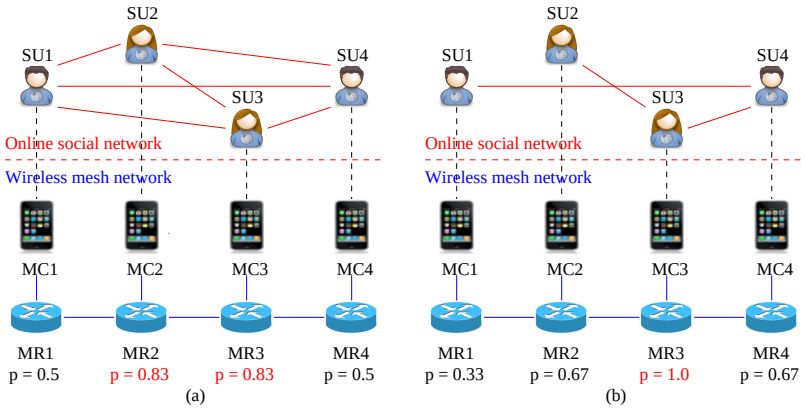

Figure 7.1: An example to present the impact of an online social network on a wireless mesh network

In order to reduce the deployment cost, wireless backhaul links have to be adopted. However, the limited capacity of the backhaul links connecting the BSs of small-cells to the core network constitutes a bottleneck, which limits the performance of small-cells. Researchers and engineers aim for directly improving the capacity of the backhaul links by conceiving more advanced communication techniques, such as millimeter wave [184] and massive MIMO techniques [185]. However, the authors of [186] proposed a femto-caching scheme, which provides us with an attractive solution from a completely different perspective.

A predominant fraction of the increased tele-traffic is generated by video streaming. However, a small fraction of video files tends to attract the majority of the subscribers. If we pre-store the popular video files in the cache memory of femto-BSs, the bottleneck incurred by the limited capacities of the backhaul links can be bypassed. The cache-refreshing operation of the femto-BSs can be carried out outside of the peak time. We may also model the connections amongst the femto-BSs and the MUs by a bipartite graph, as we did for modelling the connections between the IOs and uMUs in Chapter 5. As a result, given the different qualities of the wireless links connecting the femto-BSs and the MUs, we are capable of evaluating the importance of specific femto-BSs for the individual MUs with the aid of SNA tools. Again, the popularity of the video files can be characterised by the Zipf distribution formulated in Eq.(7.1). Eventually, an optimal video files placement scheme can be found for maximising the chances of the MUs fetching their video clips of interest. Additionally, multilayer video coding has been widely adopted, where each video file is comprised of a low-quality basic layer and several enhancement layers. Instead of placing the entire video clip in the cache of the femto-BSs, we may find a scheme for optimally pre-storing the layers of video clips in order to maximise the quality of the video viewing experience for the MUs.

7.4.5 Interplay between Online Social Networks and Wireless Networks

The design of wireless networks aims for improving their full potential. However, communication amongst people relies on their social characters, especially when pervasive online social networking services, such as Facebook and Twitter, become part of our daily life. We maintain regular contact with our friends, our colleagues and our families often relying on social media. Hence, we have to study the impact of online social networks on wireless networks.

Let us assume that a pair of MUs can only communicate with each other if they share a social relationship in an online social network. In Figure 7.1(a), we have four social users (SUs) in an online social network, in which any pair of SUs share a social relationship. In order to fulfil their communication demands, their mobile devices connect to a wireless mesh network as mesh clients (MCs), which is shown in Figure 7.1(a). The backbone of the wireless mesh network is comprised of four serially concatenated mesh routers (MRs). As depicted by the topology of the online social network in Figure 7.1(a), we have six communicating pairs,

Table 7.3: The usage of MRs corresponding to the online social network and the wireless mesh network of Figure 7.1(a)

	SU1↔SU2	SU1↔SU3	SU1↔SU4	SU2↔SU3	SU2↔ SU4	SU3↔ SU4	Usage Probility
MR1	✓	✓	✓	×	×	×	0.5
MR2	✓	✓	✓	✓	✓	×	0.83
MR3	×	✓	✓	✓	✓	✓	0.83
MR4	×	×	✓	×	✓	✓	0.5

Table 7.4: The usage of MRs corresponding to the online social network and the wireless mesh network of Figure 7.1(b)

	SU1↔SU4	SU2↔SU3	SU3↔SU4	Usage Probability
MR1	✓	×	×	0.33
MR2	✓	✓	×	0.67
MR3	✓	✓	✓	1.0
MR4	✓	×	✓	0.67

namely the SU1 and SU2 pair, the SU1 and SU3 pair, the SU1 and SU4 pair, the SU2 and SU3 pair, the SU2 and SU4 pair as well as the SU3 and SU4 pair. In order to satisfy the communication demand of the SU1 and SU2 pair, MR1 and MR2 are used as their intermediate relays. In order to serve the communication demand of the SU2 and SU4 pair, MR2, MR3 and MR4 have to be employed as intermediate relays. The employment of MRs for the remaining communicating pairs is listed in Table 7.3. As shown in Table 7.3, we observe that MR1 is employed for fulfilling the communication demands of three pairs out of six. Hence, the usage probability of MR1 is 0.5. By following the same methodology, we may evaluate the usage probabilities for all the other MRs. Apparently, MR2 and MR3 are more important than MR1 and MR4, since they are employed more frequently than the other two. For example, disabling MR2 may disconnect five communicating pairs, but disabling MR1 may only disconnect three communicating pairs.

As shown in Figure 7.1(b), we consider a different topology for the online social network, while the topology of the wireless mesh network remains the same. The potential communication demands in this case consist of three communicating pairs., which are constituted by the SU1 and SU4 pair, the SU2 and SU3 pair as well as the SU3 and SU4 pair. Table 7.4 presents the usage of MR invoked for fulfilling the communication demands of different pairs. As shown in Table 7.4, for example, we observe that MR2 is employed for fulfilling the communication demands of two pairs out of a potential of three. Hence, the usage probability of MR2 is 0.67. By following the same methodology, we may evaluate the usage probabilities for all the other MRs. Apparently, MR3 is the most important one. If it malfunctions, none of the potential communication demands can be fulfilled. By contrast, if MR1 malfunctions, only SU1 and SU4 are prevented from communicating with each other, while the remaining communication demands can still be fulfilled.

According to Tables 7.3 and 7.4, we observe that the social relationships characterised by the online social network heavily affect the usage of the MRs in the wireless mesh network. This interplay between the online social network and the wireless mesh network can be exploited for optimising the attainable communication performance. From the perspective of resource allocation, we are inclined to allocate more resources to the more important MRs after evaluating the importance of the MRs by considering the impact of the online social network. Furthermore, in order to improve the performance of disseminating the IoCI amongst the SUs, we might save the IoCI in a more important MR's cache.

7.5 Potential Applications

Our design of integrated cellular and opportunistic networks can find numerous applications, which will be briefly presented in this section.

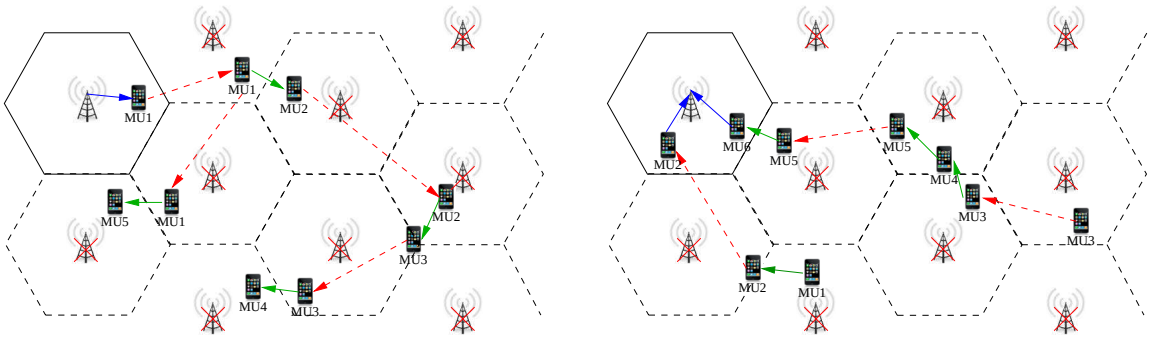

(a) An information dissemination scenario

(b) An information uploading scenario

Figure 7.2: Application in emergency communication

7.5.1 Emergency Communication

Our integrated network can be applied for delivering vital information, if most of the CI is destroyed by disasters, such as an earthquake, tsunami or volcano eruption. In Figure 7.2, we present examples of disseminating information and uploading information in the disaster-affected area.

As shown in Figure 7.2, only the BS at the top-left corner survives during a natural disaster, hence most MUs lose their connection to the cellular network. In order to provide crucial information, such as the arrival time of a rescue team and survival guides, our integrated network can be invoked for disseminating this vital information across the entire disaster-affected area. For example, we observe from Figure 7.2(a) that the information is delivered by the surviving BS to MU1 via a cellular link. MU1 then carries this information and moves around in the area, delivering the information to anyone he/she encounters. The served MU further joins the dissemination process so as to disseminate the information to as many MUs as possible with as short a delay as possible. An epidemic relaying protocol should be invoked for this scenario.

The survivors are also eager to report their personal information, such as their positions and their medical conditions, to the outside world. Since the majority of them lose their connections to the cellular network, our integrated network may be relied upon by the survivors to upload this crucial personal information. As shown in Figure 7.2(b), for example, MU1 asks MU2 to relay its information toward the surviving BS and once MU2 enters the coverage of the surviving BS, MU1's information can be successfully uploaded. The information of MU3 is also successfully uploaded to the BS via the opportunistic contact between MU4 and MU5 as well as that between MU5 and MU6. However, for the information uploading scenario, the employment of an epidemic relaying protocol is not quite appropriate, since it may rapidly drain the precious energy of the MUs' devices. Hence, the SNA aided opportunistic routing protocols of Chapter 1 may be invoked for uploading crucial personal information without excessive energy and resource consumption.

7.5.2 Hybrid Vehicular Network

Our integrated cellular and opportunistic network can be extended to a hybrid vehicular network, where roadside communication units act as the CI and vehicles may also exchange their information via their opportunistic contact. When a pair of vehicles enter each other's transmission range, an opportunistic link can be established for delivering information. When a vehicle enters the range of a roadside communication unit, a dedicated link can be established as well, as portrayed in Figure 7.3(a). In this scenario, the vehicles may share common interest in some travel information, such as the road conditions and traffic conditions. As shown in Figure 7.3(a), the vehicles travelling at the front collect the information about the road conditions as well as traffic conditions and this information can be disseminated via opportunistic links to the vehicles travelling behind. Moreover, the vehicles coming from the reverse direction may also bring back this sort

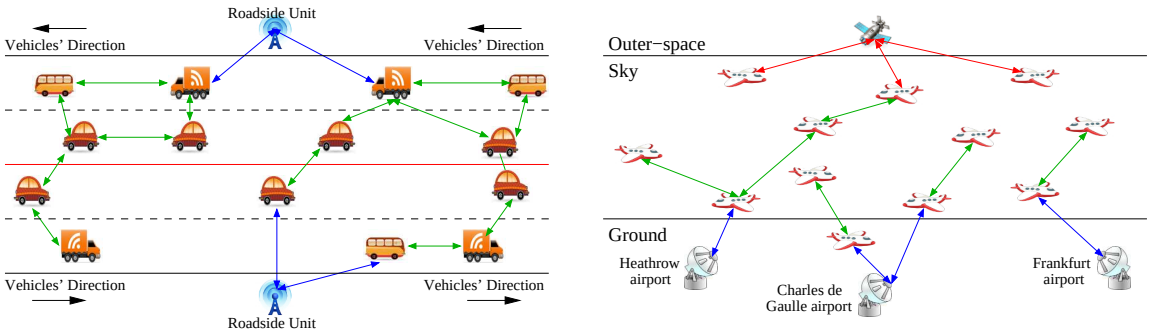

(a) Hybrid vehicular network

(b) Hybrid aircraft network

Figure 7.3: Examples of a hybrid vehiclular network and a hybrid aircraft network.

of information. If a pair of vehicles are too far away from each other, the roadside communication unit can be exploited for relaying the information between them. Furthermore, this network can be relied upon for designing smart vehicles. For example, when a vehicle in front applies emergency braking, the information related to this operation is automatically sent back to the vehicles following behind. The emergency braking system of the vehicle behind is then triggered by this information. As a result, we may be able to avoid serious pile-up collisions. The opportunistic links between a pair of vehicles can be invoked for regularly exchanging relevant information. For example, the vehicle in the front sends its speed information to its peers. As the vehicle following behind receives this information, its speed can be automatically adjusted so as to keep its safety distance.

7.5.3 Hybrid Aircraft Network

Our integrated cellular and opportunistic network can be extended to a hybrid aircraft network. As shown in Figure 7.3(b), apart from the opportunistic links amongst the aeroplanes, two types of CI exist, namely ground-stations and satellites. This hybrid network can be relied upon for disseminating important information across the aeroplanes that are interested in it. For example, when an aeroplane destined to Heathrow airport is approaching, a wireless link can be established for connecting the ground-station and the aeroplane. Then the ground-station directly delivers important information, such as the runway conditions and the weather conditions at Heathrow airport to assist the aeroplane in safe landing. Aeroplanes destined to Heathrow airport may form a community of interest. However, only a few that are within the transmission range of the ground-station can directly receive the IoCI. Consequently, the IoCI can be disseminated to all the other community members relying on their opportunistic links. Note that the conventional deterministic routing may not be fit for an aircraft network, because it cannot react as fast as the context changes imposed by the extremely high speed of the aeroplanes. By contrast, the information delivery based on opportunistic contacts may generate a reduced overhead traffic and may be more robust to near-instantaneous context changes. There are also some aeroplanes still far away from their destinations. In order to receive the relevant commands from the ground stations, they have to maintain reliable links connecting them to the satellite, which may effectively relay information to them.

7.5.4 One Laptop Per Child Scenarios

The charitable goal of the 'One Laptop Per Child (OLPC)' project is to design and distribute inexpensive laptop computers to children in developing countries around the world, in order to provide them with access to knowledge and opportunities. Based on the associated common hardware and software platform, it is convenient for content providers to disseminate useful contents of common interest to children, such as

various types of educational programs. Our integrated cellular and opportunistic network can be applied in the OLPC project in order to efficiently disseminate educational programs. Children speaking the same languages or those in the same-group form communities of interest. Since the CI is not pervasive in the developing countries, only a small fraction of children in a community are able to download the educational programs by connecting their laptops to the content provider. However, we can exploit the common interests of the users and allow them to cooperatively forward the content that they have received so far to their unserved peers. With the aid of our integrated network, the major portion of the content dissemination is completed by the ad hoc network constructed by the users. Consequently, the cost of downloading the content of common interest from the CI can be shared by the users of the same community, which remarkably reduces the total price paid by an individual and hence achieves the charitable goal of this project.

7.5.5 Privacy and Security Enhancement

Back in 2013, Edward Snowden shocked the entire world by revealing the existence of the PRISM surveillance program[3], which had been launched by the U.S. government six years earlier. In PRISM, Internet giants, who are running the most influential central data servers, e.g. Microsoft, Google, Facebook and Apple, were required to provide their users' private data to the government. As reported by *The Guardian* in 2014, Vodafone, one of the largest mobile network operators, revealed the existence of secret wires that allow government agencies to listen to all conversations on its networks, stating that they are widely used in some of the 29 countries in which it operates in Europe and beyond[4]. Although this sort of wiretapping enhances the state security, it raised global concerns related to privacy. In some special circumstances, channelling confidential information flows alongside those of third parties does increase the risk of information leakage. As a result, for some authorities or organisations, which have to exchange confidential information, our opportunistic network may provide a safe option for internal private communication. Since the information exchange in our opportunistic network is purely completed by the direct communication amongst mobile devices, who recognise each other as trusted friends, without any aid of the CI, this may minimise the chances of the confidential information being leaked to or by third parties.

7.6 Closing Remark

We believe that we are witnessing a revolution from 'Comm 1.0' to 'Comm 2.0' in the field of communication engineering, as the World Wide Web evolves from the 'Web 1.0' era to the 'Web 2.0' era. During the old 'Web 1.0' era, there were only a few content creators and the vast majority of users simply acted as content consumers. As a result, in this old era, the website of the content publishers, such as BBC, CNN and ABC, attracted the most visits. We can define the 'Comm 1.0' era in the field of communication engineering in a similar way. In the 'Comm 1.0' era, most of the communication between a pair of MUs was realised by CI-based networks, which were operated by a third party, normally regarded as a network operator. MUs are charged according to their usage of the CI-based networks. Although mobile communication techniques evolved from the well-known '1G' analog mobile networks to the emerging '5G' heterogeneous mobile networks, we are still lingering in the CI-dominated 'Comm 1.0' era because the direct interaction amongst MUs without any aid of the CI is rare. During the development of the World Wide Web, the interaction amongst the users defined the 'Web 2.0' era, where a huge amount of content is published and shared by users themselves and the function of posting comments and reviews is available for users as well. In this new era, we witness a great success of various social networking websites, such as MySpace, Facebook and Twitter, as well as the content sharing websites, such as Youtube and Allrecipes (http://allrecipes.com/). Similarly,

[3] http://en.wikipedia.org/wiki/PRISM

[4] http://www.theguardian.com/business/2014/jun/06/vodafone-reveals-secret-wires-allowing-state-surveillance

we are looking forward to more direct interaction amongst MUs so as to overcome the impediments[5] of the CI-based communication in the next 'Comm 2.0' era, since powerful mobile devices have already been popularised amongst the MUs. In the emerging 'Comm 2.0' era, if necessary, direct communication between a pair of MUs is activated for achieving a more reliable, more prompt, more energy-efficient communication experience. The 'Comm 2.0' era may become popular amongst MUs, since their communications may bypass the CI of network operators and their communications become free of charge, if the unlicensed spectrum is relied upon! By contrast, this becomes a challenge for network operators, because their profit may suffer, if their CI is becoming less frequently used. This treatise may contribute in a modest way towards the new 'Comm 2.0' era and may inspire further efforts from both the industrial and academic communities so as to embrace both the opportunities and the challenges of this new era for both the technical and economic perspectives.

[5]Please refer to Chapter 1 or the beginning of this chapter for more details.

Bibliography

[1] Cisco-Co., "Cisco visual networking index: global mobile data traffic forecast update, 2013-2018," white paper, Cisco and Its Affiliates, February 2014.

[2] M. Peng, Y. Li, T. Q. S. Quek, and C. Wang, "Device-to-device underlaid cellular networks under Rician fading channels," *IEEE Transactions on Wireless Communications*, vol. 13, pp. 4247–4259, August 2014.

[3] A. M. Ortiz, D. Hussein, S. Park, S. N. Han, and N. Crespi, "The cluster between internet of things and social networks: Review and research challenges," *IEEE Internet of Things Journal*, vol. 1, pp. 206–215, June 2014.

[4] N. Kayastha, D. Niyato, P. Wang, and E. Hossain, "Applications, architectures, and protocol design issues for mobile social networks: a survey," *Proceedings of the IEEE*, vol. 99, pp. 2130–2158, December 2011.

[5] T. Alahakoon, R. Tripathi, N. Kourtellis, R. Simha, and A. Iamnitchi, "K-path centrality: a new centrality measure in social networks," in *Proceedings of the 4th Workshop on Social Network Systems*, SNS '11, pp. 11–16, April 2011.

[6] P. V. Marsden, "Egocentric and sociocentric measures of network centrality," *Social Networks*, vol. 24, pp. 407–422, October 2002.

[7] P. Bonacich, "Some unique properties of eigenvector centrality," *Social Networks*, vol. 29, pp. 555–564, October 2007.

[8] S. Brin and L. Page, "The anatomy of a large-scale hypertextual web search engine," *Computer Networks and ISDN Systems*, vol. 30, pp. 107–117, April 1998.

[9] K. Okamoto, W. Chen, and X.-Y. Li, "Ranking of closeness centrality for large-scale social networks," *Frontiers in Algorithmics*, vol. 5059, pp. 186–195, January 2008.

[10] L. C. Freeman, "A set of measures of centrality based on betweenness," *Sociometry*, vol. 40, pp. 35–41, March 1977.

[11] P. D. Meo, E. Ferrara, G. Fiumara, and A. Ricciardello, "A novel measure of edge centrality in social networks," *Knowledge-Based Systems*, vol. 30, pp. 136–150, June 2012.

[12] M. Girvan and M. E. J. Newman, "Community structure in social and biological networks," *Proceedings of the National Academy of Sciences*, vol. 99, pp. 7821–7826, June 2002.

[13] F. Henri and B. Pudelko, "Understanding and analysing activity and learning in virtual communities," *Journal of Computer Assisted Learning*, vol. 19, pp. 474–487, December 2003.

[14] V. D. Blondel, J.-L. Guillaume, R. Lambiotte, and E. Lefebvre, "Fast unfolding of communities in large networks," *Journal of Statistical Mechanics: Theory and Experiment*, vol. 2008, October 2008.

[15] J. Travers and S. Milgram, "An experimental study of the small world problem," *Sociometry*, vol. 32, pp. 425–443, December 1969.

[16] D. J. Watts and S. H. Strogatz, "Collective dynamics of 'small-world' networks," *Nature*, vol. 393, pp. 440–442, June 1998.

[17] M. E. J. Newman and D. J. Watts, "Renormalization group analysis of the small-world network model," *Physics Letters A*, vol. 263, pp. 341–346, March 1999.

[18] J. Kleinberg, "The small-world phenomenon: an algorithm perspective," in *Proceedings of the thirty-second annual ACM symposium on Theory of computing*, STOC '00, pp. 163–170, May 2000.

[19] H. Inaltekin, M. Chiang, and H. V. Poor, "Average message delivery time for small-world networks in the continuum limit," *IEEE Transactions on Information Theory*, vol. 56, pp. 4447–4470, September 2010.

[20] H. Inaltekin, M. Chiang, and H. V. Poor, "Delay of social search on small-world graphs," *The Journal of Mathematical Sociology*, vol. 38, pp. 1–46, January 2014.

[21] J. L. Moreno and H. H. Jennings, *Who shall survive? A new approach to the problem of human interrelations*. Nervous and mental disease monograph series, Nervous and mental disease publishing company, 1934.

[22] A. Rapoport and W. J. Horvath, "A study of a large sociogram," *Behavioral Science*, vol. 6, pp. 279–291, October 1961.

[23] L. C. Freeman, S. C. Freeman, and A. G. Michaelson, "On human social intelligence," *Journal of Social and Biological Structures*, vol. 11, pp. 415–425, October 1988.

[24] W. W. Zachary, "An information flow model for conflict and fission in small groups," *Journal of Anthropological Research*, vol. 33, pp. 452–473, Winter 1977.

[25] M. E. J. Newman, "A measure of betweenness centrality based on random walks," *Social Networks*, vol. 27, pp. 39–54, january 2005.

[26] M. E. J. Newman, "Scientific collaboration networks. II. shortest paths, weighted networks, and centrality," *Physical Review E*, vol. 64, p. 016132, June 2001.

[27] L. C. Freeman, "Centered graphs and the structure of ego networks," *Mathematical Social Sciences*, vol. 3, pp. 291–304, October 1982.

[28] M. Panju, "Iterative methods for computing eigenvalues and eigenvectors," *The Waterloo Mathematics Review*, pp. 9–18, May 2011.

[29] M. E. J. Newman, "Modularity and community structure in networks," *Proceedings of the National Academy of Sciences*, vol. 103, pp. 8577–8582, May 2006.

[30] K.-C. Chen, M. Chiang, and H. V. Poor, "From technological networks to social networks," *IEEE Journal on Selected Areas in Communications*, vol. 31, pp. 548–572, September 2013.

[31] W. M. Tam, F. C. M. Lau, and C. K. Tse, "Complex-network modeling of a call network," *IEEE Transactions on Circuits and Systems I: Regular Papers*, vol. 56, pp. 416–429, February 2009.

[32] A.-L. Barabasi, R. Albert, and H. Jeong, "Mean-field theory for scale-free random networks," *Physica A: Statistical Mechanics and its Applications*, vol. 272, pp. 173–187, October 1999.

[33] J. Wu, C. K. Tse, F. C. M. Lau, and I. H. Ho, "Analysis of communication network performance from a complex network perspective," *IEEE Transactions on Circuits and Systems I: Regular Papers*, vol. 60, pp. 3303–3316, December 2013.

[34] M. Faloutsos, P. Faloutsos, and C. Faloutsos, "On power-law relationships of the Internet topology," *ACM SIGCOMM Computer Communication Review*, vol. 29, pp. 251–262, October 1999.

[35] N. Eagle and A. S. Pentland, "Reality mining: sensing complex social systems," *Personal and Ubiquitous Computing*, vol. 10, pp. 255–268, November 2005.

[36] M. Musolesi and C. Mascolo, "Designing mobility models based on social network theory," *ACM SIGMOBILE Mobile Computing and Communications Review*, vol. 11, pp. 59–70, July 2007.

[37] C. Boldrini and A. Passarella, "HCMM: modelling spatial and temporal properties of human mobility driven by users' social relationships," *Computer Communications*, vol. 33, pp. 1056–1074, June 2010.

[38] F. Li and J. Wu, "Localcom: a community-based epidemic forwarding scheme in disruption-tolerant networks," in *2009 6th Annual IEEE Communications Society Conference on Sensor, Mesh and Ad Hoc Communications and Networks*, pp. 1–9, IEEE, June 2009.

[39] E. Bulut and B. K. Szymanski, "Exploiting friendship relations for efficient routing in mobile social networks," *IEEE Transactions on Parallel and Distributed Systems*, vol. 23, pp. 2254–2265, December 2012.

[40] P. Costa, C. Mascolo, M. Musolesi, and G. P. Picco, "Socially-aware routing for publish-subscribe in delay-tolerant mobile ad hoc networks," *IEEE Journal on Selected Areas in Communications*, vol. 26, pp. 748–760, June 2008.

[41] P. Hui, J. Crowcroft, and E. Yoneki, "Bubble rap: social-based forwarding in delay-tolerant networks," *IEEE Transactions on Mobile Computing*, vol. 10, pp. 1576–1589, November 2011.

[42] E. M. Daly and M. Haahr, "Social network analysis for information flow in disconnected delay-tolerant MANETs," *IEEE Transactions on Mobile Computing*, vol. 8, pp. 606–621, May 2009.

[43] K. Akkarajitsakul, E. Hossain, and D. Niyato, "Cooperative packet delivery in hybrid wireless mobile networks: a coalitional game approach," *IEEE Transactions on Mobile Computing*, vol. 12, pp. 840–854, May 2013.

[44] T. Zhang, J. Cao, Y. Chen, L. Cuthbert, and M. Elkashlan, "A small world network model for energy efficient wireless networks," *IEEE Communications Letters*, vol. 17, pp. 1928–1931, October 2013.

[45] A. Banerjee, R. Agarwal, V. Gauthier, C. K. Yeo, H. Afifi, and F. B. Lee, "A self-organization framework for wireless ad hoc networks as small worlds," *IEEE Transactions on Vehicular Technology*, vol. 61, pp. 2659–2673, July 2012.

[46] L. Gu, S.-C. Lin, and K.-C. Chen, "Small-world networks empowered large machine-to-machine communications," in *2013 IEEE Wireless Communications and Networking Conference (WCNC)*, pp. 1558–1563, IEEE, April 2013.

[47] V. Krishnamurthy and H. V. Poor, "Social learning and bayesian games in multiagent signal processing: how do local and global decision makers interact?," *IEEE Signal Processing Magazine*, vol. 30, pp. 43–57, May 2013.

[48] V. Krishnamurthy and H. V. Poor, "A tutorial on interactive sensing in social networks," *IEEE Transactions on Computational Social Systems*, vol. 1, pp. 3–21, March 2014.

[49] M. Kobayashi, "Experience of infrastructure damage caused by the great east japan earthquake and countermeasures against future disasters," *IEEE Communications Magazine*, vol. 52, pp. 23–29, March 2014.

[50] Y. S. Soh, T. Q. S. Quek, M. Kountouris, and H. Shin, "Energy efficient heterogeneous cellular networks," *IEEE Journal on Selected Areas in Communications*, vol. 31, pp. 840–850, May 2013.

[51] A. Liu, V. K. N. Lau, L. Ruan, J. Chen, and D. Xiao, "Hierarchical radio resource optimization for heterogeneous networks with enhanced inter-cell interference coordination (eICIC)," *IEEE Transactions on Signal Processing*, vol. 62, pp. 1684–1693, April 2014.

[52] S. Singh, H. S. Dhillon, and J. G. Andrews, "Offloading in heterogeneous networks: modeling, analysis, and design insights," *IEEE Transactions on Wireless Communications*, vol. 12, pp. 2484–2497, May 2013.

[53] IEEE Standards Committee, "Information technology–telecommunications and information exchange between systems local and metropolitan area networks–specific requirements part 11: Wireless LAN Medium Access Control (MAC) and Physical Layer (PHY) Specifications," *ISO/IEC/IEEE 8802-11:2012(E)*, pp. 1–2798, November 2012.

[54] S.-J. Lee, W. Su, and M. Gerla, "On-demand multicast routing protocol in multihop wireless mobile networks," *Mobile Networks and Applications*, vol. 7, pp. 441–453, December 2002.

[55] J. Wang, S. Park, D. J. Love, and M. D. Zoltowski, "Throughput delay tradeoff for wireless multicast using hybrid-ARQ protocols," *IEEE Transactions on Communications*, vol. 58, pp. 2741–2751, September 2010.

[56] C.-H. Lee and D. Y. Eun, "On the forwarding performance under heterogeneous contact dynamics in mobile opportunistic networks," *IEEE Transactions on Mobile Computing*, vol. 12, pp. 1107–1119, June 2013.

[57] J.-T. Tsai and R. L. Cruz, "Opportunistic multicast scheduling for information streaming in cellular networks," *IEEE Transactions on Wireless Communications*, vol. 10, pp. 1776–1785, June 2011.

[58] J. Hu, L.-L. Yang, L. Hanzo, and H. V. Poor, "Bridging the social and wireless networking divide: information dissemination in integrated cellular and opportunistic networks," *accepted by IEEE Access*, September 2015.

[59] J. Hu, L.-L. Yang, and L. Hanzo, "Mobile social networking aided content dissemination in heterogeneous networks," *China Communications*, vol. 10, pp. 1–12, June 2013.

[60] J. Hu, L.-L. Yang, and L. Hanzo, "Delay analysis of social group multicast aided content dissemination in cellular system," *submitted to IEEE Transactions on Communication, under major revision*, October 2015.

[61] J. Hu, L.-L. Yang, and L. Hanzo, "Throughput and delay analysis of wireless multicast in distributed mobile social networks based on geographic social relationships," in *2014 IEEE Wireless Communications and Networking Conference (WCNC)*, pp. 1874–1879, April 2014.

[62] J. Hu, L.-L. Yang, and L. Hanzo, "Distributed cooperative social multicast aided content dissemination in random mobile networks," *IEEE Transactions on Vehicular Technology*, vol. 64, pp. 3075–3089, July 2014.

[63] J. Hu, L.-L. Yang, and L. Hanzo, "Cooperative multicast aided picocellular hybrid information dissemination in mobile social networks: delay/energy evaluation and relay selection," in *2014 IEEE Wireless Communications and Networking Conference (WCNC)*, (Istanbul, Turkey), pp. 3207–3212, April 2014.

[64] J. Hu, L.-L. Yang, and L. Hanzo, "Stochastic geometry and performance analysis of mus obeying uniform mobility model in cellular systems," *to be submitted*, October 2015.

[65] A. M. Ahmed, B. Jedari, and S. Abolfazli, "Event-based mobile social networks: services, technologies, and applications," *IEEE Access*, vol. 2, pp. 500–513, April 2014.

[66] Y. Cao and Z. Sun, "Routing in delay/disruption tolerant networks: a taxonomy, survey and challenges," *IEEE Communications Surveys & Tutorials*, vol. 15, pp. 654–677, Second Quarter 2013.

[67] L. Becchetti, A. Clementi, F. Pasquale, G. Resta, P. Santi, and R. Silvestri, "Flooding time in opportunistic networks under power law and exponential intercontact times," *IEEE Transactions on Parallel and Distributed Systems*, vol. 25, pp. 2297–2306, September 2014.

[68] Z. Zhang, "Routing in intermittently connected mobile ad hoc networks and delay tolerant networks: overview and challenges," *IEEE Communications Surveys & Tutorials*, vol. 8, pp. 24–37, First Quarter 2006.

[69] A. Jindal and K. Psounis, "Contention-aware performance analysis of mobility-assisted routing," *IEEE Transactions on Mobile Computing*, vol. 8, pp. 145–161, February 2009.

[70] P. R. Pereira, A. Casaca, J. J. P. C. Rodrigues, V. N. G. J. Soares, J. Triay, and C. Cervello-Pastor, "From delay-tolerant networks to vehicular delay-tolerant networks," *IEEE Communications Surveys & Tutorials*, vol. 14, pp. 1166–1182, Fourth Quarter 2012.

[71] A. Chaintreau, J.-Y. L. Boudec, and N. Ristanovic, "The age of gossip: spatial mean field regime," *SIGMETRICS Perform. Eval. Rev.*, vol. 37, pp. 109–120, June 2009.

[72] T. Wang, L. Song, and Z. Han, "Coalitional graph games for popular content distribution in cognitive radio vanets," *IEEE Transactions on Vehicular Technology*, vol. 62, pp. 4010–4019, October 2013.

[73] Y. Li, D. Jin, Z. Wang, L. Zeng, and S. Chen, "Coding or not: optimal mobile data offloading in opportunistic vehicular networks," *IEEE Transactions on Intelligent Transportation Systems*, vol. 15, pp. 318–333, February 2014.

[74] Bluetooth Special Interest Group (SIG), *Specification of the Bluetooth system v4.1*, Decemeber 2013.

[75] M. Zhao, Y. Li, and W. Wang, "Modeling and analytical study of link properties in multihop wireless networks," *IEEE Transactions on Communications*, vol. 60, pp. 445–455, February 2012.

[76] W. L. Huang and K. B. Letaief, "Cross-layer scheduling and power control combined with adaptive modulation for wireless ad hoc networks," *IEEE Transactions on Communications*, vol. 55, pp. 728–739, April 2007.

[77] G. Resta and P. Santi, "A framework for routing performance analysis in delay tolerant networks with application to noncooperative networks," *IEEE Transactions on Parallel and Distributed Systems*, vol. 23, pp. 2–10, January 2012.

[78] T. Camp, J. Boleng, and V. Davies, "A survey of mobility models for ad hoc network research," *Wireless Communications & Mobile Computing (WCMC): Special issue on Mobile Ad Hoc Networking: Research, Trends and Applications*, vol. 2, pp. 483–502, August 2002.

[79] R. Groenevelt, P. Nain, and G. Koole, "The message delay in mobile ad hoc networks," *Performance Evaluation*, vol. 62, pp. 210–228, October 2005.

[80] T. Spyropoulos, A. Jindal, and K. Psounis, "An analytical study of fundamental mobility properties for encounter-based protocols," *International Journal of Autonomous and Adaptive Communications Systems*, vol. 1, pp. 4–40, July 2008.

[81] A. Chaintreau, P. Hui, J. Crowcroft, C. Diot, R. Gass, and J. Scott, "Impact of human mobility on opportunistic forwarding algorithms," *IEEE Transactions on Mobile Computing*, vol. 6, pp. 606–620, June 2007.

[82] T. Karagiannis, J.-Y. L. Boudec, and M. Vojnovic, "Power law and exponential decay of intercontact times between mobile devices," *IEEE Transactions on Mobile Computing*, vol. 9, pp. 1377–1390, October 2010.

[83] M. McNett and G. M. Voelker, "Access and mobility of wireless PDA users," *SIGMOBILE Mobile Computing and Communication Review*, vol. 9, pp. 40–55, April 2005.

[84] C. Chen and Z. Chen, "Exploiting contact spatial dependency for opportunistic message forwarding," *IEEE Transactions on Mobile Computing*, vol. 8, pp. 1397–1411, October 2009.

[85] A. Passarella and M. Conti, "Analysis of individual pair and aggregate intercontact times in heterogeneous opportunistic networks," *IEEE Transactions on Mobile Computing*, vol. 12, pp. 2483–2495, December 2013.

[86] M. Abdulla and R. Simon, "The impact of inter-contact time within opportunistic networks: protocol implications and mobility models," tech. rep., Department of Computer Science, George Mason University, 2009.

[87] W. Wang, V. Srinivasan, and M. Motani, "Adaptive contact probing mechanisms for delay tolerant applications," in *Proceedings of the 13th Annual ACM International Conference on Mobile Computing and Networking*, MobiCom '07, (New York, NY, USA), pp. 230–241, ACM, September 2007.

[88] Y. Li, D. Jin, Z. Wang, L. Zeng, and S. Chen, "Exponential and power law distribution of contact duration in urban vehicular ad hoc networks," *IEEE Signal Processing Letters*, vol. 20, pp. 110–113, January 2013.

[89] X. Zhuo, Q. Li, W. Gao, G. Cao, and Y. Dai, "Contact duration aware data replication in delay tolerant networks," in *2011 19th IEEE International Conference on Network Protocols (ICNP)*, pp. 236–245, October 2011.

[90] Y. Li, M. Qian, D. Jin, P. Hui, Z. Wang, and S. Chen, "Multiple mobile data offloading through disruption tolerant networks," *IEEE Transactions on Mobile Computing*, vol. 13, pp. 1579–1596, July 2014.

[91] V. Sciancalepore, D. Giustiniano, A. Banchs, and A. Picu, "Offloading cellular traffic through opportunistic communications: analysis and optimization," *IEEE Journal on Selected Area in Communications, early access*, vol. pp, July 2015.

[92] R.-S. Chang, W.-Y. Chen, and Y.-F. Wen, "Hybrid wireless network protocols," *IEEE Transactions on Vehicular Technology*, vol. 52, pp. 1099–1109, July 2003.

[93] A. Vahdat and D. Becker, "Epidemic routing for partially connected ad hoc networks," tech. rep., July 2000.

[94] P. V. Mieghem, *Performance Analysis of Communications Networks and Systems*. New York, NY, USA: Cambridge University Press, 2005.

[95] M. W. Fackrell, *Characterization of Matrix-Exponential Distributions*. PhD thesis, The University of Adelaide, 2003.

[96] Y.-K. Ip, W.-C. Lau, and O.-C. Yue, "Performance modeling of epidemic routing with heterogeneous node types," in *2008 IEEE International Communications Conference (ICC)*, pp. 219–224, May 2008.

[97] Y. Li, G. Su, D. O. Wu, D. Jin, L. Su, and L. Zeng, "The impact of node selfishness on multicasting in delay tolerant networks," *IEEE Transactions on Vehicular Technology*, vol. 60, pp. 2224–2238, June 2011.

[98] M. V. Barbera, J. Stefa, A. C. Viana, M. D. de Amorim, and M. Boc, "VIP delegation: enabling VIPs to offload data in wireless social mobile networks," in *International Conference on Distributed Computing in Sensor Systems and Workshops (DCOSS)*, pp. 1–8, June 2011.

[99] W. Gao, Q. Li, B. Zhao, and G. Cao, "Social-aware multicast in disruption-tolerant networks," *IEEE/ACM Transactions on Networking*, vol. 20, pp. 1553–1566, October 2012.

[100] P. Hui, J. Crowcroft, and E. Yoneki, "Bubble rap: social-based forwarding in delay tolerant networks," in *Proceedings of the 9th ACM international symposium on mobile ad hoc networking and computing - MobiHoc '08*, (New York, New York, USA), pp. 241–250, ACM Press, May 2008.

[101] Q. Li, S. Zhu, and G. Cao, "Routing in socially selfish delay tolerant networks," in *Proceedings of 2010 IEEE INFOCOM*, pp. 1–9, March 2010.

[102] A. Clementi, F. Pasquale, and R. Silvestri, "Opportunistic MANETs: mobility can make up for low transmission power," *IEEE/ACM Transactions on Networking*, vol. 21, pp. 610–620, February 2013.

[103] H. Sun and C. Wu, "Epidemic forwarding in mobile social networks," in *2012 IEEE International Conference on Communications (ICC)*, pp. 1421–1425, June 2012.

[104] S. Ioannidis, A. Chaintreau, and L. Massoulie, "Optimal and scalable distribution of content updates over a mobile social network," in *proceedings of 2009 IEEE INFOCOM*, pp. 1422–1430, April 2009.

[105] C. Boldrini, M. Conti, and A. Passarella, "Contentplace: social-aware data dissemination in opportunistic networks," in *Proceedings of the 11th International Symposium on Modeling, Analysis and Simulation of Wireless and Mobile Systems*, MSWiM '08, (New York, NY, USA), pp. 203–210, ACM, October 2008.

[106] D. Niyato, P. Wang, W. Saad, and A. Hjϕrungnes, "Controlled coalitional games for cooperative mobile social networks," *IEEE Transactions on Vehicular Technology*, vol. 60, pp. 1812–1824, May 2011.

[107] B. Han, P. Hui, V. S. A. Kumar, M. V. Marathe, J. Shao, and A. Srinivasan, "Mobile data offloading through opportunistic communications and social participation," *IEEE Transactions on Mobile Computing*, vol. 11, pp. 821–834, May 2012.

[108] H. Zhu, M. Li, L. Fu, G. Xue, Y. Zhu, and L. M. Ni, "Impact of traffic influxes: Revealing exponential intercontact time in urban vanets," *IEEE Transactions on Parallel and Distributed Systems*, vol. 22, pp. 1258–1266, August 2011.

[109] P. Bellavista, A. Corradi, and E. Magistretti, "Redman: a decentralized middleware solution for cooperative replication in dense MANETs," in *Pervasive Computing and Communications Workshops, 2005. PerCom 2005 Workshops. Third IEEE International Conference on*, pp. 158–162, March 2005.

[110] G. H. Mohimani, F. Ashtiani, A. Javanmard, and M. Hamdi, "Mobility modeling, spatial traffic distribution, and probability of connectivity for sparse and dense vehicular ad hoc networks," *IEEE Transactions on Vehicular Technology*, vol. 58, pp. 1998–2007, May 2009.

[111] J.-B. Seo, T. Kwon, and V. C. M. Leung, "Social groupcasting algorithm for wireless cellular multicast services," *IEEE Communications Letters*, vol. 17, pp. 47–50, January 2013.

[112] R. K. Ganti, J. G. Andrews, and M. Haenggi, "High-SIR transmission capacity of wireless networks with general fading and node distribution," *IEEE Transactions on Information Theory*, vol. 57, pp. 3100–3116, May 2011.

[113] H. Kwon and B. G. Lee, "Cooperative power allocation for broadcast/multicast services in cellular OFDM systems," *IEEE Transactions on Communications*, vol. 57, pp. 3092–3102, October 2009.

[114] T. S. Rappaport, *Wireless Communications: Principles and Practice*. Upper Saddle River, NJ, USA: Prentice Hall PTR, 2nd ed., 2001.

[115] H. Zhang, Z. Zhang, and H. Dai, "Gossip-based information spreading in mobile networks," *IEEE Transactions on Wireless Communications*, vol. 12, pp. 5918–5928, November 2013.

[116] M. Grossglauser and D. N. C. Tse, "Mobility increases the capacity of ad hoc wireless networks," *IEEE/ACM Transactions on Networking*, vol. 10, pp. 477–486, August 2002.

[117] J. Hu, L.-L. Yang, and L. Hanzo, "Maximum average service rate and optimal queue scheduling of delay-constrained hybrid cognitive radio in Nakagami fading channels," *IEEE Transactions on Vehicular Technology*, vol. 62, pp. 2220–2229, June 2013.

[118] M. Derakhshani and T. Le-Ngoc, "Aggregate interference and capacity-outage analysis in a cognitive radio network," *IEEE Transactions on Vehicular Technology*, vol. 61, pp. 196–207, January 2012.

[119] E. T. Jaynes and G. L. Bretthorst, *Probability Theory: The Logic of Science: Principles and Elementary Applications*. Cambridge University Press, 2003.

[120] H. Yetgin, K. T. K. Cheung, M. El-Hajjar, and L. Hanzo, "Cross-layer network lifetime optimization considering transmit and signal processing power in WSNs," *IET Wireless Sensor Systems (Intelligent Wireless Sensor Networks and Applications Special Issue)*, October 2014.

[121] R. G. Maunder, B. M. Al-Hashimi, M. Zwolinski, and L. Hanzo, "Energy-conscious turbo decoder design: a joint signal processing and transmit energy reduction approach," *IEEE Transactions on Vehicular Technology*, vol. 62, pp. 3627–3638, October 2013.

[122] Ofcom, "Notice of proposed variation of Everything Everywhere's 1800 MHz spectrum licences to allow use of LTE and WiMAX technologies," *Ofcom*, March 2012.

[123] C. Bettstetter, H. Hartenstein, and X. Perez-Costa, "Stochastic properties of the random waypoint mobility model," *Wireless Networks*, vol. 10, pp. 555–567, September 2004.

[124] O. Helgason, S. T. Kouyoumdjieva, and G. Karlsson, "Opportunistic communication and human mobility," *IEEE Transactions on Mobile Computing*, vol. 13, pp. 1597–1610, July 2014.

[125] S. A. Hassan and M. A. Ingram, "A quasi-stationary markov chain model of a cooperative multi-hop linear network," *IEEE Transactions on Wireless Communications*, vol. 10, pp. 2306–2315, July 2011.

[126] G. Latouche and V. Ramaswami, *Introduction to Matrix Analytic Methods in Stochastic Modeling*. Society for Industrial and Applied Mathematics, 1999.

[127] S. R. Mirghaderi, A. Bayesteh, and A. K. Khandani, "On the multicast capacity of the wireless broadcast channel," *IEEE Transactions on Information Theory*, vol. 58, pp. 2766–2780, May 2012.

[128] C.-H. Liu and J. G. Andrews, "Multicast outage probability and transmission capacity of multihop wireless networks," *IEEE Transactions on Information Theory*, vol. 57, pp. 4344–4358, July 2011.

[129] B. Niu, H. Jiang, and H. V. Zhao, "A cooperative multicast strategy in wireless networks," *IEEE Transactions on Vehicular Technology*, vol. 59, pp. 3136–3143, July 2010.

[130] J.-H. Wui and D. Kim, "Optimal power allocation between unicast and multicast messages in wireless relay-multicasting networks using superposition coding," *IEEE Communications Letters*, vol. 15, pp. 1159–1161, November 2011.

[131] I.-H. Lee, H. Lee, and H.-H. Choi, "Exact outage probability of relay selection in decode-and-forward based cooperative multicast systems," *IEEE Communications Letters*, vol. 17, pp. 483–486, March 2013.

[132] Y. Zhou, H. Liu, Z. Pan, L. Tian, J. Shi, and G. Yang, "Two-stage cooperative multicast transmission with optimized power consumption and guaranteed coverage," *IEEE Journal on Selected Areas in Communications*, vol. 32, pp. 274–284, Feburary 2014.

[133] H. V. Zhao and W. Su, "Cooperative wireless multicast: performance analysis and power/location optimization," *IEEE Transactions on Wireless Communications*, vol. 9, pp. 2088–2100, June 2010.

[134] N. Vastardis and K. Yang, "Mobile social networks: Architectures, social properties and key research challenges," *IEEE Communications Surveys and Tutorials*, vol. 15, pp. 1355–1371, Third Quarter 2012.

[135] C. Xu, S. Jia, L. Zhong, H. Zhang, and G. Muntean, "Ant-inspired mini-community-based solution for video-on-demand services in wireless mobile networks," *IEEE Transactions on Broadcasting*, vol. 60, pp. 322–335, June 2014.

[136] C. Xu, S. Jia, M. Wang, L. Zhong, H. Zhang, and G. Muntean, "Performance-aware mobile community-based VoD streaming over vehicular ad hoc networks," *IEEE Transactions on Vehicular Technology*, vol. 64, pp. 1201–1217, March 2015.

[137] K. C.-J. Lin, C.-W. Chen, and C.-F. Chou, "Preference-aware content dissemination in opportunistic mobile social networks," in *Proceedings of IEEE INFOCOM 2012*, pp. 1960–1968, March 2012.

[138] P. TalebiFard and V. C. M. Leung, "A content centric approach to dissemination of information in vehicular networks," in *Proceedings of the Second ACM International Symposium on Design and Analysis of Intelligent Vehicular Networks and Applications*, DIVANet '12, (New York, NY, USA), pp. 17–24, ACM, October 2012.

[139] S. Bastani, B. Landfeldt, C. Rohner, and P. Gunningberg, "A social node model for realising information dissemination strategies in delay tolerant networks," in *Proceedings of the 15th ACM International Conference on Modeling, Analysis and Simulation of Wireless and Mobile Systems*, MSWiM '12, (New York, NY, USA), pp. 79–88, ACM, October 2012.

[140] L.-J. Chen, C.-H. Yu, C.-L. Tseng, H.-H. Chu, and C.-F. Chou, "A content-centric framework for effective data dissemination in opportunistic networks," *IEEE Journal on Selected Areas in Communications*, vol. 26, pp. 761–772, June 2008.

[141] M. Khabazian, S. Aissa, and M. Mehmet-Ali, "Performance modeling of safety messages broadcast in vehicular ad hoc networks," *IEEE Transactions on Intelligent Transportation Systems*, vol. 14, pp. 380–387, March 2013.

[142] A. G. Dimakis, S. Kar, J. M. F. Moura, M. G. Rabbat, and A. Scaglione, "Gossip algorithms for distributed signal processing," *Proceedings of the IEEE*, vol. 98, no. 11, pp. 1847–1864, 2010.

[143] V. Sevani, B. Raman, and P. Joshi, "Implementation-based evaluation of a full-fledged multihop TDMA-MAC for WiFi mesh networks," *IEEE Transactions on Mobile Computing*, vol. 13, pp. 392–406, February 2014.

[144] M. Crofton, *Probability, in Encyclopaedia Britannica*. Chicago, IL: Britannica Inc., 9th ed., 1885.

[145] S. Milgram, "The small world problem," *Psychology Today*, vol. 2, pp. 60–67, May 1967.

[146] B. Azimdoost, H. R. Sadjadpour, and J. J. Garcia-Luna-Aceves, "The impact of social groups on the capacity of wireless networks," *2011 IEEE Network Science Workshop (NSW)*, pp. 30–37, June 2011.

[147] D. Liben-Nowell, J. Novak, R. Kumar, P. Raghavan, and A. Tomkins, "Geographic routing in social networks," *Proceedings of the National Academy of Sciences of the United States of America*, vol. 102, pp. 11623–11628, August 2005.

[148] J.-P. Onnela, S. Arbesman, M. C. Gonzalez, A.-L. Barabasi, and N. A. Christakis, "Geographic constraints on social network groups," *PLos ONE*, vol. 6, April 2011.

[149] A. Clauset, C. R. Shalizi, and M. E. J. Newman, "Power-law distributions in empirical data," *SIAM Review*, vol. 51, pp. 661–703, November 2009.

[150] J. Hu, L.-L. Yang, and L. Hanzo, "Optimal queue scheduling for hybrid cognitive radio maintaining maximum average service rate under delay constraints," in *2012 IEEE Global Communications Conference (GLOBECOM)*, pp. 1398–1403, December 2012.

[151] I. S. Gradshteyn and I. M. Ryzhik, *Table of integrals, series, and products*. Elsevier/Academic Press, Amsterdam, seventh ed., 2007.

[152] L.-L. Yang, *Multicarrier Communication*. John Wiley & Sons, 1st ed., 2009.

[153] L. Hanzo and R. Tafazolli, "A survey of QoS routing solutions for mobile ad hoc networks," *IEEE Communications Surveys & Tutorials*, vol. 9, pp. 50–70, Second Quarter 2007.

[154] Z. Gong and M. Haenggi, "Interference and outage in mobile random networks: Expectation, distribution, and correlation," *IEEE Transactions on Mobile Computing*, vol. 13, pp. 337–349, February 2014.

[155] J.-H. Lee, Y. M. Lim, K. Kim, S.-G. Choi, and J.-K. Choi, "Energy efficient cooperative multicast scheme based on selective relay," *IEEE Communications Letters*, vol. 16, pp. 386–388, March 2012.

[156] G. Yuan, X. Zhang, W. Wang, and Y. Yang, "Carrier aggregation for LTE-Advanced mobile communication systems," *IEEE Communications Magazine*, vol. 48, pp. 88–93, February 2010.

[157] S. Mukherjee, "Distribution of downlink SINR in heterogeneous cellular networks," *IEEE Journal on Selected Areas in Communications*, vol. 30, pp. 575–585, April 2012.

[158] S. Chen and J. Zhao, "The requirements, challenges, and technologies for 5G of terrestrial mobile telecommunication," *IEEE Communications Magazine*, vol. 52, pp. 36–43, May 2014.

[159] C. Shin, H. Park, and H. M. Kwon, "PHY-supported frame aggregation for wireless local area networks," *IEEE Transactions on Mobile Computing*, vol. 13, pp. 2369–2381, October 2014.

[160] D. Fooladivanda and C. Rosenberg, "Joint resource allocation and user association for heterogeneous wireless cellular networks," *IEEE Transactions on Wireless Communications*, vol. 12, pp. 248–257, January 2013.

[161] K. Shen and W. Yu, "Distributed pricing-based user association for downlink heterogeneous cellular networks," *IEEE Journal on Selected Areas in Communications*, vol. 32, pp. 1100–1113, June 2014.

[162] S. Singh and J. G. Andrews, "Joint resource partitioning and offloading in heterogeneous cellular networks," *IEEE Transactions on Wireless Communications*, vol. 13, pp. 888–901, Februray 2014.

[163] B. H. Jung, N.-O. Song, and D. K. Sung, "A network-assisted user-centric WiFi-offloading model for maximizing per-user throughput in a heterogeneous network," *IEEE Transactions on Vehicular Technology*, vol. 63, pp. 1940–1945, May 2014.

[164] R. L. Streit, *Poisson Point Processes*. Boston, MA: Springer US, 2010.

[165] H. Zhuang and T. Ohtsuki, "A model based on Poisson point process for analyzing MIMO heterogeneous networks utilizing fractional frequency reuse," *IEEE Transactions on Wireless Communications*, vol. 13, pp. 6839–6850, December 2014.

[166] J. Wen, M. Sheng, X. Wang, J. Li, and H. Sun, "On the capacity of downlink multi-hop heterogeneous cellular networks," *IEEE Transactions on Wireless Communications*, vol. 13, pp. 4092–4103, August 2014.

[167] R. W. Heath, M. Kountouris, and T. Bai, "Modeling heterogeneous network interference using Poisson point processes," *IEEE Transactions on Signal Processing*, vol. 61, pp. 4114–4126, August 2013.

[168] C.-H. Lee and M. Haenggi, "Interference and outage in poisson cognitive networks," *IEEE Transactions on Wireless Communications*, vol. 11, pp. 1392–1401, April 2012.

[169] H. S. Chiu and K. L. Yeung, "J-CAR: An efficient joint channel assignment and routing protocol for IEEE 802.11-based multi-channel multi-interface mobile ad hoc networks," *IEEE Transactions on Wireless Communications*, vol. 8, pp. 1706–1715, April 2009.

[170] J. C. Haartsen and S. Mattisson, "Bluetooth-a new low-power radio interface providing short-range connectivity," *Proceedings of the IEEE*, vol. 88, pp. 1651–1661, October 2000.

[171] N. Lee, X. Lin, J. G. Andrews, and R. W. Heath, "Power control for D2D underlaid cellular networks: modeling, algorithms and analysis," *IEEE Journal on Selected Areas in Communications*, vol. 33, pp. 1–13, January 2014.

[172] M. J. Neely and E. Modiano, "Capacity and delay tradeoffs for ad hoc mobile networks," *IEEE Transactions on Information Theory*, vol. 51, pp. 1917–1937, June 2005.

[173] G. Sharma, R. Mazumdar, and N. Shroff, "Delay and capacity trade-offs in mobile ad hoc networks: a global perspective," *IEEE/ACM Transactions on Networking*, vol. 15, pp. 981–992, October 2007.

[174] Z. Bharucha and H. Haas, "The distribution of path losses for uniformly distributed nodes in a circle," *Research Letters in Communications*, March 2008.

[175] A. Rabbachin, T. Q. S. Quek, and M. Z. Win, "Cognitive network interference," *IEEE Journal on Selected Areas in Communications*, vol. 29, pp. 480–493, February 2011.

[176] O. Yagan, D. Qian, J. Zhang, and D. Cochran, "Conjoining speeds up information diffusion in overlaying social-physical networks," *IEEE Journal on Selected Areas in Communications*, vol. 31, no. 6, pp. 1038–1048, 2013.

[177] M. Cha, H. Kwak, P. Rodriguez, Y.-Y. Ahn, and S. Moon, "I tube, you tube, everybody tubes," in *Proceedings of the 7th ACM SIGCOMM conference on Internet measurement - IMC '07*, (New York, New York, USA), pp. 1–14, ACM Press, October 2007.

[178] M. Hefeeda and O. Saleh, "Traffic modeling and proportional partial caching for peer-to-peer systems," *IEEE/ACM Transactions on Networking*, vol. 16, pp. 1447–1460, December 2008.

[179] O. Ozel, K. Tutuncuoglu, J. Yang, S. Ulukus, and A. Yener, "Transmission with energy harvesting nodes in fading wireless channels: optimal policies," *IEEE Journal on Selected Areas in Communications*, vol. 29, pp. 1732–1743, September 2011.

[180] H. Zhu, D. Niyato, W. Saad, T. Basar, and A. Hjϕrungnes, *Game Theory in Wireless and Communication Networks: Theory, Models, and Applications*. Cambridge University Press, 2012.

[181] T. Mao, G. Feng, L. Liang, S. Qin, and B. Wu, "Distributed energy-efficient power control for macro-femto networks," *IEEE Transactions on Vehicular Technology*, vol. PP, no. 99, pp. 1–13, 2015.

[182] L. Song, Z. Han, Z. Zhang, and B. Jiao, "Non-cooperative feedback-rate control game for channel state information in wireless networks," *IEEE Journal on Selected Areas in Communications*, vol. 30, pp. 188–197, January 2012.

[183] A. Barbieri, A. Damnjanovic, T. Ji, J. Montojo, Y. Wei, D. Malladi, O. Song, and G. Horn, "LTE femtocells: system design and performance analysis," *IEEE Journal on Selected Areas in Communications*, vol. 30, pp. 586–594, April 2012.

[184] T. S. Rappaport, R. Mayzus, Y. Azar, K. Wang, G. N. Wong, J. K. Schulz, M. Samimi, and F. Gutierrez, "Millimeter wave mobile communications for 5G cellular: t will work!," *IEEE Access*, vol. 1, pp. 335–349, May 2013.

[185] J. Hoydis, S. T. Brink, and M. Debbah, "Massive MIMO in the UL/DL of cellular networks: how many antennas do we need?," *IEEE Journal on Selected Areas in Communications*, vol. 31, pp. 160–171, February 2013.

[186] K. Shanmugam, N. Golrezaei, A. G. Dimakis, A. F. Molisch, and G. Caire, "FemtoCaching: Wireless content delivery through distributed caching helpers," *IEEE Transactions on Information Theory*, vol. 59, pp. 8402–8413, December 2013.

Subject Index

S

T

U

W

Author Index

D

E

F

G

H

I

J

K

L

M

N

O

P

Q

R

S

T

U

V

W

X

Y

Z